STATE OF CALIFORNIA • DEPARTMENT OF TRANSPORTATION

TECHNICAL REPORT DOCUMENTATION PAGE

TR0003 (REV 10/98)

ADA Notice

For individuals with sensory disabilities, this document is available in alternate formats. For alternate format information, contact the Forms Management Unit at (916) 445-1233, TTY 711, or write to Records and Forms Management, 1120 N Street, MS-89, Sacramento, CA 95814.

1. REPORT NUMBER	2. GOVERNMENT ASSOCIATION NUMBER	3. RECIPIENT'S CATALOG NUMBER
CA15-2417		

4. TITLE AND SUBTITLE

Concrete-Filled Tube Bridge Pier Connections for Accelerated Bridge Construction

5. REPORT DATE

May 18, 2015

6. PERFORMING ORGANIZATION CODE

7. AUTHOR

Max Taylor Stephens, Dawn E. Lehman, Charles W. Roeder

8. PERFORMING ORGANIZATION REPORT NO.

9. PERFORMING ORGANIZATION NAME AND ADDRESS

Department of Civil and Environment Engineering
University of Washington
3935 University Way NE
Seattle, WA 98105-6613

10. WORK UNIT NUMBER

11. CONTRACT OR GRANT NUMBER

65A0446

12. SPONSORING AGENCY AND ADDRESS

California Department of Transportation
Engineering Service Center
1801 30th Street, MS 9-2/5i
Sacramento, CA 95816

California Department of Transportation
Division of Research, Innovation, and System Information
P.O. Box 942873
Sacramento, CA 94273-0001

13. TYPE OF REPORT AND PERIOD COVERED

Final Report
5/14/2012 to 3/15/2015

14. SPONSORING AGENCY CODE

913

15. SUPPLEMENTARY NOTES

Prepared in cooperation with the State of California Department of Transportation.

16. ABSTRACT

Concrete filled tubes (CFTs) consist of a steel tube with concrete infill. CFT columns offer an efficient and economical alternative to conventional reinforced concrete bridge columns, in that CFT columns can offer larger strength and stiffness and facilitate rapid construction.

This report is the second in a series. The prior report focused on engineering methods for CFT components and seismically resilient CFT column-to-foundation connections. This report focuses on CFT column-to-cap beam connections. In contrast to column-to-footing connections the cap-beam connection has unique design considerations including inverted construction and geometric limitations.

The research project uses experimental methods to develop design procedures for various CFT column-to-cap beam connections. Three connections were studied,namely: (1) an embedded flange connection in which the CFT is embedded in the cap beam, (2) a welded dowel connection in which a series of headed dowels is welded inside the tube and embedded into the cap beam (both fully bonded and partially deboned conditions were studied), and (3) a dowel connection in which an independent cage of headed dowels and transverse reinforcing is developed into the CFT and embedded into the cap beam. All specimens were constructed using precast cap-beam components to demonstrate the feasibility of using these connections for accelerated bridge construction (ABC). The experimental program included specimens that simulated either the transverse or longitudinal direction of the bridge. Results showed that the three connection types provide excellent ductility under reversed-cyclic loading while all super-structure elements remained essentially elastic. The report provides design expressions, a design example and proposed codified language to facilitate immediate implementation of the research results into practice.

17. KEY WORDS	18. DISTRIBUTION STATEMENT
Concrete filled tubes, CFT,Columns, Rapid Construction, Earthquake Engineering, Seismic Design, Accelerated Bridge Construction	No restrictions. This document is available to the public through the National Technical Information Service, Springfield, VA 22161

19. SECURITY CLASSIFICATION *(of this report)*	20. NUMBER OF PAGES	21. COST OF REPORT CHARGED
Unclassified	210	

DISCLAIMER STATEMENT

This document is disseminated in the interest of information exchange. The contents of this report reflect the views of the authors who are responsible for the facts and accuracy of the data presented herein. The contents do not necessarily reflect the official views or policies of the state of California or the Federal Highway Administration. This publication does not constitute a standard, specification, or regulation. This report does not constitute an endorsement by the Department of any product described herein.

For individuals with sensory disabilities, this document is available in Braille, large print, audiocassette, or compact disk. To obtain a copy of this document in one of these alternate formats, please contact: the Division of Research and Innovation, MS-83, California Department of Transportation, P.O. Box 942873, Sacramento, CA 94273-0001.

Concrete-Filled Tube Bridge Pier Connections for Accelerated Bridge Construction

by

Max T. Stephens,
Dawn E. Lehman,
and
Charles W. Roeder

Department of Civil and Environmental Engineering
University of Washington
Seattle, WA 98195

May 18, 2015

Final Report No. CA15-2417

Final Report submitted to the California Department of Transportation under Contract No. 65A0446

ABSTRACT

Concrete filled tubes (CFTs) consist of a steel tube with concrete infill. CFT columns offer an efficient and economical alternative to conventional reinforced concrete bridge columns, in that CFT columns can offer larger strength and stiffness and facilitate rapid construction.

This report is the second in a series. The prior report focused on engineering methods for CFT components and seismically resilient CFT column-to-foundation connections. This report focuses on CFT column-to-cap beam connections. In contrast to column-to-footing connections the cap-beam connection has unique design considerations including inverted construction and geometric limitations.

The research project uses experimental methods to develop design procedures for various CFT column-to-cap beam connections. Three connections were studied, namely: (1) an embedded flange connection in which the CFT is embedded in the cap beam, (2) a welded dowel connection in which a series of headed dowels is welded inside the tube and embedded into the cap beam (both fully bonded and partially deboned conditions were studied), and (3) a dowel connection in which an independent cage of headed dowels and transverse reinforcing is developed into the CFT and embedded into the cap beam. All specimens were constructed using precast cap-beam components to demonstrate the feasibility of using these connections for accelerated bridge construction (ABC). The experimental program included specimens that simulated either the transverse or longitudinal direction of the bridge. Results showed that the three connection types provide excellent ductility under reversed-cyclic loading while all super-structure elements remained essentially elastic. The report provides design expressions, a design example and proposed codified language to facilitate immediate implementation of the research results into practice.

ACKNOWLEDGEMENTS

Leadership and administration of the grant was deftly provided by the California Department of Transportation. The following individuals are thanked for their participation in the project: Ron Bromenshenkel, Michael Cullen, and Peter Lee.

TABLE OF CONTENTS

LIST OF FIGURES

LIST OF TABLES

ANNOTATION LIST

A_c = cross-sectional area of concrete. (in.^{2})

A_{cap}^{top} = total area of primary flexural reinforcing in the top of the cap beam. (in.^{2})

A_{cap}^{bop} = total area of primary flexural reinforcing in the bottom of the cap beam. (in.^{2})

A_{cc} = cross-sectional area of concrete in compression. (in.^{2})

A_{st} = cross-sectional area of steel of steel tube. (in.^{2})

A_h = area of mechanical anchor on headed reinforcing. (in.^{2})

$A_{st,b}$ = total cross section area of longitudinal reinforcing in column. (in.^{2})

$A_{st,c}$ = cross-sectional area of steel tube in compression. (in.^{2})

A_s^{jh} = total area of horizontal stirrups in joint region. (in.^{2})

A_s^{jv} = total area of vertical stirrups in joint region. (in.^{2})

A_s^{sf} = total area of side reinforcing in the cap beam. (in.^{2})

C_c = compressive force in the concrete as calculated using PSDM. (lbs)

C_s = compressive force in the steel tube as calculated using PSDM. (lbs)

C_3 = constant for calculation of effective CFT flexural rigidity (EI_{eff}).

C’ = constant for calculation of effective CFT flexural rigidity (EI_{eff}).

d_b = diameter of reinforcing bar. (in.)

d_f = required depth of footing to eliminate the potential for punching shear failure when using ER connection type. (in.)

d_{hb} = diameter of mechanical anchor for headed reinforcing. (in.)

D = steel tube outer diameter. (in.)

D_o = outer diameter of annular ring when CIP cap is used. Outer diameter of corrugated pipe when precast cap is used. (in.)

E_c = modulus of elasticity of concrete. (ksi)

E_s = modulus of elasticity of steel. (ksi)

EI_{eff} = effective flexural stiffness. (kip-in^2)

$EI_{measured}$ = experimentally measured flexural stiffness. (kip-in^2)

f'_c = specified strength of concrete. (May be taken in psi or ksi. When √ is present, must be taken in psi)

$f'_{c,cap}$ = specified strength of cap beam concrete. (May be taken in psi or ksi. When √ is present, must be taken in psi)

f'_{cf} = specified strength of concrete fill in CFT. (May be taken in psi or ksi. When √ is present, must be taken in psi)

$f'_{c,foot}$ = specified strength of concrete in footing. (May be taken in psi or ksi. When √ is present, must be taken in psi)

f_{cr} = cracking stress of concrete. (May be taken in psi or ksi. When √ is present, must be taken in psi)

f'_g = specified strength of fiber reinforced grout. (May be taken in psi or ksi. When √ is present, must be taken in psi)

f_t = softening relationship for post-cracking tensile behavior of concrete. (May be taken in psi or ksi. When √ is present, must be taken in psi)

f_h = horizontal normal forces at the center of the joint. (May be taken in psi or ksi. When √ is present, must be taken in psi)

f_v = vertical normal forces at the center of the joint. (May be taken in psi or ksi. When √ is present, must be taken in psi)

$F_{y,st}$ = yield strength of steel tube. (May be taken in psi or ksi. When √ of concrete strength is present, must be taken in psi)

$F_{y,b}$ = yield strength of longitudinal dowels. (May be taken in psi or ksi. When √ of concrete strength is present, must be taken in psi)

$F_{u,st}$ = ultimate tensile strength of steel tube. (May be taken in psi or ksi. When √ of concrete strength is present, must be taken in psi)

$F_{u,b}$ = ultimate tensile strength of longitudinal dowels. (May be taken in psi or ksi. When √ of concrete strength is present, must be taken in psi)

F_{EXX} = ultimate tensile strength of weld metal. (ksi)

I_c = moment of inertia of concrete. (in^4)

I_{st} = moment of inertia of steel tube. (in^4)

L_d = development length of longitudinal dowels extending into the CFT column for RC type connection. (in.)

L_e = embedment depth of CFT into cap beam for ER type connections, embedment depth of longitudinal headed dowels into cap beam for WD and RC type connections. (in.)

L_{db} = de-bonded length of longitudinal dowel. (in.)

L_{pc} = distance between top of embedded CFT and top of deck for ER type connections, and distance between the top of the headed dowels and top of deck for WD and RC type connections. (in.)

L_s = soffit depth for WD type connection. (in.)

L_w = length of weld between longitudinal dowels and steel tube. (in.)

M_{max} = maximum measured moment. (kip-in. or kip-ft)

M_n = nominal moment capacity. (kip-in. or kip-ft)

$M_{p,CFT}$ = plastic moment capacity of composite CFT. (kip-in. or kip-ft)

M_o^{col} = Predicted overstrength moment of column, 1.2 M_p^{col}. (kip-in. or kip-ft)

M_p^{col} = idealized plastic moment capacity of bridge column. (kip-in. or kip-ft)

M_y = yield moment capacity of steel tube. (kip-in. or kip-ft)

p_c = principal compression stresses in joint. (kip-in. or kip-ft)

p_t = principal tensile stresses in joint. (kip-in. or kip-ft)

P_{cr} = critical buckling load. (kip-in. or kip-ft)

P_e = elastic buckling load by Euler equation. (kip-in. or kip-ft)

P_o = ultimate compression strength of column. (kip-in. or kip-ft)

R_n = strength of weld between longitudinal dowels and steel tube. (kip)

t = steel tube thickness. (in.)

t_e = effective throat thickness of weld. (in.)

v_{jh} = horizontal shear stress in joint.

v_{jv} = vertical shear stress in joint.

V_o^{col} = predicted overstrength shear of column.

w = minimum weld size between tube and annular ring (ER type connection) or between tube and flange (WD type connection). (in.)

ε_c = strain in concrete. (in./in.)

ε_{cr} = cracking strain of concrete. (in./in.)

ε_s = strain in steel. (in./in.)

ε_{su} = ultimate steel strain. (in./in.)

θ_u = target drift at longitudinal bar fracture. (rad)

ϕ_u = curvature at ultimate strain of longitudinal dowels. (1/in.)

ψ_e = reinforcing bar coating factor defined in ACI 318 (1.0 for uncoated bars, and 1.2 for epoxy coated bars.

Chapter 1

INTRODUCTION

Concrete filled tubes (CFTs) are composite structural elements which provide large strength and stiffness while permitting accelerated bridge construction (ABC). The steel tube serves as formwork and reinforcement to the concrete fill, negating the need for reinforcing cages, shoring, and temporary formwork. In relation to ABC, the placement of the concrete fill may be further enhanced using self-consolidating concrete (SCC), so that concrete vibration is not required.

The steel tube is placed at the optimal location to resist bending forces, thereby maximizing strength and stiffness while minimizing weight and material requirements. In addition, the steel tube provides optimal confinement and much greater shear strength than spiral reinforcement, which is typically used for circular reinforced concrete columns. In addition, the concrete fill restrains local tube buckling, supports compressive stress demands, and offers large stiffness to meet functionality seismic performance objectives and non-seismic load requirements. Shear stress transfer must occur between the steel tube and concrete fill to ensure full composite action, which increases efficiency, resistance, and ductility, all of which are desirable properties for seismic design (Roeder et al. 1999; Roeder et al. 2009; Roeder et al 2010; Lehman and Roeder, 2012; Brown et al. 2013).

CFTs are not widely used in bridge construction in the United States due to a lack of practical, economical and standardized seismic connection details. A limited amount of research has been conducted on CFT connections for use in moderate and high seismic regions.

Prior research by the PIs developed a foundation connection (Lehman and Roeder, 2012). Results from that experimental program provided unique and valuable data and design expressions to support the use of CFT columns in bridge construction. Full realization of the system requires a wider range of connections; connections to the cap beam are needed. This research is focused on the development and experimental investigation of robust CFT column-to-cap beam connections capable of sustaining cyclic lateral load demands while minimizing damage and degradation. Specifically, the study investigates connections between the CFT component and precast bent caps for the optimization of accelerated bridge construction (ABC), with the ultimate objective of characterizing engineering properties of the connections and developing practical design expressions. The work presented herein provides a concise description of the test program and the test results to support CFT cap beam connection design.

1.1 Proposed Connections

This research focused on developing a range of CFT column-to-cap beam connections that facilitate ABC and provide superior seismic performance. The proposed CFT column-to-cap beam connections are illustrated in Fig. 1.1. There are three connection types: (1) embedded ring connections (Fig. 1.1a), (2) welded dowel connections (Fig. 1.1b and Fig. 1.1c), and (3) embedded dowel connections (Fig. 1.1d). This provides a suite of connections for designers, each option offering advantages as the bridge may require.

Fig. 1.1a shows a full strength embedded ring connection (herein referred to as ER); this connection is similar to the embedded flange column-to-foundation connection that was developed in the prior project (Lehman and Roeder 2012). The connection uses a grouted connection detail, with a void cast into a precast cap beam (shown as cast into an inverted-t beam

in Fig. 1.1a; note an RC cap beam can also be utilized). A circular ring is welded to the steel tube to provide anchorage and transfer stress to the concrete and reinforcing in the cap beam. The flange extends a distance 8 times the thickness of the tube (8t) both inside and outside of the tube. The external projection of 8t is smaller than previous recommendations for the embedded foundation connection (Lehman and Roeder, 2012). The precast cap beam is placed onto the column after the column is set, and the recess between the tube and corrugated pipe is filled with high strength fiber reinforced grout.

The connections illustrated in Fig. 1.1b – Fig. 1.1d utilize T-headed reinforcing dowels that extend from the CFT column into the cap beam to provide axial, moment, and shear transfer. These connections can be used in traditional cast-in-place construction, or can be integrated into precast elements using a void similar to that described from grouted CFT connection as shown in Fig. 1.1b - Fig. 1.1d, or individual ducts.

Fig. 1.1b shows a welded dowel connection (herein referred to as WD). The WD connection utilizes headed dowels to resist the flexural demand. The shear transfer to the tube is accomplished by welding the dowels to the steel tube. The dowels are developed into the cap beam using a high-strength, fiber-reinforced grouted connection. Welding the dowel directly to the tube, as opposed to embedding the dowel directly into the connection, which is shown in Fig. Fig. 1.1d, maximizes the moment capacity of the dowel connection. A soffit fill depth is included between the steel tube and cap beam. An annular ring with an outer diameter of D+8t is welded to the exterior of the steel tube to increase compressive bearing area on the soffit fill.

The connection shown in Fig. 1.1c employs the same welded detail within the tube; however the reinforcing bars are de-bonded in the column-to-cap beam interface to increase the ductility (Stringer, 2010). This connection is also referred to as the WD connection.

Fig. 1.1d shows a reinforced concrete connection (referred to as RC connection) in which a short independent cage for both transverse and longitudinal reinforcing extends from the CFT column into the cap beam, and cover is provided between the reinforcing cage and steel tube within the column. A gap is left between the steel tube and cap beam to help focus the plastic hinging location between the CFT component and the cap beam (Montejo et al. 2009).

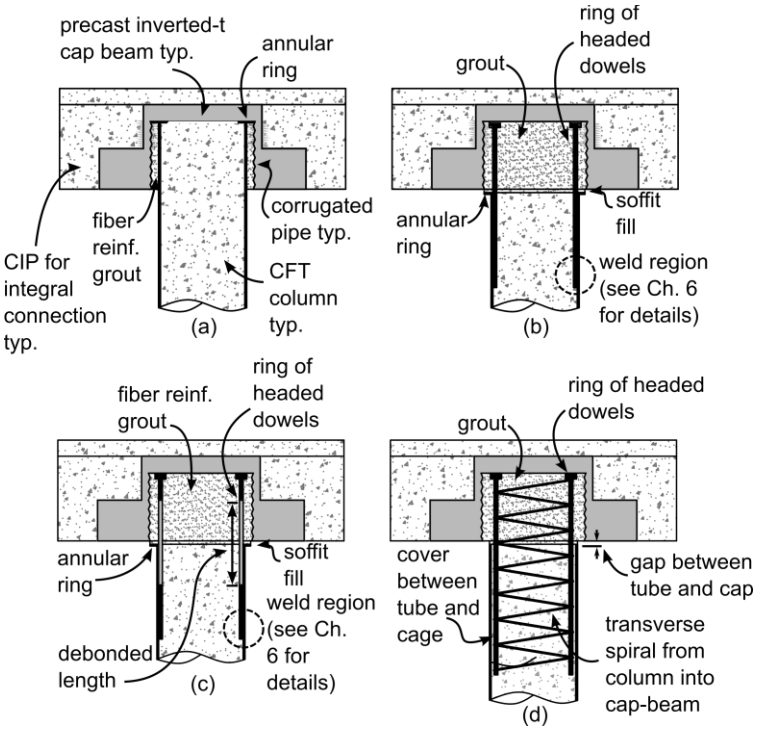

Fig. 1.1. Proposed Connection Types, (a) Embedded Ring Connection (ER), (b) and (c) Welded Dowel Connections (WD), and (d) Reinforced Concrete Connections (RC)

1.2 Overview of Research Program and Report

The research program utilized experimental methods to investigate the proposed connection types. The components of the research program were as follows:

1. Conduct a comprehensive review of past literature and research related to the development of both CFT connections and precast concrete connections.

2. Identify and select connections for study.
3. Develop high-resolution finite element models to evaluate the behavior of each connection type.
4. Utilize results from the finite element analyses to select specimens for experimental investigation.
5. Use successful experimental results to develop practical design expressions for the proposed CFT column-to-cap beam connections.

This document summarizes current design specifications for CFT components, reviews previous research conducted on CFT and precast concrete connections, and presents proposals for efficient CFT connections for rapid and economical construction of highway bridges.

Chapter 2 outlines current design provisions for CFT members available in the AASHTO LRFD Bridge Design Specifications (AASHTOa, 2011) (herein referred to as the AASHTO LRFD) as well as the 14th Edition of the American Institute for Steel Construction (AISC) Steel Design Manual (AISC, 2011). Joint detailing requirements from the AASHTO Guide Specifications for LRFD Seismic Bridge Design (AASHTOb, 2011b) (herein referred to as the AASHTO Seismic Specifications) as well as the California Department of Transportation (Caltrans) Seismic Design Criteria (SDC) Version 1.7 (Caltrans, 2013) are also introduced.

Chapter 3 reviews extensive research which has previously been conducted on CFT and precast concrete connections, while Chapter 4 summarizes the design of specimens for numerical and experimental investigations. Chapters 5 describes a limited numerical study used to evaluate the behavior of the proposed cap beam connections, and Chapter 6 summarizes several ancillary tests which were conducted leading up to the large scale connection tests. Chapter 7 describes the

test setup and instrumentation used in the connection tests, while Chapter 8 evaluates the experimental results and compares the behaviors of the connections as well as the influence of several parameters on connection performance. Chapter 9 presents design-office ready expressions for the seismic design of the proposed connections, and Chapter 10 describes future work.

The recommendations presented in Chapter 9 provide a comprehensive review of the design requirements for a range of CFT column-to-cap beam connections, and provide a solid basis for moving forward with CFT bridge piers in practice. In addition, several service load design examples have been included in Appendix A. These examples re-design several common RC bridges using CFT piers to illustrate the design procedure. Specimen details are given in Appendix B, proposed code language is included in Appendix C, and standard connection drawings of the proposed connections are given in Appendix D.

Chapter 2

DESIGN PROVISIONS

This chapter summarizes design provisions for CFT components specified in AASHTOa (2011), AISC (2011), and ACI (2011), as well as joint detailing requirements for RC bridges in seismic regions specified in the Caltrans Seismic Design Criteria V. 1.8 (2010). These provisions are reviewed because they are relevant to the design of CFT components and dowel-type cap-beam connections for use in seismic regions, and were referenced heavily in this research.

2.1 Design Provisions for CFT Components

2.1.1 Current AASHTO LRFD Design Provisions

The AASHTO LRFD (AASHTOa, 2015) provides design rules for CFT construction. These AASHTO provisions are primarily in Articles 6.9.6 and 6.12.2. The local stability of the steel tube is ensured by limiting the diameter to thickness (D/t) ratio. The limiting value is defined in AASHTO Eq. 6.9.6.2-1 as:

$$\frac{D}{t} \leq 15\sqrt{\frac{E_s}{F_{y,st}}} \tag{2.1}$$

where E_s and F_{yst} are the elastic modulus and nominal yield stress of steel, respectively.

The effective flexural stiffness of a CFT member, EI_{eff}, is defined in AASHTO Eq. 6.9.6.3.2-6 as:

$$EI_{eff} = E_s I_{st} + C' E_c I_c \tag{2.2a}$$

$$C' = 0.15 + \frac{P}{P_o} + 2\frac{A_{st}}{A_{st}+A_c} < 0.9 \quad (2.2b)$$

where the subscripts c and st indicate that the properties are of the concrete or steel sections, respectively, n is a tabulated value which approximates the ratio of the modulus of elasticity for steel and concrete, and I and A are the moment of inertia and area of the respective material sections.

The maximum compressive resistance, P_o, of a CFT member is the summation of the yield capacity of the steel tube and the crushing strength of the concrete fill as defined in AASHTO Eq. 6.9.6.3.2-4 as:

$$P_o = 0.95f'_{cf}A_c + F_{y,st}A_{st} \quad (2.3)$$

where f'_{cf} is the compressive strength of the concrete fill and other variables have been defined previously. The member buckling capacity, P_{cr}, is based on conventional steel buckling equations as defined in AASHTO Eqs. 6.9.6.3-2 and 6.9.6.3.2-3 as:

$$P_{cr} = 0.658^{\frac{P_o}{P_e}}P_o \quad (2.4a)$$

$$P_{cr} = 0.877P_e \quad (2.4b)$$

where P_e is the elastic buckling load. Note that the above equations look slightly different than the equations appearing in the LRFD specification, because internal reinforcement is not included, and some terms have been combined.

Combined loading is an important design consideration as CFTs are commonly used as columns with full moment-resisting connections. The current AASHTO LRFD provisions permit

the use of plastic stress distribution (PSDM) or strain-compatibility methods to calculate combined axial-flexural resistance of CFTs along with a stability based interaction curve to incorporate global buckling. The PSDM assumes that the section develops the full yield stress of the steel in tension and compression and a uniform compressive stress of $0.95f'_c$ for concrete over the compression region in circular CFT as illustrated in Fig. 2.1. The 0.95 coefficient on f'_c for circular CFT is larger than the 0.85 typically used for a Whitney's stress block calculation in recognition of the concrete confinement provided by circular tubes. For each neutral axis depth, pairs of axial and bending resistances are determined by satisfying equilibrium over the cross section for the given stress distribution as illustrated in Fig. 2.1. This calculation results in a material-based, closed-form axial load-bending moment (P-M) curve.

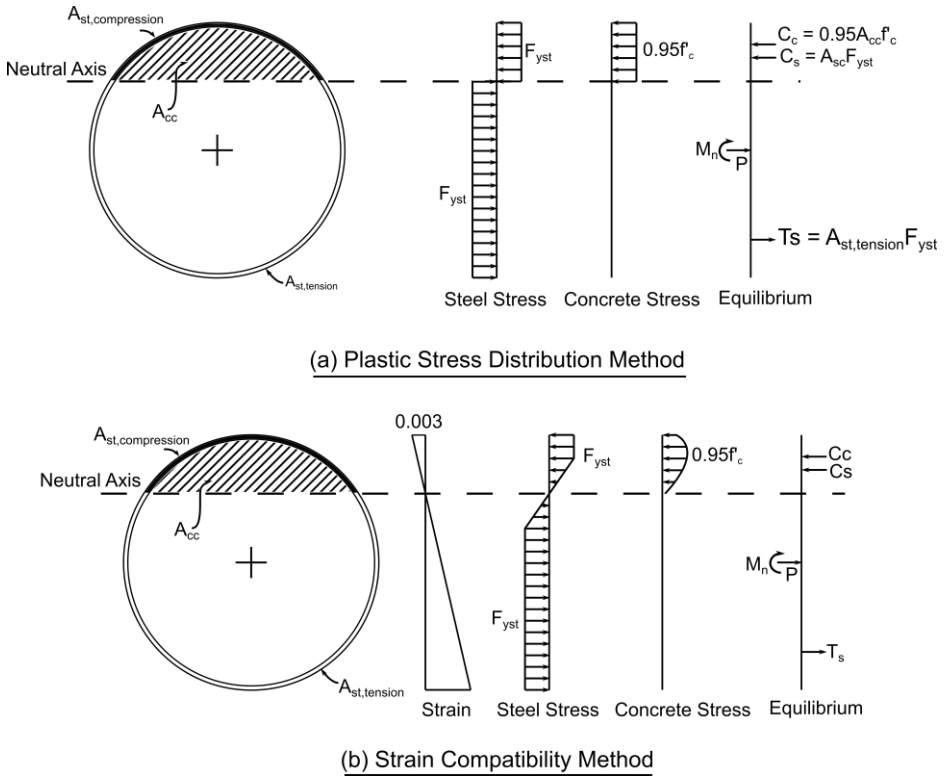

Fig. 2.1. AASHTO Model for Prediction of CFT Resistance Using (a) Plastic Stress Distribution and (b) Strain Compatibility Methods

Strain-compatibility methods are typically used to compute the resistance of reinforced concrete members. For reinforced concrete components, a maximum concrete compressive strain of 0.003 is assumed. To develop the full P-M interaction curve, the strain profile is constructed for each neutral axis depth, and pairs of axial and bending resistances are determined by satisfying equilibrium. A single instance of this is illustrated in Fig. 2.1b.

The stability based P-M interaction curve of CFTs is constructed by joining points A', A'', D, and B as illustrated in Fig. 2.2. This curve accounts for global buckling as a nominal failure mode.

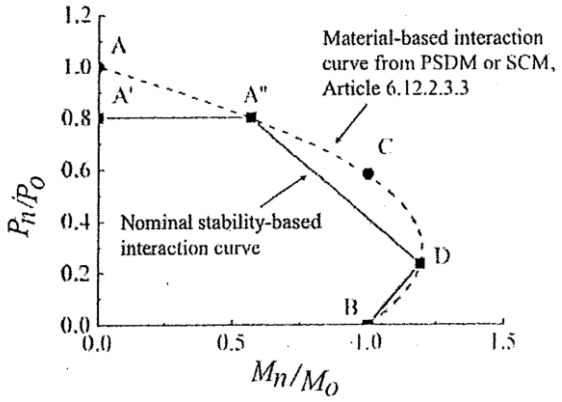

Fig. 2.2. Construction of the Normalized Stability-Based P-M Interaction Curve (AASHTO, 2015)

Point A corresponds to the nominal crushing load of the CFT column as calculated using Equation 2.3, while point A' corresponds to the axial compression resistance with moment as calculated in Equation 2.4. Point A'' is the intersection of the material-based interaction curve as calculated using the PSDM or SCM. Point B corresponds to the composite plastic moment resistance without axial load, and point C corresponds to the axial force on the material based interaction curve as calculated using the PSDM or SCM which corresponds to the composite plastic moment resistance without axial load. Point D is located on the material-based interaction curve as calculated using the PSDM or SCM, and is taken at an axial of load $P_D = 0.5P_c(P_n/P_o)$.

2.1.2 Current AISC Design Provisions

AISC (AISC, 2010) also provides design guidelines of CFT construction in Chapter I of the 2010 steel manual. The local stability of the tube is provided using a D/t ratio limit provided in AISC Table I1.1A. This limit is defined as:

$$\frac{D}{t} \leq 0.15\frac{E}{F_{y,st}} \tag{2.5}$$

The effective flexural stiffness of a CFT member is defined in AISC Eq. I2-I2 as:

$$EI_{eff} = E_s I_{st} + C_3 E_c I_c \tag{2.6a}$$

$$C_3 = \left(\frac{A_{st}}{A_c + A_{st}}\right) \leq 0.9 \tag{2.6b}$$

The compressive capacity of a circular CFT member is defined in AISC Eq. I2-9b as:

$$P_o = 0.95 f'_{cf} A_c + F_{y,st} A_{st} \tag{2.7}$$

where the coefficient 0.95 is taken in recognition of the confinement provided by the steel tube. The member buckling capacity is calculated using the steel buckling equations defined in Eq. 2.4 above. AISC permits the use of the PSDM or SCM to calculate the combined axial-flexure resistance of CFTs.

2.1.3 Current ACI Design Provisions

ACI (ACI, 2010) also provides design guidelines of CFT construction. The local stability of the tube is provided using a D/t ratio limit provided in ACI Article 10.13.6.1. This limit is defined as:

$$\frac{D}{t} \leq 2.8\sqrt{\frac{E_s}{F_{y,st}}} \tag{2.8}$$

ACI requires use of strain compatibility methods to calculate the combined P-M interaction for CFT columns. The ACI strain compatibility procedure is similar to the AISC strain compatibility method in Fig. 2.1a, except that the concrete stress distribution is a

rectangular stress block with a $0.85f'_c$ compressive stress acting over a depth, $\beta_1 d_c$. The variable β_1 depends on the concrete strength and d_c is the maximum depth of the concrete in compression.

2.2 Superstructure Joint Design Provisions for Reinforced Concrete Bridges

In CFT column-to-cap beam connections, the joint region is subjected to large shear and is required to transfer the axial, shear and bending moment demands from the superstructure to the column. As such, this region is critical to the performance of the connection. CFT-to-cap beam connections will need to be reinforced using an adaptation of the current joint design provisions. Therefore, these provisions are the basis for the new connection design and a review of the current provisions is important.

In California, the Caltrans Seismic Design Criteria (SDC) V. 1.7 (Caltrans, 2013) govern the design of bridges. These requirements are intended to capacity protect non-yielding components of the superstructure to ensure that they remain essentially elastic when plastic hinges form in adjacent substructure elements. Within the SDC there are specific detailing requirements for reinforcement in the joint regions of RC bridges. Joint region provisions in the Caltrans SDC V. 1.8 are in Section 7.4. Because this research is primarily concentrated on the behavior of interior joints in non-skewed multi-column bents, only requirements for joints of this type are discussed.

2.2.1 Joint Capacity

Moment resisting connections between the superstructure and column are designed to resist the maximum overstrength moment, M_o^{col}, and corresponding shear generated by the column, V_o^{col}. The quantity M_o^{col} is defined in Eq. 4.4 of the SDC as $1.2M_p^{col}$ where M_p^{col} is the idealized plastic moment strength of the column.

2.2.2 Joint Stresses

Requirements for proportioning superstructure-to-column joints as well as requirements for reinforcing details in the joint region are based on the principal tension, p_t, and compression stresses, p_c, in the joint. The equations for calculating these stresses are defined in Eqns. 7.11 and 7.12 (SDC 2013) as:

$$p_t = \frac{(f_h+f_v)}{2} - \sqrt{\frac{(f_h+f_v)^2}{2} + v_{jv}^2} \tag{2.9a}$$

$$p_c = \frac{(f_h+f_v)}{2} - \sqrt{\frac{(f_h+f_v)^2}{2} + v_{jv}^2} \tag{2.9b}$$

where f_h and f_v are the horizontal and vertical normal stresses at the center of the joint respectively, and v_{jv} is the vertical shear stress. The equations for calculating these stresses are defined in Eqns. 7.13, 7.15, and 7.17 (SDC 2013). The loads which induce these stresses, M, P and V, and the location of the stresses in the joint are shown in Fig. 2.3; the equations have not been included here for brevity.

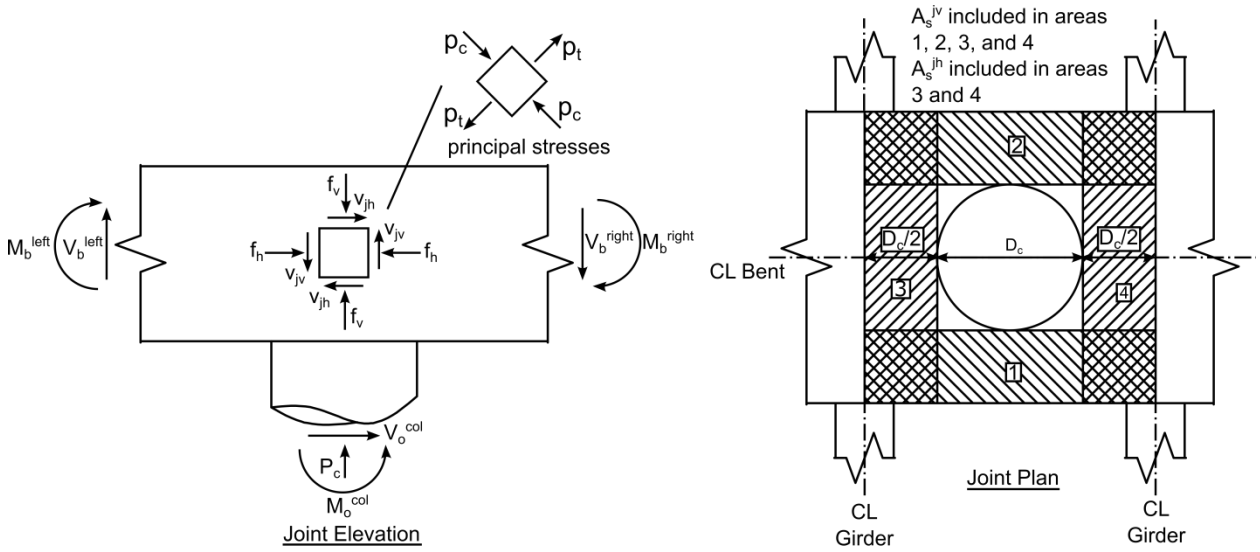

Fig. 2.3. (a) Caltrans SDC Joint Shear Definition and (b) Transverse Reinforcing Requirements (Caltrans, 2013)

2.2.3 Joint Proportioning

The proportions of the superstructure-to-column joints must be selected such that the principal stresses do not exceed $0.25f'_c$ in compression ($p_c \leq 0.25f'_c$ (psi)) and $12\sqrt{f'_c}$ in tension ($p_t \leq 12\sqrt{f'_c}$ (psi)). Larger widths may be required to develop a compression strut outside the joint for larger diameter columns.

2.2.4 Joint Reinforcing

The amount of joint shear reinforcing depends the value of the principal tension stress in the joint, p_t. For $p_t < 3.5\sqrt{f'_c}$ (psi), a minimum joint shear reinforcing ratio of $\rho_{s,min} = 3.5\sqrt{f'_c}/f_{yh}$ is required and may be provided as continuation of the column transverse reinforcement into the cap beam. For $p_t \geq 3.5\sqrt{f'_c}$ (psi), additional joint reinforcing is required in the form of vertical stirrups, horizontal stirrups, and horizontal side reinforcing. The required area of vertical and horizontal stirrups extending a distance of the column diameter, D_c, from either side of the

column centerline are defined in Eqns 7.19 and 7.20 of the Caltrans SDC, which are repeated here:

$$A_s^{jv} = 0.2A_{st,b} \tag{2.10}$$

$$A_s^{jh} = 0.1A_{st,b} \tag{2.11}$$

where A_a^{jv} is the required vertical stirrup area, A_s^{jh} is the horizontal stirrup area, and $A_{st,b}$ is the total area of column steel extending from the column into the bent cap. Note that the variable $A_{st,b}$ is represented as A_{st} in the SDC, but has been changed here as A_{st} represented the cross sectional area of the steel tube in a CFT in AASHTO (2015). The horizontal stirrups are required to be placed around the vertical stirrups in two or more layers spaced vertically at a maximum distance of 18-in. Areas 1-4 are the locations where transverse vertical and horizontal reinforcing are required for multi-column interior t-type joints, as shown in Fig. 2.3. Steel located in overlapping areas is counted towards meeting the requirements for both areas (SDC, 2013). The area of longitudinal side reinforcing is specified in Equation 7.21 of the SDC as:

$$A_s^{sf} \geq \begin{cases} 0.1A_{cap}^{top} \\ 0.1A_{cap}^{bot} \end{cases} \tag{2.12}$$

where A_s^{sf} is the required area of side reinforcing, and A_{cap}^{top} and A_{cap}^{bot} are the areas of the primary top and bottom flexural steel in the bent cap respectively.

Chapter 3

LITERATURE REVIEW

This chapter reviews research that was conducted and provided the basis of the connection studied here. First, CFT to RC component connections are studied; CFT to precast components were not found in the literature search. Second, because some of the connections will emulate standard connection details for all precast components, this type of connections that were specifically developed for ABC are reviewed. As such, this chapter reviews previous work in two primary categories: (1) CFT connections and (2) connection details for precast components.

3.1 CFT Connections

Research that has been conducted on CFT connections demonstrates that they exhibit large strength and ductility. These connections generally fall under two categories: (1) fully restrained connection intended to transfer the full moment strength of the CFT, and (2) partial strength connections in which the strength emulates RC construction and is less than that of the CFT component. This chapter evaluates experimental and numerical research conducted on both connection types.

3.1.1 Partial Strength Connections

The following section provides a summary of relevant research programs that studied partial strength connections with a focus on connections utilizing reinforced concrete in the transition region. Studies using either circular or rectangular CFTs were included because the research is so limited.

Kawaguchi and Morino (2006) developed a CFT-to-foundation connection consisting of an exposed base plate with multiple anchor bolts as well as internal reinforcing bars as shown in Fig. 3.1. The central reinforcing bars are included to increase the stiffness and strength of the exposed base plate, as this connection type has been shown to provide limited rotational stiffness. These bars are cast into the foundation prior to placement of the CFT, and extend through holes in the base plate into the CFT column.

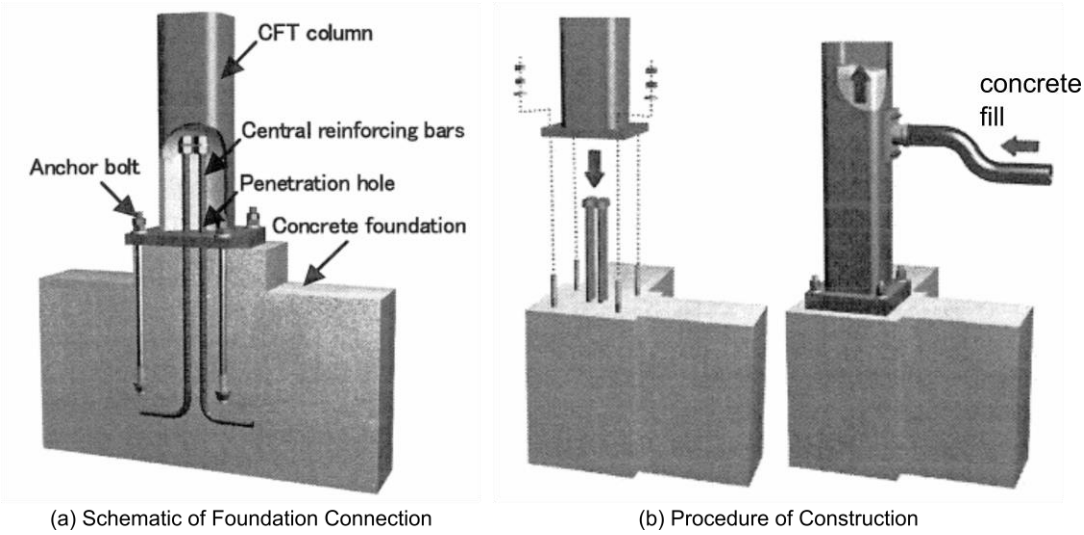

Fig. 3.1. CFT-to-Foundation Connection Developed by Kawaguchi and Morino (2006)

Ten specimens were constructed to evaluate the performance of the connection. The specimen geometry consisted of a 62-in. high column anchored into 40x27.5-in. foundation with an 82-in. length. Two different types of tubes were evaluated: (1) 12x12-in. square steel tubes with 0.75-in. wall thickness and (2) 16-in. diameter circular tubes with 0.5-in. wall thickness. The shape and size of the base plate and the size and number of anchor bolts were identical for all specimens. The primary parameters were: (1) axial force: zero, constant tension, constant

compression, and reversed cyclic (2) type of connection; base plate or internally reinforced CFT, and (3) strength of the CFT column.

Results from the experiments showed that the internally reinforced CFT connection exhibited larger stiffness and strength compared to base plate connections. Specifically, the connections with internal bars showed increases in stiffness and yield strengths of 1.2 and 1.8 respectively compared to the traditionally detailed connections.

Montejo et al. (2009, 2013) evaluated the behavior of a jacketed reinforced concrete column which utilized a traditional reinforced concrete column-to-foundation connection. Jacketed reinforced concrete columns utilize a conventional steel cage placed within the steel tube as is illustrated in Fig. 3.2. This reinforcing steel is also used to transfer the moment, shear and axial forces to the adjacent RC component and vise versa. To ensure the tube does not contribute to the strength or in the transfer mechanism, a gap is left between the tube and adjacent members. As such, this member and connection does not respond as a CFT but instead responds as a jacketed RC component and connection.

In the study by Montejo et al. (2009,2013), a total of six connections were tested experimentally; two flexure dominated RC columns with an 18-in. diameter and 65-in. height and four flexure dominated jacketed RC columns with an 18-in. diameter tube that had a 1/4-in. wall thickness (D/t=72), and 65-in. height. The primary parameters were: (1) axial load ratio (ranging from 3.3% - 6.4%), (2) longitudinal reinforcing ratio (ranging from 2.1% to 3.1%), and (3) ambient temperature (ranging from -33˚F - 72˚F). An overview of the specimen geometry and test setup is shown in Fig. 3.2.

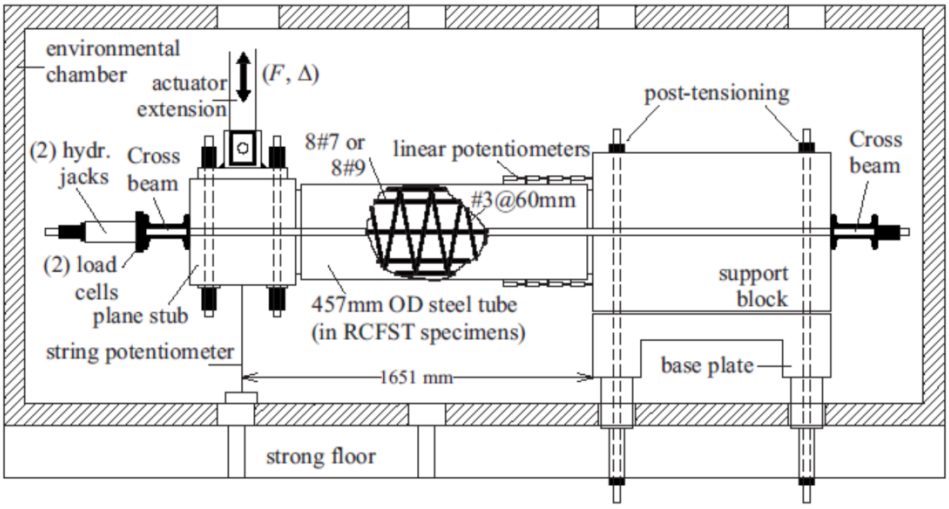

Fig. 3.2. Schematic of Test Setup and Specimen Tested by Montejo et al. (2009, 2013)

Results from the experiments showed that the jacked RC column connection performed largely similar to the RC connection. Differences were, however, noted in the length of the damaged region of the two different components. The RCFT components exhibited a significant reduction in the damage length.

3.1.2 Full Strength Connections

A full strength structural steel connection was developed by Marson and Bruneau (2004). The connection was constructed by welding the steel tube to structural steel members and encasing the built-up base into a concrete foundation, as shown in Fig. 3.3. The steel members act both to fully develop the moment capacity of the CFT, and as flexure reinforcement in the foundation. Four specimens were constructed with D/t ratios of 34, 51, 42, and 64 and diameters of 12.75-in. 12.75-in., 16.16-in., and 16.16-in. respectively to experimentally evaluate the performance of the structural steel connection, and axial load ratio was the primary parameter.

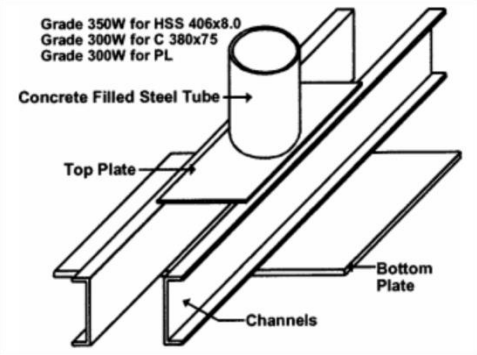

Fig. 3.3. Schematic of Connection Tested by Marson and Bruneau (2004)

The embedded structural steel connection was able to develop the full plastic moment capacity of the CFT with failure modes characterized by local buckling of the steel tube. All columns exhibited large energy dissipation, and exceeded 7% drift without significant strength loss or foundation damage. Strain gage data from the embedded structural steel suggested that the CFT was primarily anchored by the foundation concrete as opposed to the built up base.

The strength of an embedded CFT column-to-pier cap connection (shown in Fig. 3.4) was evaluated by Kappes et al. (2012). To simplify construction and transfer the moment at the pier cap connection, the tube was extended into the pier cap. Mechanical anchors were not included in the connection, thus there was only chemical bond between the tube and the concrete. This represented standard construction practice for CFT bridge bent connections in the state of Montana.

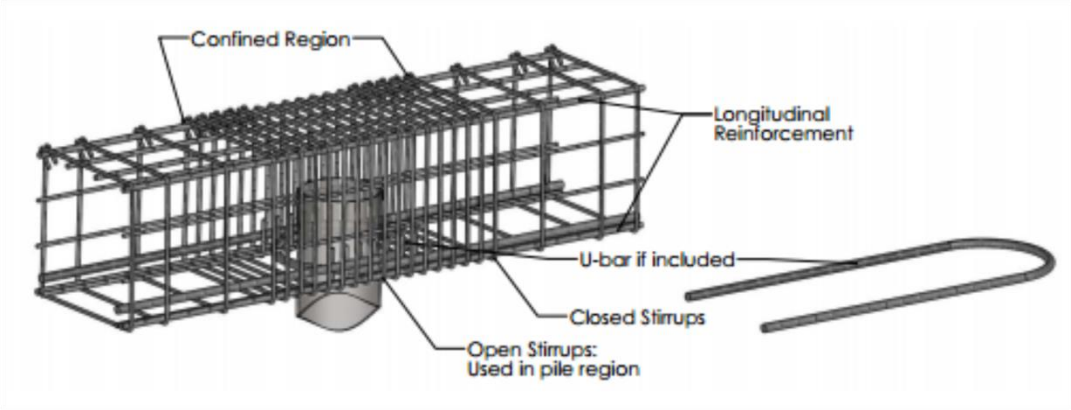

Fig. 3.4. Overview of Connection Evaluated by Kappes et al. (2012)

Nine 50% scale specimens with D/t ratios varying from 18-28 were constructed to evaluate the strength of the connection. The primary parameter evaluated in the experiment was the reinforcing details in the pier cap; several specimens were constructed with standard practice detailing, and several were constructed using detailing intended to increase the strength of the connection. Results from the experiments showed that the pier cap could be detailed to achieve the plastic moment capacity of the CFT with limited damage to the pier for D/t ratios of 28. In this case, the failure of the connection was characterized by yielding of the CFT column as a plastic hinge developed in the column adjacent to the pier cap. Significant cap beam reinforcing beyond standard practice was included to achieve this failure mode. As it was the intent of the experiment to evaluate the capacity of the connection, larger steel tubes with a D/t ratio of 18 were introduced which resulted in the failure of the pier cap from prying effects.

3.1.3 Embedded CFT Column to Footing tests at University of Washington

Several research program undertaken at the University of Washington studied a CFT foundation connection capable of developing the full plastic moment capacity of a CFT component

(Kingsley, 2005; Williams, 2006; Lee, 2011; Lehman and Roeder, 2012). The latter research program was the prior phase to the program discussed in this report.

The embedded CFT connection studied was a fully restrained moment connection that employs a flanged annular ring that was welded to the base of the steel tube. This flange provides anchorage and efficient shear and moment transfer to the surrounding concrete and reinforcement, as illustrated by the compression struts in Fig. 3.5a. There are no reinforcing bars in the tube or dowels penetrating from the tube into the foundation; the force transfer is solely accomplished by the anchored portion of the tube and the flange. The foundation or pile cap is designed to normal geometric limits, design loads, and shear and flexural reinforcement.

Two variations of the embedded foundation connection have been developed, as shown in Fig. 3.5b and Fig. 3.5c, a monolithic option and a grouted option. For the monolithic option, the steel tube and annular ring are temporarily anchored within the foundation reinforcing, and the foundation and CFT-column are cast simultaneously, as shown in Fig. 3.5b. For the grouted variation, the footing is cast with a recess formed by a lightweight corrugated steel tube with an inner diameter slightly larger than the outside diameter of the annular ring, as shown in Fig. 3.5c. The tube and ring are placed into the void after the foundation is cast, and the recess between the tube and corrugated pipe is filled with high-strength, fiber-reinforced grout to anchor the column into the foundation. For both options, the steel tube is filled with low-shrinkage self-consolidating concrete to complete the CFT member, and no vibration is required (Lehman and Roeder, 2012).

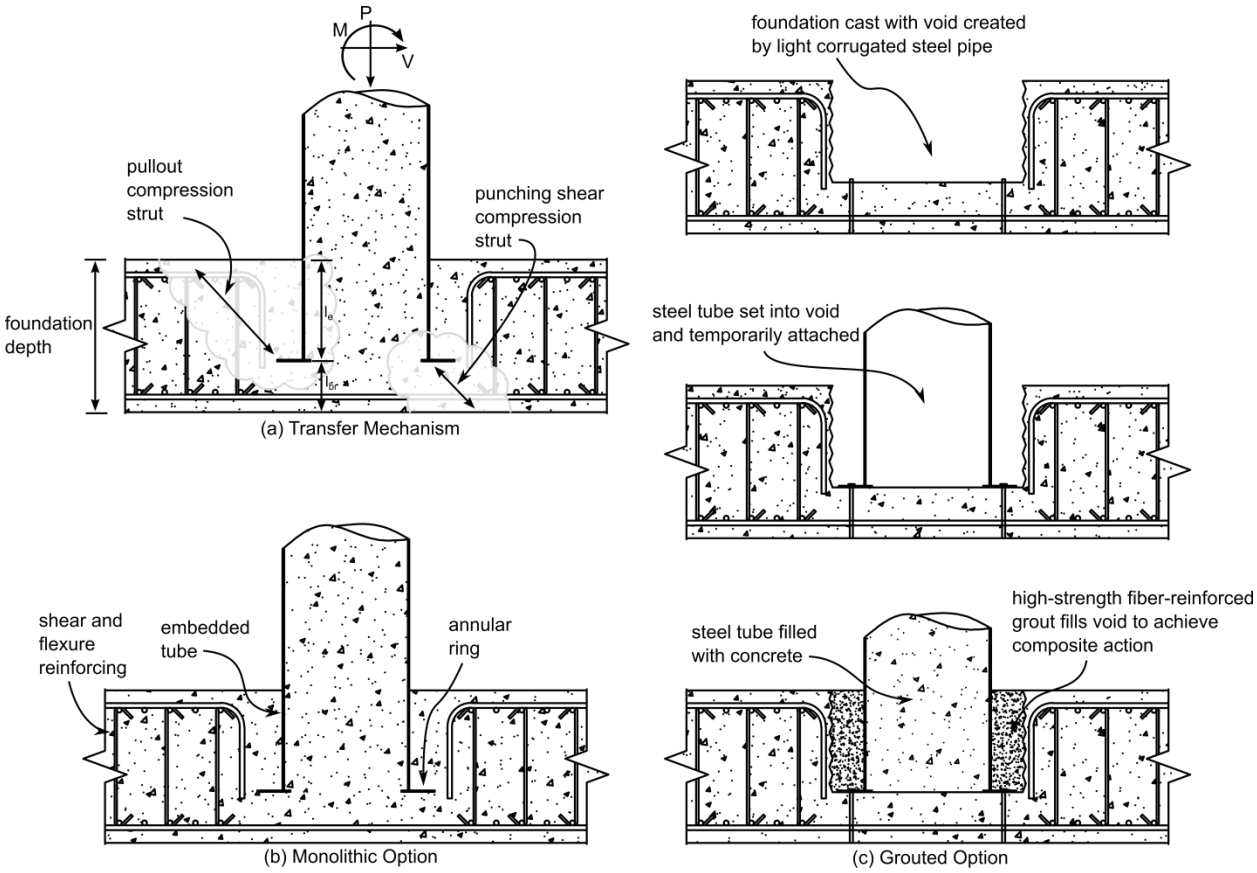

Fig. 3.5. Foundation Connection Proposed at the University of Washington

The compilation of the experimental programs to evaluate the CFT column-to-foundation connections consisted of a series of 19 large-scale specimens, which simulated approximately a half-scale bridge column (Kingsly, 2005; Williams, 2006; Lee, 2011; Lehman and Roeder, 2012). The details and geometry of a typical specimen are shown in Fig. 3.6, while specimen descriptions and nominal material strengths are summarized in Table 3.1.

The diameter and thickness of the steel tube in a majority of the specimens were 20-in. and 0.25-in. respectively, resulting in a diameter-to-thickness ratio D/t of 80. This exceeds the limiting D/t ratio specified in ACI (2010) , but meets the slenderness requirements in AISC

(2010) and AASHTO (2012). The annular ring in all specimens extended 16t (4-in.) out from and 8t (2-in.) in to the steel tube respectively.

Table 3.1. Experimental Parameters and Material Properties from Prior Research

Spec.	l_e/D	Connection Type Study Parameter	F_y, ksi (MPa)	F_u, ksi (MPa)	f'c, ksi (MPa)	Tearing Drift	$M_{max}/M_{P,PSDM}$	Failure Mode
1	0.6	Monolithic connection No vertical reinforcing	75 (520)	88 (605)	11 (76)	3.5%	0.88	Cone pullout
2	0.6	Monolithic connection Vertical Reinforcing	75 (520)	88 (605)	11 (76)	4.2%	0.92	Cone pullout
3	0.9	Monolithic connection Embedment depth	75 (520)	88 (605)	10 (69)	8.0%	1.13	Ductile tearing
4	0.6	Recessed connection Embedment depth	75 (520)	88 (605)	10 (69)	6.5%	0.98	Partial pullout
5	0.9	Recessed connection Flexible underlay	75 (520)	88 (605)	11.3 (78)	6.0%	1.15	Ductile tearing
6	0.75	Recessed connection Flexible underlay	75 (520)	88 (605)	11.9 (82)	6.0%	1.22	Ductile tearing
7	0.75	Monotonic axial load only Punching with 9-in (225-mm) depth	75 (520)	88 (605)	9.3 (64)	NA	NA	Monotonic punching
8	0.75	Cyclic axial load only Punching with 9-in (225-mm) depth	75 (520)	88 (605)	9.4 (65)	NA	NA	Cyclic punching
9	0.9	Recessed connection Galvanized tube	75 (520)	88 (605)	10 (69)	7.8%	1.27	Ductile tearing
10	0.9	Recessed connection – galvanized Near-fault load history	75 (520)	88 (605)	9.7 (67)	9.5%	1.30	Ductile tearing
11	0.9	Recessed connection $0.15P_o$ axial load	75 (520)	88 (605)	9.3 (64)	9.2%	1.14	Ductile tearing
12	0.9	Recessed connection $0.2P_o$ axial load	75 (520)	88 (605)	69 (10)	9.0%	1.23	Ductile tearing
13	0.8	Monolithic connection Straight seam tube	49 (340)	60 (417)	8.7 (60)	11.6%	1.17	Ductile tearing
14	0.775	Recessed connection Straight seam tube	49 (340)	60 (417)	9.4 (65)	10.4%	1.17	Ductile tearing
15	0.775	Recessed connection Spiral weld tube/evaluate l_e	51 (355)	78 (540)	7.8 (54)	10.2%	1.14	Ductile tearing
16	0.8	Monolithic connection Spiral weld tube/evaluate l_e	51 (355)	78 (540)	8.7 (60)	7.3%	1.07	Ductile tearing
17	0.7	Recessed connection Spiral weld tube/evaluate l_e	51 (355)	78 (540)	9.9 (68)	7.4%	1.31	Ductile tearing w/ cracking
18	0.6	Recessed connection Spiral weld tube/evaluate l_e	51 (355)	78 (540)	10.2 (70)	7.4%	1.22	Ductile tearing w/ cracking
19	0.62	Recessed connection Larger, 762-mm tube $0.05P_o$ axial load	50 (355)	78 (540)	11.2 (77)	7.0%	1.30	Ductile tearing w/ cracking

The dimensions of the footing as well as the primary flexure reinforcing were selected to provide adequate strength for the foundation to minimize the influence of footing size on the failure mode, resist M_p of the CFT without yielding, and to represent a scale model of a typical bridge footing. The imposed displacement history for a majority of the specimens was based on

the ATC-24 protocol (ATC-24, 1992). The majority of the specimens were subjected to approximately 10% of the gross compressive load capacity of the CFT column; however several additional axial load ratios were evaluated. A summary of the experimental results is included in Table 3.1, the moment-drift behaviors of several specimens are plotted in Fig. 3.8, and typical failure modes are shown in Fig. 3.9. The moment-drift response curves were normalized to the theoretical capacity calculated using the PSDM.

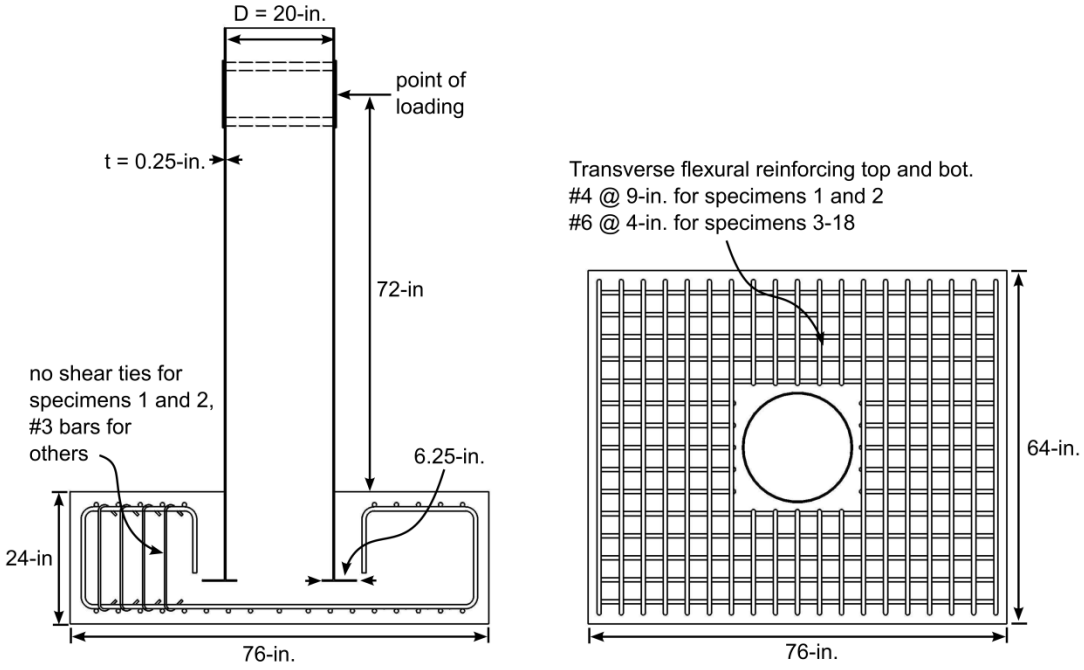

Fig. 3.6. Typical Specimen Geometry and Reinforcing

As the testing program was so large, only the hysteretic performances of selected specimens are discussed here to highlight the influence of several different parameters on performance of the connection. These parameters include connection type, tube embedment depth, axial load ratio, and column diameter.

Specimens 13 and 14 (as summarized in Table 3.1) demonstrate the strength and ductility of the monolithic and grouted connection types respectively. As is illustrated by the hysteretic curves in Fig. 3.7, using a grouted connection type did not influence the performance of the embedded connection.

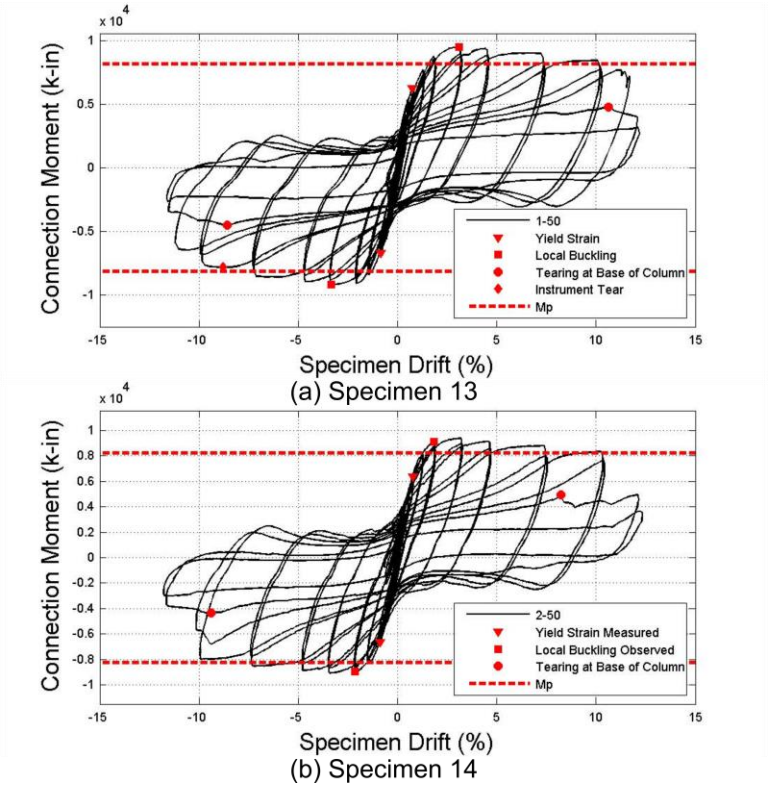

Fig. 3.7. Typical Moment-Drift Response From Monolithic and Grouted Connection Types (Lee, 2011)

Specimens 1 and 3 demonstrate the strength and ductility as well as typical failure modes of adequately and inadequately embedded specimens. In summary, ductility of the inadequately embedded connections (Specimen 1) was ultimately limited by foundation damage as illustrated in Fig. 3.9a, while the failure mode of the adequately embedded connections (Specimen 3) was

characterized by ductile tearing of the steel tube as shown in Fig. 3.9c, which occurred at the location of local buckling (see Fig. 3.9b).

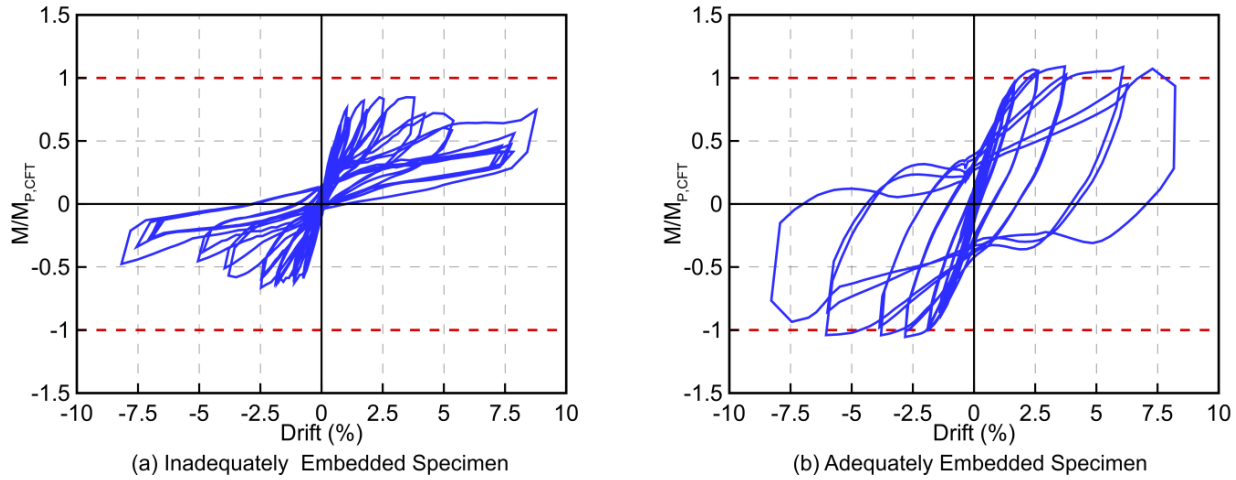

Fig. 3.8. Typical Moment-Drift Response from Adequately and Inadequately Embedded Specimens (Kingsly, 2005)

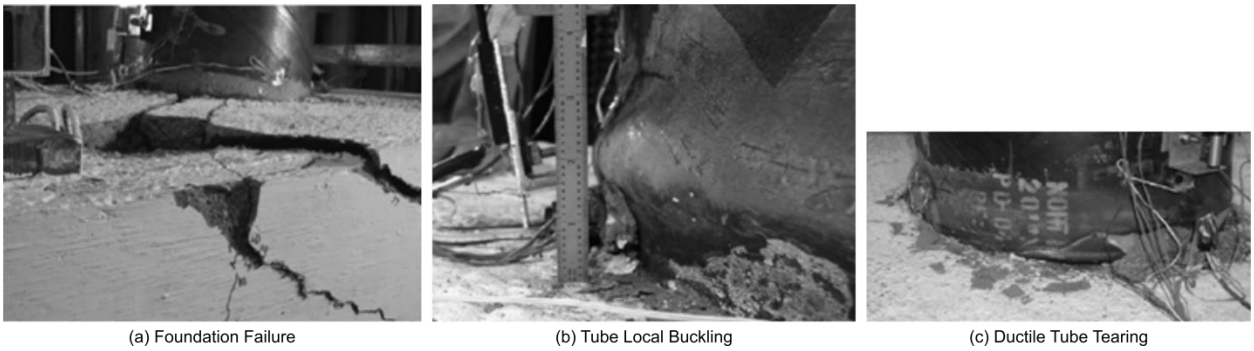

Fig. 3.9. Photos of connection behavior (Kingsley, 2005)

Specimens 11, 12, and 19 evaluated the influence of the axial load ratio on the behavior of the embedded connections. These specimens were subjected to constant axial load ratios of 15%, 20%, and 5% respectively, and were subjected to an increased cyclic lateral loading. Specimen 19 was tested as part of the prior phase of the research discussed in this report. The

axial load ratio did not greatly influence the behavior of the embedded connection as is illustrated by the hysteretic curves shown in Fig. 3.10.

In addition to evaluating the influence of varying axial load ratio on the embedded connection, the hysteretic curves shown in Fig. 3.10 illustrate that the embedded connection can develop the full plastic capacity of the CFT for fairly large connection diameters. Specimen 19 is the largest CFT ever tested, with a diameter of 30-in.

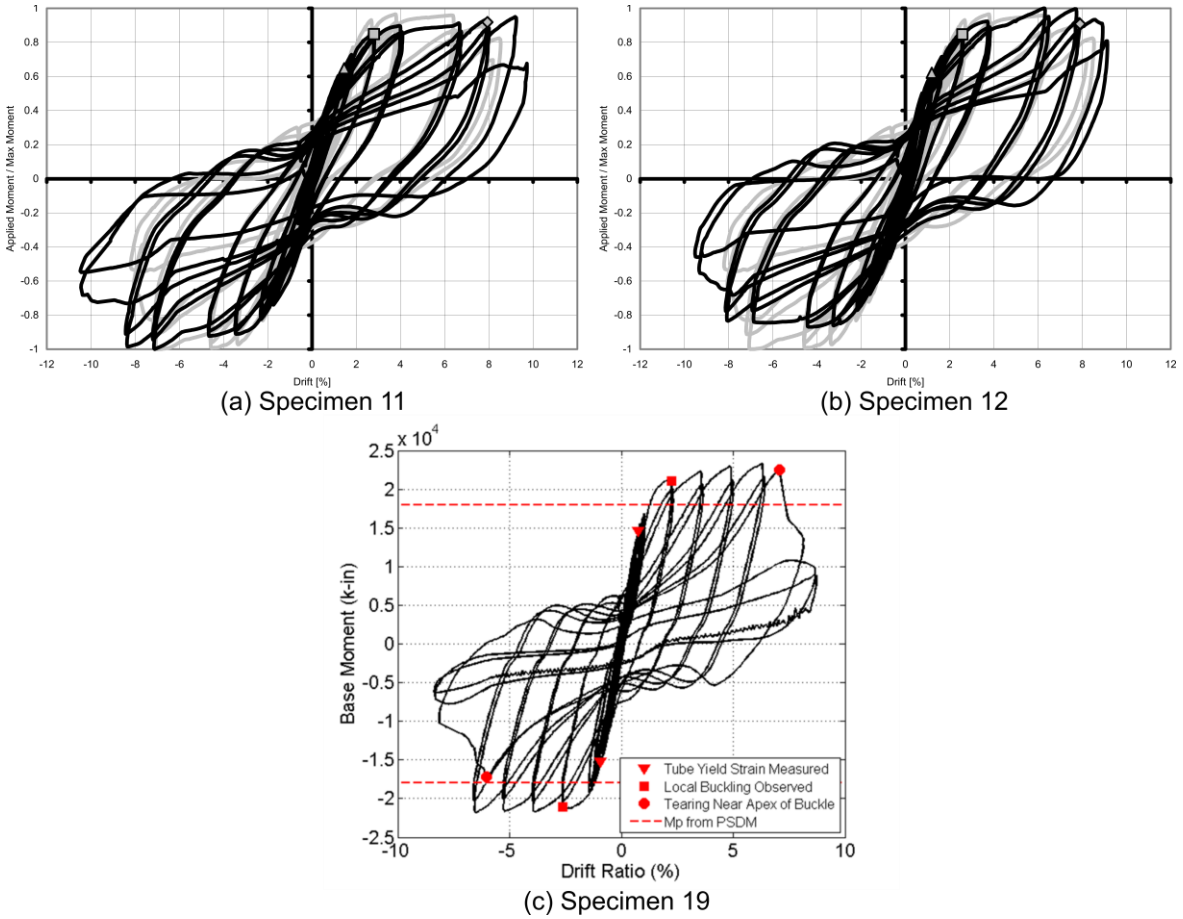

Fig. 3.10. Typical Moment-Drift Response for Embedded Connection Specimens Subjected to Axial Load Ratios of (a) 15%, (b) 20%, and (c) 5%

3.1.4 Design Expressions from the University of Washington Tests

Results from the experimental investigation were used to develop design expressions for a CFT column-to-foundation equation capable of transferring the plastic moment capacity of the CFT. The proposed design expressions are introduced briefly here with detailed explanations available in reference material (Lehman and Roeder 2012).

Annular Ring

The annular ring is welded to tube using complete joint penetration welds or fillet welds on both the inside and outside of the column designed to transfer the full strength of the tube to provide anchorage and stress transfer. The ring is made of steel of the same thickness and similar yield stress as the steel tube. The ring extends into and out from the tube 8 times the tube thickness to provide adequate anchorage. This dimensioning is different than the dimensioning used in the foundation connection experiments, and is a result of experimental testing conducted on the cap beam connection discussed below.

Embedment Depth

The required embedment depth, l_e, of the CFT was determined using a conical pullout model discussed in detail in reference material (1). The required embedment depth to eliminate the potential for foundation failure is given in Equation 1 as:

$$L_e = \sqrt{\frac{D_o^2}{4} + \frac{DtF_{u,st}}{6\sqrt{f'_{c,foot}}}} - \frac{D_o}{2} \ (psi) \qquad [1]$$

where D_o is the outside diameter of the annular ring and corrugated pipe for the monolithic and grouted connections respectfully, D, t, and $F_{u,st}$ are the diameter, thickness, and ultimate stress of

the steel tube, and $f'_{c,foot}$ is the compressive strength of the foundation concrete in psi.

Punching Shear

Adequate concrete depth must be provided below the tube to eliminate the potential for punching shear failure in the foundation. The ACI 318 (7) provisions for footings in single shear were used as a basis to develop an expression for the minimum foundation depth, d_f, to avoid this failure mode. This expression is given in Equation 2 as:

$$d_f \geq \sqrt{\frac{D^2}{4} + \frac{C_c + C_s}{4\sqrt{f'_{cfoot}}}} - \frac{D}{2} \ (psi) \qquad [2]$$

where C_c and C_s are the compressive forces in the concrete and steel due to the combined axial load and bending moment as computed using the PSDM.

3.1.5 Numerical Analysis on the Embedded Ring Foundation Connection

A comprehensive series of nonlinear analyses were performed using the commercially available finite analysis software ABAQUS to extend the experimental results to a wider range of the experimentally studied parameters and include unstudied parameters (Moon et al., 2012). An overview of the numerical model is shown in Fig. 3.11. Model geometry included the embedded CFT column-to-foundation connection, the CFT column, and the reinforced concrete foundation. A half model was developed taking advantage of symmetry in the plane parallel to the direction of loading and the center of the specimen; this increased computational efficiency. The nodes at the base of the footing were fully restrained, and lateral loading was applied by assigning displacements Δ_y along the y-axis to the top nodes of the concrete fill and steel tube. A distributed axial load was applied to the top of the concrete and steel tube using the pressure load

option in ABAQUS. A constant axial load of $0.1P_o$ was applied in for most models unless the axial load ratio was being evaluated.

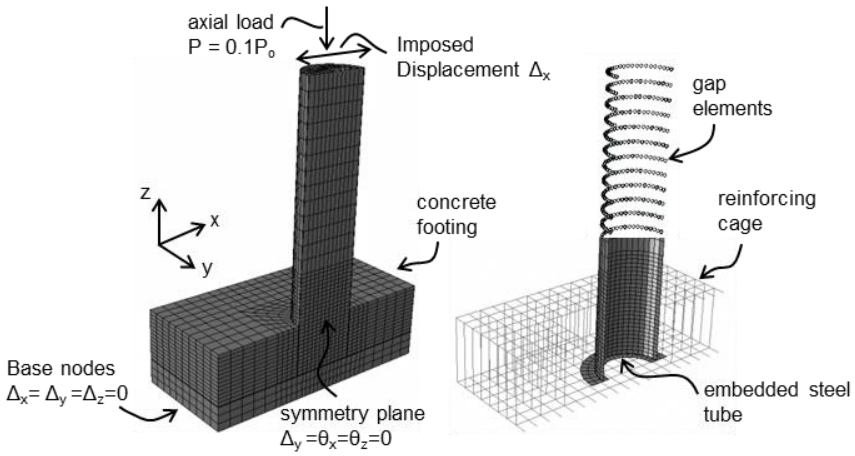

Fig. 3.11. Overview of Finite Element Model of CFT Column-to-Foundation Connection

The 4-node shell element with reduced integration (S4R), 2-node truss element (T3D2), and 8-node solid element with reduced integration (C3D8R) were used to model steel tube, reinforcing steel, and concrete elements, respectively. Gap elements were used at every nodal point that was geometrically common to the steel tube and concrete fill elements to simulate bond stress between the concrete by combining the confining contact stress with a coefficient of friction to develop shear stresses at the interface; penetration of the concrete element by the steel element was prevented. The reinforcing steel and concrete components in the footing were spatially assembled, and interactive constraint relationships were defined using the ABAQUS Embedded constraint to perfectly embed the reinforcing bar in the concrete. This constraint does not allow for relative slip between the reinforcing bar and concrete components.

Material nonlinearity was incorporated using the concrete damaged plasticity model for concrete and a trilinear stress strain relationship with isotropic hardening for steel. The numerical

values to define the properties in these constitutive models were calibrated to numerical properties of past CFT column-to-foundation connection experiments. Mesh refinement in the CFT column-to-foundation model was primarily concentrated in the plastic hinge and embedded regions of the steel tube due to the load and deformation demands in these regions. Global mesh convergence of the concrete components in the foundation and the steel and concrete components in the CFT was conducted by analyzing the maximum numerical moment capacity of each specimen.

The experimental and numerical base moment-drift relationships from Specimens 1 and 3 (as defined in Table 3.1) are shown in Fig. 3.12. From this figure, it can be seen that the numerical results accurately predict the stiffness, strength, and post-peak behavior of the CFT and CFT column-to-foundation connection for adequate and inadequate embedment depths. Furthermore, the experimental failure modes characterized by extensive cracking in the footing or local buckling in the tube for inadequate and adequate embedment depths respectively were accurately captured in the numerical results.

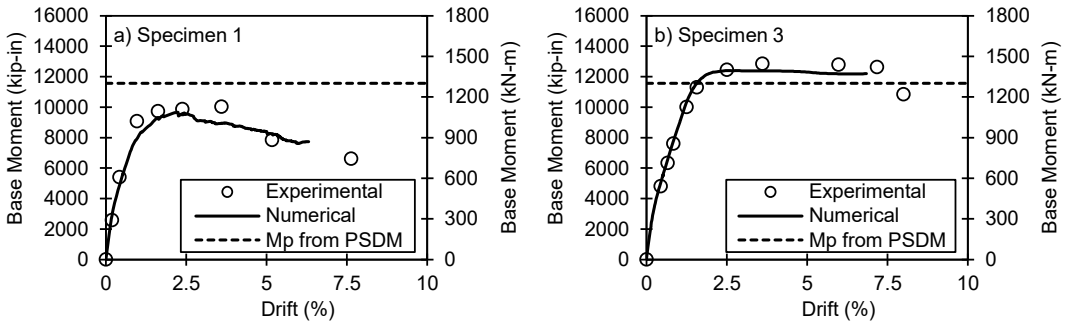

Fig. 3.12. Comparison of Predicted and Measured Base Moment vs. Drift for (a) Specimen 1 and (b) Specimen 3

As described above, Specimen 1 failed due to extensive footing damage. The numerical and experimental crack formation results for this specimen are compared in Fig. 3.13. In both

cases, cracks radiating diagonally from the column are observed. Note that cracking in the numerical results was predicted using the maximum principal plastic strain output variable. The direction of the vector normal to the crack plane is assumed to be parallel to the direction of the line of action of the maximum principal plastic strain tensor (Simulia, 2013). Specimen 3 developed the full flexural capacity of the CFT and sustained large load and deformation demands. The failure mode of this specimen was characterized by local buckling and ductile tearing of the steel tube near the footing interface. The local buckling behavior was captured in the numerical results as is shown in Fig. 3.13.

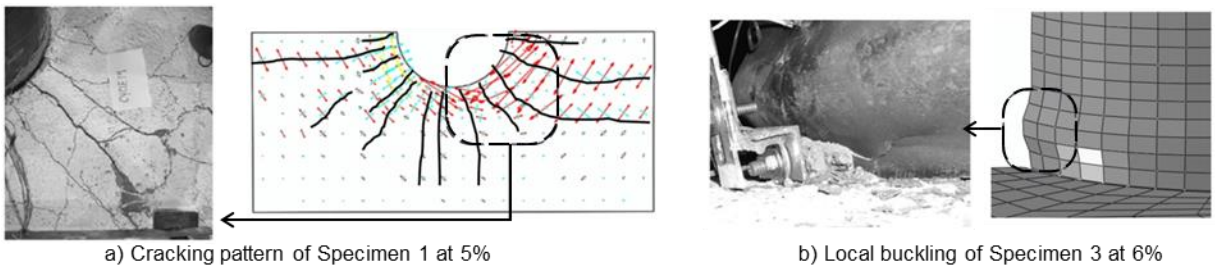

Fig. 3.13. Simulated and Observed Damage Patterns for (a) Specimen 1 and (b) Specimen 3

3.2 Dowel Connections for Precast Concrete Components

Using precast concrete elements in highway bridge construction is a method to achieve ABC. These elements are fabricated in a controlled environment off site which improves material quality and product durability. Once on site, they can be rapidly assembled without the construction of temporary shoring or flexible reinforcing cages which decreases construction time and cost and minimizes traffic impacts.

A significant amount of research has been conducted to develop construction details for precast elements, and they have successfully been implemented around the United States (NCHRP, 2011). However, the use of precast elements in regions of high seismicity is still

limited due to uncertainty about performance; especially regarding the strength and ductility of the connections. Of particular concern are the column connections to the bent cap, because these connections are needed for force transfer and therefore connection damage can lead to system failure. As connections between precast substructure elements typically occur in these critical regions, a large amount of research has been conducted to develop precast connections which exhibit adequate performance during lateral loading events. Since this research is focused on using precast components with dowel-type connections to the cap beam, a review of these connections offers options for CFT to precast cap beam connections.

A research program was undertaken at the University of Washington to evaluate the feasibility of using large bars grouted into individual ducts (Raynore et al. 2002), and to develop and evaluate column-to-cap beam connections for ABC (Stueck et al., 2007, 2009; Pang et al. 2008, 2010).

Raynor et al. (2002) and Stueck et al. (2007, 2009) conducted full-scale pullout tests on No. 8, No. 10, and No. 18 bars grouted into ducts. An overview of the test setup is shown in Fig. 3.14 The experiments showed that yielding of the bars could be achieved in lengths as low as $6d_b$, while the ultimate strength could be achieved in $14d_b$. These tests demonstrated that grouted large bar connections could practically be used within the depth of common precast bent cap sections.

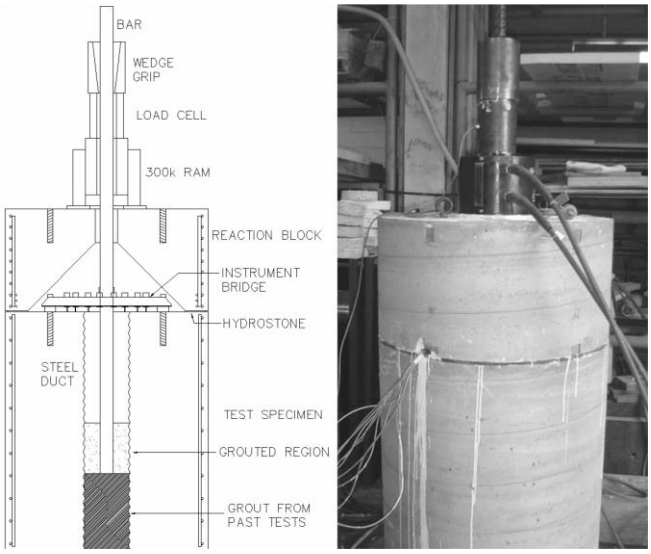

Fig. 3.14. Grouted Large Bar Pullout Test Apparatus

A survey of column-to-cap beam connections was completed by Pang et al. (2008) and Stueck et al. (2007) which evaluated fabrication and construction difficulties as well as the structural behavior of several reinforcing concrete connection types. Based on the results of the survey, a large bar connection type was selected for experimental investigation. The concept of this connection is the improvement of construction tolerances through use of a reduced number of large longitudinal column bars in the place of a large number of smaller longitudinal bars. Transitioning to larger bars, however, is challenging because of the increased development lengths.

Pang et al. (2008, 2010) and Stueck et al. (2007, 2009) conducted tests on four 42% scale columns to evaluate the performance of the large bar connection. One of the columns served as a base-line specimen with 16 No. 5 longitudinal bars constructed using typical CIP methods. The other three columns used 6 No. 8 bars with differing de-bonded lengths. The purpose of the de-bonding was to distribute plastic strain across a longer effective length to decrease stress

concentrations at the column-to-cap interface. An overview of the large bar connection specimen is shown in Fig 3.15.

The columns were subjected to a constant axial load and cyclic lateral loading protocol. Results from the experiments showed that the large bar connections perform similarly to comparative CIP connections. Furthermore, de-bonding the bars had a limited influence on the performance, as the fully bonded specimens naturally de-bonded during testing.

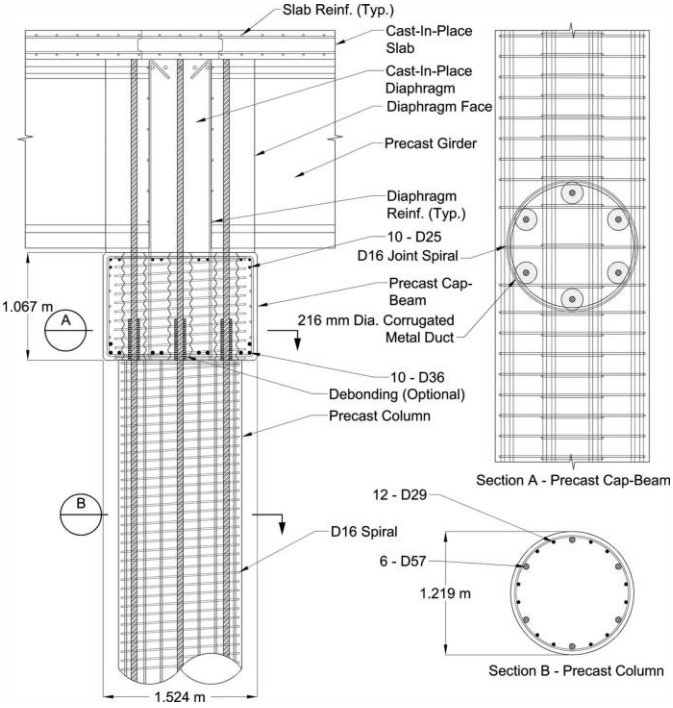

Fig. 3.15. Typical Large Bar Connection Specimen (Stueck et al., 2009; Pang et al. 2008)

The National Cooperative Highway Research Program Project 12-74 was conducted by Restrepo et al. (2011) with the objective of developing and validating design methodologies, specifications, design examples, and example connections details for precast bent systems for use in seismic areas in the United States. This project conducted a survey of existing practice precast

bent cap systems, developed a series of connection details for experimental analysis, and ultimately provides recommendations to facilitate the implementation of precast bent cap systems. The types of connections evaluated in this report ranged from emulative (designed to emulate the behavior of typical CIP RC connections) to hybrid details which include self-centering post-tensioned concrete and concrete filled tube columns. The 12-74 document provides valuable information regarding state-of-practice and innovative connections for precast components.

As part of the NCHRP 12-74, tests were conducted tests on four 42% scale column to cap beam connections. The specimen geometry consisted of a 35-in high, 20-in. diameter column connected to a 12-ft long cap beam with a height and width of 25-in. The four connection types consisted of a typical CIP connection, a grouted bar connection similar to the large bar connections evaluated by Pang et al. (2008, 2010) (shown in Fig. 3.16a), and two pocket connections in which a void was created in the cap beam using a corrugated pipe as illustrated in Fig. 3.16b. Typical specimen geometry is illustrated in Fig. 3.17.

(a) Duct Connection

(b) Pocket Connection

Fig. 3.16. Grouted duct and pocket cap beam connection evaluated by Matsumoto (2009).

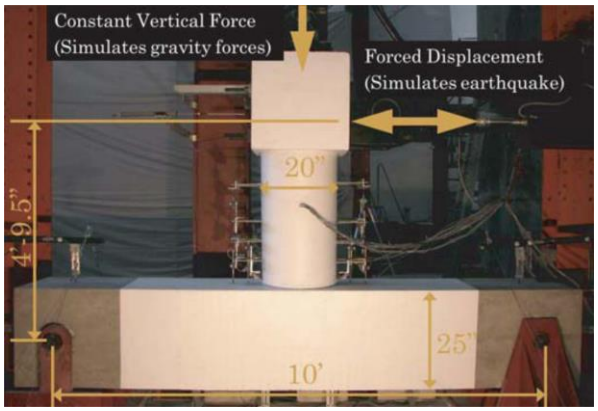

Fig. 3.17. Typical Specimen Geometry from Matsumoto (2009)

The columns were subjected to constant axial load and a cyclic lateral loading protocol. Results from the experiments showed that the emulative precast connection types performed as well as the CIP connection detail.

A research program was undertaken at the University of Washington to develop damage-resistant wharf pile connections (Jellin, 2007; Stringer, 2010). These connections utilized bearing pads between the wharf-pile and pile-cap to reduce spalling, and de-bonded longitudinal reinforcing to increase the inelastic deformation capacity of the dowel bar steel. Four large scale damage-resistant wharf pile connections were tested by Stringer (2010). The specimens consisted of a 24-in. diameter prestressed concrete pile embedded 3-in. into a CIP deck segment. The connections consisted of eight No. 10 T-headed dowel bars, which were grouted into the pile for a length of $16d_b$. An overview of specimen geometry is shown in Fig. 3.18. The primary parameter of interest in these experiments was the inclusion of a bearing pad between the precast wharf-pile and CIP pile cap to limit damage at the interface. These research has been included here as the proposed WD connection utilized both headed dowels and de-bonding along the length of the dowels at the interface.

The specimens were subjected to a constant axial load ranging from 10% to 20% of the theoretical crushing load of the wharf pile, and an reversed cyclic lateral load was applied according to the ATC-24 protocol. In general, all of the connections exhibited largely stable hysteretic behaviors. Furthermore, all of the connections appeared to displace in near rigid body rotation. The inclusion of the bearing pad between the wharf pile and pile cap delayed the onset of pile cover spalling by up to 3.5% drift.

Fig. 3.18. Specimen Geometry from Stringer (2010)

Chapter 4

REFERENCE SPECIMEN DESIGN

Eight large-scale specimens were designed to evaluate the performance of the proposed connections under constant axial and reversed cyclic lateral loading. The specimens were designed using the Laguna De Santa Rosa Bridge located outside of Santa Rosa, California as a prototype. An overview of the prototype bridge is shown in Fig. 4.1. The columns in this bridge are reinforced concrete with 1.22m (48-in.) diameter, and are detailed using 32 bundled No. 11 longitudinal bars, and No. 8 hoops at 152-mm (6-in.) on-center in the transverse direction. These columns were redesigned using CFT columns with equivalent strength under combined axial-moment (P-M) loading as well as equivalent stiffness, which resulted in CFT members with a thickness and diameter of 12.7 (0.5-in.) and 1.07-m (42-in.) respectfully and a diameter to thickness ratio (D/t) of 84. The CFT connection specimens were scaled using the redesigned CFT column as a prototype column. The original RC column and redesigned CFT column are shown in Fig. 4.1.

Specimen geometries are illustrated in Fig. 4.2 and Fig. 4.3 for loading in the transverse and longitudinal directions of the bridge respectively. Four 20-in. diameter and one 24-in. diameter CFTs were selected to evaluate the performance of the proposed connections for loading in the transverse direction of the bridge (resulting in scale factors of 48% and 57%, respectively), while two 25.75-in. CFTs and one 24-in. diameter CFT were selected to evaluate performance for loading in the longitudinal direction (resulting in scale factors of 57% and 61%, respectively).

All tubes had a thickness of 0.25-in, resulting in D/t ratios of 80, 96, and 103 for the 20-in, 24-in, and 25.75-in. tubes, respectively.

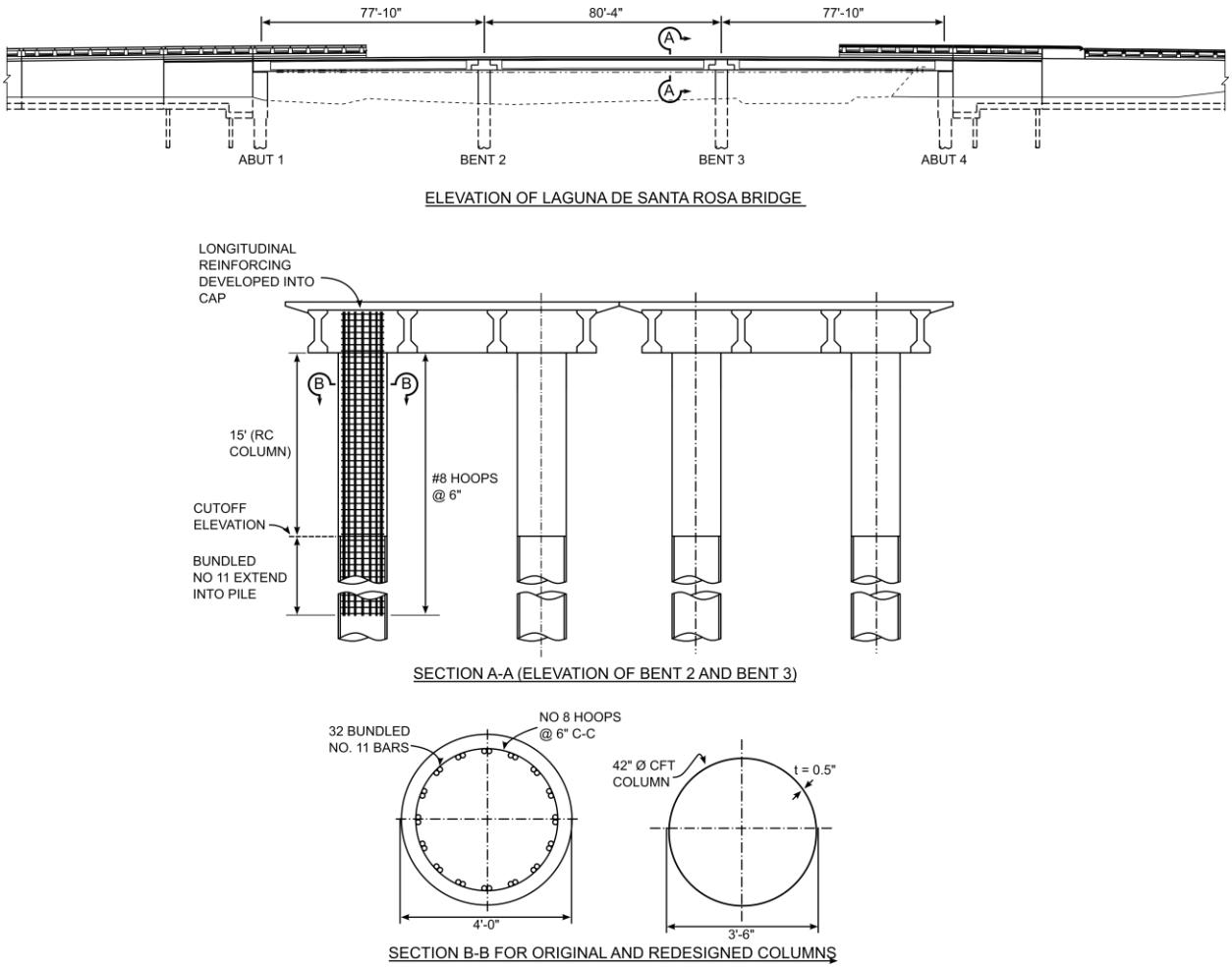

Fig. 4.1. Prototype Bridge

Specimen nomenclature used here refers to the connection type, as illustrated in Fig. 1.1, followed by the D/t ratio, and a letter to denote the direction of loading (T for transverse and L for longitudinal), i.e., ER96T describes an embedded connection with D/t = 96 for loading in the transverse direction of the bridge.

All of the specimens were constructed using pre-cast cap beams cast with a recess formed by light-gauge corrugated metal pipe, and the columns were grouted into place using high

strength fiber reinforced grout. The specimens were cantilever columns anchored into a cap beam as illustrated in Fig. 4.2 and Fig. 4.3. Joint shear reinforcing in the welded dowel and reinforced concrete connection specimens was scaled from the prototype bridge and checked against the California Department of Transportation Seismic Design Criteria (Caltrans, 2013), while vertical shear reinforcing in the joint region of the cap beam was designed according to recommendations by Lehman and Roeder (2012). Flexural reinforcement in the cap beam was designed to resist 1.2 times the theoretical flexural strength of $1.25M_{p,cft}$ of the CFT columns. Reinforcing details for all specimens are located in Appendix A.

4.1 Embedded Ring (ER) CFT Connections

Two transverse and two longitudinal specimens were designed to evaluate the performance of the proposed ER CFT column-to-cap beam connection. Specimen connection geometries are illustrated in Fig. 4.4 The specimens were designed: (1) to investigate the performance for smaller cap beam widths than had previously been evaluated for the embedded foundation connection (the final cap beam width was determined using a numerical analysis discussed in the next chapter), (2) to evaluate a smaller exterior annular ring projection of 8t (in contrast to 16t that had been used on the prior foundation connections studied in Phase 1), (3) to evaluate the influence of using API or ASTM grade tube steel, (4) to compare a straight seam and spirally welded tube, and (5) to evaluate the performance for loading in the transverse and longitudinal direction of the bridge.

Specimen ER80T was designed with embedment depth of 18-in. (0.9D), and utilized a 61-ksi ASTM A1018 spiral welded steel tube with an annular ring with a 2-in. projection both inside and outside of the tube. Specimens ER96T and ER96L were embedded 20-in (0.83D) into

the cap beam (note the lesser relative embedment depth was possible because of the lower steel strength), and both utilized a 53-ksi API 5L X-42 grade straight seam tube with an annular ring that projected 51-mm (2-in.) inside and outside of the tube. Specimen ER103L was embedded 20.25-in. (0.8D) into the cap beam, and utilized a 69.3-ksi ASTM A1018 spiral welded steel tube with an annular ring with a projection of 2-in. inside and outside of the tube.

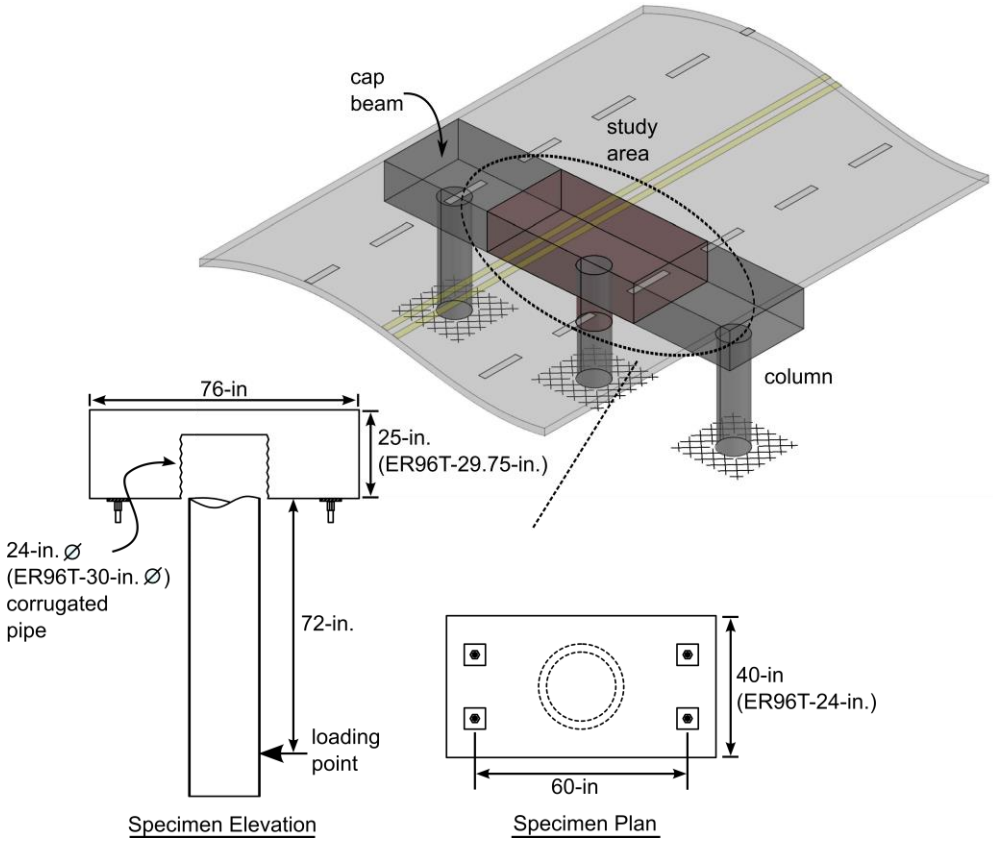

Fig. 4.2. Overview of Transverse Specimen Geometry

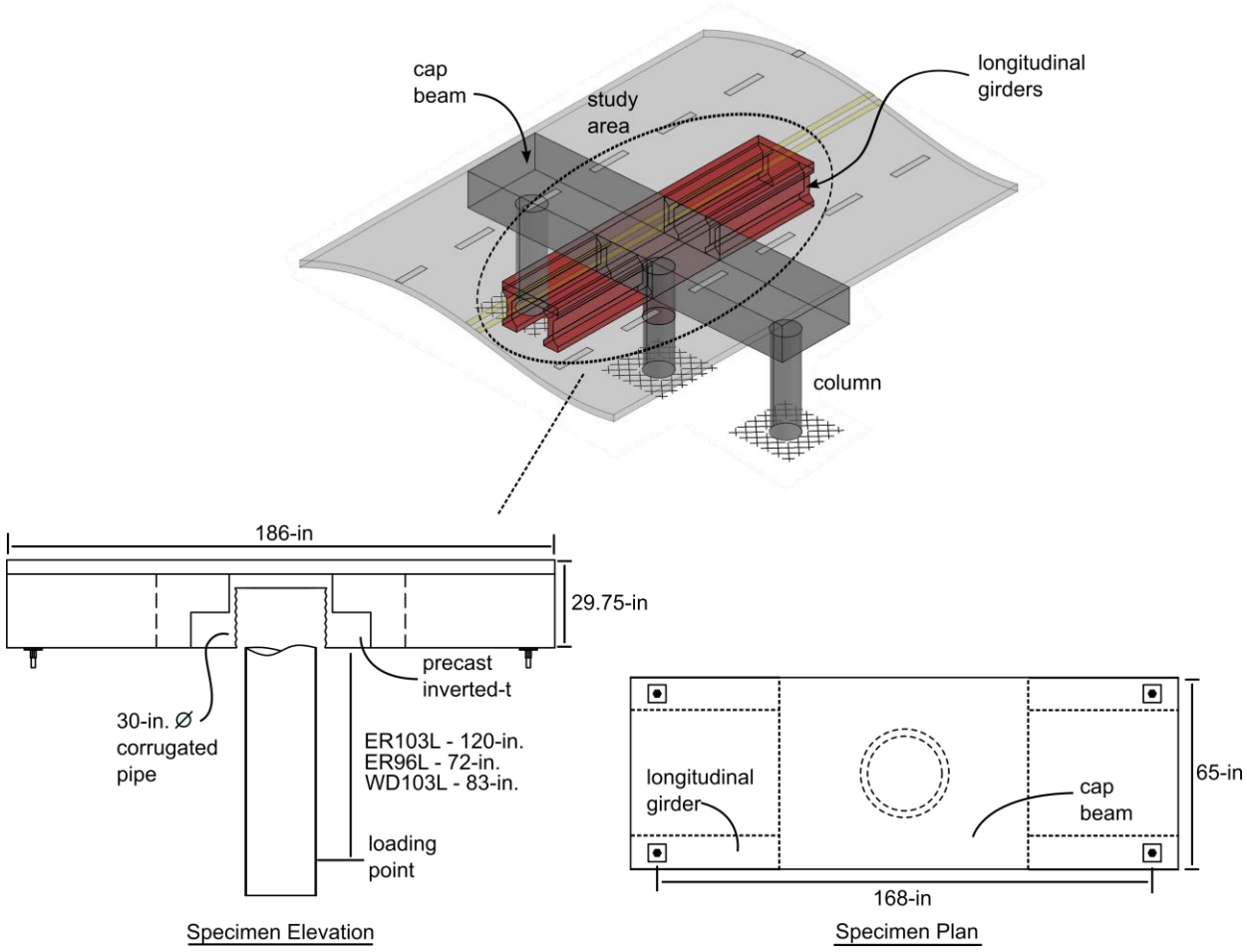

Fig. 4.3. Overview of Longitudinal Specimen Geometry

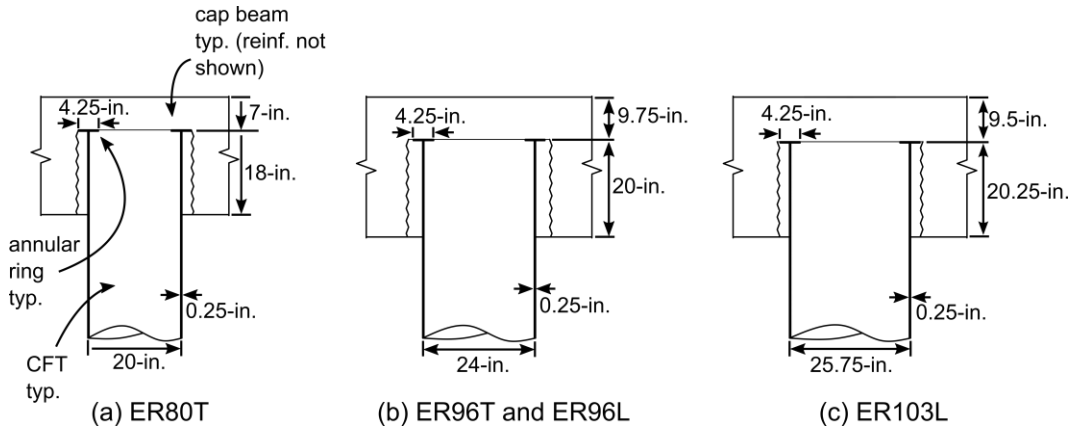

Fig. 4.4. Connection Details for Embedded Dowel Connection Specimens

4.2 Welded Dowel (WD) Connections

Three specimens were designed using the welded dowel connection detail: one specimen with fully bonded bars (WD80T1), and two specimens with bars de-bonded along the length (WD80T2 and WD103L). In all cases, the longitudinal reinforcing in the connection region was selected with a target longitudinal reinforcing ratio of 3%, resulting in eight evenly distributed No. 9 bars in WD80T1 and WD80T2 and ten evenly distributed No. 11 bars in WD103L.

The bars in all welded dowel specimens were embedded $12d_b$ into the cap beam per ACI 318 requirements for the development of headed reinforcing bars (ACI, 2011), and $24d_b$ into the CFT column based on weld pullout tests discussed in Chapter 6. The bars were welded to the inside of the steel tubes using flare bevel groove welds formed by requirements of AWS D1.4 designed to exceed F_{ub}, where F_{ub} is the ultimate steel strength of the reinforcing bars.

All of the specimens used flanges that projected 2-in. from the exterior of the steel tube and a 1-in. thick soffit fill, which extended below the surface of the cap beam. Specimen WD103L also included transverse No. 5 hoops with the intention of providing additional confinement to the soffit fill and joint region, as illustrated in Fig. 4.5.

PVC pipe was used to de-bond the longitudinal reinforcing bars in specimens WD80T2 and WD103L for lengths of 22-in. and 24-in., respectively. The de-bonded lengths were calculated according to Equation 4.1 to achieve a connection rotation demand of 10% drift prior to fracture of the longitudinal dowel bars where θ_u is the target drift, and ϕ_u is the curvature at the fracture strain of the dowels (Stringer, 2010).

$$L_{db} = \frac{\theta_u}{\phi_s} \quad [4.1]$$

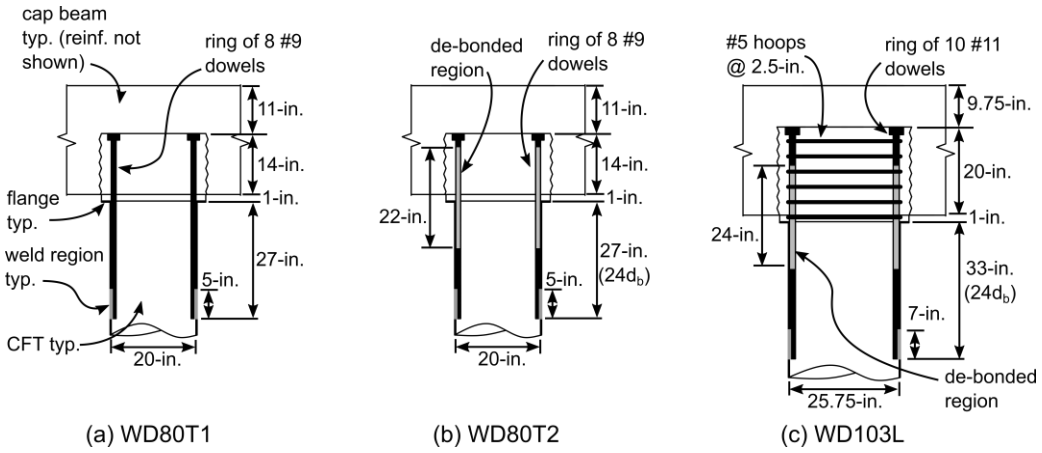

Fig. 4.5. Connection Details for Welded Dowel Connection Specimens

4.3 Reinforced Concrete (RC) Connections

One specimen (RC80T) was designed to evaluate the behavior of the reinforced concrete connection. As illustrated in Fig. 4.6, the longitudinal reinforcement consisted of eight evenly distributed No. 9 headed bars in an effort to achieve a longitudinal reinforcing ratio of 3%, and to allow for comparison to the welded dowel connections. The bars were embedded $12d_b$ into the cap beam per the ACI 318 development requirements for headed reinforcing, and $30d_b$ into the CFT column per development requirements for deformed bars (ACI, 2011). Transverse column reinforcing was scaled from the prototype column, resulting in a No. 3 spiral at a spacing of 2.5-in. as shown in Fig. 4.6. A clear cover of 1-in. was provided between the steel tube and the transverse reinforcing.

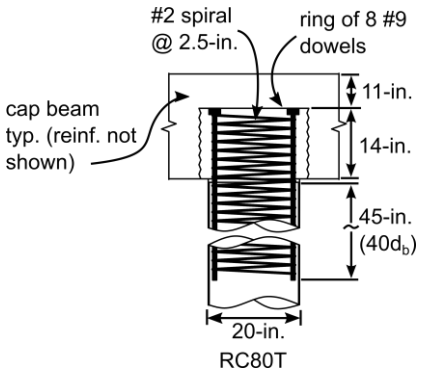

Fig. 4.6. Connection Details for Embedded Dowel Connection Specimen

Chapter 5

NUMERICAL ANALYSIS FOR SUPPORT OF EXPERIMENTS

A limited numerical study was conducted in both the transverse and longitudinal directions to evaluate the behavior of the proposed cap beam connections. This chapter introduces the numerical methods used to evaluate the different connection types and summarizes the results of the numerical study.

The commercially available finite element analysis software ABAQUS was used to perform a preliminary series of nonlinear analyses on the ER, WD, and RC cap beam connections in the transverse direction, and the ER connection in the longitudinal direction. An overview of the numerical model for the transverse analyses is shown in Fig. 5.1, while the longitudinal model is summarized in Fig. 5.2.

Model geometry in the transverse direction included the CFT column-to-cap beam connection, the CFT column, and the reinforced concrete cap beam. Geometry in the longitudinal direction included the CFT column-to-cap beam connection, the CFT column, a precast inverted-T, a CIP diaphragm, dapped ended precast girders, and a deck. A half model was developed taking advantage of symmetry in the plane parallel to the direction of loading and the center of the specimen; this increased computational efficiency. The CFT column was modeled using 3-dimensional elements for a length of 2 times the theoretical plastic hinge length of the column. The remainder of the length was modeled using the ABAQUS MPC constraint tied to a reference point. This approach models the remaining length of the column as a rigid beam to decrease computation time. The nodes at the top of the cap beam were restrained to simulate the boundary

conditions of future experimental tests, and lateral loading was applied by assigning monotonic displacements Δ_x along the x-axis to the reference point.

A distributed axial load was applied to the top of the concrete and steel tube using the pressure load option in ABAQUS. A constant axial load of $0.1P_o$ was applied for most models unless the axial load ratio was being evaluated.

The 4-node shell element with reduced integration (ABAQUS element type S4R), 2-node truss element (ABAQUS element type T3D2), 2-node beam element (ABAQUS element type B31), and 8-node solid element with reduced integration (ABAQUS element type C3D8R) were used to model steel tube, cap beam reinforcing steel, connection reinforcing steel (for WDC, WDCDB, and EDC), and concrete elements, respectively.

Gap elements were used at every nodal point that was geometrically common with the steel tube and concrete fill elements to simulate bond stress between the concrete by combining the confining contact stress with a coefficient of friction to develop shear stresses at the interface; penetration of the concrete element by the steel element was prevented.

The reinforcing steel and concrete components in the cap beam were spatially assembled, and interactive constraint relationships were defined using the ABAQUS Embedded constraint to perfectly embed the cap beam reinforcement in the cap beam concrete. This constraint does not allow for relative slip between the reinforcing bar and concrete components. The interaction between the connection reinforcing steel and the concrete is more complex and required a more robust interaction approach. Spring elements were used to connect every nodal point that was geometrically common between the concrete and connection reinforcing. These elements

allowed for the definition of a bond-slip interaction, as well as de-bonding of the reinforcing in the cases when the longitudinal dowels were de-bonded in the WD connection.

Mesh refinement in the CFT column-to-cap beam model was primarily concentrated in the plastic hinge and embedded regions of the steel tube due to the load and deformation demands in these regions. Global mesh convergence of the concrete components in the cap beam and the steel and concrete components in the CFT was conducted by analyzing the maximum numerical moment capacity of each specimen.

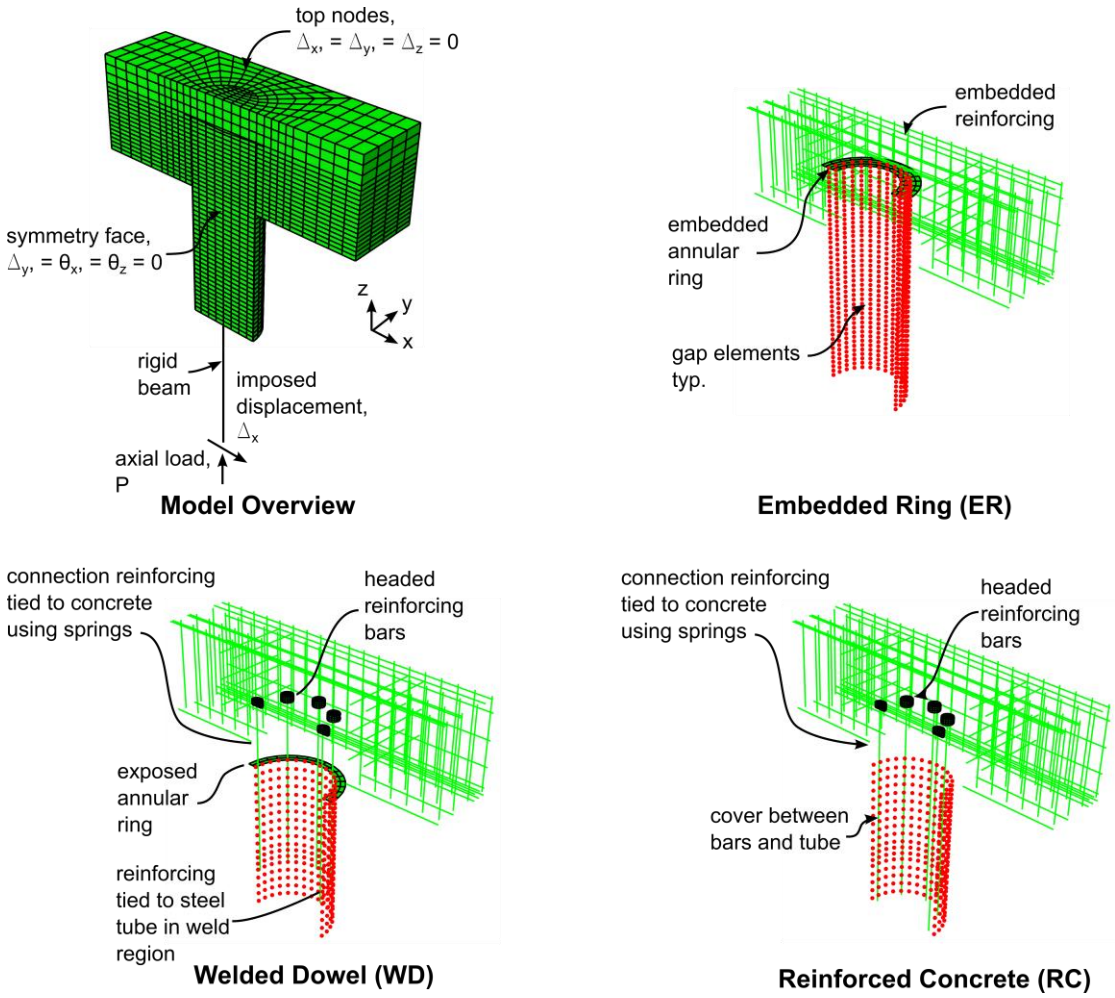

Fig. 5.1. Transverse Model Overview

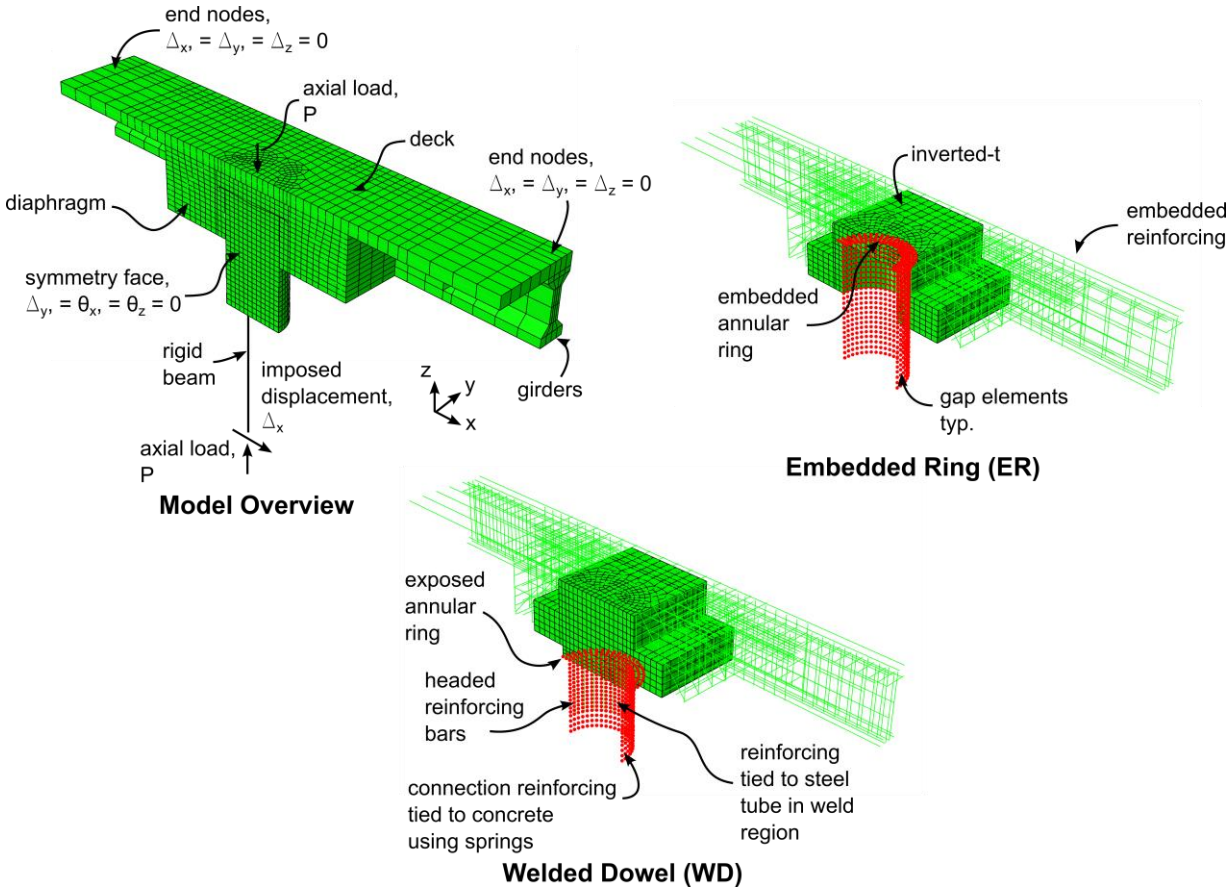

Fig. 5.2. Longitudinal Model Overview

Material nonlinearity was incorporated using the concrete damaged plasticity model for concrete and a trilinear stress strain relationship with isotropic hardening for steel. The concrete damaged plasticity model utilizes a non-associative flow rule and can capture the influence of tri-axially dependent plastic hardening as well as a reduction in tensile and compressive stiffness in cyclic loading applications (Lee and Fenves, 1998). The compressive stress-strain behavior of the concrete was defined using a relationship proposed by Saenz (1964) in which linear elastic behavior is assumed up to a concrete stress of $0.5f'_c$ and a maximum compressive stress is achieved at a compressive strain of 0.003. The tensile stress strain behavior was modeled using a

relationship developed by Hsu and Mo (2010) where linearity is assumed up to the cracking stress of the concrete, $f_{cr} = 7\sqrt{f'_c}$, and the softening relationship is defined as:

$$f_t = f_{cr}\left(\frac{\varepsilon_{cr}}{\varepsilon_c}\right)^{0.4} \tag{5.1}$$

where ε_{cr} is the cracking strain of concrete. The compressive and tensile stress-strain relationships used to define the concrete behavior are shown in Fig. 5.3.

A tri-linear stress strain relationship with isotropic hardening was used to define the behavior of the tube steel and reinforcing bars. The plastic plateau was terminated when the strain in the steel, ε_s was 10 times the yield, and the ultimate stress, $F_{u,st}$, was assigned at an ultimate steel strain $\varepsilon_{su} = 0.1$. The stress-strain relationship used to define the steel components is shown in Fig. 5.3.

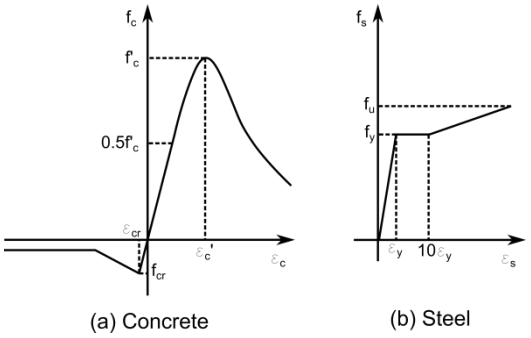

Fig. 5.3. Material Models of Concrete and Steel

Note that as of the writing of this document the materials have only been calibrated for monotonic loading. Extending the concrete constitutive models available in ABAQUS to cyclic applications has presented many problems; specifically with regards to crack closure in reversed cyclic tension-to-compression loading applications. Ongoing research is being conducted to

overcome the deficiencies in the concrete constitutive models in ABAQUS. Specifically, damage implementation has been investigated for the concrete damaged plasticity model. The use of a smeared cracking formulation has also been investigated. Furthermore, more complex constitutive models which include combined isotropic and kinematic hardening are being investigated for use in the steel components for applications of cyclic loading.

5.1 Numerical Studies in the Transverse Direction

A limited series of numerical studies were conducted to evaluate the influence of differing parameters on the performance of the proposed CFT column-to-cap beam connections in the transverse direction. The parameters investigated included: (1) the type of connection (ER, WD, and RC), (2) limits on cap beam width with the ER connection, (3) limits on the annular ring diameter with the ER connection, and (5) de-bonding the bars with the WD connection detail. The parameter studies were conducted on the transverse specimens discussed in Ch. 4. The steel tube and reinforcement were assigned nominal yield strengths of 49-ksi and 60-ksi respectively, while the concrete was assigned a nominal compressive capacity of 6-ksi. The following sections will discuss the results of the parameter studies.

5.1.1 Type of Connection

Moment-drift relationships for the differing connection types are plotted in Fig. 5.4a, while inelastic deformations at 10% drift are plotted in Fig. 5.4b. The moments have been normalized to the plastic moment capacity of the CFT as calculated using the PSDM. The plastic strain for all connection types was isolated to the connection region with limited inelastic deformation in the cap beam.

Although the yielding mechanism in the WD, WD with de-bonded dowels, and RC connections was characterized by inelastic deformation in the column reinforcing, these connections did not achieve the plastic moment capacity of the CFT due to lower effective longitudinal reinforcing ratios. Additionally, the RC connection did not provide as much strength as the WD and WD with de-bonded dowel connections due to a smaller moment arm. De-bonding the reinforcing bars reduced inelastic deformation in both the grout region of the cap beam and the extreme tension reinforcing bar as is illustrated in Fig. 5.4b and Fig. 5.5.

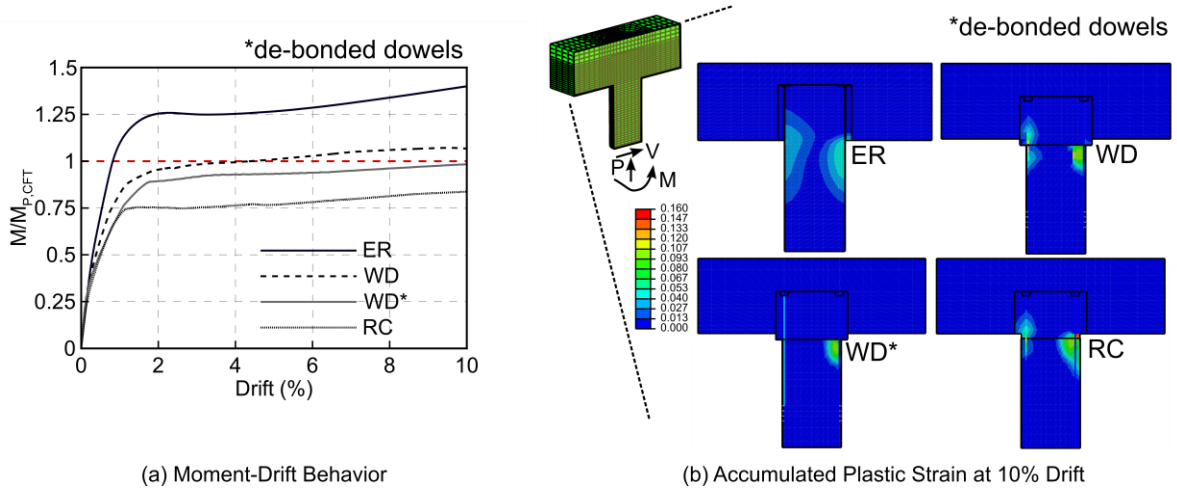

(a) Moment-Drift Behavior (b) Accumulated Plastic Strain at 10% Drift

Fig. 5.4. Moment-Drift and Inelastic Strains in the Proposed Connection Types

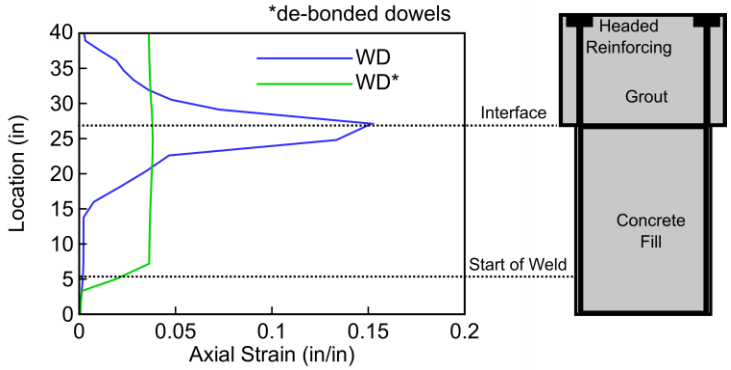

Fig. 5.5. Connection Reinforcing Strain at 10% Drift

5.1.2 Embedded Flange Connection Numerical Studies

The performance of the embedded connection was evaluated for differing cap widths and annular ring diameters. The cap width parameter study was conducted using an annular ring outer diameter D_o = D+32t per design recommendations developed for the embedded flange footing connection (Lehman and Roeder, 2012), while the cap beam width for the annular diameter study was held constant at 2D or 40-in. An embedment depth of 0.7D was selected for all parameter studies.

Moment-drift relationships for the cap beam width and annular ring diameter parameter studies are plotted in Fig. 5.6a and Fig. 5.7a, while inelastic deformations at 10% drift are shown in Fig. 5.6b and Fig. 5.7b. Fig. 5.6b illustrates that although cap beam cracking increased as the width decreased, the strength of the embedded connection exceeded the plastic moment capacity of the CFT for all widths analyzed. This suggests that the embedded connection can achieve strength and ductility performance objectives within the geometric constraints of the cap. Fig. 5.7b shows that decreasing the outer diameter of the annular ring, D_o from D+32t to D+8t does not influence the moment-drift relationship or influence the distribution of plastic strain in the cap beam or column.

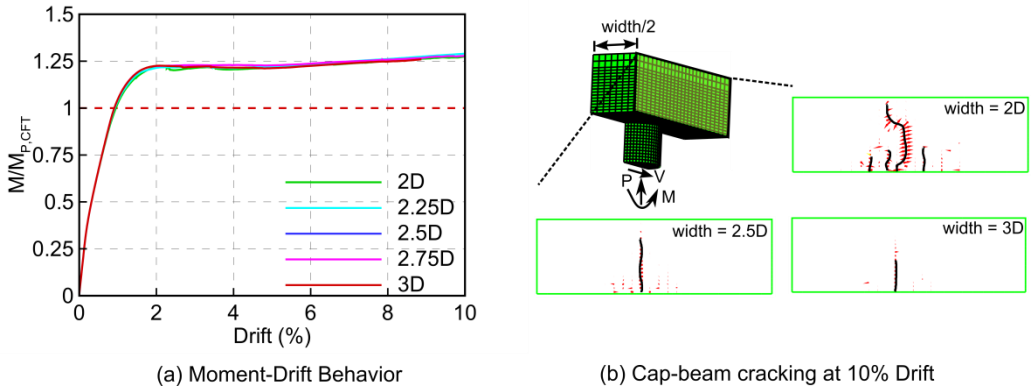

(a) Moment-Drift Behavior (b) Cap-beam cracking at 10% Drift

Fig. 5.6. ER Connection Cap-Beam Width Parameter Study (a) moment-drift behaviors and (b) cap beam cracking

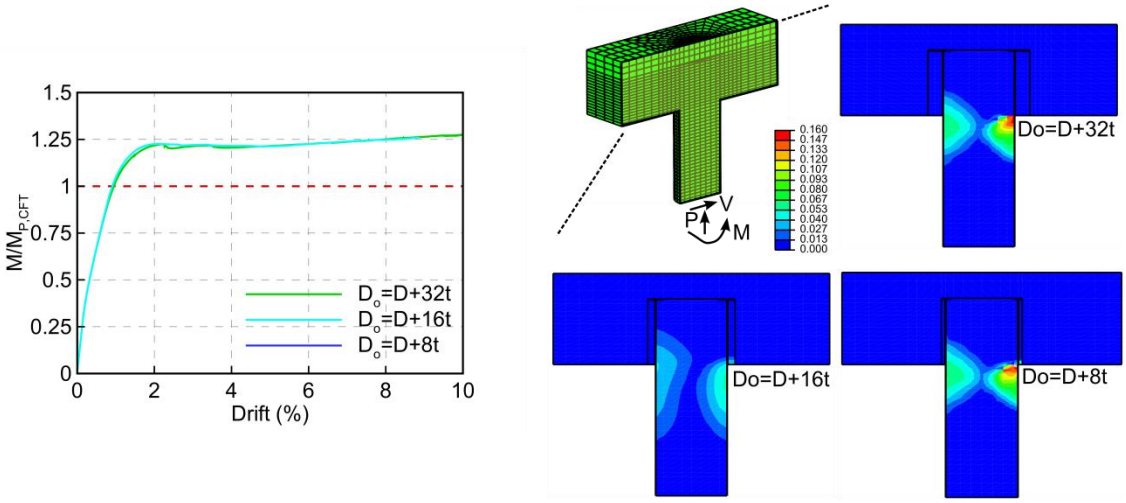

(a) Moment-Drift Behavior (b) Maximum Principal Strain at 10% Drift

Fig. 5.7. ER connection Annular Ring Diameter Parameter Study

5.2 Numerical Studies in the Longitudinal Direction

Limited numerical studies were conducted on the ER connection and WDC connection with de-bonded dowels in the longitudinal direction to ensure the connections could achieve strength and ductility requirements. The primary parameter of interest in the preliminary study was the axial load ratio, P/P_o.

The moment drift relationships for the two connection types subjected to axial load ratios of 0.05, 0.10, and 0.15 are shown in Fig. 5.8 for drifts up to 5%. The ER and WD connections exceeded the theoretical plastic moment capacity of the CFT column and the longitudinal connection reinforcing respectively. This indicated that these connections could achieve strength and ductility performance objectives within the geometric constraints of the precast cap beam.

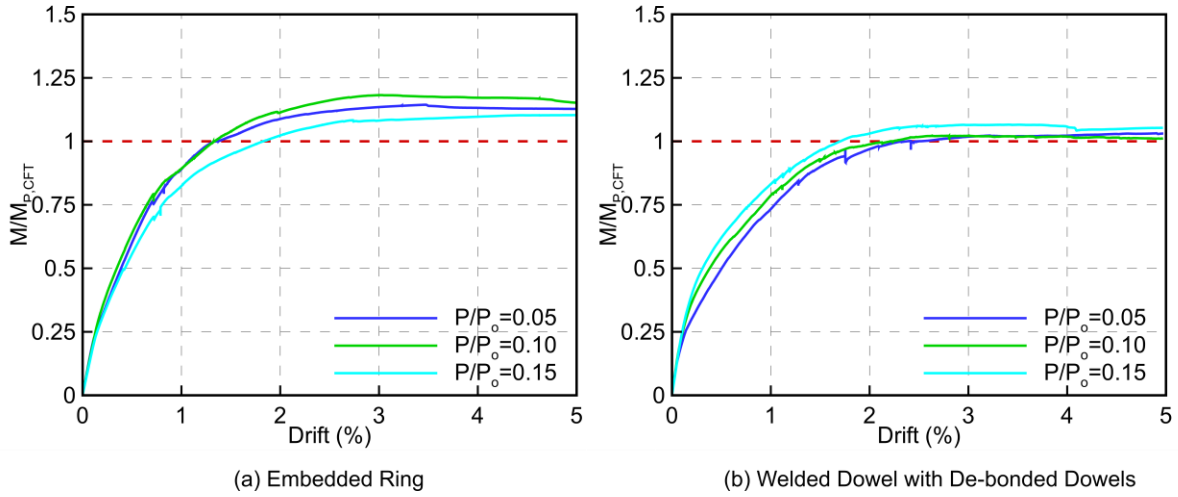

Fig. 5.8. Moment-Drift Relationships for Axial Load Parameter Study in the Longitudinal Direction

Chapter 6

WELDED DOWEL PULLOUT EXPERIMENTS AND STEEL TUBE-TO-CONCRETE-FILL BOND EXPERIMENTS

The experimental program to investigate the performance of the proposed cap beam connections was completed in two primary phases: (1) welded dowel pullout and bond slip experiments were conducted to evaluate the dowel-to-steel tube welds and the bond characteristics between the concrete core and steel tube, and (2) large scale connection experiments were conducted to evaluate the seismic performance of the proposed connections. This chapter discusses the welded dowel pullout tests and bond slip tests.

6.1 Welded Dowel Pullout Tests

Initial analysis of WD connections showed potential problems with the welds joining the dowel bars to the inside of the steel tube. Questions regarding the size and location of the welds in the tube and potential damage to the tube and CFT member were apparent. Therefore, an experimental investigation was conducted to evaluate the performance of the dowel-to-tube weld detail, prior to evaluating the connection-level performance of those connections. Of particular concern was the ability of the relatively thin tube to develop the full capacity of large dowels subjected to tensile forces. AWS D1.4 (2010) provides specifications for welding dowels to steel plates; the specified weld type is a flare bevel groove weld (as illustrated in Fig. 6.1), and the weld strength is calculated as:

$$\phi R_n = \phi 0.6 F_{EXX} t_e (2L_w) \quad (5.1)$$

where ϕ is the resistance factor, R_n is the weld strength, F_{EXX} is the tensile strength of the electrode, L_w is the weld length, and t_e is the weld throat thickness defined as $0.2d_b$ (as illustrated

in Fig. 6.1.). A factor of 2 is placed in front of L_w to account for welds on both sides of the reinforcing bar.

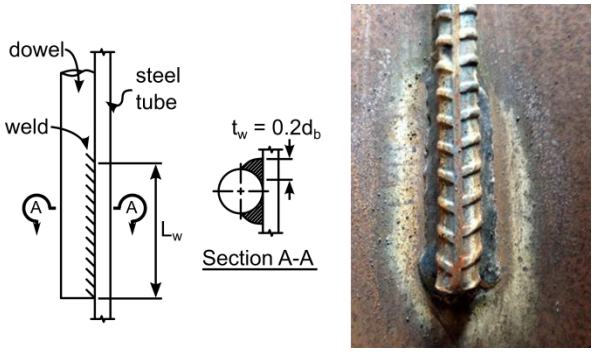

Fig. 6.1. Flare Bevel Groove Weld

Sixteen No. 7, four No. 9, and four No. 11 dowels were welded to inside of 4 20-in. diameter steel tubes with 0.25-in. wall thickness, and the tubes were filled with self-consolidating low shrinkage concrete. The primary test parameters included weld strength, de-bonding the dowels from the concrete, and the length which the bar extended into the steel tube as summarized in Table 6.1. Weld strengths ranging from 80% to 120% of the dowel strength based upon the AWS D1.4 were designed, and the dowels were extended into the steel tubes for lengths of $18d_b$ and $24d_b$ based on discussions with the California Department of Transportation. Weld strengths in Table 6.1 are presented as a strength ratio, $\phi R_n/P_n$, where ϕR_n is the reduced design capacity of the weld, and P_n is the ultimate capacity of the longitudinal dowel (i.e. a weld designed to resist 80% of the capacity of the dowel has a strength ratio of 0.8). The actual strength ratios were calculated based on the measured lengths of the welds after the specimens were fabricated. In all cases, the welds were longer than specified, resulting in larger theoretical strength ratios than intended. The weld type for each dowel was a flare bevel groove weld (as

shown in Fig. 6.1) , and the weld process was a self-shielded flux core arc welding method with E71T8 electrodes.

In each tube, bonded and de-bonded dowels were alternated around the circumference to limit the influence of conical concrete pullout on neighboring dowels. The de-bonded dowels were de-bonded through the entire depth of the concrete using duct-tape to cover the dowel deformations. The bars were pulled using a hydraulic ram placed into a self-reacting system as illustrated in Fig. 6.2a. A gap was left between the top of the steel tube and the concrete surface to allow for dowel pullout, and a transfer plate was used to transfer force through the steel tube and into the floor. Global bar displacement was monitored using string-pots, and load was monitored using a load cell.

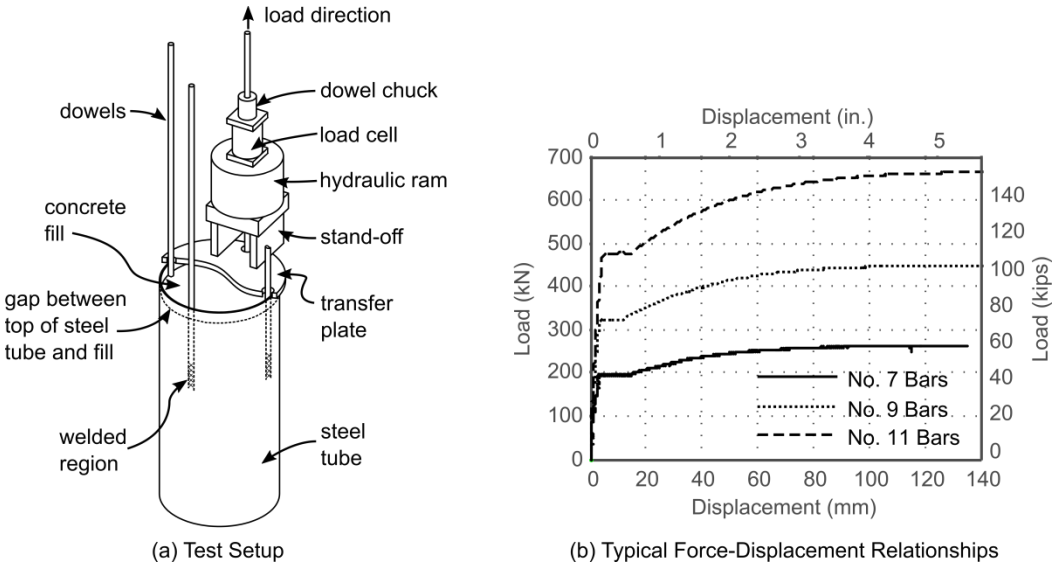

Fig. 6.2. (a) Test Setup and (b) Typical Force-Displacement Behavior

Table 6.1. Welded Dowel Pullout Test Matrix

Specimen Number`	Dowel Size	De-bonded	Specified Strength Ratio ($\phi R_n/P_n$)	Actual Strength Ratio from Measured Length ($\phi R_n/P_n$)	Length Dowel Extended into Tube
1	No. 7	No	0.8	1.06	$24d_b$
2	No. 7	No	1.0	1.27	$24d_b$
3	No. 7	No	1.1	1.08	$24d_b$
4	No. 7	No	1.2	1.40	$24d_b24d_b$
5	No. 7	Yes	0.8	0.99	$24d_b$
6	No. 7	Yes	1.0	1.24	$24d_b$
7	No. 7	Yes	1.1	1.36	$24d_b$
8	No. 7	Yes	1.2	1.31	$24d_b$
9	No. 7	No	0.8	0.99	$24d_b$
10	No. 7	No	1.0	1.18	$24d_b$
11	No. 7	No	1.1	1.19	$24d_b$
12	No. 7	No	1.2	1.31	$24d_b$
13	No. 7	Yes	0.8	0.92	$24d_b$
14	No. 7	Yes	1.0	1.16	$24d_b$
15	No. 7	Yes	1.1	1.23	$24d_b$
16	No. 7	Yes	1.2	1.29	$24d_b$
17	No. 9	No	1.0	0.98	$18d_b$
18	No. 9	Yes	1.0	1.0	$18d_b$
19	No. 9	No	1.0	0.98	$24d_b$
20	No. 9	Yes	1.0	0.95	$24d_b$
21	No. 11	No	1.0	1.03	$18d_b$
22	No. 11	Yes	1.0	1.01	$18d_b$
23	No. 11	No	1.0	1.00	$24d_b$
24	No. 11	Yes	1.0	1.06	$24d_b$

The failure mode in all tests was characterized by dowel yielding followed by strain hardening and fracture. Typical force displacement curves are illustrated in Fig. 6.2b. The steel tube was removed following the experiments to evaluate the influence of de-bonding the dowels on the amount of concrete damage. De-bonding the reinforcing tended to decrease the amount of visible concrete damage (as illustrated in Fig. 6.3), and no damage to the tubes in the weld region was observed in any of the tests.

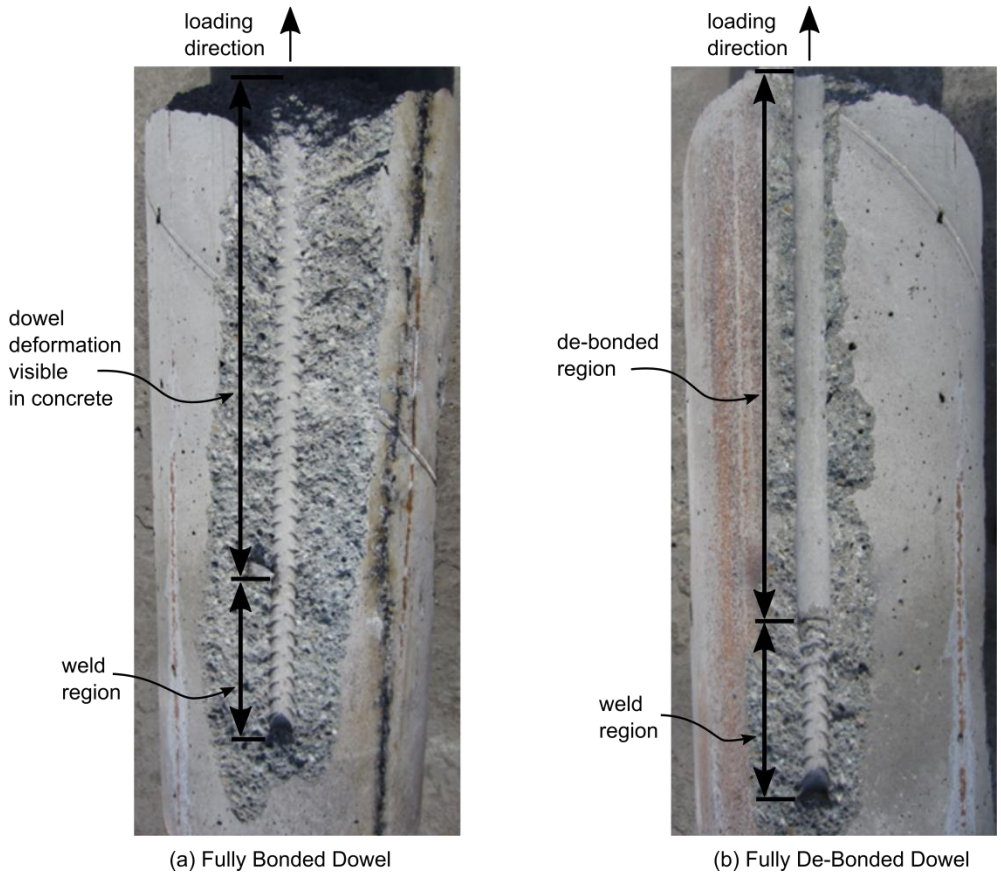

Fig. 6.3. Concrete Damage in Pullout Specimens with (a) Fully Bonded Dowel and (b) Fully De-bonded Dowel

6.2 Steel Tube-to-Concrete-Fill Bond Experiments

To help characterize the composite nature of CFTs which utilize straight seam and spiral welded tubes, an ancillary experimental investigation was conducted. Of particular interest were the bond slip characteristics of two different tube types using a concrete fill both with and without a low shrinkage admixture.

Four bond-slip specimens were constructed to evaluate the bond-slip characteristics of CFTs with spiral weld and straight seam tubes. A full specimen matrix including tube type and material properties is summarized in Table 6.2. Two CFT's with spiral welded and straight seam

tubes were cast using concrete with a low shrinkage admixture, and two were cast with a concrete without a low shrinkage admixture. The specimens were cast with a 1-in. gap on the bottom to allow for push through of the concrete fill (as illustrated in Fig. 6.4).

Table 6.2. Bond Slip Specimen Matrix

Specimen	Type of Tube	D, in.	t, in.	D/t	Test Day f'_c, ksi	Concrete Admixture
SS-I	Straight Seam	20	0.25	80	7.95	Low Shrinkage
SW-I	Spiral Welded	24	0.25	96	7.95	None
SS-II	Straight Seam	20	0.25	80	7.53	Low Shrinkage
SW-II	Spiral Welded	20	0.25	80	7.53	None

The specimens were instrumented using linear Duncan potentiometers, vibrating wire gages, and strain gages, and were tested under a 2.4-million lb capacity Universal testing machine. An overview of the instrumentation and test setup is illustrated in Fig. 6.4.

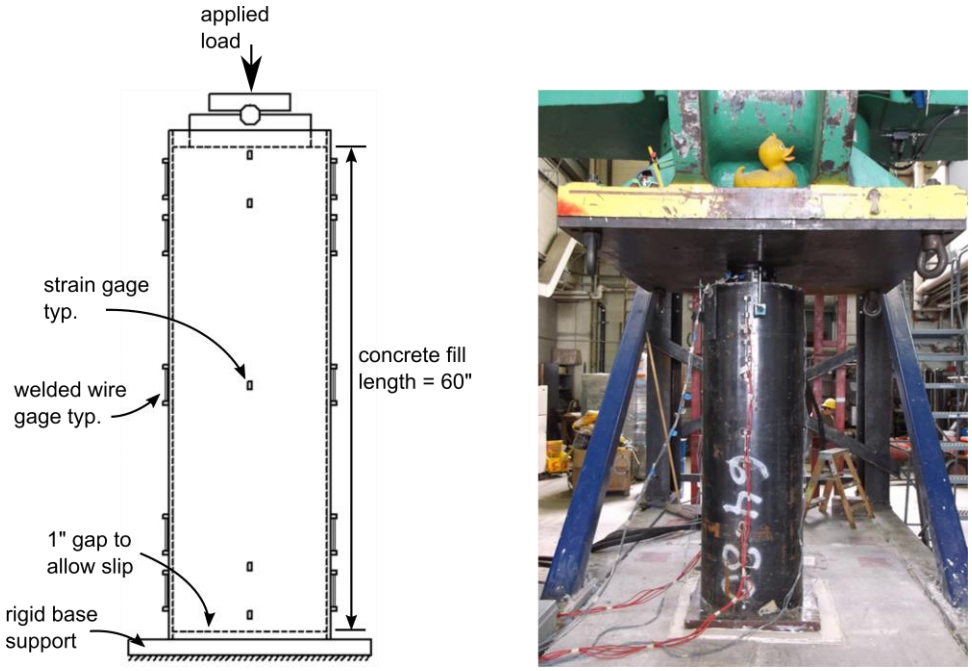

Fig. 6.4. Bond Slip Test Setup and Instrumentation

The concrete core was loaded axially until a 1-in. displacement was recorded. The force-displacement behaviors of the specimens have been plotted in Fig. 6.5. The addition of a low shrinkage admixture did not influence the bond-slip characteristics of the spiral welded tubes. This is because the primary bonding mechanism in this type of tube is mechanical; the spiral weld acts to force composite action between the concrete fill and steel tube. In contrast, the addition of low shrinkage admixture greatly improved the bond strength for straight seam tubes. This is because the primary bonding mechanism in this type of tube is chemical, and if the concrete shrinks away from the steel tube as it cures, a majority of the bond is lost.

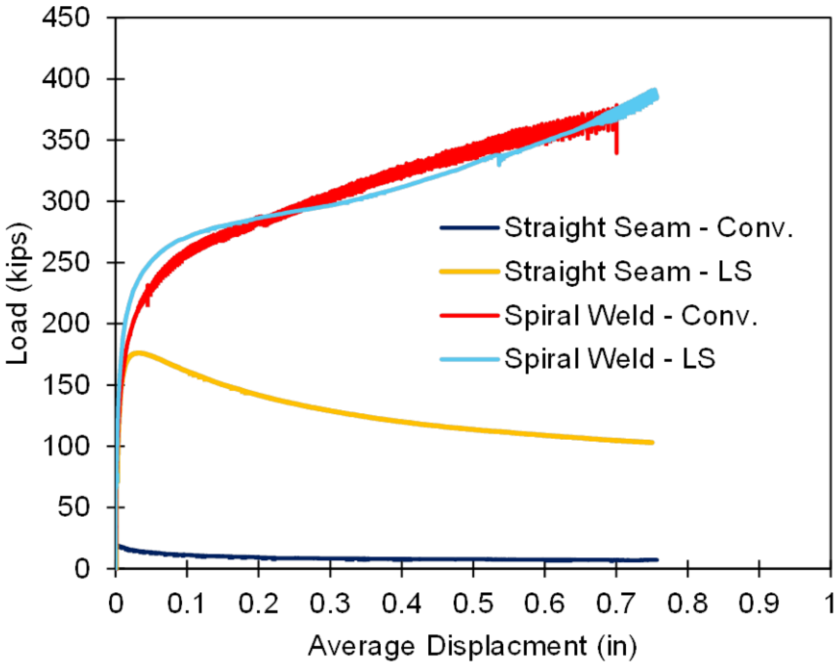

Fig. 6.5. Bond Slip Force-Displacement Behaviors

Chapter 7

CONNECTION TESTS: EXPERIMENTAL PROGRAM

Eight large scale specimens were tested to evaluate the performance of the proposed connections under constant axial and reversed cyclic lateral loading. An overview of the full experimental matrix is given in Table 7.1. The specimens consisted of five large scale transverse specimens which simulated approximately a half scale bridge column, and three longitudinal specimens which simulated approximately a 60% scale bridge column. The specimens were tested in an inverted configuration due to constraints of the available testing apparatus. An overview of the transverse and longitudinal specimen geometry is presented in Fig. 7.1, and details of the specimen reinforcing are provided in Appendix B. The following sections describe the construction of the specimens and provide an overview of the testing apparatus and instrumentation.

Table 7.1. Connection Experiment Test Matrix

Specimen	Loading Direction	Steel Tube Type	D, in.	t, in.	D/t	L_e, in.	L_{pc}, in.	L_s, in.	L_{db}, in.	Long. Dowels	Trans. Reinf.	P, %
ER80T	Trans.	ASTM A 1018 Spiral Welded	20	0.25	80	18	7	-	-	-	-	5
ER96T	Trans.	API 5 L X42 Straight Seam	24	0.25	96	20	9.75	-	-	-	-	4
WD80T1	Trans.	ASTM A 1018 Spiral Welded	20	0.25	80	14	11	1	0	8-No. 9	None	2.5
WD80T2	Trans.	ASTM A 1018 Spiral Welded	20	0.25	80	14	11	1	22	8-No. 9	None	2.5
RC80T	Trans.	ASTM A 1018 Spiral Welded	20	0.25	80	14	11	1	0	8-No. 9	No. 3 @ 63.5-mm	2.5
ER103L	Long.	ASTM A 1018 Spiral Welded	25.75	0.25	103	20.25	9.5	-	-	-	-	4
ER96L	Long.	API 5 L X42 Straight Seam	24	0.25	96	20	9.75	-	-	-	-	4
WD103L	Long.	ASTM A 1018 Spiral Welded	25.75	0.25	103	20	9.75	1	24	10-No. 11	No. 5 @ 127-mm	3

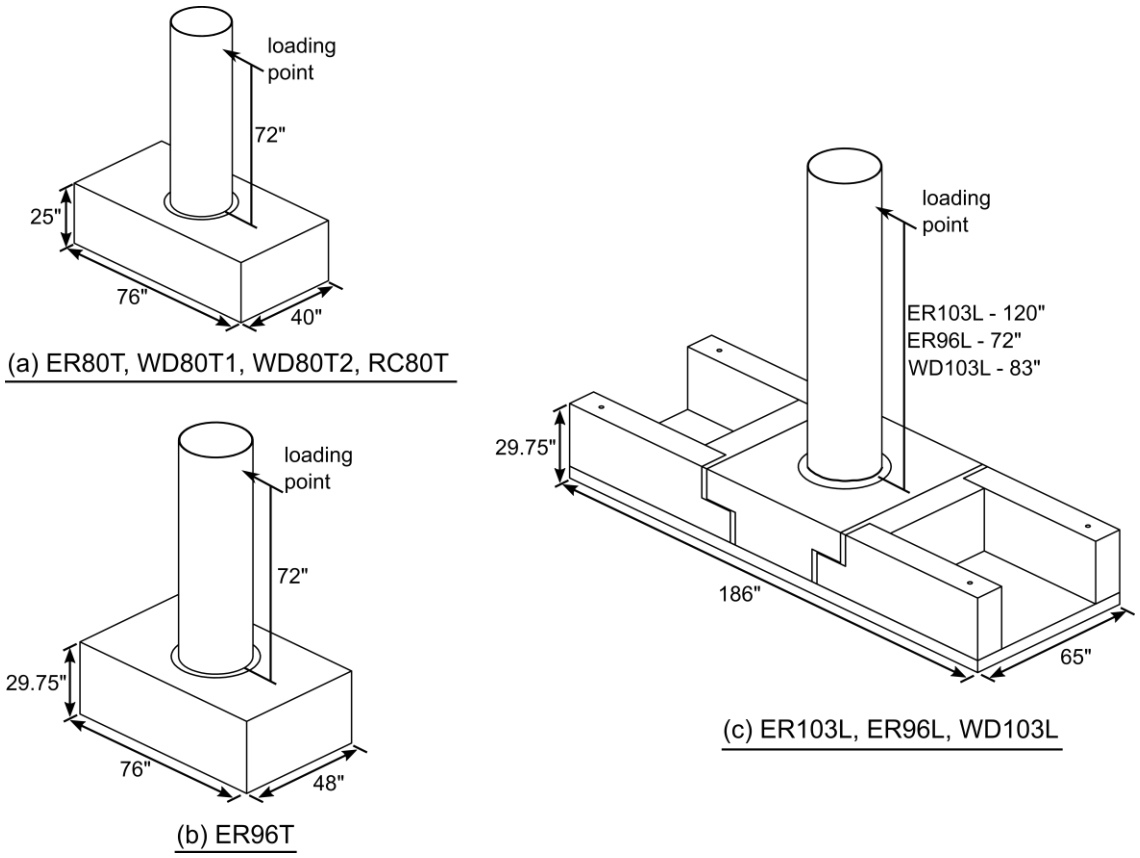

Fig. 7.1. Overview of Longitudinal and Transverse Specimen Geometries

7.1 Specimen Construction

The specimens were constructed in the Structural Testing Laboratory at the University of Washington. To eliminate the need for the construction of temporary shoring, all of the specimens were constructed upside-down (i.e. the columns were cast into the cap-beams while the cap-beams rested on the floor). This resulted in construction sequences and practices which would not be used in the field. The following sections will briefly describe the sequence used to construct each specimen.

7.1.1 Transverse Specimens

The construction sequences for cap beams in the transverse specimens were identical, as each connection utilized a void cast into the cap using a corrugated pipe. The cap beams were cast on the floor with the void facing the ceiling as is shown in Fig. 7.2. The remaining construction sequence for each specimen is described below, construction photos for the ER, WD, and RC specimens are shown in Fig. 7.3 - Fig. 7.5, and the construction sequence for all transverse specimens is illustrated in Fig. 7.6.

ER – (1) The annular ring was welded to the base of the steel tube using a ¼-in. fillet weld on the inside and outside of the tube, (2) the column was leveled and grouted into the void, and (3) the column was cast using-self consolidating concrete with low shrinkage admixture.

WD – (1) The annular ring was welded to the exterior of the tube using a ¼-in. fillet weld, (2) the reinforcing bars were temporarily supported and welded to the inside of the steel tube, (3) in the case of WD80T2, PVC was placed around the reinforcing bars in the connection region to provide de-bonding, (4) the reinforcing bars were grouted into the void, and (5) the column was cast using self-consolidating concrete with low shrinkage admixture.

RC – (1) The reinforcing cage was assembled and grouted into the void, (2) the steel tube was temporarily supported above the reinforcing cage, and (3) the column was cast using self-consolidating concrete with low shrinkage admixture.

Fig. 7.2. Transverse Formwork

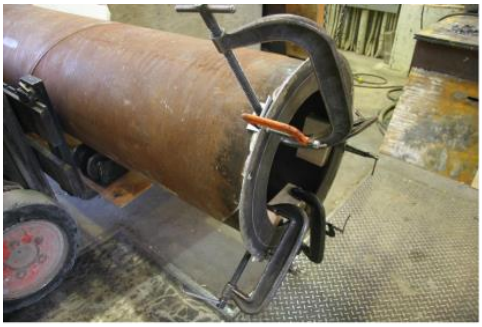

(a) annular ring

(b) steel tube placed into void in cap

Fig. 7.3. ER Construction Photos

(a) annular ring

(b) welded dowels

(b) dowels placed into void in cap

Fig. 7.4. WD Construction Photos

Fig. 7.5. Cage Used in RC Specimen

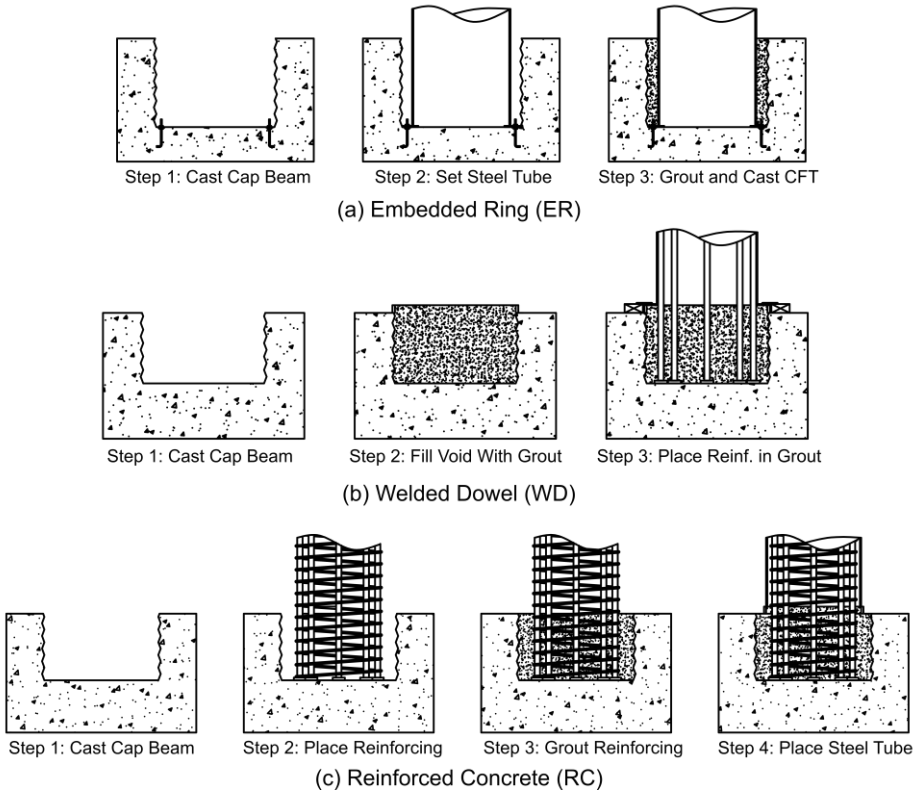

Fig. 7.6. Transverse Specimen Construction Sequence

7.1.2 Longitudinal Specimens

The longitudinal specimens were constructed to evaluate the behavior of the ER and WD connections for loading in the longitudinal direction of the bridge, and to demonstrate that these

connections can be integrated into a precast inverted-t pier cap. Thus the superstructure of each of the specimens were constructed in 4 steps: (1) the inverted-t component was precast with a void created using a corrugated pipe, (2) the superstructure including diaphragm, deck, and longitudinal girders were cast around the inverted-t, (3) the annular ring or flange was welded to the base of the tube, and (4) the columns were grouted into the superstructure. Typical construction photos of the precast inverted-t and diaphragm and girder reinforcing cages are shown in Fig. 7.7, and the construction sequence is illustrated in Fig. 7.8.

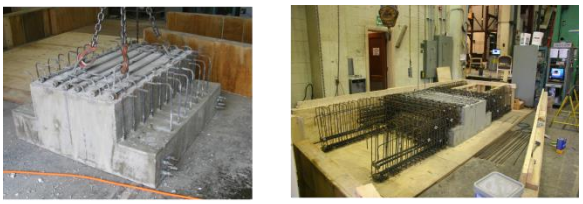

(a) Inverted-t (b) Superstructure Cage

Fig. 7.7. Longitudinal Construction Photos

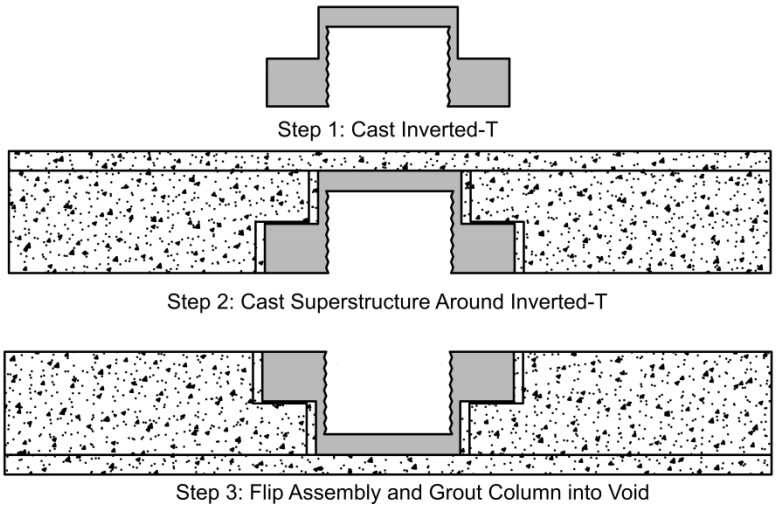

Fig. 7.8. Longitudinal Construction Sequence

7.2 Test Setup

The specimens were tested using a self-reacting test frame with a horizontal actuator to apply lateral load, and a Baldwin Universal Testing Machine to apply a constant lateral load as shown

in Fig. 7.9. The transverse specimens were fully supported on the reaction block, while the longitudinal specimens were supported under the column and at the ends of the longitudinal girders as illustrated in Fig. 7.10. The fully supported condition in the transverse experiments represents a conservative estimation of connection performance in terms of ductility, as flexural deformation in the cap beam is neglected. The longitudinal specimens were supported under the column to allow flexural deformation of the superstructure, while eliminating a transfer of the column dead load into the longitudinal girders. The length of these girders was restricted by the geometric limitations of the cap beam; supporting the column dead load ensured shear failure would not develop at the longitudinal girder-to-cap beam interface, since the longitudinal beam connection was not the focus of this research and was based upon a prior Caltrans research study.

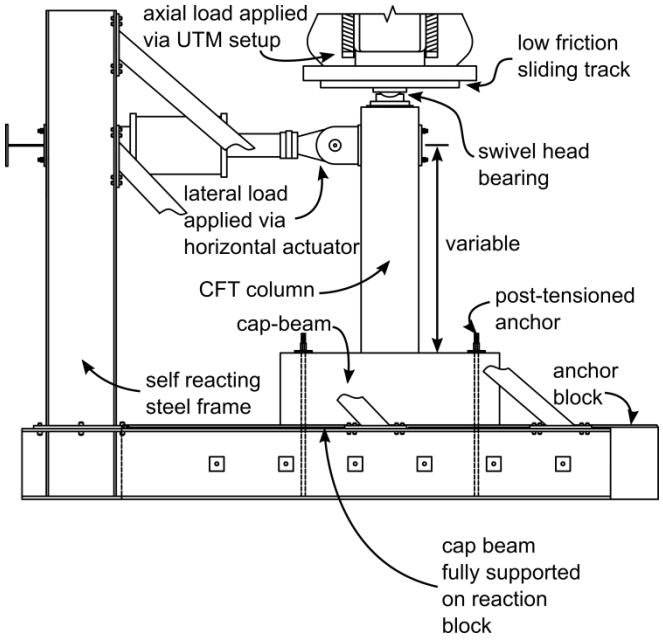

Fig. 7.9. Test Apparatus with Transverse Specimen

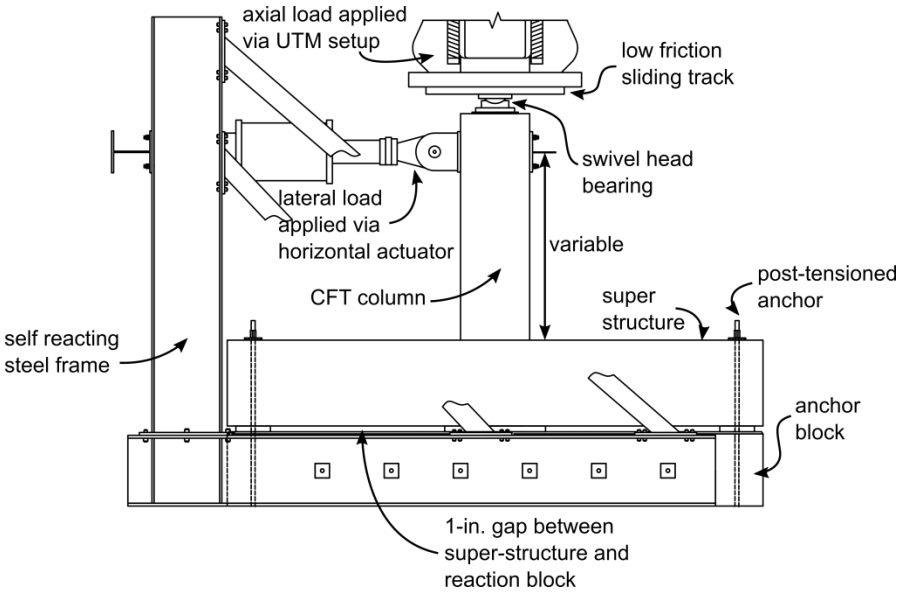

Fig. 7.10. Test Apparatus with Longitudinal Specimen

The self-reacting rig was centered under a Baldwin Universal Testing machine with a compressive capacity of 2400-kips. Each specimen was leveled, and grouted into place using Hydrostone, and the specimen was anchored and post-tensioned to the base of the test apparatus with 4-1 ¼-in. Williams Form Engineering All-Thread high-strength steel bars post-tensioned to 120-kips. The anchor rods were placed at a position to minimize confinement of concrete and to avoid development of additional resistance to the foundation in the area where cone pullout failure of the foundation could occur.

The actuator was clamped to the CFT column by a pair of machined blocks, which conformed to the outside diameter of the tube, and were post-tensioned to the tube using four 1 ¼-in. Williams All Thread bars to prevent all slip and movement during loading. The actuator had a pin swivel connection at each end, to prevent development of moment in the actuator or the specimen.

A spherical, swivel-head bearing was fixed to the top of the CFT column to allow for lateral displacements while still maintaining a constant axial load. The bearing sat within a recessed steel plate, which was lined with a dimpled polytetrafluoroethylene (PTFE) sliding surface, as shown in Fig. 7.11. Under lateral loading, the PTFE slid within a stainless steel-lined channel, which was fixed to the bottom of the Baldwin head to prevent out-of-plane movement. A silicone grease lubricant was applied between the PTFE and stainless steel to create a low-friction sliding surface. Research has shown that this arrangement results in friction less than one tenth of one percent of the applied load.

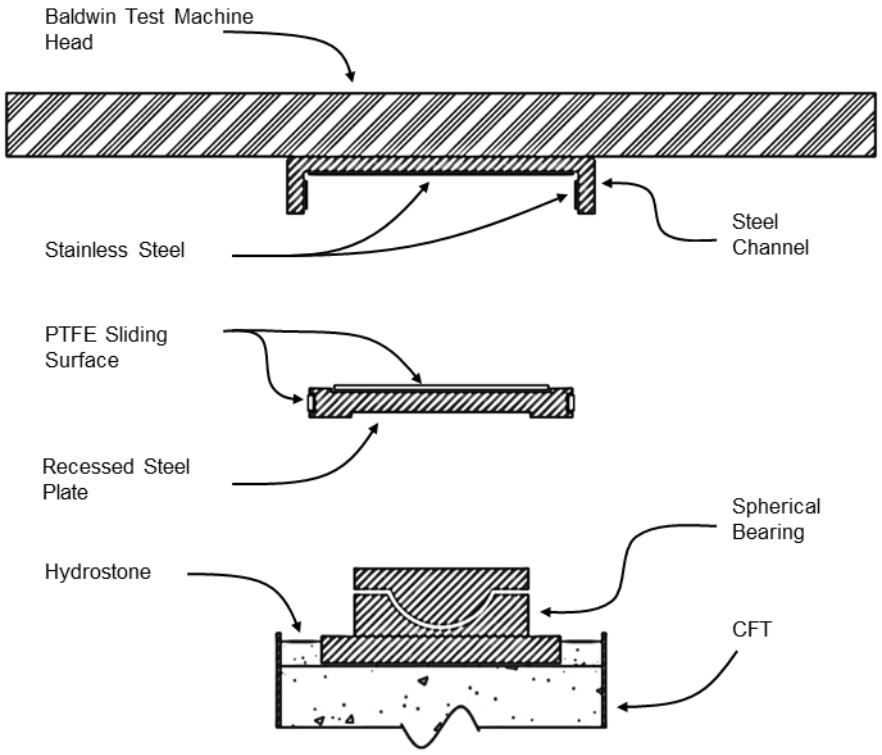

Fig. 7.11. Spereical Bearing and Low Friction Sliding Surface

Each specimen was subjected to a constant axial load of either 10% or 5% of the gross crush capacity $P_o=(A_{st}F_{y,st}+0.95Acf'_{cf})$ of the column as indicated in Table 8.1, as well as a reversed cyclic lateral load with incrementally increasing displacements. The lateral load

displacement protocol was adapted from that of previous University of Washington tests, and the ATC-24 guidelines (ATC, 1992), in which the imposed displacements are based on incremental multiples of the member's yield displacement. The target lateral load protocol for each specimen is illustrated in Fig. 7.12.

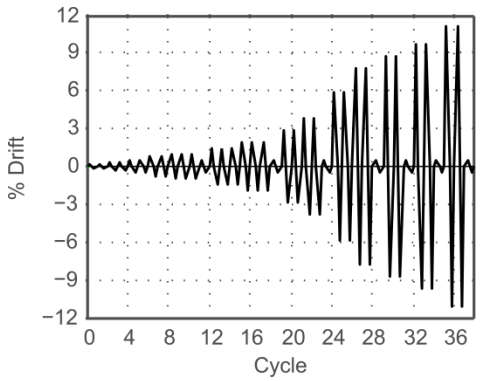

Fig. 7.12. Typical Lateral Deformation Test Protocol

7.3 Instrumentation

Significant instrumentation was attached to each specimen including strain gages, linear potentiometers, string potentiometers, and an Optotrak motion capture system. The instruments were electronically recorded using computer controlled data acquisition systems.

The applied gravity and lateral loads were directly measured using load cells, which were calibrated prior to testing for all tests. Strain gages were attached to the steel tube and reinforcing dowels as illustrated in Fig. 7.13, and were used primarily to measure elastic strains in the steel tube and dowels for evaluation of elastic curvature, elastic bending moments, and the plastic strain distribution the critical regions of the connections.

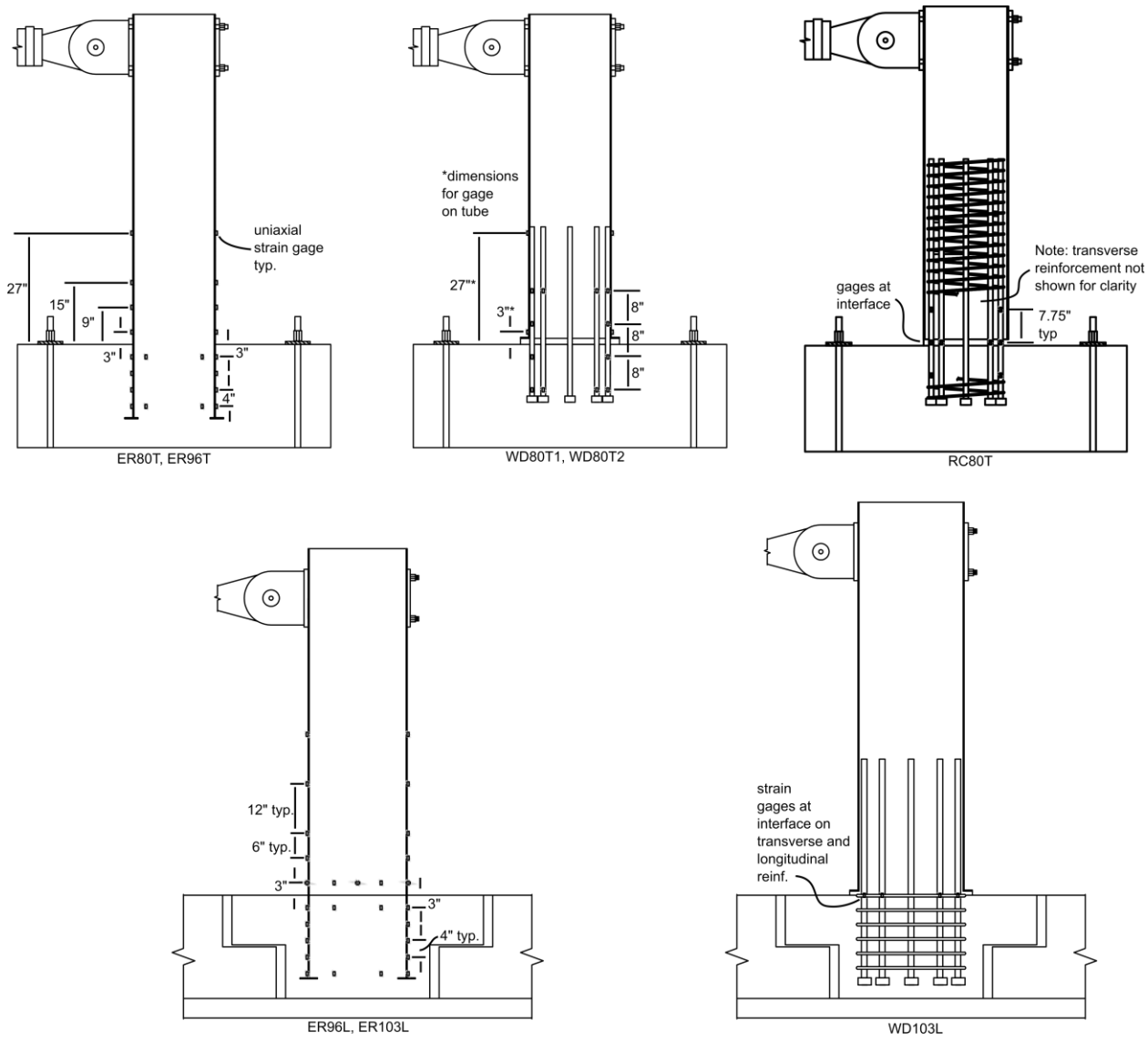

Fig. 7.13. Strain Gage Schematic

Displacements were measured using string potentiometers and short stroke Duncan potentiometers. String potentiometers can measure a large range of displacement (typically 10 to 20-in.), and they were used to measure the actual top displacement of the tube as illustrated in Fig. 7.14. String potentiometers were additionally used to measure tube displacement at 3 additional locations along the height of the tube to allow for development of a displaced profile

of the column, and track displacements within the plastic hinge region. Small stroke Duncan potentiometers were placed at locations where small displacements were expected as illustrated in Fig. 7.14. In particular, they measured slip or uplift of the specimen and the test rig. They were additionally used to monitor deformations along the length of the longitudinal girders in the longitudinal specimens as illustrated in Fig. 7.14.

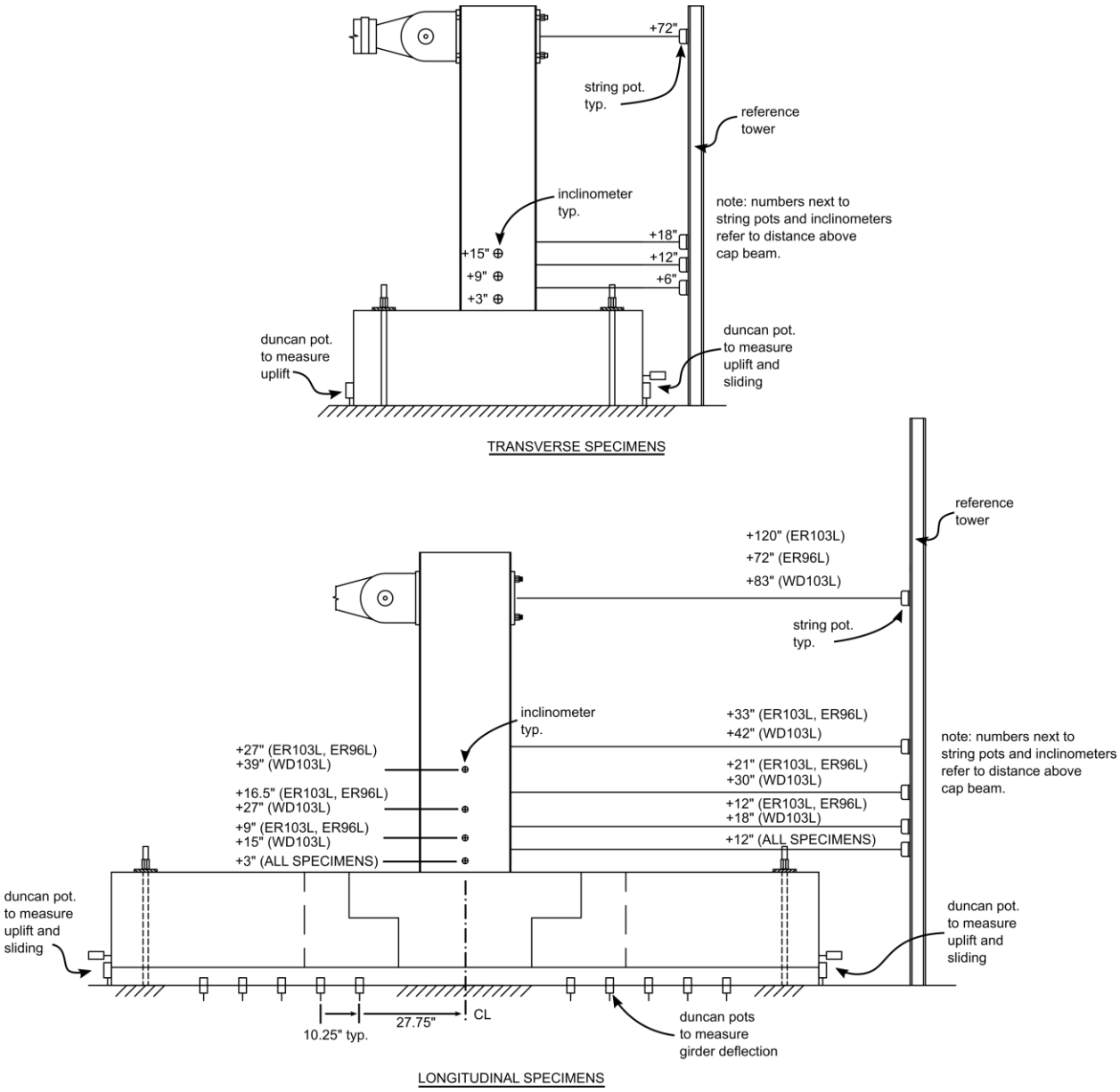

Fig. 7.14. String Potentiometer, Duncan Potentiometer, and Inclinometer Locations

Inclinometers were used to provide a redundant measurement of rotation along the height of the column. The inclinometers were spaced at varying intervals (depending on the specimen geometry) from the surface of the cap beam as illustrated in Fig. 7.14. The inclinometers were fixed to the East side of the column, which was closest to the data acquisition system.

Finally, an Optotrak Certus motion capture system was used to monitor the deformed shape of the columns during testing. The system consists of a 3-dimensional optical sensor and a series of LED markers, which were attached to the specimen using adhesive foam pads, and emit an electronic signal that is photographed by optical sensors. The optical sensors consist of 3 precision cameras, which locate the position of each LED marker in 3-dimensional space by triangulation of the relative positions noted by each camera. This system was used to capture the buckled shape of the tube as well as inelastic rotation, and relative displacement fields in the plastic hinge region of the columns. Measurements from the Optotrak system were compared to the string potentiometer and inclinometer data, and provided the most accurate and consistent measurements of the inelastic performance of the system. The placement of the LED targets is illustrated in Fig. 7.16 for all specimens.

Fig. 7.15. LED Emitters for Optotrak Measuring System on Specimen WD103L

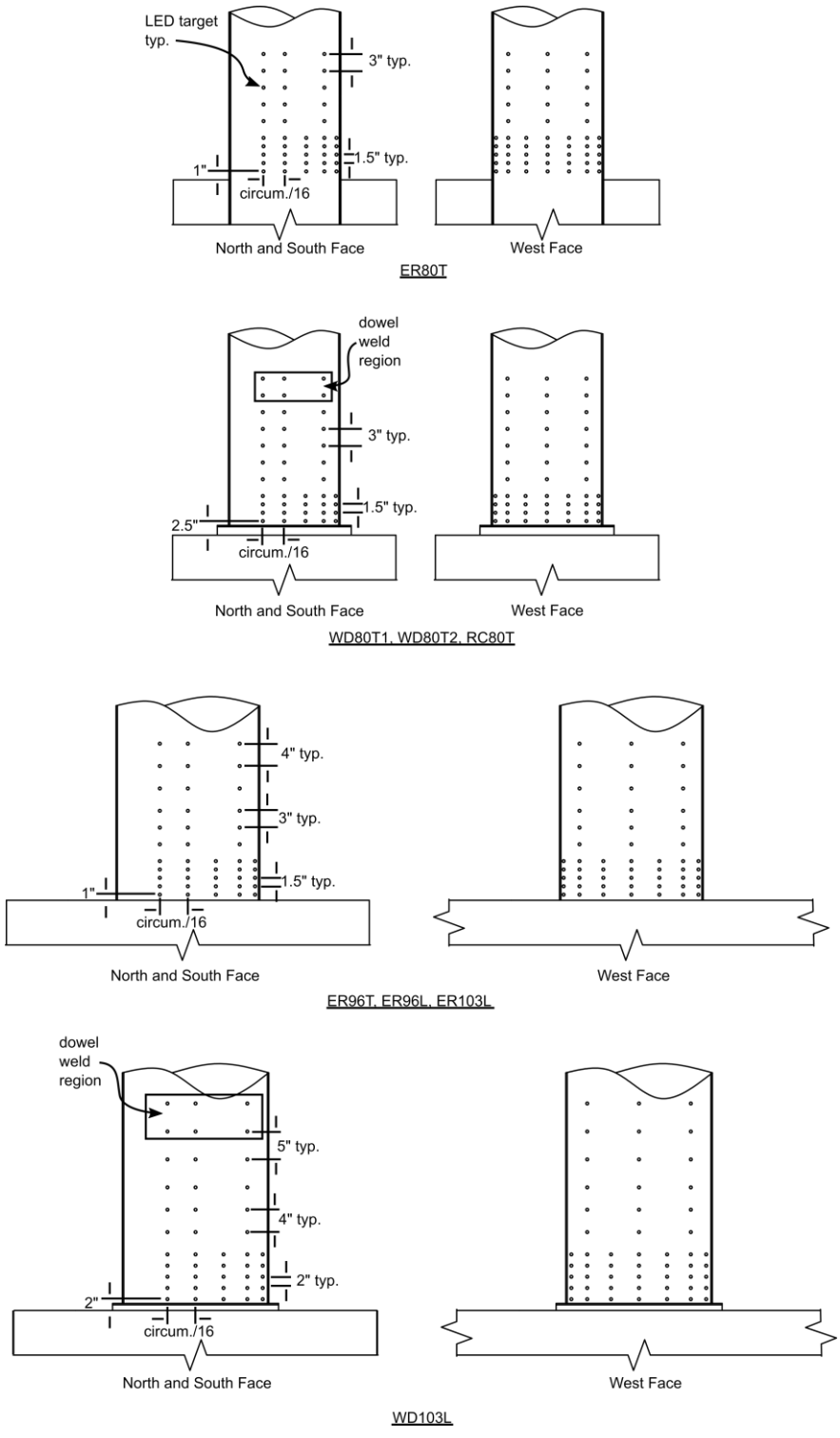

Fig. 7.16. Optotrak Target Layout

Chapter 8

CONNECTION TESTS: EXPERIMENTAL RESULTS

The primary focus of the research was the experimental testing of the eight (8) CFT column-to-cap beam connection specimens described previously. The specimens investigated the influence of several design parameters including type of tube, type of connection, and the effect of longitudinal and transvers loading, as shown in Table 7.1. The tests were completed during the period between October 2013 and September 2014. The specimens were designed, built, and instrumented as summarized in Chapter 4 and Chapter 7. The experimental results are summarized here.

8.1 Overview of Test Matrix

Key results from the experiments for the eight specimens are summarized in Table 8.1, while test day material strengths are given in

Table **8.2**. The performance of each connection was assessed based on the secant stiffness to $0.8M_y$ of the CFT, maximum moment resistance, maximum drift, and the drift where the resistance decreased to 80% of its maximum.

Secant stiffness was measured when the moment resistance achieved approximately 80% of the yield moment of the CFT. Specimen stiffness is expresses as the ratio of the measured stiffness to the theoretical stiffness of the CFT ($EI_{measured}/EI_{eff}$) as calculated using the stiffness expression in AASHTO (2015). Using this method, $EI_{measured}/EI_{eff}$ values greater than 1.0 would suggest a larger stiffness than the theoretical stiffness of the CFT component, while $EI_{measured}/EI_{eff}$ values less than 1.0 would suggest a smaller initial stiffness.

Similarly, the moment resistance of each connection was evaluated by calculating the ratio of the maximum observed moment to the theoretical moment capacity of the CFT ($M_{max}/M_{p,CFT}$) as calculated using the PSDM. This method for estimating the combined moment-axial capacity of CFT components is discussed in detail in literature (Lehman and Roeder 2012). Using this method, $M_{max}/M_{p,CFT}$ values greater than 1.0 suggest that the connection exceeded the theoretical plastic moment capacity of the CFT, while $M_{max}/M_{p,CFT}$ values less than 1.0 suggest that the connection did not provide as much resistance as the theoretical plastic capacity expected for the CFT component.

Table 8.1. Experimental Results

Specimen	Axial Load Ratio (%)	Initial Stiffness $EI_{measured}/EI_{eff}$	Yield Drift[1] (%)	$M_{peak}/M_{P,PSDM}$	Drift at peak Moment (%)	Drift at 20% Degradation (%)
ER80T	10	0.98	1.3	1.2	7	7
ER96T	5	0.77	0.97	1.12	4.5	8.6
WD80T1	10	0.86	0.56	1.4	9.5	11.5
WD80T2	10	0.71	0.69	1.05	9.75	12.2
RC80T	10	0.69	0.67	0.92	7	10
ER103L	10	0.96	1.4	1.13	1.8	5
ER96L	5	0.6	1.1	1.19	4.4	7
WD103L	10	0.65	1.08	1.1	11.8	-

[1]Yield drift determined using strain gage data at cap beam interface.

Table 8.2. Test Day Material Strengths.

Specimen	$F_{y,st}$, ksi	$F_{u,st}$, ksi	$F_{y,b}$, ksi	$F_{u,b}$, ksi	f'_{cc}, ksi	$f'_{c,cap}$, ksi	f'_g, ksi
ER80T	60.2	68.5	-	-	10.7	9.9	6.8
ER96T	53	68.9	-	-	8.3	10.1	8.7
WD80T1	60.2	68.5	68.8	95.6	7.9	9.8	7.9
WD80T2	60.2	68.5	68.8	95.6	7.5	9.5	8.1
RC80T	60.2	68.5	68.8	95.6	9.7	10	10.6
ER103L	58	69.3	-	-	8.4	9.9	4.3
ER96L	53	68.9	-	-	7.9	7.7	8.9
WD103L	58	69.3	68.1	95	7.7	7.8	8.6

8.2 Summary of Individual Test Results

The following section provides a summary of the test results for each specimen including the hysteretic response, and damage progression. Note that the moment-drift behaviors have been

normalized by the theoretical plastic moment capacity of the CFT component as calculated using the PSDM.

8.2.1 ER80T

ER80T utilized a 20-in. diameter spiral welded ASTM A1018 grade steel tube with an embedded flange connection. The thickness of the steel tube was ¼-in., resulting in D/t = 80, and it was evaluated for loads and deformation transverse to the axis of the bridge. The purpose of this specimen was to evaluate the performance of the connection and cap beam using a reduced annular ring outer diameter (D+16t) and a reduced cap beam width of 2D. The revisions were proposed based upon a series of non-linear analysis of design parameters for this connection discussed in Chapter 5. The measured moment-drift response is illustrated in Fig. 8.1. This specimen exhibited an initial stiffness $EI_{measured}/EI_{eff}$ = 0.98, and a maximum moment $M_{max}/M_{p,CFT}$ = 1.2.

During loading at 1.3% drift, yielding of the steel tube was measured by strain gauges located on the CFT column 3-in. from the surface of the cap beam on both the North and South sides of the column. At 1.45% drift, circumferential hairline cracks initiated along the grout interface on the North side of the specimen, as shown in Fig. 8.2a. At this same drift, cracks were observed propagating radially in the grout pad and the cap beam, as shown in Fig. 8.2a. These cracks were hairline in width, and they continued propagating down the East and West sides of the cap beam. During the third cycle at 1.45% drift, slight flaking of the grouted region was observed near the grout-cap beam interface, as shown in Fig. 8.2. The portions of grout that flaked off ranged between ½-in. and 1-in. in diameter, and were less than ¼-in. in thickness.

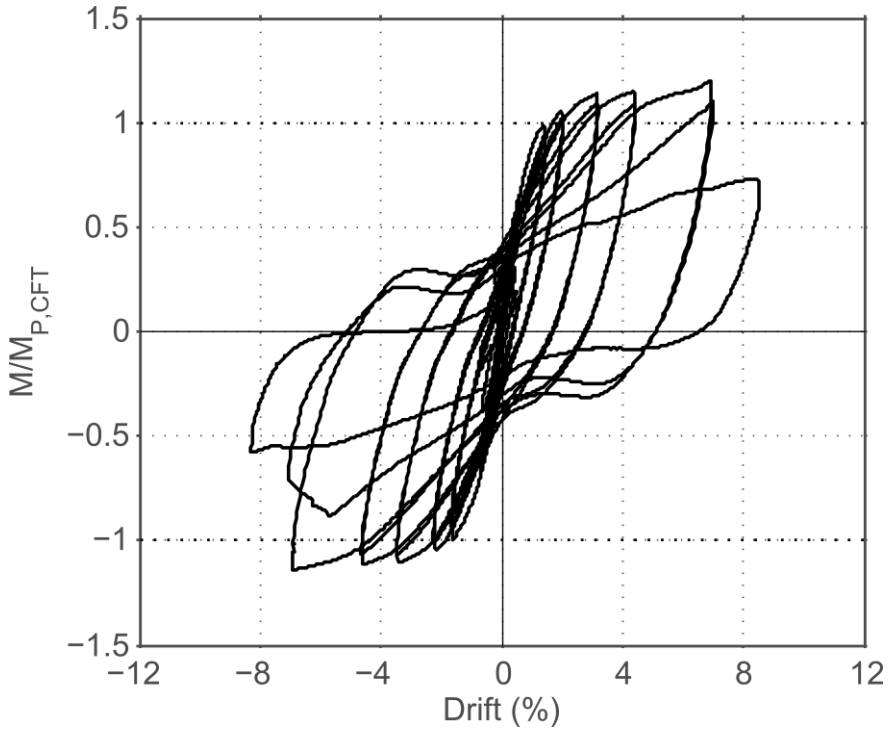

Fig. 8.1. Moment-Drift Behavior of Specimen ER80T

Initial buckling of the North and South sides of the steel tube was observed visually during loading at 3.19% and -3.45% drift, respectively. The apex of the buckled region was approximately 1.75-in. above the surface of the cap beam and had very small amplitude, as shown in Fig. 8.2b. Additional hairline cracks formed radially in the top surface of the cap beam, as well as vertically and diagonally down the East and West faces of the cap beam. No cracks were observed on the North and South faces of the cap beam. Cyclic deformation continued to increase with virtually no deterioration in resistance, but increased amplitude of the buckled shape up to 7.7% drift.

Tearing initiated at the apex of the buckled region on both the North and South sides of the column during cycling at 7% drift, and continued to grow with increasing lateral deformations. At 8.54% drift, the tearing propagated around the base of the column. The test was

stopped after cycling at 8.75% drift as tearing continued to propagate around the base of the column as illustrated in Fig. 8.2f. However, the lateral resistance remained at around 50% of the maximum at this damaged state. The concrete was well confined at the point. There was no spalling or significant damage to the concrete fill, and the column retained its ability to support the full axial load.

(a) 1.5% Drift

(b) 3.75% Drift

(c) 7.5% Drift

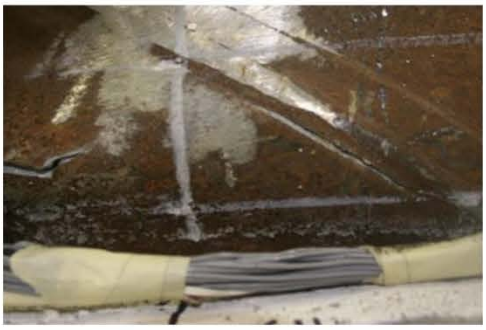

(d) 7.5% Drift

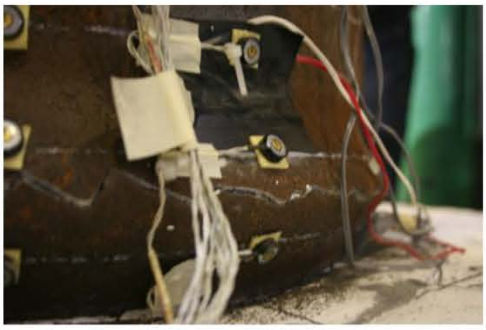

(e) 7.5% Drift

(f) final state (8.75% Drift)

Fig. 8.2. Photos Primary Damage States of Specimen ER80T

8.2.2 ER96T

ER96T utilized a 24-in. diameter straight seam API 5L X-42 grade steel with an embedded ring connection. The thickness of the steel tube was ¼-in., resulting in D/t = 96. This specimen had similarities with ER80T, but used a larger D/t ratio and a different grade of steel. The API 5L specification has tighter requirements on the material properties and manufacturing of the tube. However, the increased D/t ratio is generally expected to to cause earlier buckling and deterioration of resistance. The D/t ratio of this specimen satisfies the D/t requirement for the current AASHTO LRFD (2015) specification, but is approximately within 7% of the limit. The measured moment-drift response is illustrated in Fig. 8.3. This specimen exhibited an initial stiffness $EI_{measured}/EI_{eff} = 0.77$, and a maximum moment $M_{max}/ M_{p,CFT} = 1.12$.

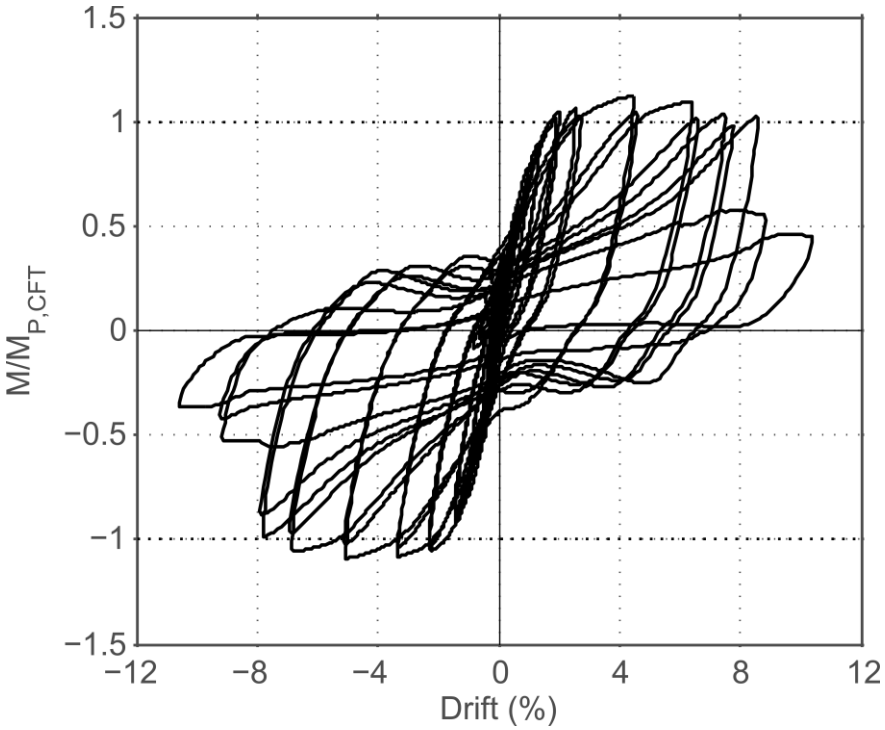

Fig. 8.3. Moment-Drift Response of Specimen ER96T

There was no visible damage to the cap beam or column during the initial load cycles up to 0.5% drift. At 0.5% drift, circumferential hairline cracks initiated along the column-grout interface on both the North and South sides of the specimen, as each side was respectively subjected to tensile loading. Yielding was measured by strain gages located on the CFT column 3-in. from the surface of the cap beam during cycling at 0.97% drift.

Local buckling was observed during the 3% drift cycle as illustrated in Fig. 8.4. The apex of the buckle was approximately 2.5-in. from the surface of the cap beam, but the amplitude of the buckle was quite small as shown in Fig. 8.4a. There was no significant cracking observed in the cap beam or grout region during subsequent cycles, and the out of plane displacement of the buckled region continued to grow as shown in Fig. 8.4b. Tearing initiated at the apex of the buckled region on the North side of the column, and at the interface between the column and cap beam on the South side of the column during cycling at 8.75% as shown in Fig. 8.4. Tearing propagated around the base of the column during cycling at 9.15% drift, and the test was stopped due to significant strength degradation. The CFT column retained approximately 35% of its maximum moment capacity at 9.75% drift, while supporting the full axial load. There was virtually no damage to the concrete fill at these large deformations as shown in Fig. 8.4d.

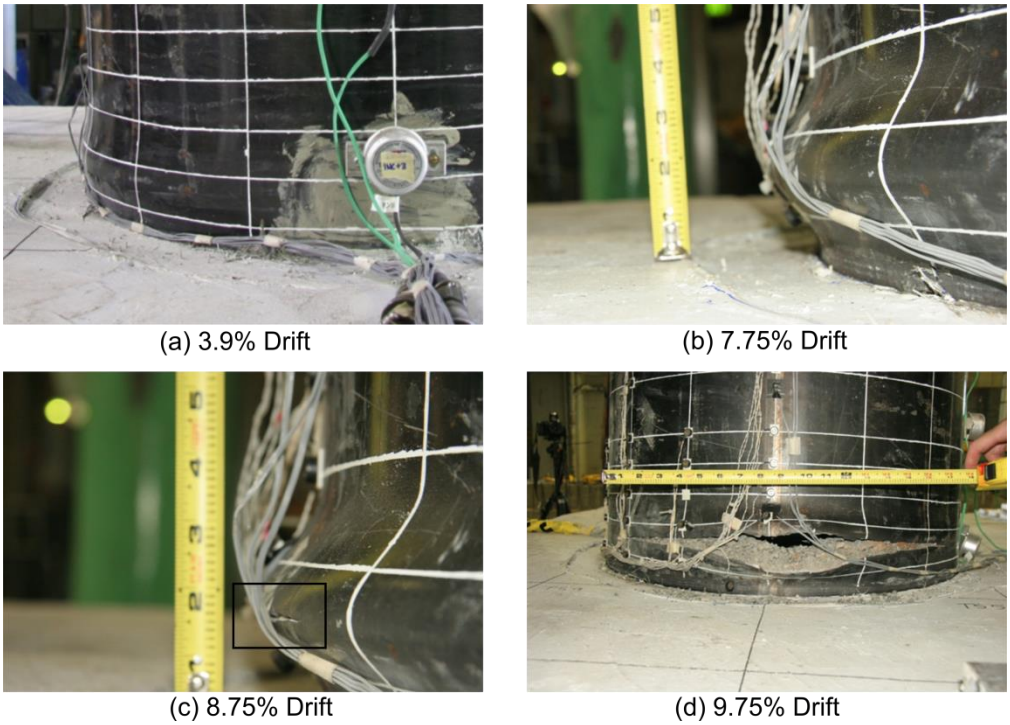

(a) 3.9% Drift (b) 7.75% Drift

(c) 8.75% Drift (d) 9.75% Drift

Fig. 8.4. Photos of Specimen ER96T

8.2.3 ER96L

EMB96L utilized a 24-in. diameter straight seam API 5L X-42 grade steel with an embedded flange connection. The thickness of the steel tube was ¼-in., resulting in D/t = 96. The specimen was similar to ER96T except that it evaluated the effect of loads and deformations in the longitudinal axis of the bridge instead of the transverse direction as for ER96T.

The measured moment-drift response is illustrated in Fig. 8.5. This specimen exhibited an initial stiffness $EI_{measured}/EI_{eff,CFT}$ = 0.6, and a maximum moment $M_{max}/ M_{CFT,PSDM}$ = 1.19. It should be noted that the reduced stiffness is at least partially due to increased deformation caused by the longer length of the longitudinal beams compared to the beam cap length for the transverse specimens.

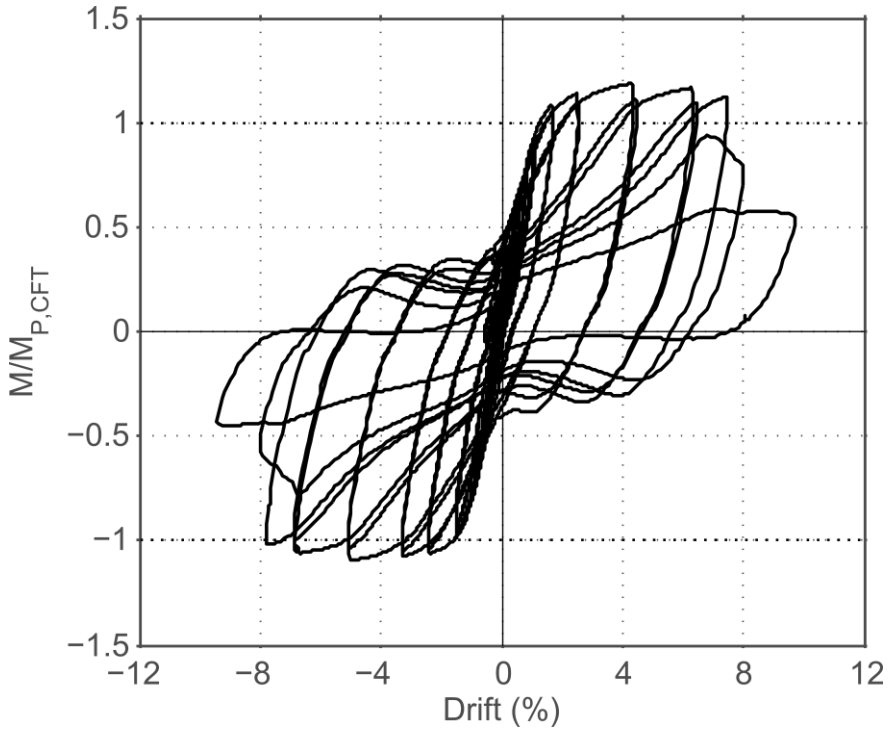

Fig. 8.5. Moment-Drift Behavior of Specimen EMB96L

There was very limited visible damage to the column or cap beam through cycling at 0.5% drift. At this point, several circumferential hairline cracks developed at the grout-to-corrugated pipe interface. Several hairline cracks additionally extended radially into the cap beam from the column. Yielding was measured by the strain gages on the CFT column located 3-in. from the surface of the cap beam during cycling at 1.1% drift.

Local buckling was observed during cycling at 3% drift, and the amplitude of the bulge was relatively small at 3.5% drift as illustrated in Fig. 8.6a. The apex of the buckle was approximately 2-in. above the surface of the cap beam. There was no significant cracking observed in the cap beam or grout region during subsequent cycling, and the out-of-plane deformation of the buckled region continued to grow as shown in Fig. 8.6b. Tearing initiated at the apex of the buckled region on both the North and South side of the column during cycling at

7.5% drift as seen in Fig. 8.6c. Tearing propagated around the base of the column at 9% drift, and the test was stopped due to degradation of resistance. The specimen retained approximately 40% of its maximum moment capacity and support the full axial load at more than 9% drift.

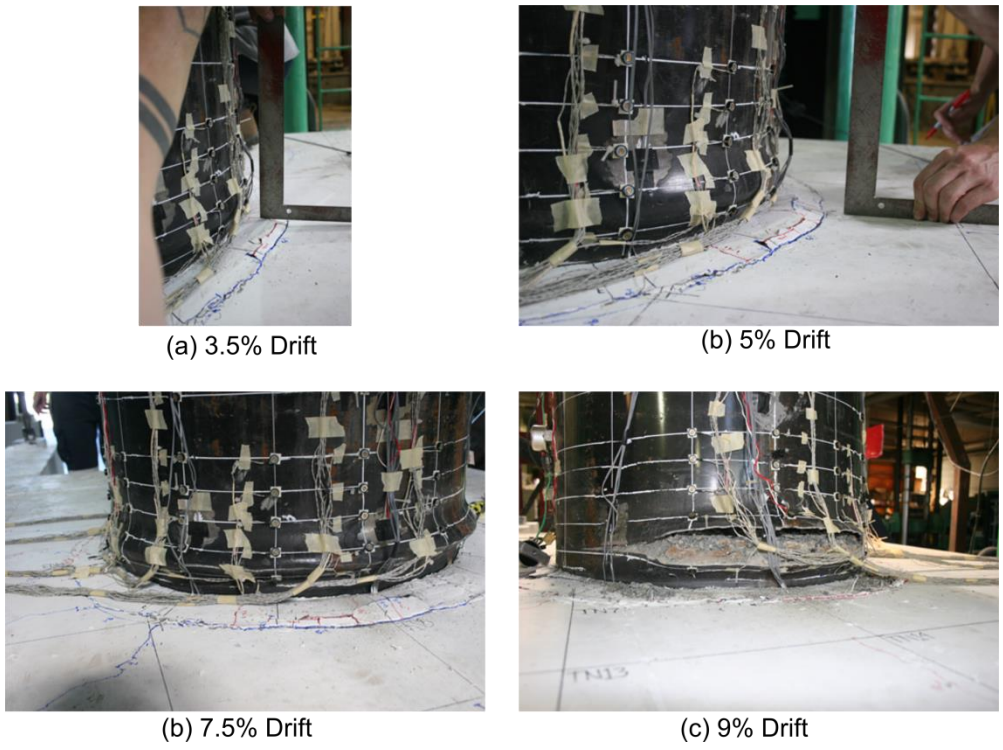

Fig. 8.6. Photos of Specimen EMB96L

8.2.4 ER103L

ER103L utilized a 25.75-in. diameter spiral welded ASTM A1018 grade steel with an embedded flange connection. The thickness of the steel tube was ¼-in., resulting in D/t = 103. This specimen was loaded and deformed in the longitudinal direction of the bridge as for ER96L, but it employed a lower grade of steel than ER96L. It also had a larger D/t ratio than the prior ER connection specimens, and it was expected to buckle at smaller deformations and to sustain earlier deterioration of resistance and tearing of the buckled steel. The CFT member exceeds the D/t limit permitted by the current AASHTO LRFD specification by approximately 18%.

The purpose of this specimen was to evaluate the performance of the connection and cap beam for loading in the longitudinal direction of the bridge with a different grade of steel tube.

The measured moment-drift response is illustrated in Fig. 8.7. This specimen exhibited an initial stiffness $EI_{measured}/EI_{eff,CFT}$ = 0.96, and a maximum moment $M_{max}/ M_{CFT,PSDM}$ = 1.13. It is interesting to note that this specimen did not experience the reduced stiffness for longitudinal deformation noted with the other specimens.

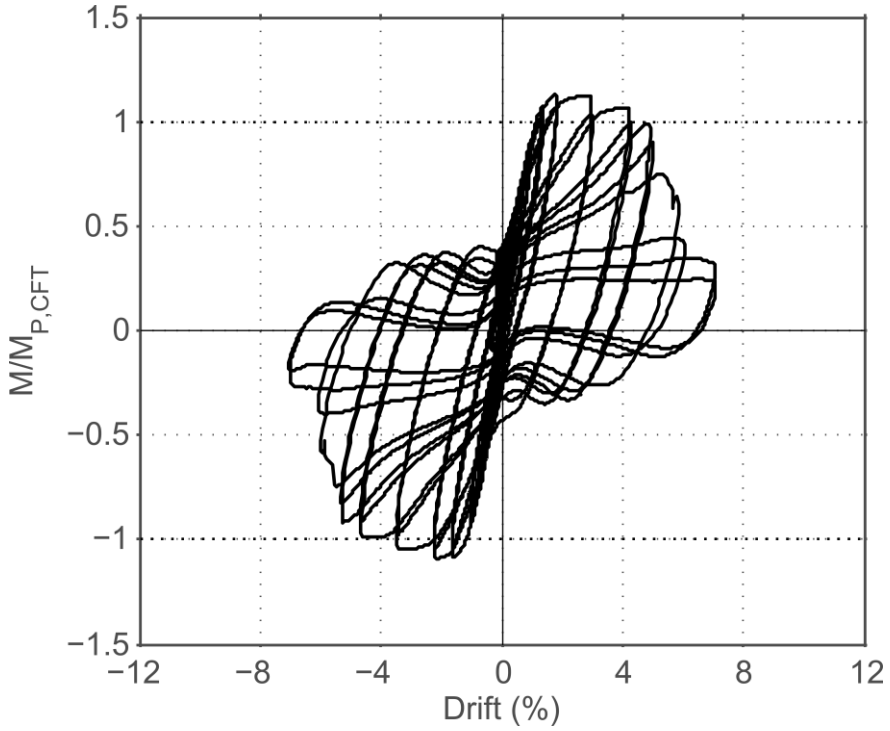

Fig. 8.7. Moment-Drift Behavior of Specimen ER103L

There was very limited visible damage to the column or cap beam through cycling at 0.75% drift. At this point, several circumferential hairline cracks developed at the grout-to-corrugated pipe interface. Several hairline cracks additionally extended radially into the cap

beam from the column. Yielding was measured by the strain gages located in the CFT column 3-in. from the surface of the cap beam during cycling at 0.96% drift.

Local buckling was observed during cycling at 3.5% drift as shown in Fig. 8.8a. The apex of the buckle was approximately 1.5-in from the surface of the cap beam. Tearing initiated at the apex of the buckled region on the North and South sides during the 5.5% drift cycles. The length of the initial observed tear was rather large (~6-in.) as illustrated in Fig. 8.8b. Tearing propagated around the base of the steel tube during cycling at 7.5% drift, and the test was stopped due to significant strength degradation. The moment capacity was approximately 20% of the maximum tearing of the tube, and the full axial compression capacity was maintained. The earlier buckling and tearing of this tube illustrate the importance of the D/t slenderness limit.

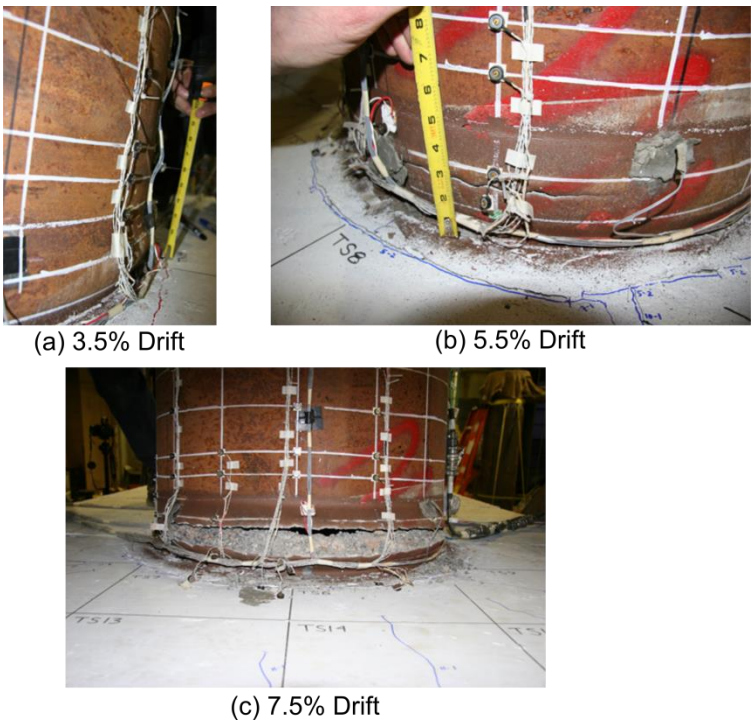

(a) 3.5% Drift (b) 5.5% Drift

(c) 7.5% Drift

Fig. 8.8. Photos of Specimen ER103L

8.2.5 WD80T1

WD80T1 utilized 20-in. diameter spiral welded ASTM A1018 grade steel tube with a welded dowel connection consisting of 8 No. 9 headed bars embedded into the cap beam and welded to the steel tube. The purpose of this specimen was to evaluate the behavior of this connection type, and to provide comparison to the embedded ring connections. The measured moment-drift response is given in Fig. 8.9. The steel tube was similar to that of ER80T. The area of the 8 No. 9 bars was significantly smaller than the area of the steel tube, but the tensile capacity of the bars and the tube were similar, because the ultimate tensile stress of the reinforcing bars was significantly larger than that of the tube. The rebar was bonded to the concrete throughout the connection. The specimen exhibited an initial stiffness $EI_{measured}/EI_{eff,CFT} = 0.86$, and a maximum moment $M_{max}/ M_{CFT,PSDM} = 1.4$.

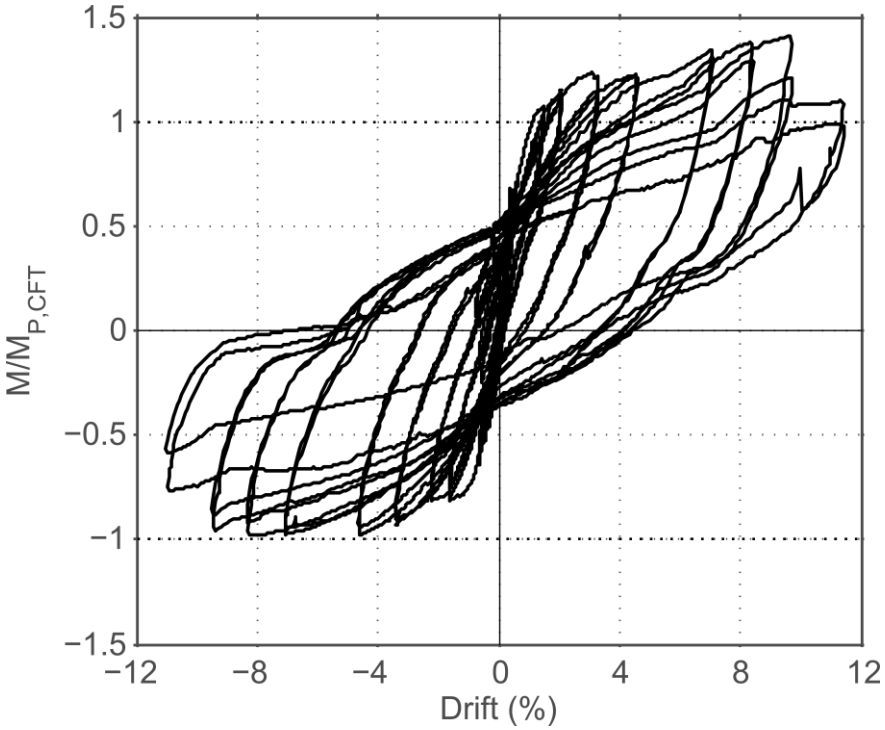

Fig. 8.9. Moment-Drift Behavior of Specimen WD80T1

There was no observed damage to the specimen during cycling up to 0.5% drift. During the third drift set at 0.5% drift, a hairline crack initiated circumferentially along the grout soffit fill-steel flange interface on both the North and South sides of the specimen. On the South side of the specimen, a circumferential hairline crack also initiated along the base of the soffit fill, at the grout-cap beam interface. The existing circumferential cracks along the grout soffit fill gradually widened with increasing drift levels. During the 7th drift set, the openings between the soffit fill and the flange on both the North and South sides of the column opened to approximately 4-mm while they were each subjected to tensile loading. The existing opening between the soffit fill and cap beam on the South side of the specimen increased to approximately 3-mm, while circumferential hairline cracks began to just initiate at the base of the soffit fill on the North side of the specimen. Yielding was measured by the strain gages on the longitudinal dowels during cycling at 0.56% drift. During the cycling at 1.5% drift, hairline cracks initiated radially in the grouted soffit fill, as well as in the cap beam. The cap beam cracks formed at approximate angles of 30-45° of one another, and continued vertically down the East and West faces of the cap beam.

For drifts greater than 2%, cracks continued to initiate radially from the column as target drift levels increased. During the 2.5% drift set, some of the existing radial cracks in both the cap beam and grout pad were observed to have widened slightly, such that they were no longer hairline in width. In addition, the opening between the grout pad and the column flange increased to approximately 6-mm as each side of the specimen was cycled into tensile loading (illustrated in Fig. 8.10b). The longitudinal reinforcing became visible during cycling at 7.08% drift, and soffit fill and cap beam damage continued to grow. The column began to pull out of the cap beam during cycling at 8.33% drift, as large cracks developed between the anchor rods and

column. These cracks continued to grow until cycling at 13% drift at which point the test was terminated as a result of cap beam damage as illustrated in Fig. 8.10f. The specimen developed large resistance and deformation, but did great damage to the cap beam. The resistance shown in Fig. 8.9 is much larger in one direction than the other, and this is partially attributed to the severe damage to the to the concrete caused by the initial yielding cycles of the rebar. The bonded bar contributes greater resistance, but the greater structural damage is expected with bonded bars.

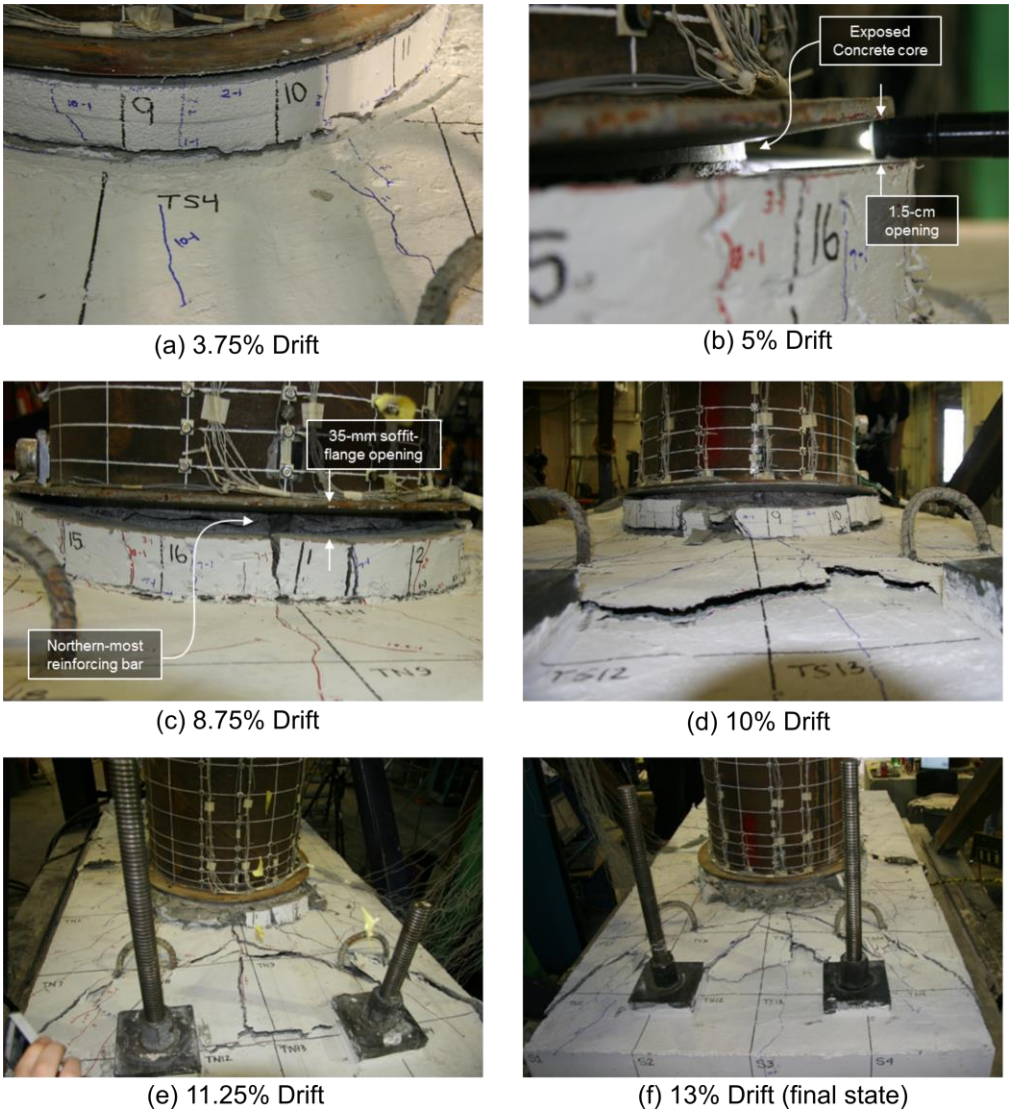

(a) 3.75% Drift

(b) 5% Drift

(c) 8.75% Drift

(d) 10% Drift

(e) 11.25% Drift

(f) 13% Drift (final state)

Fig. 8.10. Photos of Specimen WD80T1

8.2.6 WD80T2

WD80T2 has the same tube, reinforcing bars, and connection details of WD80T1, except the longitudinal dowels were de-bonded for a length of 20-in. The dowels were de-bonded to improve the inelastic deformation capacity and significantly reduce the concrete damage in the connection.

The measured moment-drift response is given in Fig. 8.11. The specimen exhibited an initial stiffness $EI_{measured}/EI_{eff,CFT} = 0.71$, and a maximum moment $M_{max}/ M_{CFT,PSDM} = 1.05$.

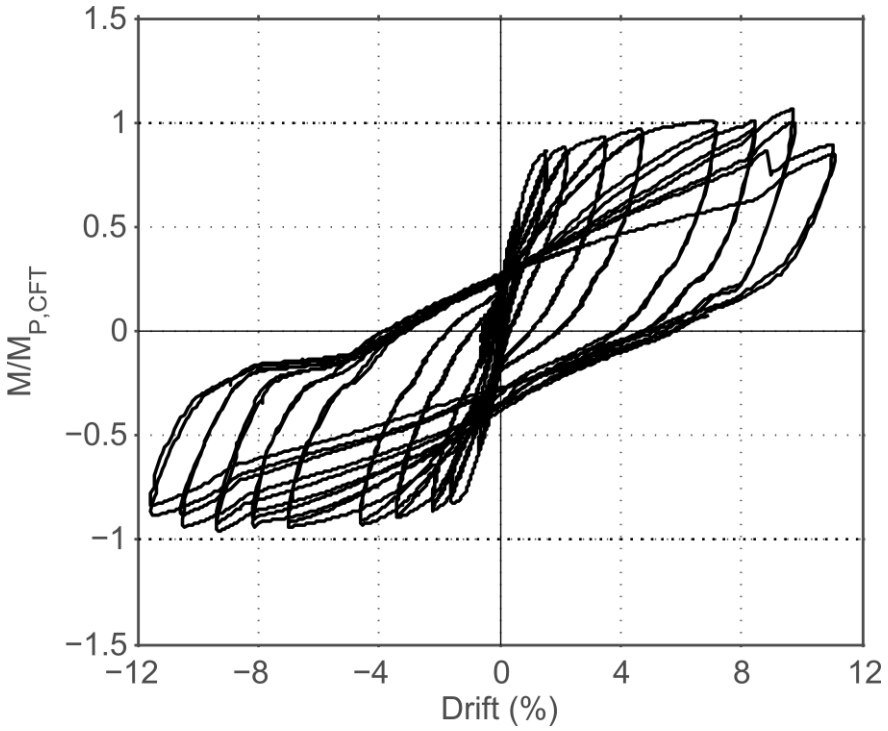

Fig. 8.11. Moment-Drift Behavior of Specimen WD80T2

Yielding was measured by strain gages on the longitudinal dowels during cycling at 0.69% drift. A circumferential crack initiated on the North side of the soffit fill as the specimen was subjected to 1.58% drift in South direction. At this drift level, radial hairline cracking was observed in the grouted soffit fill region, as well as in the cap beam. The cap beam cracks

initiated radially from the grouted region, and propagated vertically and diagonally down the East and West sides of the cap beam. As the column cycled back and forth, an opening formed between the soffit fill and the annular ring on the side of the specimen subjected to tensile loading as shown in Fig. 8.12a.

As drift levels increased, new radial cracks continued to develop throughout the grout pad and the cap beam. While the majority of the cracks remained hairline in width for several proceeding cycles, a few of the cracks increased slightly in width during the 1.5% drift set. At 2.24% drift to the South, the cracks propagating in the NE and NW directions increased to approximately 0.5-mm in width. The opening between the soffit fill and the flange on the North side of the specimen reached approximately 10-mm as it was subjected to peak tensile loading, as shown in Fig. 8.12. A majority of the cracks remained hairline during subsequent cycling, and the longitudinal dowels became visible at 7% drift as shown in Fig. 8.12. At the same time, radial cracks in the cab beam between the column and anchors began to grow.

The northern most longitudinal dowel fractured during the first excursion to 11% drift, resulting in 33% degradation in strength. A second reinforcing bar fractured on the north side on the second excursion to 11% drift, resulting in 46% degradation in strength. Although the cap-beam appeared to remain elastic for loading in the Southern direction (i.e. when tension was applied to the Northern most bars), large radial cracks developed on the South side of the cap beam during cycling at 11% drift as illustrated in Fig. 8.12d.

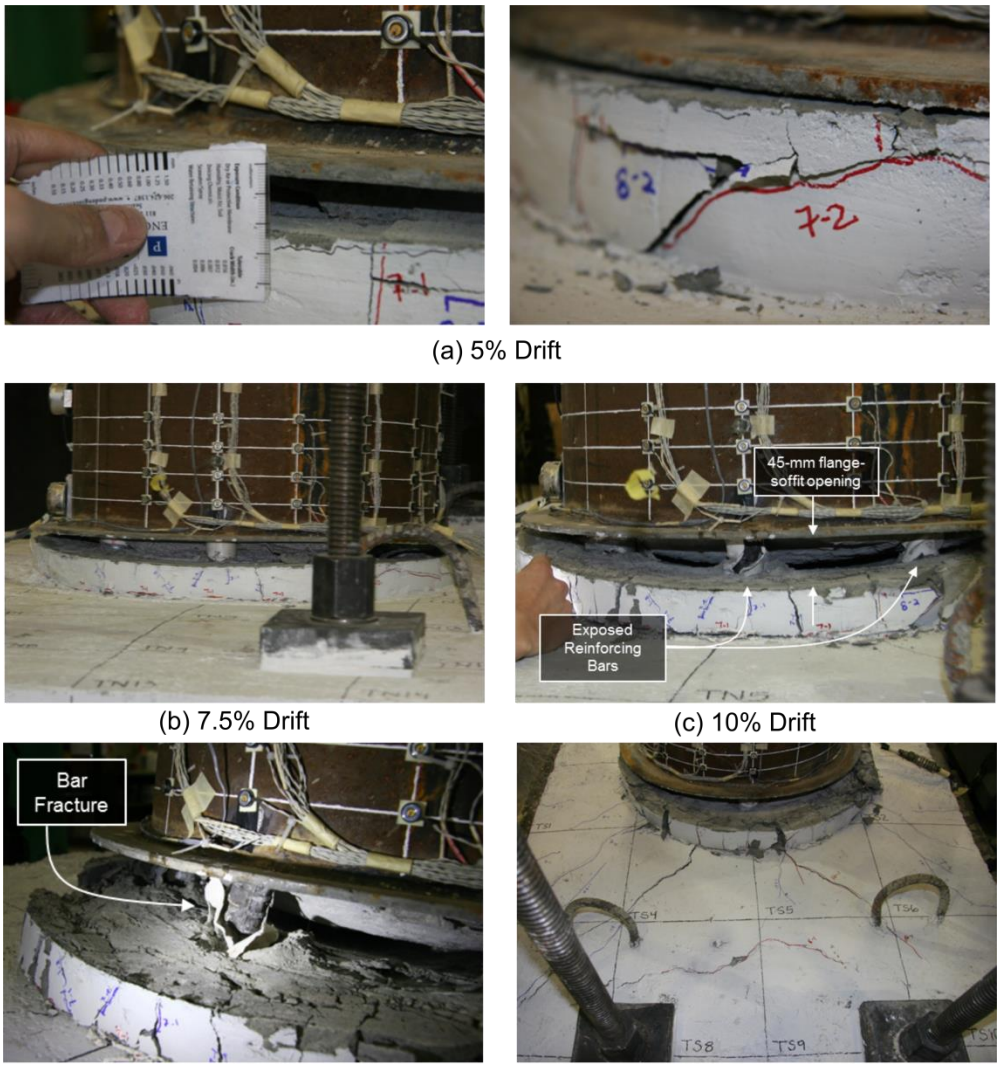

Fig. 8.12. Photos of Specimen WD80T2

8.2.7 WD103L

WD103L utilized 25.75-in. diameter spiral welded ASTM A1018 grade steel tube with a welded dowel connection consisting of 10 No. 11 headed bars embedded into the cap beam and welded into the steel tube. This steel tube is the same as that of ER103L. The area of the steel tube is 34% larger than the area of the 10 No. 11 longitudinal dowels, but the tensile strength of the

dowels is 63% larger than the yield stress of the steel tube. Hence this specimen was expected to be relatively stronger comparted to ER103L.

The purpose of this specimen was to evaluate the behavior of this connection type for loading in the longitudinal direction of the bridge. Additionally, transverse reinforcing was included in the joint region with the intent of increasing confinement in the joint region (transverse reinforcing in the joint region was not included in the transverse welded dowel connections).

The measured moment-drift response is given in Fig. 8.13. The specimen exhibited an initial stiffness $EI_{measured}/EI_{eff,CFT} = 0.65$, and a maximum moment $M_{max}/ M_{CFT,PSDM} = 1.1$.

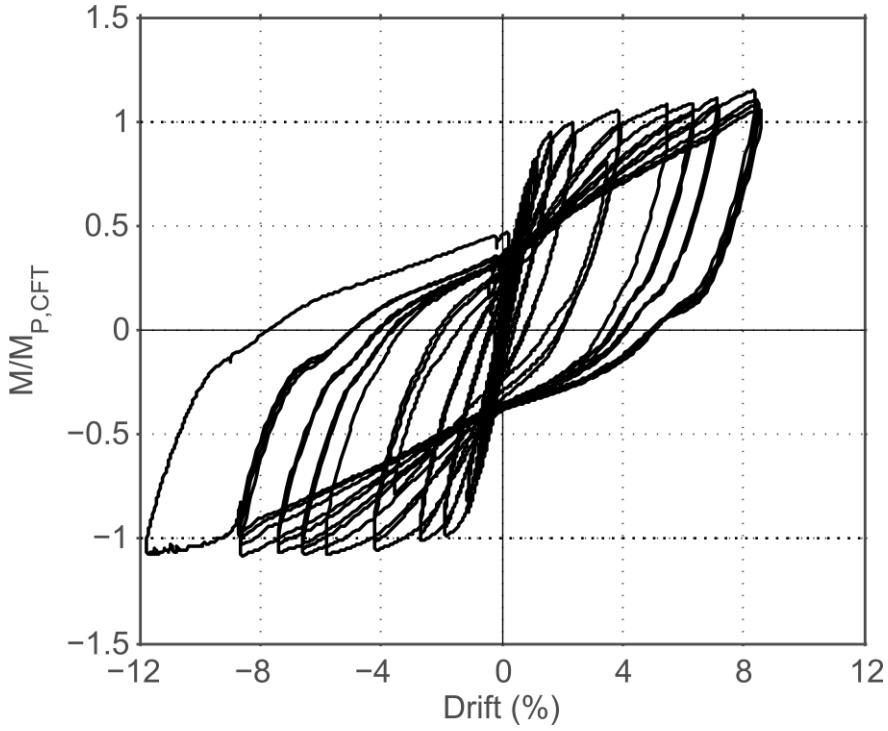

Fig. 8.13. Moment-Drift Behavior of Specimen WD103L

Very limited cap beam or soffit fill damage was observed during cycling at low drift levels (<2%), and dowel yielding was recorded by strain gages on the longitudinal dowels during cycling at 1.08% drift.

The PVC used to de-bond the longitudinal dowels was exposed during cycling at 5% drift, as a gap of 21-mm (0.83-in) was recorded between the annular ring and soffit fill. Moderate soffit fill crushing was to the exterior of the grout pad under the annular ring at 8% drift, as the transverse hoop in the soffit fill region provided confinement for the grout to the interior of the column. Large cracks developed in the soffit fill during cycling at 8.4% drift, and significant crushing was observed.

The displacement capacity of the actuator was achieved at 9.5% drift, and no strength degradation was observed. Significant grout pad crushing was observed, and the transverse hoop through the thickness of the soffit fill was entirely exposed in regions of the extreme fibers as illustrated in Fig. 8.14. The transverse hoop appeared un-deformed, suggesting that longitudinal bar buckling had not developed.

In an attempt to fail the specimen, the actuator was retracted, and spacers were placed between the actuator head and column such that a large monotonic push could be applied. The specimen was pushed for ½ cycle to 12% drift with no strength degradation or increase in visual damage. A maximum moment $M_{max}/ M_{CFT,PSDM} = 1.1$ was recorded at 12% drift.

This specimen provided good resistance with little damage to the cap beam. The grout pad sustained some limited damage. These de-bonded connections sustained great benefit through uplift of the flange from the grout pad in tension, and increased moment arm contributed by the CFT on the grout pad in compression through the flange. The specimen was slightly weaker than ER103L, but it was considerably more flexible than that specimen.

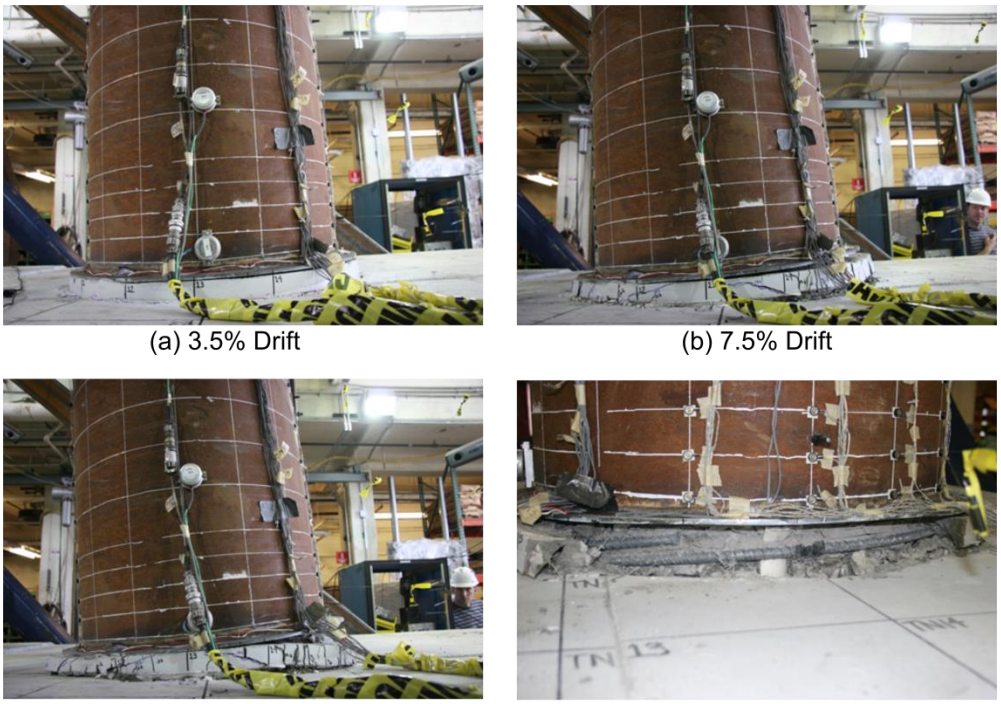

(a) 3.5% Drift (b) 7.5% Drift

(c) 9% Drift

Fig. 8.14. Photos of Specimen WD103L

8.2.8 RC80T

RC80T utilized 20-in. diameter spiral welded ASTM A1018 grade steel tube with a reinforced concrete connection consisting of 8 No. 9 headed bars embedded into the cap beam and developed into the steel tube. No. 3 spiral was additionally included for the length of the longitudinal dowels, and a concrete cover of 1-in. was provided between the steel tube and reinforcing cage. This connection is clearly a reinforced concrete connection, and it is somewhat comparible to ER80T and WD80T1.

The measured moment-drift response is given in Fig. 8.15. The specimen exhibited an initial stiffness $EI_{measured}/EI_{eff,CFT} = 0.69$, and a maximum moment $M_{max}/ M_{CFT,PSDM} = 0.92$.

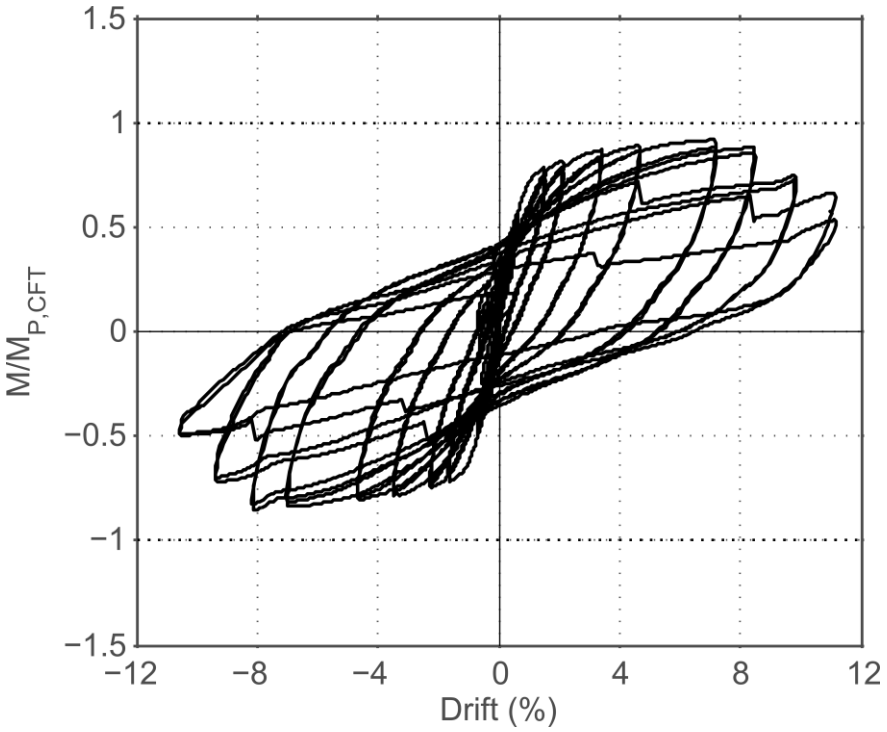

Fig. 8.15. Moment-Drift Behavior of Specimen EDC

Very limited cap beam or soffit fill damage was observed during cycling at drifts less than 2%, and dowel yielding was recorded by strain gages on the longitudinal dowels during cycling at 0.67% drift. The embedded dowel connection exhibited a ductile hysteretic response, as inelastic deformation was limited to the longitudinal dowels and grout in the soffit fill region. Severe soffit fill crushing developed during cycling at 5% drift. Deterioration of moment began at around 7% drift, as the soffit fill continued to crush. Transverse and longitudinal reinforcing became visible at 8.15% drift. The transverse reinforcing was bent around the longitudinal dowels, suggesting that dowel buckling had developed. The dowels located at the north and south extreme fibers fractured during cycling at 9.4% drift. The NE, NW, SE, and SW dowels fractured in the subsequent cycle leaving only the dowels at the center of the column in-tact. The

test was terminated at 10% drift, as the strength degradation exceeded 20%. The damaged soffit fill and exposed transverse reinforcing are show in Fig. 8.16.

(a) 2.5% Drift

(b) 5% Drift (c) 11.25% Drift

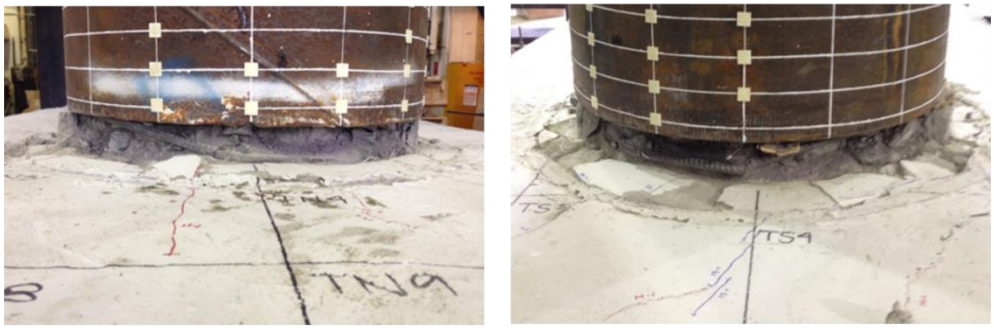

(c) 11.25% Drift (spalled grout removed)

Fig. 8.16. Photos of Specimen RC80T

8.3 Comparison of Test Results

Comparison of these experiments clearly demonstrates the different behaviors of the proposed connections as well as the influence of varying parameters on each connection type. The hysteresis of the transverse and longitudinal specimens have been plotted next to each other in

Fig. 8.17 and Fig. 8.18 respectively to provide a comparison of the hysteretic response exhibited by each connection type, while the cumulated energy dissipation has been plotted in Fig. 8.19.

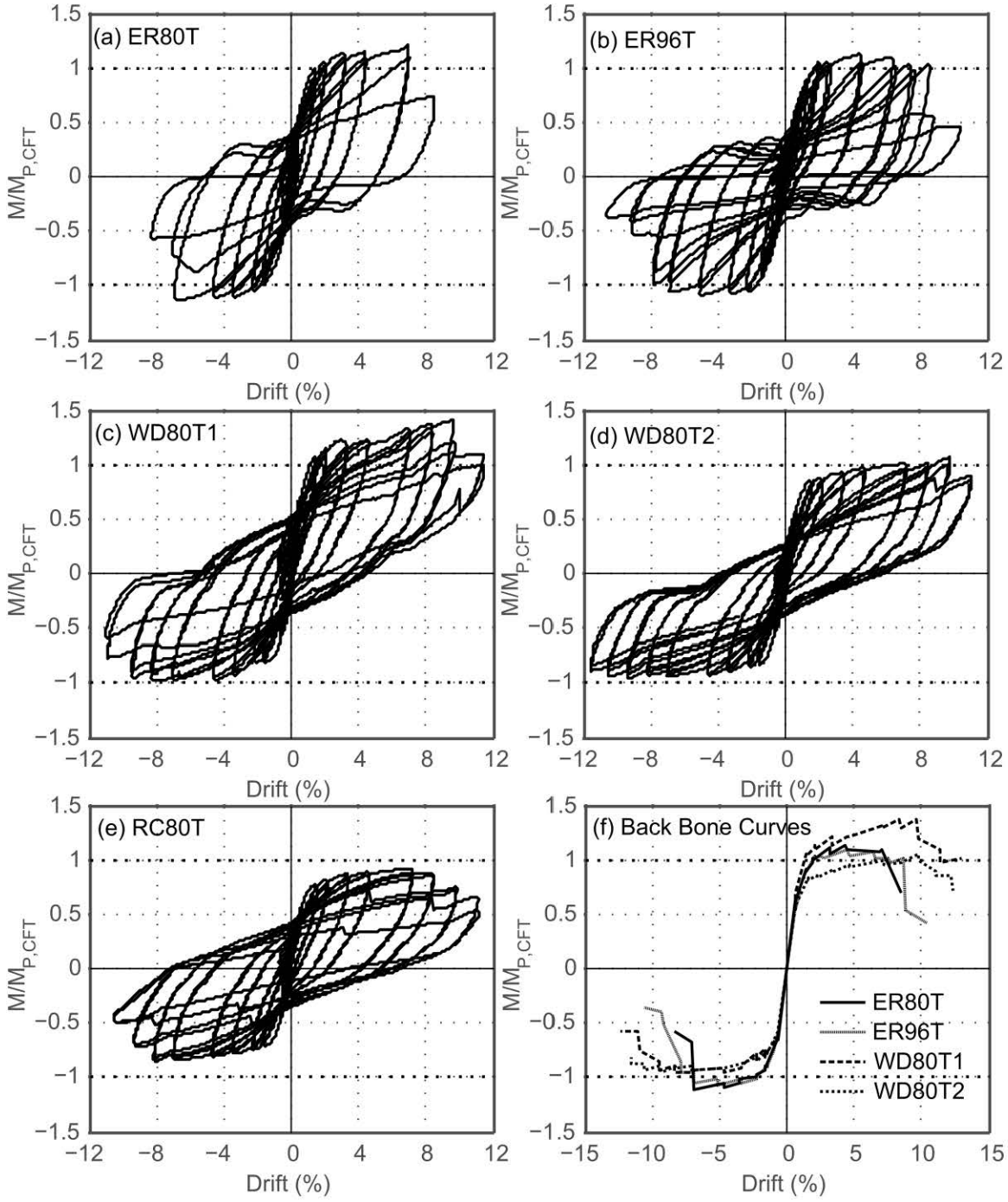

Fig. 8.17. Hysteretic Response of Transverse Specimens

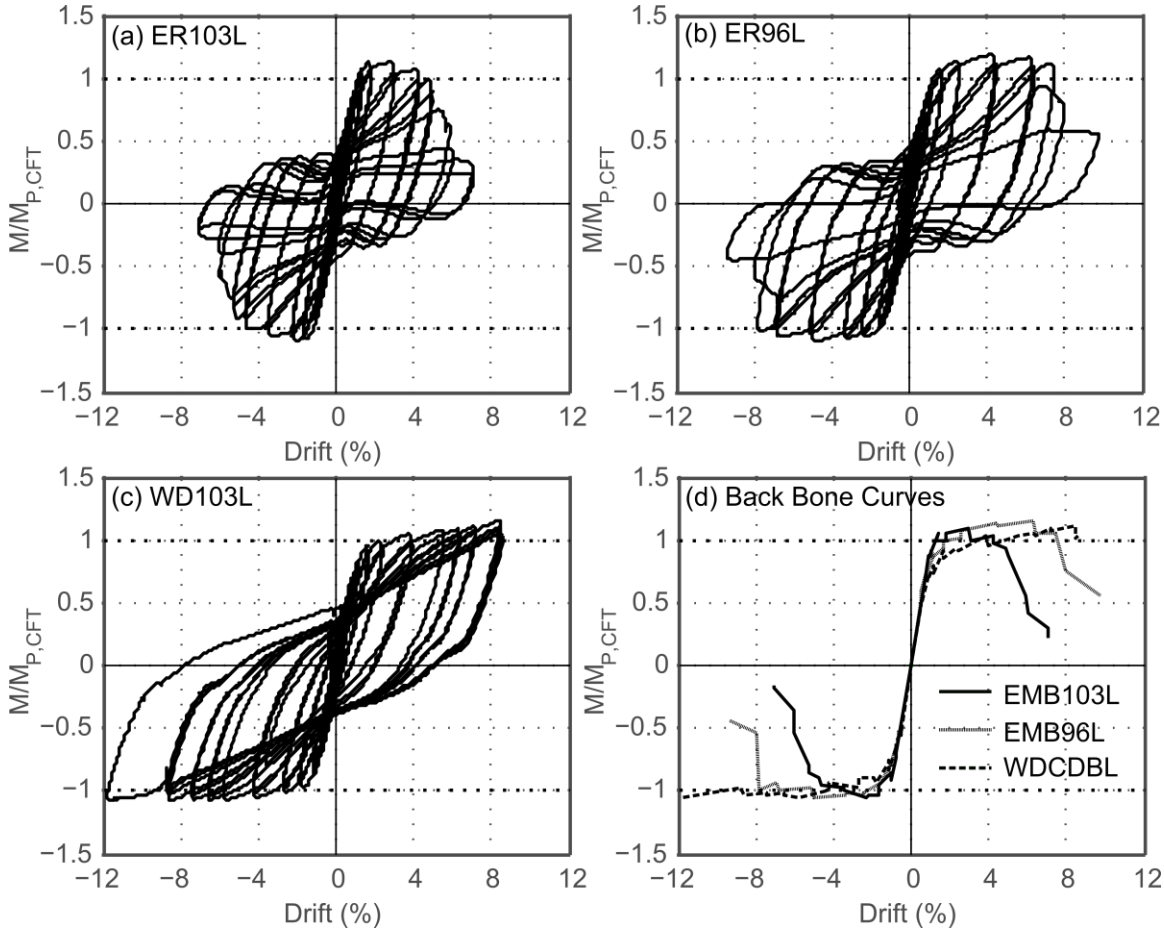

Fig. 8.18. Hysteretic Response of Longitudinal Specimens

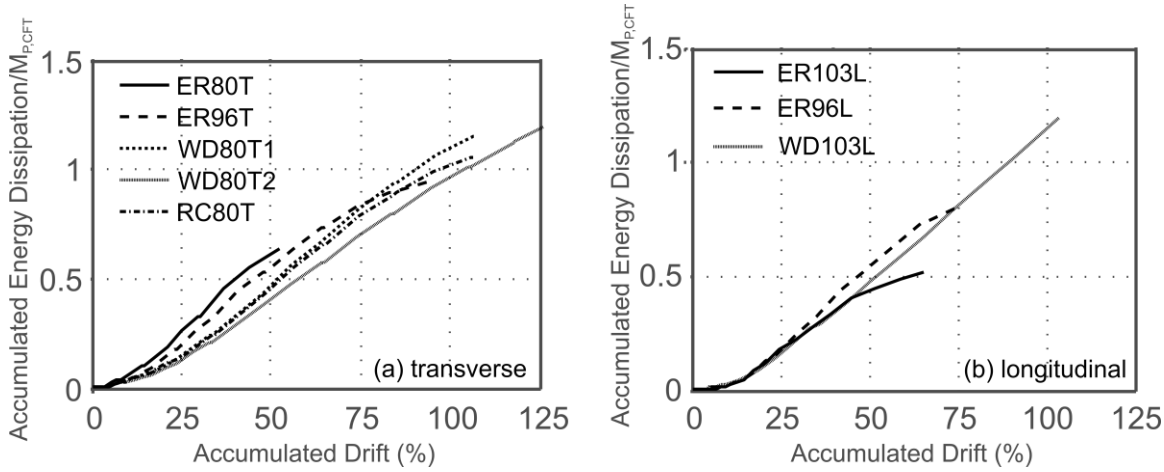

Fig. 8.19. Energy Dissipation Characteristics

The ER connections exhibited larger stiffness, and comparable strength, and energy dissipation characteristics to the WD connections. The larger stiffness of the embedded connection specimens is a result of the location of the tube as well as the confinement of the concrete fill. The comparable strengths are a result of the fact that the ER and WD connections had similar effective reinforcing ratios and moment arms (effective and actual longitudinal reinforcing ratios are given in Table 1).

To provide a direct comparison of the performance of the different connection types in terms of stiffness and strength, only columns with the same diameter, axial load, and loading direction are directly compared (i.e. ER80T is compared with WD80T1, WD80T2, and RC80T for loading in the transverse direction, while RC103L is compared with WD103L for loading in the longitudinal direction). Furthermore, the direction of loading (transverse or longitudinal) did not have a large impact on the performance of the embedded connection. ER96T and ER96L are used to provide a comparison in response for the two different loading directions.

8.3.1 Effective Stiffness and Strength

ER80T and ER103L achieved the theoretical stiffness of the CFT component, with $EI_{measured}/EI_{eff,CFT}$ values of 0.98 and 0.96 respectively. The initial stiffness values of WDC80T1, WD80T2, and RC80T were 12.2%, 27.5%, and 29.6% lower than the initial stiffness recorded in ER80T respectively. The initial stiffness of WD103L was 32.2% lower than the stiffness recorded in ER103L.

The embedded ring connections also exhibited larger peak capacities than the comparable dowel connections. The peak moment capacities of WD80T2 and RC80T were 12.5% and 23% lower than the peak capacity recorded in ER80T, while the peak moment capacity of WD103L

was 2% lower than the peak capacity of ER103L. (Note that WD80T1 has been excluded from the peak moment comparison due to the large asymmetry observed in the hysteresis as discussed above.)

Finally, the energy dissipation characteristics of the embedded and dowel connections are compared in Fig. 8.19. Note that although energy dissipation is largely a function of the applied displacement history, all of the connections were subjected to the same protocol. The energy dissipation in Fig. 7.19 has been normalized by the theoretical plastic moment capacity of the CFT as calculated using the PSDM. From the figure, the embedded connections exhibited slightly larger energy dissipations at moderate drifts, however the energy dissipation characteristics of all the connection types were largely similar.

8.3.2 De-bonding Longitudinal Dowels and Transverse Reinforcing in Joint Region

De-bonding the longitudinal bars in the connection region and providing transverse reinforcing in the joint improved the performance of the welded dowel connection. De-bonding the longitudinal connection reinforcing at the interface between the cap beam and steel tube significantly decreased the severity of damage to the cap beam. Including transverse reinforcing in the joint region further helped to improve the performance of the connection. WD103L incorporated de-bonded longitudinal dowels as well as transverse hoops in the joint region, and achieved 12% drift with extremely limited cap beam damage and no strength degradation.

8.3.3 Comparison of Transverse and Longitudinal Loading

The direction of loading did not influence the behavior of the embedded connection type. EMB96T and EMB96L were selected to evaluate the influence of the direction of loading as these specimens had the same cap-beam reinforcing details and axial load; the only variable was

the direction of loading. Both specimens exhibited similar moment-drift behaviors and energy dissipation characteristics as shown in Fig. 8.20. The moment-drift behaviors in Fig. 8.20exhibit similar strengths and overall hysteretic shape. The accumulated energy dissipation and drift were larger in the transverse specimen because this specimen was subjected to additional cycles after tearing propagated around the base of the column. Very similar accumulated energy dissipation characteristics were exhibited up to this point. The stiffness of the transverse specimen was greater than that of the longitudinal specimen as is shown in Fig. 8.20, however this is due to the boundary conditions used during testing; the longitudinal specimen developed some rotation through flexural deformation in the girders.

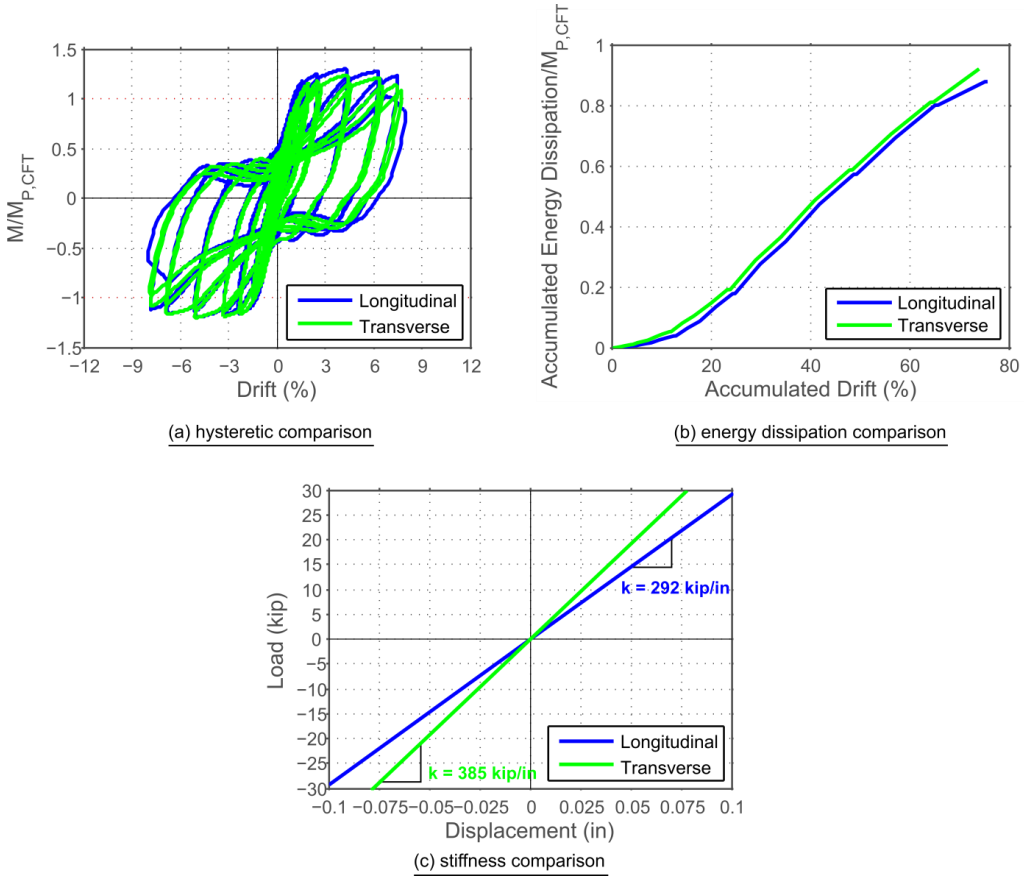

Fig. 8.20. Comparison of Transverse (EMB96T) and Longitudinal (EMB96L) Specimens

Chapter 9

DESIGN EXPRESSIONS FOR CFT PIER TO CAP BEAM CONNECTION

9.1 Overview

The experimental results and observations were used to develop practical engineering expressions for the CFT column-to-cap beam connections. The connection should be designed as one of the following options:

1. An embedded CFT connection in which the CFT column is embedded into the cap beam as illustrated in Figure 1.3.1.
2. A welded dowel connection in which a ring of partially deboned vertical headed reinforcing bars are welded inside the CFT column and extend into the cap beam as illustrated in Figure 1.4.1.
3. A grouted dowel connection in which a ring of headed reinforcing bars is developed into the steel tube and extend into the cap beam as illustrated in Figure 1.5.1.

Each of these options can be employed using cast-in-place (CIP) or precast super-structure cap beam. For precast construction, a void must be included in the precast elements through use of a corrugated pipe, which meets the specifications outlined below. For CIP construction either a monolithic or grouted connection can be used although only the grouted connection was studied in this phase, the prior phase evaluated monolithic connections.

The connections are grouted into place using a high-strength fiber-reinforced grout to ensure shear transfer and bond strength precluding failure of the grout. Embedded ring connections embed the end of the tube with the annular ring into the RC cap beam. Welded dowel connections use vertical reinforcing that is welded to the steel tube and extended into the

cap beam. Reinforced concrete connections use an internal reinforcing cage, including spiral and headed longitudinal reinforcement that extend into the CFT column and into the cap beam.

Cap beam design for the embedded ring connection requires vertical cap beam reinforcement within a horizontal distance equal to the embedment depth to minimize crack widths. The cap beam design for the welded dowel and reinforced concrete connections shall conform to the joint shear requirements in Section 7.4 of the Caltrans SDC V. 1.7 (2013).

The following sections summarize the materials and design expressions for the three connection types. Specification language for inclusion in the SDC has been drafted and is provided in Appendix C of this report.

9.2 Materials

Materials for the specified connections shall conform to the Caltrans standards, with several specific provisions included in this section.

9.2.1 Grout

When precast components are used, the fiber-reinforced grout consisting of prepackaged, cementitious grout and meeting ASTM C-1107 for grades A, B, and C non-shrink grout is used. The grout conforms to several additional performance requirements including compressive strength, compatibility, constructability, and durability. These requirements are summarized in Table 9.1. The 28-day grout strength f'_g must exceed f'_c of the surrounding concrete components. Grout using metallic formulations shall not be permitted, and grout shall be free of chlorides. No additives shall be added to pre-packaged grout.

These requirements ensure the grout has properties that provide adequate strength and longevity. These requirements adapted from recommendations provided in NCHRP Report 651 (Restrepo et al., 2011). Grouts with chloride are not permitted as these materials can accelerate corrosion in the connection reinforcing and steel tube. Additives are not permitted because pre-packaged grouts are proprietary mixes which should not be modified.

Table 9.1. Grout Specifications

Property	Permitted Values
Mechanical Compressive Strength	Must exceed f'_c of surrounding concrete at 28-days. Minimum grout strength f'_g must exceed 6-ksi.
Compatibility Non-Shrink	Grade A, B, or C Per ASTM C-1107.
Constructability Flow	Mix to flowable consistency according to manufacturer specification.
Durability Freeze thaw Sulfate resistance	300 cycles, relative durability factor 90% per ASTM C666. Expansion at 26 weeks < 0.3% per ASTM C1012

9.2.2 Fiber Reinforcing

Macro polypropylene fiber with a minimum volume of 0.2% is included to provide crack resistance and bounding characteristics between the tube and corrugated metal duct. Test results to date have not evaluated the use of alternative fibers such as steel fibers.

9.2.3 Corrugated Metal Duct

Corrugated metal ducts are used to provide voids in precast components. The ducts are galvanized steel according to ASTM A653. Duct diameter is selected based on construction tolerances. Plastic ducts should not be used as the purpose of the ducts it to be a bond crack arrestor, act as confinement and provide shear transfer from the grout to the outer concrete. The

use of corrugated metal ducts for grouted connections is supported by this research as well as a wealth of seismic precast connection data, such as the references discussed in Section 3.2.

9.2.4 Reinforcement

Reinforcing in the connection region shall conform to ASTM A706 Gr. 60 (or Gr. 80 if allowed) requirements for weldable reinforcing. ASTM A706 places restrictions on the chemical composition of reinforcing bars to enhance welding properties. Weld properties are discussed below.

9.2.5 Tube Steel

Steel tubes may either be straight seam or spiral welded and must conform to either ASTM 1018 or API 5L requirements. Spiral welded tubes must be welded using a double submerged arc welding process, and weld metal properties must match properties of the base metal and meet minimum toughness requirements of AISC demand critical welds (AISC 2010).

Selection of tube material designation (ASTM 1018 or API 5L) plays a role in the ductility of the full strength embedded CFT connection. API 5L grade steel has more strict requirements regarding chemical composition than ASTM 1018 steel, and can therefore provide additional ductility for both spiral welded and straight seam tubes. Experiments were conducted on API 5L and ASTM 1018 tubes which slightly exceeded the upper bound slenderness requirements for CFTs specified in the AASHTO LRFD (2015). Results from these tests showed that embedded ring connections which utilize API 5L steel can exceed 8% drift prior to tube fracture, while connections which use ASTM 1018 steels tend to fracture at 6% drift.

9.3 Embedded Ring Connection

The embedded ring connection utilizes a CFT fully embedded into the cap beam. The CFT pier or column controls the strength and ductility of this connection type, not the cap beam or other superstructure or foundation components. The precast cap is placed on the column after the concrete is set, and the recess between the tube and corrugated pipe would be filled with high strength fiber reinforced grout.

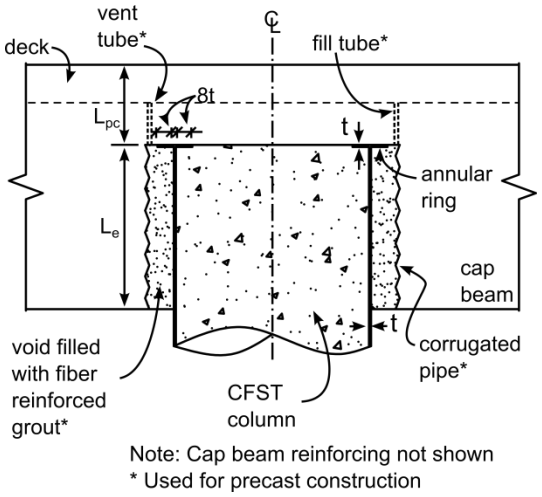

Fig. 9.1. Embedded Ring Connection

9.3.1 Annular Ring

The annular ring is welded to the end of the steel tube to provide anchorage and stress transfer to the concrete and reinforcing in the cap beam. The ring is made of steel of the same thickness and yield strength as the steel tube. The ring projects both in to and out from the steel tube a distance 8 times the thickness of the steel tube.

The ring is welded to the steel tube using complete joint penetration (CJP) welds, or fillet welds designed to develop the tensile capacity of the steel tube. The minimum fillet weld size is:

$$w \geq \frac{1.31 \times F_{u,st} \times t}{F_{exx}} \quad [9.1]$$

where $F_{u,st}$ is the ultimate strength of the steel tube, and F_{EXX} is the minimum tensile strength of the weld metal. The CJP or fillet welds should, as a minimum, satisfy the AISC 341-10 (2010) toughness criteria for demand critical welds.

9.3.2 Embedment Depth

The required embedment depth to transfer the plastic moment capacity of the CFT component has been previously derived (Lehman and Roeder, 2012) for the embedded flange connection using the cone pullout model illustrated in Fig. 9.1. Using equilibrium, the ultimate tensile strength of the steel tube is resisted by principal tensile stress in the cap beam concrete of $n\sqrt{f'_c}$.

This value for *n* was determined using data from specimens that exhibited failure modes ranging from (1) embedment failure prior to achieving $M_{p,CFT}$ in the CFT column to (2) embedment failure prior to just achieving $M_{p,CFT}$ in the CFT column, to (3) CFT column fracture without connection failure. These data were used to determine a limiting principal stress to eliminate a conical failure mode in the connection. Specimens with n values less than 6 were shown to develop large stable drift capacities and strengths before sustaining degradation of strength. As a result, the minimum embedment depth to develop the plastic moment capacity of the CFT was calculated as:

$$L_e \geq \sqrt{\frac{D_o^2}{4} + \frac{DtF_{u,st}}{6\sqrt{f'_{c,cap}}}} - \frac{D_o}{2} \; (psi) \qquad [9.2]$$

where D_o is the outer diameter of the annular ring for connections with CIP construction, and the diameter of the corrugated pipe for connections which utilize precast components, and $f'_{c,cap}$ is the compressive strength of the concrete in the cap beam in psi, and $f_{u,st}$ is the ultimate strength of the steel tube in psi (Lehman and Roeder, 2012).

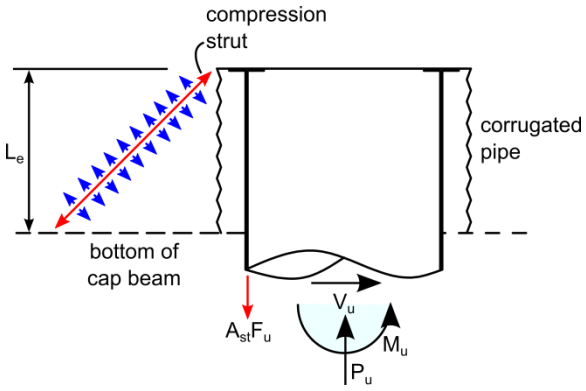

Fig. 9.2. Transfer Mechanism for Calculating the Required Embedment Depth of the Embedded Ring Connection

9.3.3 Punching Shear Requirements

The required depth above the embedded tube to eliminate the potential for punching shear failure (L_{pc}) has been previously derived (Lehman and Roeder, 2012) for the embedded flange foundation connection, and is presented in Equation 9.1, where C_c and C_s are the compressive forces in the concrete and steel due to the maximum combined axial load and bending moment as calculated using the PSDM (as illustrated in Fig. 9.3).

$$L_{pc} \geq \sqrt{\frac{D_o^2}{4} + \frac{C_c + C_s}{6\sqrt{f'_{c,cap}}}} - \frac{D}{2} - L_e \; (psi) \qquad [9.3]$$

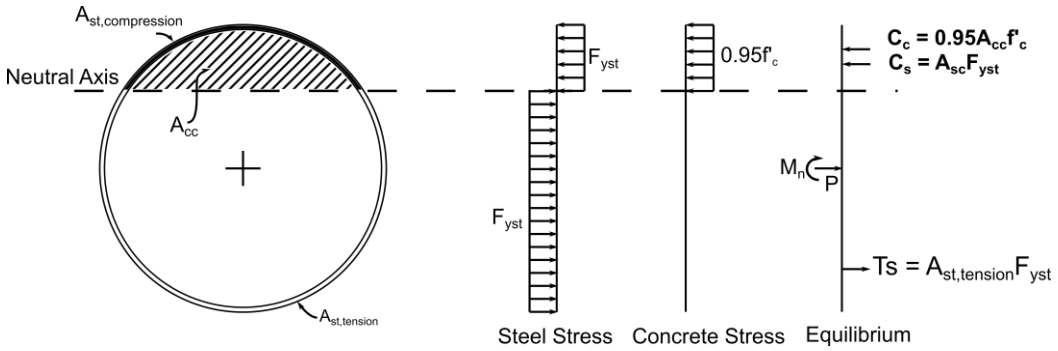

Fig. 9.3. PSDM for Calculation of Cs and Cc

9.3.4 Cap Beam Reinforcing

Flexural Reinforcing

Longitudinal flexural reinforcing in the column region is required to resist $1.25M_{p,CFT}$ to ensure the cap beam does not yield. Longitudinal flexural reinforcing is spaced uniformly across the width of the cap beam.

To ensure continuity, a minimum of one layer of upper reinforcing shall pass above the embedded CFT in the cap beam as shown in Fig. 9.4.

Some longitudinal reinforcing in the bottom layer will be interrupted by the embedded corrugated pipe. The bottom layer of flexural reinforcing not interrupted by the corrugate pipe shall be designed to resist $1.25M_p$ of the CFT column. Interrupted bars shall still be included and arranged as illustrated in Fig. 9.4.

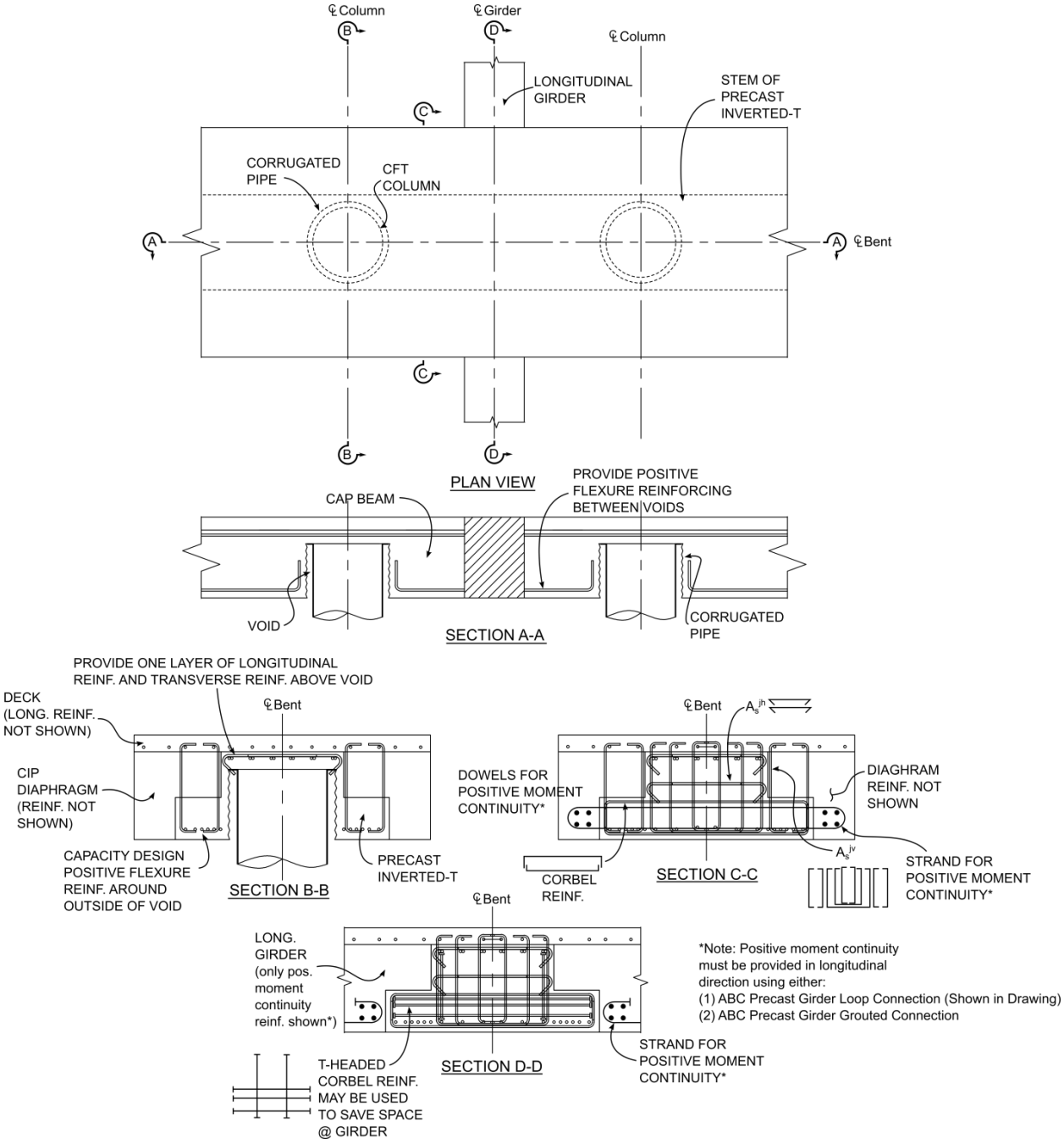

Fig. 9.4. Cap Beam Details for Embedded Connection

Vertical Cap-Beam Reinforcement

Vertical reinforcing, A_s^{jv}, shall be included according to Equation 9.4 where A_{st} is the total area of the steel tube embedded into the cap beam.

$$A_s^{jv} = 0.65A_{st} \quad [9.4]$$

where A_s^{jv} is the area of vertical reinforcing required within a distance L_e extending from the end of the annular ring when monolithic construction is used, and extending from the outer diameter of the corrugated pipe when the grouted option is used. L_e is the length the steel tube extends into the cap beam as illustrated in Fig. 9.1.

Equation 9.4 was derived using the conical failure mode illustrated in Fig. 9.2. Using this model a limiting joint shear stress of $4\sqrt{f'_c}$ (psi) is assumed. The concrete along the compression strut is assumed to carry a stress of $2\sqrt{f'_c}$ (psi), while vertical reinforcing in the joint region carries the remaining stress, up to $4\sqrt{f'c}$. Thus the area of vertical reinforcing required to resist a conical pullout failure can be calculated as a function of the embedment depth, Le, and D_o. This relationship can be simplified to relate the ratio of the required vertical reinforcing area to the area of the tube, A_s^{jv}/A_{st}, to the D/t ratio of the steel tube as is illustrated in Fig. 9.5. From Fig. 9.5, $0.65A_{st}$ provides a conservative amount of vertical reinforcing steel for all D/t ratios that would be commonly seen in practice.

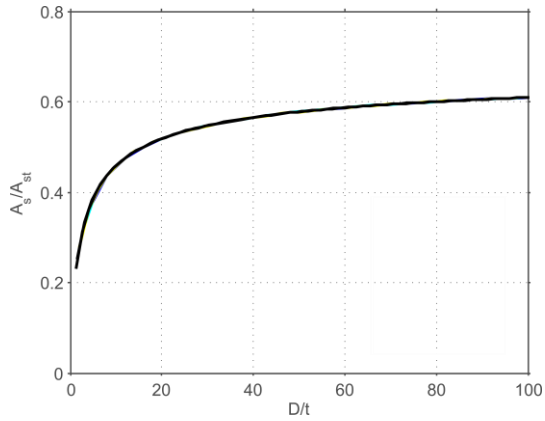

Fig. 9.5. Required Area of Vertical Stirrups Related to D/t for Embedded Ring Connection

Vertical stirrups or ties are distributed uniformly within a distance $D/2+L_E$ extending from the column centerline as shown in Fig. 9.4 and Fig. 9.6. These stirrups can be used to meet other requirements documented elsewhere including shear in the bent cap.

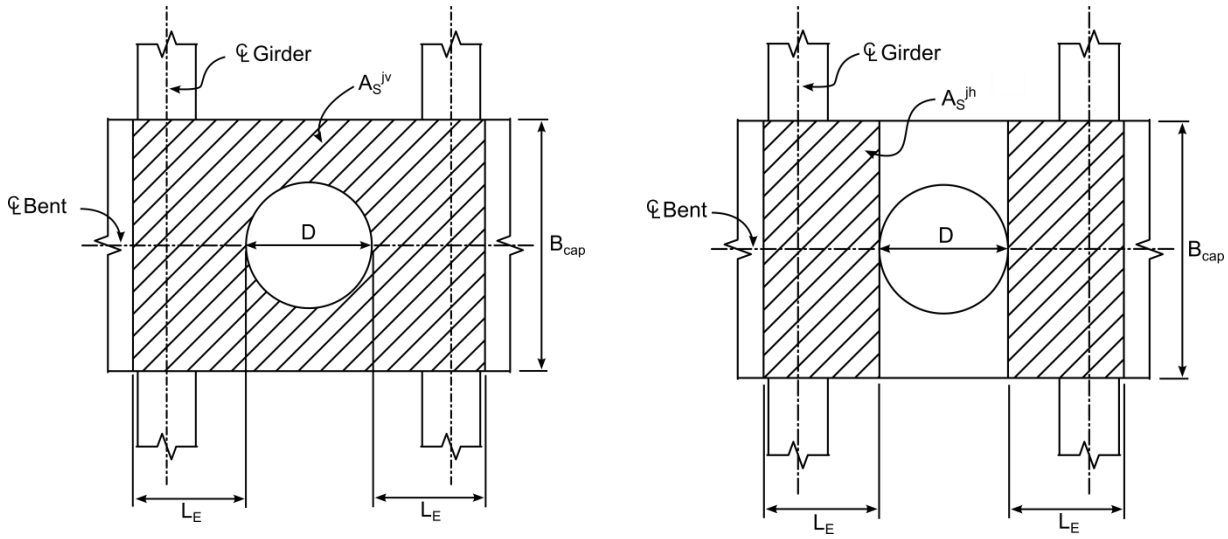

(a) location of vertical stirrups

(b) location of horizontal stirrups

Fig. 9.6. Required Location of (a) Vertical and (b) Horizontal Stirrups for the Embedded Ring Connection

Horizontal Stirrups

Horizontal stirrups or ties shall be placed transversely around the vertical stirrups or ties in two or more intermediate layers spaced vertically at not more than 18-in apart. The horizontal reinforcing area, A_s^{jh}, is determined using Equation 9.5 where A_{st} is the area of the steel tube embedded into the cap beam. The horizontal reinforcing shall be placed within a distance $D/2+L_E$ extending from the column centerline as illustrated in Fig. 9.4 and Figure Fig. 9.6.

$$A_S^{jh} = 0.1 \times A_{st} \quad [9.5]$$

In addition, the top layer of transverse reinforcing shall continue across top of the void in the cap beam as illustrated in Figure Fig. 9.4.

Horizontal Side Reinforcement

Horizontal side reinforcing shall be included according to Article 7.4.4.3 of the Caltrans SDC V. 1.8.

9.3.5 Configuration of Columns and Longitudinal Girders for ER Connection

When using the embedded connection, the column shall be laid out between the longitudinal girders as illustrated in Fig. 9.4 and Fig. 9.6.

9.4 Welded Dowel Connection

The welded dowel connection design expressions are provided in this section. The connection utilizes a ring of headed reinforcing bars that are welded into the tube and developed into the cap beam. The strength is controlled by the reinforcing ratio of the longitudinal reinforcing which extends from the column into the cap beam. The welded detail is designed to carry the full strength of the reinforcing bar. The advantage of this connection is a shorter embedment length into the CFT column and a maximized moment arm.

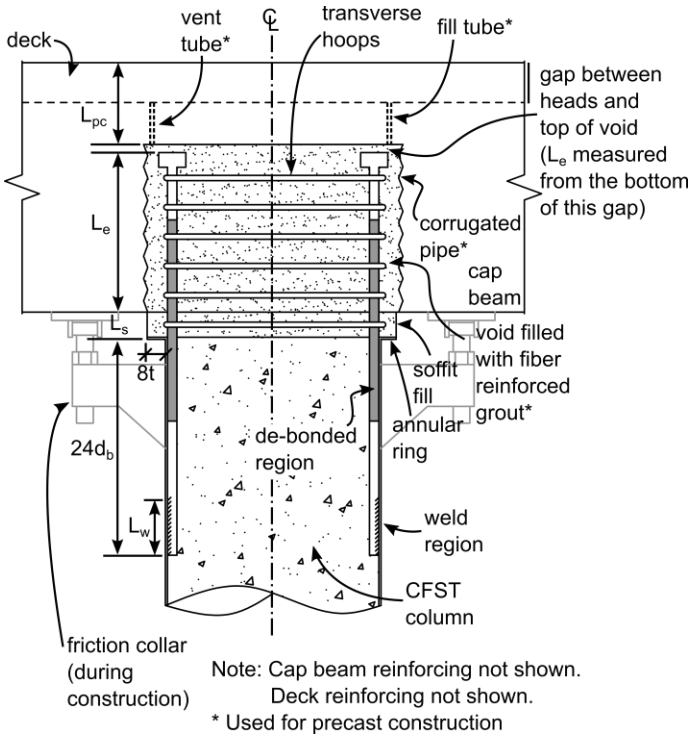

Fig. 9.7. Welded Dowel Connection with De-bonded Reinforcing

9.4.1 Annular Ring

The annular ring is welded to end of the steel tube to provide a larger area to transfer compressive stress from the steel tube into the soffit fill. In this connection the ring does not transfer tensile stresses but does provide some compressive force transfer.

The ring is made from steel of the same thickness and yield strength as the steel tube. The ring projects outside of the steel tube a distance 8 times the thickness of the steel tube. The annular ring is welded to end of the steel tube using CJP welds, or fillet welds on the exterior of the tube. The minimum fillet weld size to attach the annular ring is defined in Equation 9.1. Welds meet a minimum CVN toughness of 40-ft-lbs at 70˚F.

9.4.2 Length Reinforcing Extends into the Cap Beam and Column

The headed reinforcing extends into the cap beam to fully develop the longitudinal dowels while also eliminating the potential for a conical pullout failure. The headed dowels must extend into the cap beam for the largest length calculated using Equation 9.6a, 9.6b, and 9.6c. Equation 9.6a defines the required development length to develop reinforcing bars with mechanical anchors as specified in ACI 318 (2011), where ψ_e is the reinforcing bar coating factor defined in ACI 318 and $F_{y,b}$ is the yield strength of the longitudinal dowels. Note that ACI is referenced because neither the AASHTO nor the SDC provide development expressions for headed bars.

Equation 9.6b defines the required embedment depth to eliminate a conical pullout as determined using the transfer mechanism illustrated in Fig. 9.8 where $A_{st,b}$ is the total area of longitudinal dowels which extend into the cap beam, and $F_{y,b}$ and f'_g are in psi. In lieu of a large pool of experimental data on the welded dowel connection, Equation 9.6b was derived assuming a limiting tensile principal stress of $6\sqrt{f'_c}$ (Lehman and Roeder, 2012) where $F_{u,b}$ and f'_{cc} are in psi.

A final embedment depth requirement has been specified in Equation 9.6c to ensure a minimum bonded length of $3d_b$ is included adjacent to the head on the end of the dowel where L_{db} is the total length over which the longitudinal dowels are de-bonded. This equation is presented assuming one half of the full de-bonded length extends into the cap beam, and must be modified in cases in which a different de-bonded length is extended into the cap.

$$L_e \geq \frac{0.016\psi_e F_{y,b}}{\sqrt{f'_g}} d_b \qquad [9.6a]$$

$$L_e \geq \sqrt{\frac{D^2}{4} + \frac{1.2 * F_{y,b} * A_{st,b}}{6\pi\sqrt{f'_{cc}}}} - \frac{D}{2} \quad [9.6b]$$

$$L_e \geq 3d_b + 0.5L_{db} \quad [9.6c]$$

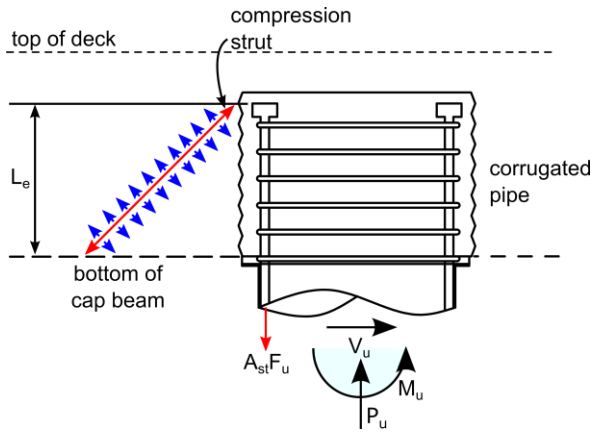

Fig. 9.8. Transfer Mechanism for Calculating the Required Development of Headed Reinforcement Bars into the Cap-Beam

The longitudinal dowels must also extend into the CFT for a distance adequate to develop the full strength of the dowels. Results from the welded dowel tests (discussed above) suggest that the embedment can be as low as $18d_b$ for full dowel development, however a distance of $24d_b$ is recommended here to provide a reasonable factor of safety.

9.4.3 Joint Region Reinforcing

Cap beam detailing requirements specified in the California Department of Transportation Seismic Design Criteria V. 1.8 should be followed when designing the welded dowel connection.

9.4.4 Soffit Fill Depth

The soffit fill depth, L_s, is calculated according to Equation 9.7 to ensure that the annular ring does not come in to contact with the bottom of the cap beam at the maximum expected drift angle, θ_u where D is the outer diameter of the annular ring.

$$L_s \geq \sin(\theta_u)\left(\frac{D}{2} + 8t\right) \quad [9.7]$$

9.4.5 Dowel De-bonded Length

Longitudinal dowels should be de-bonded from the concrete in the connection region with the intent of increasing connection ductility. The required de-bonded length the achieve a pre-determined connection rotation, θ_u, prior to bar fracture is calculated using Equation 9.8 or 9.9, where ϕ_u is a curvature limit corresponding to a maximum steel strain as obtained from a moment-curvature analysis. Half of the de-bonded length extends into the cap beam, and half of the de-bonded length extends into the CFT column as illustrated in Fig. 9.9.

$$L_{db} = \frac{\theta_u}{\phi_u} \quad [9.8]$$

$$L_{db} = \frac{\tan\theta(D - t - d_b/2)}{0.7\varepsilon_u} \quad [9.9]$$

Equation 9.9 is a simplified method for estimating the required de-bonded length of the longitudinal reinforcing to achieve a pre-determined drift ratio prior to bar fracture. Although this method does not require a moment curvature analysis, it results in larger de-bonded lengths than those calculated using a moment-curvature analysis, as required in Equation 9.8.

The method for de-bonding the reinforcing shall be specified. Several de-bonding methods have been evaluated in previous research including encasing the bars in tight-fitting PVC pipe, or wrapping the bars with duct tape. Other methods may be considered if it has been shown to adequately de-bond the reinforcing from the surrounding concrete.

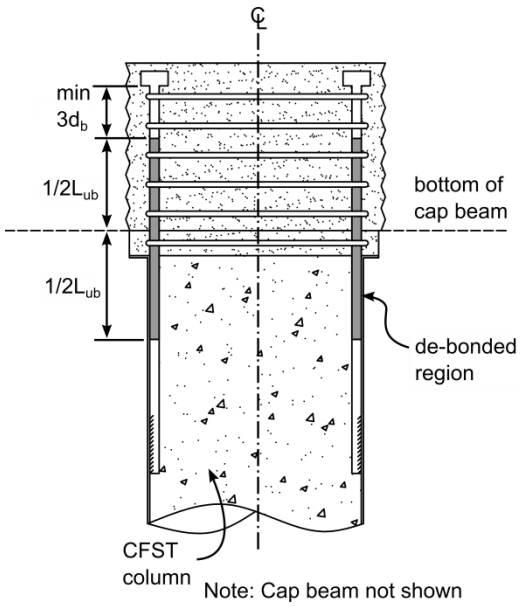

Fig. 9.9. Welded Dowel Connection De-bonding Dimensions

9.4.6 Dowel-to-Steel Tube Welds

Longitudinal dowels are welded to the inside of the steel tube using flare bevel groove welds on both sides of the dowels, as illustrated in Fig. 6.1. The required weld lengths to develop the rupture capacity of the longitudinal dowels are specified in Equation 9.10 and are based on typical weld limit states for flare bevel groove welds. Equation 9.10a is based on failure of the weld metal, Equation 8.10b is based on yielding of the tube steel, and Equation 9.10c is based on rupture of the tube steel. A strength reduction factor of 0.9 has been included for yielding limit states in Equations 9.10a and 9.10b, while a strength reduction factor of 0.75 has been included based on a tube steel rupture limit state in Equation 9.10c.

$$L_w \geq \frac{5.6 A_b F_{y,b}}{F_{EXX} d_b} \quad [9.10a]$$

$$L_w \geq \frac{0.83 A_b F_{y,b}}{F_{y,st} t} \quad [9.10b]$$

$$L_w \geq \frac{1.11 A_b F_{y,b}}{F_{u,st} t} \quad [9.10c]$$

9.4.7 Use of Spiral Reinforcement in Column and Extension into the Joint Region

Spiral reinforcing should be included around the longitudinal dowels, which extend into the cap beam according to requirements in the California Department of Transportation Seismic Design Criteria V. 1.7. At least one hoop must be placed in the soffit fill depth if individual hoops are used.

9.4.8 Longitudinal Girder and Column Layout for the Welded Connection

When using the welded dowel connection, the column shall be laid out between the longitudinal girders.

9.4.9 Requirements for Headed Reinforcing

Minimum cover shall be provided when headed reinforcing is anchored into the cap beam. These requirements are summarized in Fig. 9.10.

1. The thickness of side cover around the head must be equal to or greater than the diameter of the head.
2. A minimum depth of $3d_h$ shall be included above the heads in the headed reinforcing where d_h is the diameter of the head.

3. Nominal amounts of longitudinal reinforcing (e.g. reinforcing steel in the plane orthogonal to the headed reinforcement) shall be placed above the head.

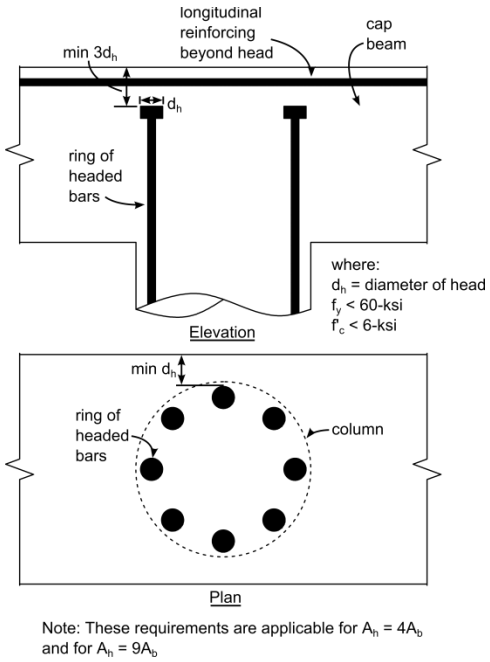

Fig. 9.10. Cover Requirements for Headed Reinforcing

9.5 Reinforced Concrete Connection

The reinforced concrete connection consists of a more traditional reinforced concrete dowel connection, as both transverse and longitudinal reinforcing extend from the CFT column into the cap beam. The strength and ductility of this connection type is controlled by the amount and placement of the headed reinforcement. Note that construction of this connection using precast super-structure components requires use of a friction collar to temporarily support the cap beam.

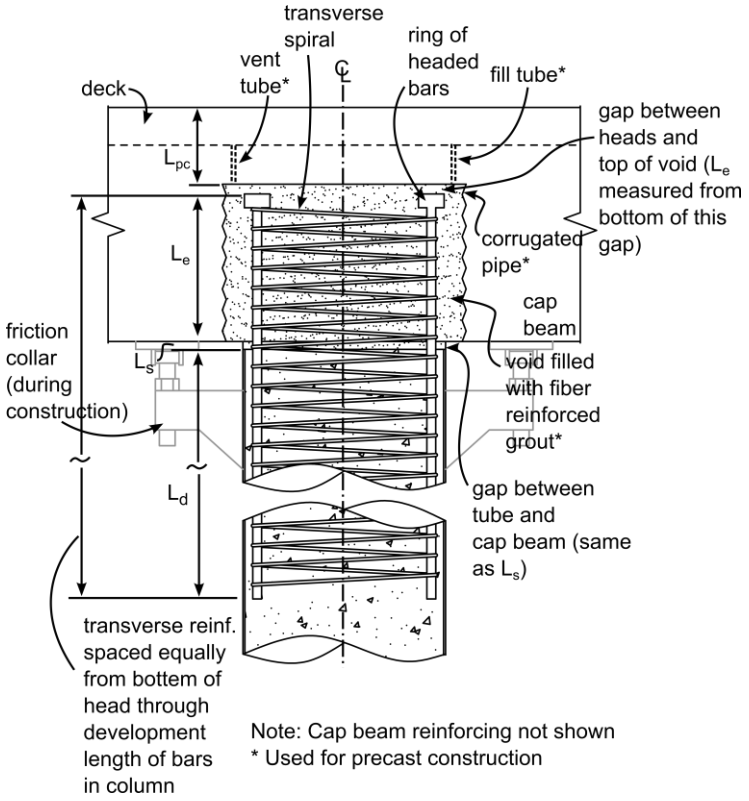

Fig. 9.11. Reinforced Concrete Connection

9.5.1 Reinforcing Embedment Length into Cap Beam and Column

Longitudinal dowels shall extend into the cap beam as specified in Section 9.4.2. Longitudinal dowels shall extend a distance L_d into the CFT column according to Equation 9.11 where ψ_e is the reinforcing bar coating factor as defined in ACI 318 (1.0 for uncoated bars, and 1.2 for epoxy coated bars) and F_y and f'_{cf} are in psi.

$$L_d = \left(\frac{F_{y,b}\psi_e}{25\sqrt{f'_{cf}}}\right) d_b \qquad [9.11]$$

The headed reinforcing must extend into the CFT column for a length sufficient to fully develop the reinforcing bar. Equation 9.11 defines the required development length as specified in Article 12.2 of ACI 318 for deformed reinforcing. Equation 9.11 is a simplified development

length equation which pertains to geometries commonly found in reinforced concrete bridge columns. For uncommon geometries or reinforcing layouts, The Engineer shall reference Article 12.2 of ACI 318.

9.5.2 Punching Shear Requirements

Punching shear requirements are consistent with Section 8.4.3.

9.5.3 Transverse Reinforcing

Discrete hoops or spiral shall extend from the cap beam and into the column for a distance L_d as illustrated in Fig. 9.11.

9.5.4 Joint Region Reinforcing

Cap beam detailing requirements specified in the California Department of Transportation Seismic Design Criteria V. 1.8 should be followed when designing the welded dowel connection.

9.5.5 Requirements for Headed Reinforcing

Cover for headed reinforcing is sized according to requirements in Section 8.4.10.

9.5.6 Longitudinal Girder and Column Layout for RC Connection

The bridge layout shall correspond to requirements in Section 8.4.9.

Chapter 10

SUMMARY, CONCLUSIONS AND FUTURE WORK

10.1 Summary

Several new CFT column-to-cap beam connections were proposed and experimentally studied using increasing cyclic deformations. These connections include (1) an embedded ring connection in which an annular ring is welded to the top of the steel tube and embedded into the cap beam (2) a welded dowel connection in which a ring of headed dowels is welded to the inside of the steel tube and developed into the cap beam, and (3) an reinforced concrete connection in which a traditional reinforcing cage consisting of a ring of headed dowels with transverse reinforcing is developed into the CFT column and cap beam. All of the connections were demonstrated using a grouted connection detail, which can be integrated with precast cap beam components for ABC; however the connections can also be used in tradition CIP construction. Further, the benefits of ABC vary somewhat with the 3 connection types.

A series of transverse and longitudinal test specimens was developed (note that transverse and longitudinal refers to the direction of the bridge). Initially salient design parameters including the width of the cap beam, geometry of the ring at the end of the tube for the embedded connection and axial load ratio were numerically evaluated. From this study, a series of specimens were tested to evaluate the behavior of the different connection types, and to assess the influence of several parameters on the performance of the connections. The experimental results were used to develop practical engineering expressions for the proposed connections. Based on the experiences and recorded results, the following observations and conclusions were drawn from the study.

10.2 Conclusions

10.2.1 Embedded Ring Connection

The embedded ring connection uses a circular ring welded to the base of the steel tube to provide anchorage and stress transfer to the concrete and reinforcing in the cap beam. The flange extends a distance 8 times the thickness of the tube (8t) both inside and outside of the tube. When precast super-structure elements are used, a void is cast into the precast elements using a galvanized corrugated pipe. The precast cap beam is placed onto the column after the column is set, and the recess between the tube and corrugated pipe is filled with high strength fiber reinforced grout.

Experimental results demonstrated that this connection provides large strength, stiffness, and deformation capacity, and the predictions were accurate with modest and predictable over-strength. All of the specimens which utilized this connection type achieved the theoretical plastic moment capacity of the CFT component as calculated using the PSDM. The failure mode in all cases was characterized by ductile tearing near the column-to-cap beam interface. Local buckling was observed in the steel tube at around 4% drift in all cases, however the initiation of buckling did not influence the stiffness or moment resistance of the connection. The influence of several parameters on the behavior the ER connection are noted below.

- The cap beam width for this connection may be as narrow as 2 times the diameter of the CFT column.
- Decreasing the external projection of the annular ring to 8 times the thickness of the steel tube does not influence the performance of the embedded connection. This is lower than the external projection of 16 times the thickness of the steel tube recommended in previous research

The ER connection offers several distinct advantages in terms of optimizing the objectives of accelerated construction and decreasing labor. After the column is cast, precast super-structure elements can be placed directly onto the CFT; no shoring, friction collars, or temporary support is required. Furthermore, this connection does not require any internal transverse or longitudinal reinforcing. There are no dowels or flexible reinforcing cages that need to be tied and placed.

The ER connection also offers several advantages in terms of post-event inspection and repair. The damage state of the ER connection can be readily identified based on the condition of the steel tube in the connection region; the concrete in the tube is generally in pristine condition. In addition, the accessibility to the steel tube (which acts as the primary longitudinal reinforcing) provides a unique opportunity for repair which will be more difficult in dowel or RC type connections in which extensive spalling and concrete damage are noted, and the longitudinal steel is embedded in the column concrete. Developing robust repair strategies for the ER connection will be a focus of future work.

10.2.2Welded Dowel Connection

The WD connection utilizes a ring of headed dowels to resist the flexural demand. The tensile forces in the dowels is developed by welding the dowels to the steel tube. The dowels then transfer forces and moment into the cap beam using a high-strength, fiber-reinforced grouted connection. Welding the dowel directly to the tube, as opposed to embedding the dowel directly into the connection maximizes the moment capacity of the dowel connection. A soffit fill is included between the steel tube and cap beam. A flange with an outer diameter of D+8t is welded to the exterior of the steel tube, and this flange bears on the soffit fill and the surface of the cap beam thereby increasing the moment arm and moment capacity of the connection.

Experimental results demonstrated that this connection can offer large strength, stiffness, and deformation capacity. However, the stiffness and strength of this connection is controlled by the effective reinforcing ratio of the dowels which extend from the CFT into the cap beam, and therefore lower stiffness and strength values were recorded than comparable ER connections. The strength of the WD connection may be similar to that of the ER connection if adequate reinforcing ratios are used. However some of this resistance is contributed by the compressive bearing of the flange on the steel tube, and this added strength which is not considered in the current design equations. Hence, the WD connection is prone to large and variable over-strength to the design values.

Two distinct failure modes were observed: (1) cap beam failure in which the headed dowels pulled out of the cap beam and (2) yielding and fracture of the longitudinal dowels within the soffit fill region. In all cases, significant soffit fill crushing was observed. The specimens that exhibited yielding and fracture of the longitudinal dowels demonstrated that extending the longitudinal dowels for a length of $24d_b$ into the CFT column and welding them to the steel tube using a flare bevel groove weld will assure good performance, good distribution of stress to the steel, and prevent damage to the tube. The influence of several parameters on the WD connection are noted below.

- De-bonding the longitudinal dowel in the connection region increases deformation capacity and significantly decreases cap beam damage.

- Providing transverse steel in the connection region with at least one hoop through the thickness of the soffit fill increases ductility and decreases cap beam damage by providing additional confinement in the joint region.

The WD connection in its current form has several disadvantages in terms of optimizing the objectives of accelerated bridge construction and decreasing labor. After the column is cast, precast super-structure elements must be supported using temporary shoring or a friction collar until the void can be grouted. Using individual ducts in place of a large corrugated pipe can potentially solve this issue (while decreasing construction tolerances), however using individual ducts was not evaluated in the testing program described in this report. Furthermore, dowels must be welded to the inside of the steel tube which requires skilled labor and additional time. Further, the welds are well inside the tube, and this increases the difficulty of welding and inspection of the welds. As these welds provide the primary load transfer from the steel tube into the connection dowels, they should be inspected according to requirements for fracture critical welds. As a final point, transverse reinforcing must be placed around the dowels before they are inserted into the cap beam, which requires additional labor.

The WD connection offers the same challenges encountered with traditional RC columns in terms of post-event inspection and repair. The longitudinal dowels are encased in concrete and grout, which makes it difficult to determine the damage state of the connection. This also increases the difficulty of developing repair strategies for this connection type. Further, significant damage to the concrete in the soffit fill is expected, while the concrete within the tube remains in very good condition.

10.2.3 Reinforced Concrete Connection

The RC connection utilizes both longitudinal and transverse reinforcing to transfer forces from the CFT column into the cap beam. A traditional reinforcing cage is extended from the CFT column into the cap beam, and cover is provided between the reinforcing cage and steel tube within the column. A gap is left between the steel tube and cap beam to permit development of the dowel bars. Tensile forces in the bars are developed by bond transfer between the bars and the concrete, shear stress and strain within the concrete, and ultimately bond stress transfer between the concrete fill and the steel tube. The concrete fill is very well confined by the steel tube to facilitate this transfer.

Experimental results demonstrated that the RC connection exhibits stiffness and strength significantly lower than the stiffness and strength of the CFT component, because the stiffness and strength of the RC connection is controlled both by the effective longitudinal reinforcing ratio in the connection region and the reduced moment arm. Failure of this connection was characterized by yielding and fracture of the longitudinal reinforcing in the gap between the steel tube and cap beam. Significant grout crushing was also observed in this region. As only one specimen which used the RC connection was tested, there is currently no basis to report the influence of any parameters on the behavior of this connection type.

The RC connection has many disadvantages in terms of optimizing the objectives of accelerated construction and decreasing labor. A flexible reinforcing cage must be constructed and temporarily supported within the steel tube. After the column is cast, precast super-structure elements must be supported using temporary showing or a friction collar until the void can be grouted. Similar to the WD connection, using individual ducts in place of a large corrugated pipe

can potentially solve this issue (while decreasing construction tolerances), however this configuration was not evaluated in this testing program.

The RC connection offers the same challenges encountered with traditional RC columns in terms of post-event inspection and repair. The longitudinal dowels are encased in concrete and grout, which makes it difficult to determine the damage state of the connection. This also increases the difficult of developing repair strategies for this connection type.

10.3 Future Work

Additional research should be conducted to further refine the design expressions, and evaluate the behavior of the connections for a much wider range of parameters. An evaluation of possible repair methods would be beneficial to demonstrate the advantages of using CFTs in highway bridge construction. Thus four primary areas of future work are recommended:

1) Utilize the detailed finite element models developed for the initial connection evaluation to conduct extensive parameter studies on the proposed connections.
2) Evaluate repair strategies for columns which have been moderately damaged following lateral load events.
3) Develop additional connections such that CFTs are more versatile for bridge construction; specifically a CFT-to-pile connection is needed.
4) CFTs should have larger torsional strength and deformability relative to RC columns. A research program aimed at evaluating the response of CFT columns and connections subjected to combined torsional, shear, flexure and axial loading is needed. In addition

this program should develop a connection capable of transferring torsion to the superstructure for skewed bridges.

ACKNOWLEDGMENTS

Research was sponsored by the California Department of Transportation under Agreement Number 65A0446. The views and conclusions contained in this document are those of the authors and should not be interpreted as representing official policies, either expressed or implied, of the California Department of Transportation. The authors gratefully acknowledge the financial support of the California Department of Transportation. In addition, the advice and assistance provided by Ron Bromenschenkel, Michael Cullen, and Peter Lee of the California Department of Transportation.

REFERENCES

AASHTOa (2011). AASHTO LRFD Bridge Design Speci cation. American Association of State Highway and Transportation Official, Washington, DC.

AASHTOb (2011). AASHTO Guide Speci caitons for LRFD Seismic Bridge Design. American Association of State Highway and Transportation Official, Washington, DC, 2 edition.

ACI 318(2011). "Building Code Requirements for Structural Concrete". American Concrete Institute, Farmington Hills, MI.

AISC (2011). Steel Construction Manual. American Institute of Steel Construction, Chicago, IL, 14 edition.

ATC-24. (1992). Guidelines for Testing Steel Components. Applied Technology Council: Redwood City, CA.

AWS D1.4 (2010). "Structural Welding Code – Reinforcing Steel." *American Welding Society*, Miami, FL.

Bishop, E. (2009). Evaluation of the flexural resistance and stiffness models for circular concrete- filled steel tube members subjected to combined axial- flexural loading. Master's thesis, University of Washington.

Brown, N.K., Kowalsky, M., and Nau, James. (2013). Strain Limits for Concrete Filled Steel Tubes in AASHTO Seismic Provisions. *North Carolina State University*. Report Number FHWA-AK-RD-13-05.

Caltrans, (2010) “Seismic Design Criteria Version 1.6,” California Department of Transportation.

Goode, C. and Lam, D. (2008). Concrete Filled Tube Columns - Tests Compared with Eurocode 4. In Engineering Foundation Conference, Devils Thumb Ranch, CO.

Haraldsson, O., James, T., Eberhard, M., and Stanton, J. (2012a). Laboratory tests of column-to-footing socket connections. Technical report, U.S. Department of Transportation, Federal Highway Administration.

Haraldsson, O., James, T., Eberhard, M., and Stanton, J. (2012b). Seismic resistance of socket connections between footing and precast column. Journal of Bridge Engineering.

Hitaka, T., Suita, K., and Kato, M. (2003) CFT Column Base Design and Practice in Japan, *Proceedings of the International Workshop on Steel and Concrete Composite Construction (IWSCCC-2003)*, Report No. NCREE-0.-0.26, National Center for Research in Earthquake Engineering, Taipei, Taiwan.

Hsu, H. and Lin, H. (2003) Performance of Concrete-Filled Tube Base Connections Under Repeated Loading, *Proceedings of the International Workshop on Steel and Concrete Composite Construction (IWSCCC-2003)*, Report No. NCREE-0.-0.26, National Center for Research in Earthquake Engineering, Taipei, Taiwan.

Janes, T. (2011). Precast column socket connections for thin spread footings. Master's thesis, University of Washington.

Kappes, L., Berry, M., Stephens, J., and McKittrick, L. (2012) Concrete Filled Steel Tube Piles to Concrete Pile-Cap Connections, *Proceedings of the 2012 Structures Congress and Exposition,* 29 March – 31 March, Chicago IL.

Kappes, L. Berry, M., and Stephens, J. (2013). Performance of Steel Pipe Pile-To-Concrete Cap Connections Subject To Seismic or High Transverse Loading: Phase III Confirmation of Connection Performance. *Montana State University*. Report Number FHWA/MT-13-001/8203.

Kawaguchi, J. and Morino, S. (2006). Experimental Study on Strength and Stiffness of Bare Type CFT column Base with Central Reinforcing Bars. *Composite Construction in Steel and Concrete V.*

Kingsley, A. (2005). Experimental and analytical investigation of embedded column base connections for concrete filled high strength steel tubes. Master's thesis, University of Washington.

Lee, J. (2011). Experimental investigation of embedded connections for concrete- lled steel tube columns subjected to combined axial- exural loading. Master's thesis, University of Washington.

Lee, J. and Fenves, G. (1998). Platic-damage modeling for cyclic loading of concrete structures. Journal of Engineering Mechanics, 124(8):892{900.

Lehman, D.E. and Roeder, C.W. (2012) Foundation Connection for Circular Concrete Filled Tubes, *Journal of Constructional Steel Research,* Vol. 78, November 2012, pgs. 212-25, Elsevier.

Marson, J. and Bruneau, M. (2004). Cyclic Testing of Concrete-Filled Circular Steel Bridge Piers Having Encased Fixed-Base Detail, *ASCE Journal of Bridge Engineering*, Vol. 9, No. 1,pp. 14-23.

Matsumoto, E. (2009). Emulative precast bent cap connections for seismic regions: Grouted duct and cap pocket test results: Grouted duct and cap pocket test results, design and construction specifications, design examples, and connection details. Technical Report ECS-CSUS-2009-05, Sacramento State University.

Montejo, L., Kowalsky, M., and Hassan, T. (2009). Seismic Behavior of Flexural Dominated Reinforced Concrete Bridge Columns at Low Temperatures, *Journal of Cold Regions Engineering*, Vol. 23, pp. 18-42.

Montejo, L. Gonzalez-Roman, L. a., and Kowalsky, M. (2013). Seismic Performance Evaluation of Reinforced Concrete-Filled Steel Tube Pile/Column Bridge Bents, *Journal of Earthquake Engineering*, Vol. 16, No. 3, pp. 401-424.

Morino, S., Kawaguchi, J., Tsuji, A., and Kadoya, H. (2003). Strength and Stiffness of CFT Semi-Embedded Type Column Base, *Proceedings of ASSCCA 2003*, Sydney Australia.

Pang, J., Eberhard, M., and Stanton, J. (2010). Large-Bar Connection for Precast Bridge Bents in Seismic Regions. Journal of Bridge Engineering, pages 231-239.

Pang, J., Steuck, K., Cohagen, L., Stanton, J., and Eberhard, M. (2008). Rapidly constructable large-bar precast bridge-bent seismic connections. Technical Report WA-RD 684.2, Washington State Department of Transportation.

Raynor, D., Lehman, D., and Stanton, J. (2002). Bond-slip response of reinforcing bars grouted in ducts. ACI Structural Journal, 99(5):568{576.

Restrepo, J., Tobolski, M., and Matsumoto, E. (2011). Development of a Precast Bent Cap System for Seismic Regions. Technical Report 681, NCHRP.

Roeder, C.W., Cameron, B., and Brown, C.B., (1999) Composite action in concrete filled tubes, *Structural Engineering*, ASCE, Vol 125, No. 5, May 1999, pp. 477-84.

Roeder, C.W., Lehman, D.E., and Bishop, E. (2010). Strength and Stiffness of Circular Concrete Filled Tubes, *ASCE Journal of Structural Engineering*, Vol 135, No. 12, pgs 1545-53, Reston, VA.

Roeder, C., Lehman, D., and Stephens, M. (2014). Concrete filled tubes for accelerated bridge construction. In Transportation Research Record, Washington, D.C.

Roeder, C.W, Lehman, D.E., and Thody, R. (2009) Composite Action in CFT Components and Connections, *AISC Engineering Journal*, AISC, Vol 46, No. 4, pp. 229-42

Saenz, L. (1964). Discussion of equation for the stress-strain curve of concrete. ACI Journal, 61:12229-1235.

Stueck, J., Eberhard, M., and Stanton, J. (2009). Anchorage of large diameter reinforcing bars in ducts. ACI Structural Journal, pages 506{513.

Stueck, K., Eberhard, M., and Stanton, J. (2007). Anchorage of large bars in grouted ducts. Technical Report WA-RD 684.1, Washington State Department of Transportation.

Thody, R. (2006). Experimental investigation of the exural properties of high-strength concrete-filled steel tubes. Master's thesis, University of Washington.

Tran, H., Eberhard, M., and Stanton, J. (2012). Seismic-resistant connections between precast concrete columns and drilled shafts. Technical report, TRANSNOW.

Williams, T. (2006). Experimental investigation of high strength concrete filled steel tubes in embedded column base foundation connections. Master's thesis, University of Washington.

APPENDIX A: DESIGN EXAMPLES

This example aims to re-design conventional reinforced concrete bridge columns and cap beam connections using the design recommendations and expressions provided in this report using the Laguna De Santa Rosa bridge as a prototype bridge. The two column bridge bent was redesigned using CFT columns and column-to-cap beam connections. The columns are 15-ft in height (from the bottom of the cap beam to the start of a drilled shaft), and the column was originally designed as a reinforced concrete column with a diameter of 48-in., 32 bundled No. 11 bars in the longitudinal direction, and No. 8 hoops at 6-in. in the transverse direction. The resulting longitudinal reinforcing ratio is 2.8%, and the effective horizontal reinforcement was approximately 1.1%. Note that the purpose of this example is to highlight the design requirements specific to the ER connection. Corbel reinforcing and side reinforcing which are consistent with requirements in the Caltrans SDC are not designed. The requirements for horizontal stirrups are consistent with the requirements in the SDC, however design of these stirrups has been included to show that one layer must pass above the embedded CFT.

Design Process

The columns were re-designed using the following procedure. This procedure is similar to the procedure currently used by Caltrans to design RC columns.

1. Determine the factored load demands (axial, bending, and shear) on the columns (Note: These demands were supplied by a Caltrans engineer for this example).
2. Find an initial estimate of the column diameter and tube thickness to sustain the axial load such that $0.1<P/P_o<0.2$ for the full range of loading. Initial D/t estimates should range between 80 and 100.
3. Determine the effective stiffness of the column.
4. Using the effective stiffness, determine the moment magnification factor for the column.
5. Magnify the moments by the magnification factor.
6. Determine the required M_n and P_n combinations for each load case, i.e., M_u/ϕ and P_u/ϕ where $\phi = 0.75$ for most live loads and $\phi = 1.0$ for seismic loads.
7. Compute the P-M interaction curve.
8. Compare the computed demands and capacity.
9. For the designed CFT, find the required embedment depth into the cap beam.
10. Calculate the required concrete depth above the embedded CFT to eliminate punching shear failure during construction (for precast construction).
11. Size the initial depth of the cap beam based on the results of steps 9 and 10.
12. Capacity design the cap beam for the plastic moment capacity of the CFT.

Material Properties

f'_c = 6-ksi
E_c = 4415-ksi
$F_{y,st}$ = 50-ksi
E_s = 29000-ksi

Loads

Service → P_u = 790-kip, M_u = 1920 kip-ft
Controlling Limit State Load → P_u = 1300-kip, M_u = 5300 kip-ft

Size Initial Section Based on Axial Load Range

The initial section is designed to have an axial load in the range of $0.1P_o - 0.2P_o$ where

$P_o = \pi*D*t*F_{y,st} + 0.95*(D^2/4)*\pi*f'_c)$

Using a target D/t = 90

→ t = D/90

Solving for D (taking the service load as P_o):

$10(790/0.75) = 10(1053.33) = \pi*D*(D/90)*50+0.95*(D^2/4)*\pi*6) \rightarrow D = 41.145$-in.

Try → D = 44-in., t = 0.5-in. (D/t = 88)

Calculate the Effective Stiffness of the CFT Component

$EI_{eff} = E_sI_{st} + C'E_cI_c$

→ I_{st} = 16726 – in.

→ I_c = 183984 – $in.^4$

→ A_{st} = 68.72-$in.^2$

→A_c = 1486.17-$in.^2$

→ $C' = 0.15+P/P_o+A_{st}/(A_{st}+A_c)=0.15+1300/11700+68.72/(68.72+1486.17) = 0.305$

$EI_{eff} = 29000*16726 + 0.305*4415*183984 = 7.33*10^8$ kip-in^2

Calculate the Moment Magnification Factor

$\delta_s = 1/(1-P_u/(\phi P_e))$

→ $P_e = \pi^2*EI_{eff}/(Kl)^2 = \pi^2*7.33*10^8/(0.5*15*12)^2$=893138-kip

$\delta_s = 1/(1-1300/(0.9*893138)) = 1$

Compute the P-M Interaction Diagram

The P-M interaction diagram was computed using the procedure specified in AASHTO (2015) and described in Chapter 2. First, the material based interaction surface was developed using the PSDM. Then, the influence of geometric non-linearity was considered to develop the design interaction diagram. The demands are shown on the plot. As can be seen from the plot, the CFT component has adequate capacity to sustain the combined loading combination, and the axial loads are in the range of $0.1P_o$.

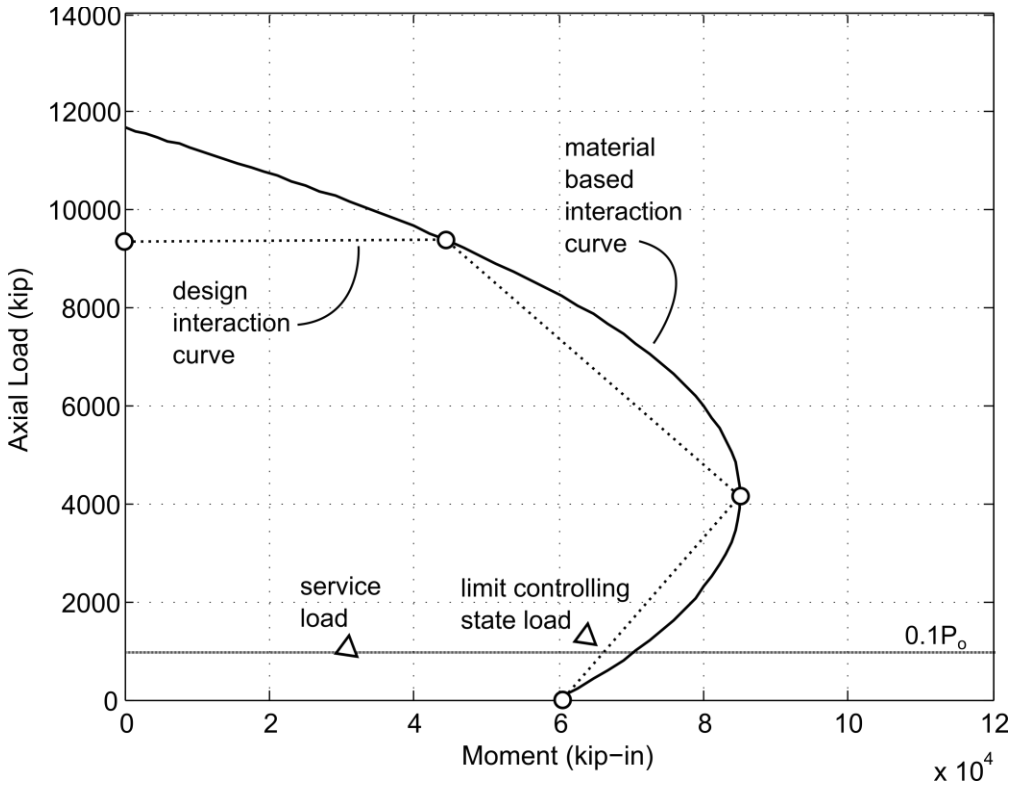

Fig. A1. P-M Interaction Curve

Calculate the Shear Strength

The shear strength of the section is computed assuming that only the steel tube contributes to the strength. Current research being conducted at the University of Washington is being conducted to evaluate the contribution of the concrete to the shear strength. The following shear strength expression has been adopted from the AISC steel construction manual (AISC, 2010).

$\phi V_n = \phi 0.6 F_{y,st} A_v$

→ $A_v = 0.5A_{st} = 0.5*68.72 = 34.36\text{-in.}^2$

$\phi V_n = 0.75*0.6*50*34.36 = 773\text{-kip}$

Size the Inverted-T

Determine the Required Width of the Stem

The outer diameter of the annular ring is 52-in. The inner diameter of the corrugated pipe must exceed this. Galvanized corrugated pipe with an inner diameter of 54-in. is readily available. Thus the width of the stem must exceed this diameter with standard cover requirements.

Try a stem width of 60-in.

Calculate the Required Tube Embedment Depth into the Cap Beam

Calculate the required tube embedment depth into the cap beam using Equation 9.2 in this document.

$$L_e \geq \sqrt{\frac{D_o^2}{4} + \frac{DtF_{u,st}}{6\sqrt{f'_{c,cap}}}} - \frac{D_o}{2} \ (psi)$$

$D_o = D + 16t = 44 + 16*0.5 = 52\text{-in.}$

$$L_e \geq \sqrt{\frac{52^2}{4} + \frac{44 * 0.5 * 60000}{6\sqrt{6000}}} - \frac{52}{2} = 33.3in.$$

Use L_e = 33.5-in.

Calculate the Required Depth Above the Embedded Tube

For the purpose of sizing the inverted-t, the depth above the embedded tube is calculated to resist punching shear failure during construction prior to grouting the connection. This calculation is made according to ACI requirements for punching shear conservatively assuming 1-way shear.

Assumed construction dead load = 55-kip

$$\phi V_c = \phi 2\sqrt{f'_c} b_o d$$

→ $b_o = \pi(D_o + d) = \pi(52 + d)$

$$\frac{55000}{0.75} = 2\sqrt{6000}\pi(52 + d)d \rightarrow d = 2.75in.$$

Next, calculate the total required depth (deck and inverted-t) above the embedded CFT to eliminate the potential for punching shear failure during seismic loading using Equation 9.3 in this document. Note that C_c and C_s are in lbs.

$$L_{pc} \geq \sqrt{\frac{D_o^2}{4} + \frac{C_c + C_s}{6\sqrt{f'_{c,cap}}}} - \frac{D}{2} - L_e\ (psi)$$

$$L_{pc} \geq \sqrt{\frac{52^2}{4} + \frac{1850000}{6\sqrt{6000}}} - \frac{44}{2} - 33.5 = 13in.\ for\ seismic$$

So the inverted-t requires a depth above the tube of 2.75-in. for construction loads, while the total required depth is 13-in. for seismic loading. Assuming a deck depth of around 8-in. this allows 5-in. of depth above the embedded CFT in the inverted-t. Allowing additional space for reinforcing in the cap beam, a depth above the embedded CFT of 8.5-in. is selected.

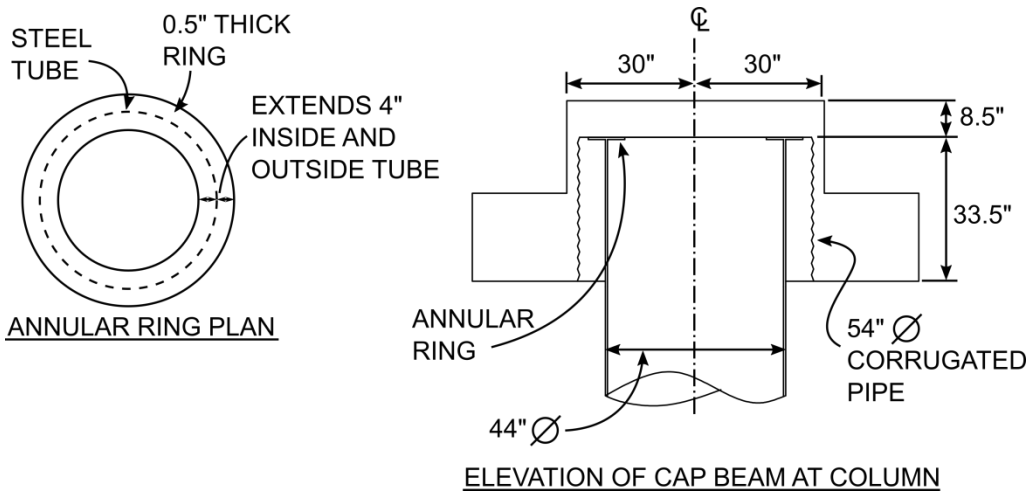

Fig. A2. Cap Beam Dimensions

Capacity Design the Cap Beam to Resist 1.25M_p of the CFT Column

Note that it is the intention of this example to demonstrate the design method in terms of using the ER connection. Thus the design of the corbels to carry the longitudinal girders and diaphragm is not shown. A ledge width of 22-in. is assumed based on the dimensions of the prototype bridge.

$1.25M_{p,CFT}$ = 85000 kip-in.

Try 20 No. 10 bars in the bottom of the inverted-t and 12 No. 10 bars in the top of the inverted-t. Additional cap beam reinforcing consisting of 14 No. 10 bars is included in the deck. The primary flexural reinforcing is arranged as shown in Fig. A2. The resulting flexural capacity of the cap beam are calculated as:

M_n^+ = 86382 kip-in.
M_n^- = 85593 kip-in.

Check that longitudinal reinforcing spacing requirements have been met in the ledge:

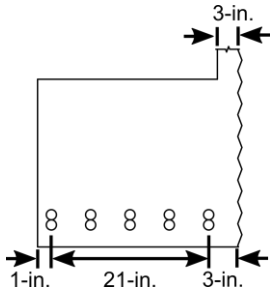

Spacing between bars = 21/4 = 5.25-in. OK

Determine the Required Area of Shear Reinforcing in the Joint Region

The required shear reinforcing in the joint region is calculated using Equation 9.4 in this document. This reinforcing must be evenly distributed in the area highlighted in Fig. 9.6.

$A_s^{jv} = 0.65A_{st} = 0.65*68.72 = 44.67 – in.^2$

Use 100 No. 6 vertical stirrup legs evenly distributed around the column → A_s^{jv} = 44-in.^{2} (See Fig. A4 for plan view of vertical stirrups)

Determine the Required Area of Horizontal Stirrups

The required area of horizontal stirrups is consistent with the requirements in the Caltrans SDC. This reinforcing must be placed in the highlighted regions in Fig. 9.6, and one layer of horizontal stirrups must pass above the embedded CFT as shown in Fig. A2.

$A_s^{jh} = 0.1A_{st} = 0.1*68.72 = 6.872\text{-in.}^2$

Use 3 rows of No. 7 hooks → $A_s^{jh} = 7.2\text{-in.}^2$

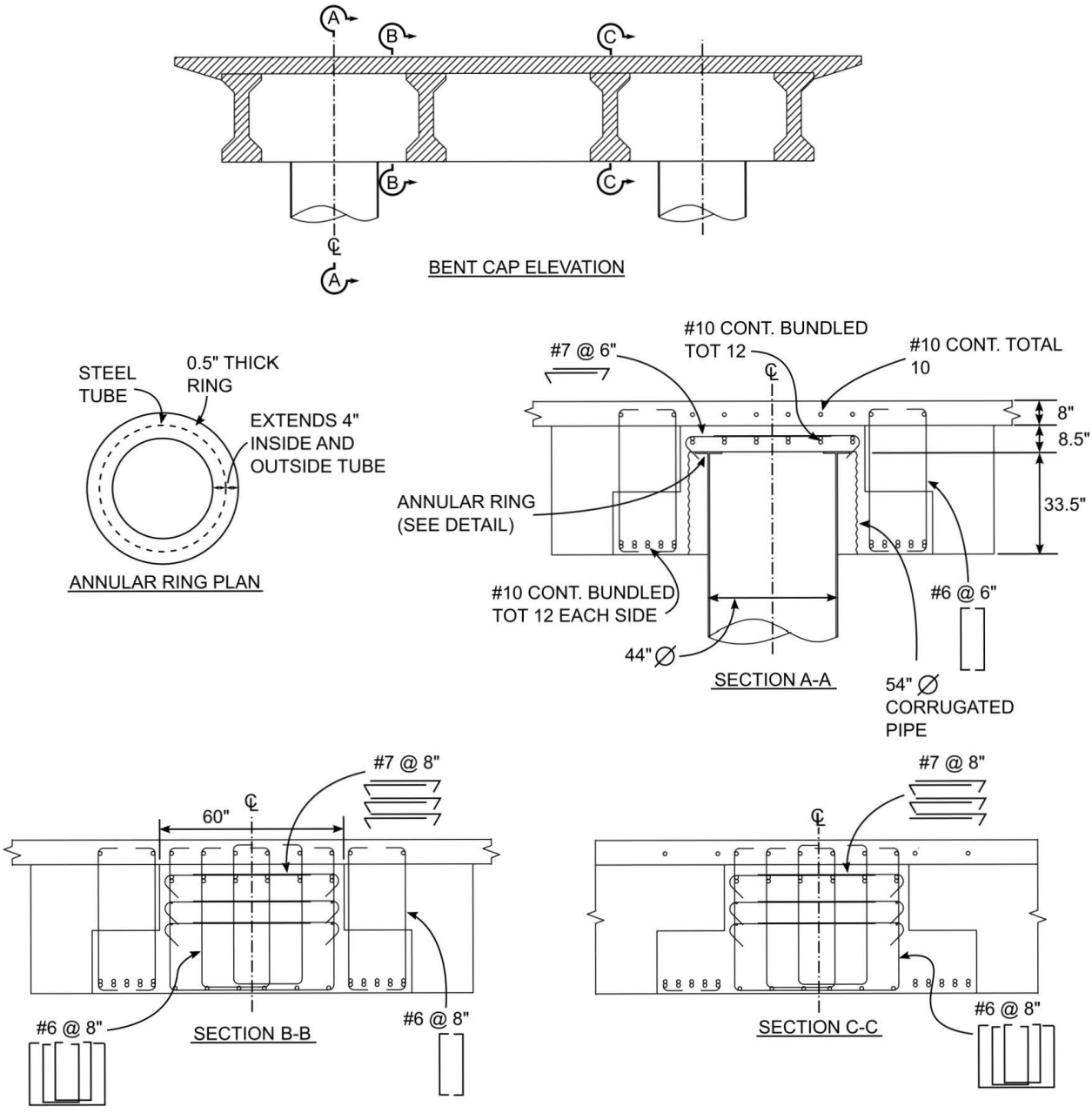

NOTE: DECK REINFORCING, DIAPHRAGM REINFORCING, CORBEL REINFORCING AND SIDE REINFORCING NOT SHOWN

Fig A3. Final Cap Beam Design

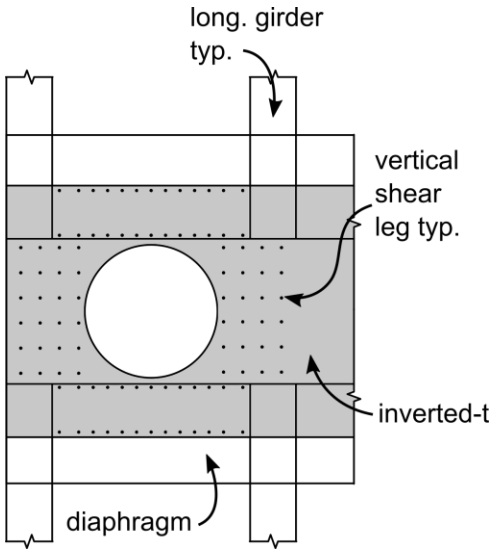

Fig A4. Plan View of Vertical Stirrup Distribution

Design Example #2: Design of WD Connection

This example aims to re-design conventional reinforced concrete bridge columns and cap beam connections using the design recommendations and expressions provided in this report for the WD connection using the Laguna De Santa Rosa Bridge as a prototype bridge. The two column bridge bent was redesigned using CFT columns and WD CFT column-to-cap beam connections. The columns are 15-ft in height (from the bottom of the cap beam to the start of a driven pile), and the column was originally designed as a reinforced concrete column with a diameter of 48-in., 32 bundled No. 11 bars in the longitudinal direction, and No. 8 hoops at 6-in. in the transverse direction. The resulting longitudinal reinforcing ratio is 2.8%, and the effective horizontal reinforcement was approximately 1.1%. Note that the purpose of this example is to highlight the design requirements specific to the WD connection. Thus things like corbel reinforcing and side reinforcing which are consistent with requirements in the Caltrans SDC are not designed. The requirements for vertical and horizontal stirrups are consistent with the requirements in the SDC, however design of these stirrups has been included to demonstrate the design.

Design Process

The columns were re-designed using the following procedure. This procedure is similar to the procedure currently used by Caltrans to design RC columns.

1. Determine the factored load demands (axial, bending, and shear) on the columns (Note: These demands were supplied by a Caltrans engineer for this example).
2. Find an initial estimate of the column diameter and tube thickness to sustain the axial load such that $0.1<P/P_o<0.2$ for the full range of loading. Initial D/t estimates should range between 80 and 100.
3. Determine the effective stiffness of the column.
4. Using the effective stiffness, determine the moment magnification factor for the column.
5. Magnify the moments by the magnification factor.
6. Determine the required M_n and P_n combinations for each load case, i.e., M_u/ϕ and P_u/ϕ where $\phi = 0.75$ for most live loads and $\phi = 1.0$ for seismic loads.
7. Compute the P-M interaction curve for the CFT.
8. Select a dowels for the connection.
9. Compute the P-M interaction curve for the connection.
10. Compare the computed demands and capacity.
11. Find the required length the dowels should extend into the CFT column.
12. Design weld between the dowels and steel tube.
13. Find the required length the dowels should extend into the cap beam.

14. Calculate the required concrete depth above the embedded CFT to eliminate punching shear failure.
15. Size the initial depth of the cap beam based on the results of steps 13 and 14.
16. Size the flange.
17. Calculate the soffit fill depth.
18. Calculate the required de-bonded length.
19. Design column transverse reinforcing which extends into the cap beam.
20. Capacity design the cap beam for the plastic moment capacity of the CFT.

Material Properties

f'_c = 6-ksi
E_c = 4415-ksi
$F_{y,st}$ = 50-ksi
E_s = 29000-ksi

Loads

Service → P_u = 790-kip, M_u = 1920 kip-ft
Limit Controlling State Load → P_u = 1300-kip, M_u = 5300 kip-ft

Size Initial Section Based on Axial Load Range

The initial section is designed to have an axial load in the range of $0.1P_o - 0.2P_o$ where

$P_o = \pi*D*t*F_{y,st} + 0.95*(D^2/4)*\pi*f'_c)$

Using a target D/t = 90

→ t = D/90

Solving for D (taking the service load as P_o):

$10(790/0.75) = 10(1053.33) = \pi*D*(D/90)*50+0.95*(D^2/4)*\pi*6) \rightarrow D = 41.145$-in.

Try → D = 44-in., t = 0.5-in. (D/t = 88)

Check the Crushing Capacity of the WD Connection. Assume 32 No. 11 Dowels.

$P_o = A_{st,b}F_y + 0.85*(D^2/4)*\pi*f'_c$

→ $A_{st,b} = 32*1.56 = 49.92\text{-in.}^2$

$P_o = 49.92*68 + 0.85*(43^2/4)*\pi*6 = 10800$-kip

Calculate the Effective Stiffness of the CFT Component

$EI_{eff} = E_sI_{st} + C'E_cI_c$

→ I_{st} = 16726 – in.

→ I_c = 183984 – in.^{4}

→ A_{st} = 68.72-in.^{2}

→A_c = 1486.17-in.^{2}

→ C' = 0.15+P/P_o+A_{st}/(A_{st}+A_c)=0.15+1300/11700+68.72/(68.72+1486.17) = 0.305

EI_{eff} = 29000*16726 + 0.305*4415*183984 = 7.33*10^8 kip-in^2

Calculate the Effective Stiffness of the WD Connection

EI_{eff} = 4415*92691.25 = 4.09*10^8 kip-in^2 (From SAP2000)

Calculate the Moment Magnification Factor

δ_s = 1/(1-P_u/(ϕP_e))

→ P_e = π^2*EI_{eff}/(Kl)^2 = π^2*7.33*10^8/(0.5*15*12)^2=893138-kip

δ_s = 1/(1-1300/(0.9*893138)) = 1

Compute the P-M Interaction Diagrams

The P-M interaction diagram for the CFT component was computed using the procedure specified in AASHTO (2015) and described in Chapter 2. First, the material based interaction surface was developed using the PSDM. Then, the influence of geometric non-linearity was considered to develop the design interaction diagram. The demands are shown on the plot. As can be seen from the plot, the CFT component has adequate capacity to sustain the combined loading combination, and the axial loads are in the range of 0.1P_o.

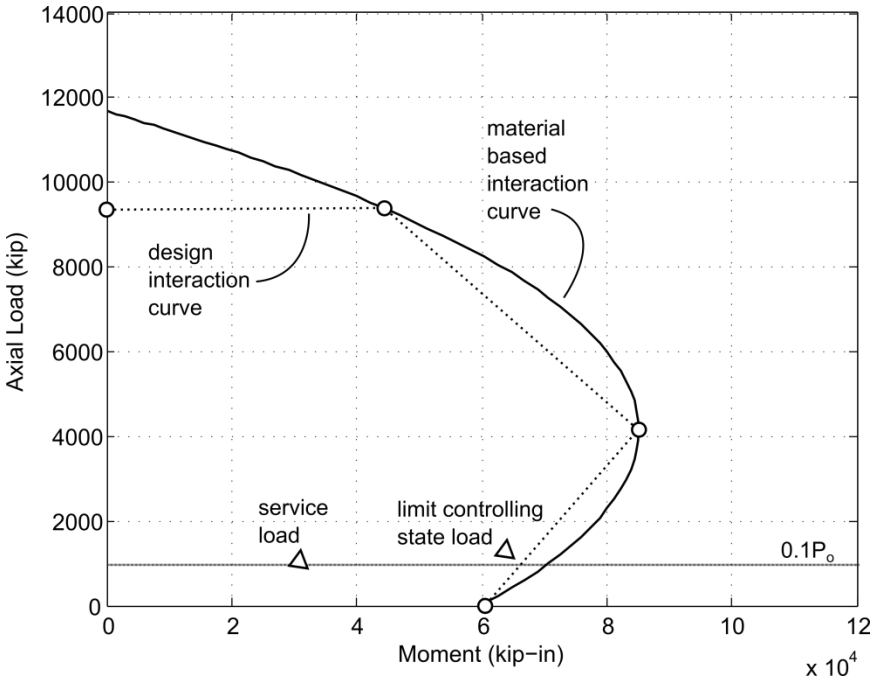

Fig. A5. P-M Interaction Curve for CFT Component

The P-M interaction diagram for the connection region was developed using SAP2000 and is shown below along with the demands.

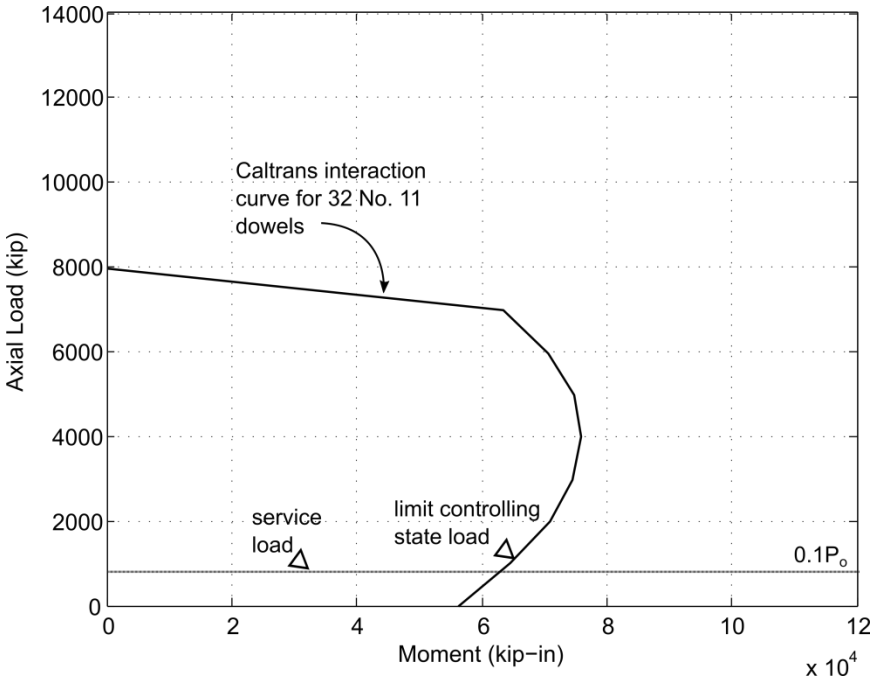

Fig. A6. P-M Interaction for Connection Region

Calculate the Required Length the Dowels Should Extend into the Steel Tube

The dowels are required to extend into the steel tube for a distance $24d_b$ as specified in Section 9.4.2 of this report.

→ $24d_b = 24*(11/8) = 33$-in.

Design the Weld between the Dowels and Steel Tube

The weld length is the greatest of Equations 9.10a through 9.10c in this report. Assume a 70XX electrode with a tensile strength of 70-ksi.

$$L_w \geq \frac{5.6A_bF_{y,b}}{F_{EXX}d_b} = \frac{5.6(1.56)(68)}{70(1.375)} = 6.17 - in.$$

$$L_w \geq \frac{0.83A_bF_{y,bar}}{F_{y,st}t} = \frac{0.83(1.56)(68)}{50(0.5)} = 3.52 - in.$$

$$L_w \geq \frac{1.11A_bF_{y,b}}{F_{u,st}t} = \frac{1.11(1.56)(68)}{70(0.5)} = 3.36 - in.$$

→ $L_w = 6.25$-in.

Calculate the Required Length the Dowels Should Extend into the Cap Beam

The dowels are required to extend into the cap beam according to Equations 9.6a through 9.6c in this report.

$$L_e \geq \frac{0.016\psi_eF_{y,b}}{\sqrt{f'_g}}d_b = \frac{0.016(1.0)(68000)}{\sqrt{6000}} * 1.375 = 19.31 - in.$$

$$L_e \geq \sqrt{\frac{D^2}{4} + \frac{1.2 * F_{y,b} * A_{st,b}}{6\pi\sqrt{f'_{cc}}}} - \frac{D}{2} = \sqrt{\frac{44^2}{4} + \frac{1.2 * 68000 * 49.92}{6\pi\sqrt{6000}}} - \frac{44}{2} = 35.2 - in.$$

→ $L_e = 35.25$-in.

Note: Need to check Equation 9.6c after the debonded length is calculated.

Calculate the Required Depth Above the Headed Dowels to Eliminate Punching Shear Failure

The required depth above the headed reinforcing is defined in Section 9.4.9 of this report.

$L_{pc} \geq 3d_h = 3(3.25) = 9.75\text{-in.}$

Size the Inverted-T

→ A total super structure depth of at least $L_e + L_{pc}$ is required. Assuming we have an 8-in. thick slab on this bridge, a clear cover above the headed reinforcing of at least 1.75-in. is required in the inverted-t. Use a clear distance of 6.75-in. in the inverted-t in the interest of maintaining the same super-structure depth as Example 1.

→ The depth of the inverted-t = 6.75 + 35.25 = 42-in.

Calculate the Flange Dimensions

→ Flange Diameter $D_o = D + 16t = 44+16(0.5) = 52\text{-in.}$

Calculate the Required Soffit Fill Depth

The required soffit fill depth is calculated according to Equation 9.7 of this report.

$$L_s \geq \sin(\theta_u)\left(\frac{D}{2} + 8t\right) = \sin(0.08)\left(\frac{44}{2} + 8 * 0.5\right) = 2 - in.$$

→ Use a soffit fill depth L_s = 2-in.

Note: One transverse hoop must be placed through the depth of the soffit.

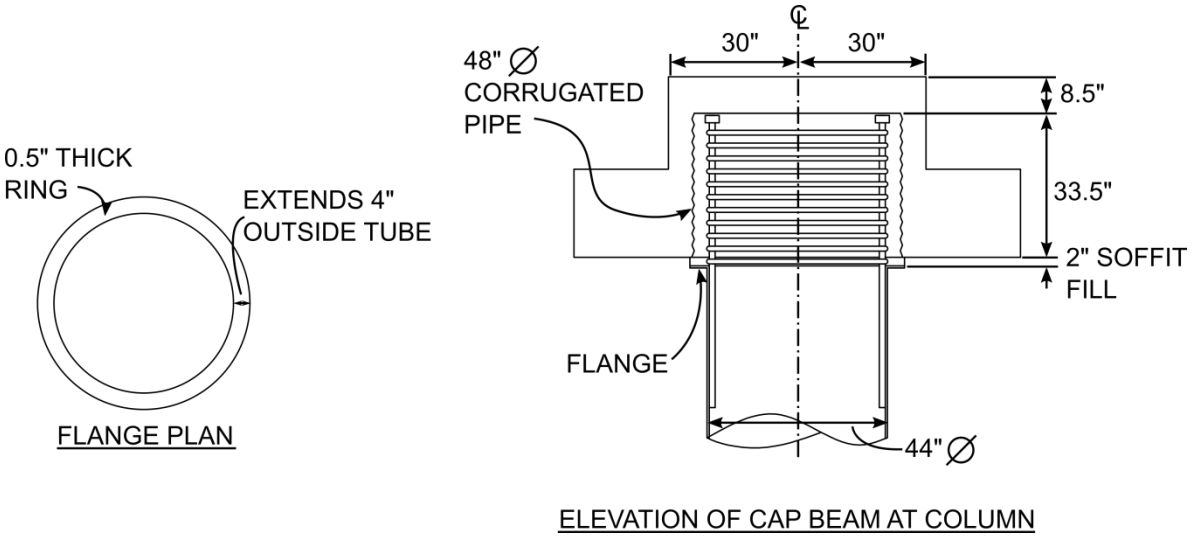

Fig. A7. Cap Beam Dimensions

Calculate the Required De-bonded Length

The de-bonded length is calculated using Equation 9.9 in this report assuming a target rotation demand of 8% and a steel ultimate strain of 0.09-in/in:

$$L_{db} = \frac{\tan\theta(D - t - d_b/2)}{0.7\varepsilon_u} = \frac{\tan(0.08)(44 - 0.5 - 1.375/2)}{0.7(0.09)} = 54.5 - in.$$

→ Use a de-bonded length L_{db} = 54.5-in.

Note: Need to check Equation 9.6c:

$$L_e \geq 3d_b + 0.5L_{db} = 3 * \left(\frac{11}{8}\right) + 0.5 * 54.5 = 31.375\ OK$$

Design Transverse Column Reinforcing which Extends into the Cap Beam

The required transverse reinforcing ratio which extends into the joint region is defined in Equation 7.23 of the Caltrans SDC.

$$\rho_s = 0.4 \times \frac{A_{st,b}}{{L_e}^2} = 0.4 \times \frac{49.92}{35.25^2} = 0.016$$

→ Use No. 9 hoops at 3-in. c-c → ρ_s = 0.016

Capacity Design the Cap Beam to Resist 1.2M_p of the Connection

Note that it is the intention of this example to demonstrate the design method in terms of using the ER connection. Thus the design of the corbels to carry the longitudinal girders and diaphragm is not shown. A ledge width of 22-in. is assumed based on the dimensions of the prototype bridge.

$1.2M_{p,CFT}$ = 79800 kip-in.

Try 20 No. 10 bars in the bottom of the inverted-t and 12 No. 10 bars in the top of the inverted-t. Additional cap beam reinforcing consisting of 14 No. 10 bars is included in the deck. The primary flexural reinforcing is arranged as shown in Fig. A3. The resulting flexural capacity of the cap beam are calculated as:

M_n^+ = 86382 kip-in.
M_n^- = 85593 kip-in.

Check that longitudinal reinforcing spacing requirements have been met in the ledge:

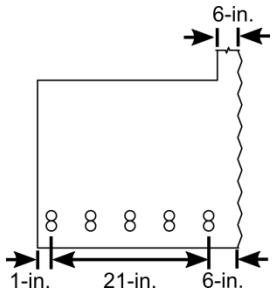

Fig. A8. Longitudinal reinforcing space check.

Determine the Required Area of Shear Reinforcing in the Joint Region

The required shear reinforcing in the joint region is calculated using Equation 7.19 in the Caltrans SDC.

$A_s^{jv} = 0.2A_{st,b} = 0.2*49.92 = 10 - in.^2$

Use No. 6 vertical stirrups as shown in Fig. A8

Determine the Required Area of Horizontal Stirrups

The required area of horizontal stirrups is consistent with the requirements in the Caltrans SDC. This reinforcing must be placed in the highlighted regions in Fig. 9.6, and one layer of horizontal stirrups must pass above the void as shown in Fig. A9.

$A_s^{jh} = 0.1A_{st} = 0.1*49.92 = 5\text{-}in.^2$

Use 3 rows of No. 6 hooks as shown in Fig. A9

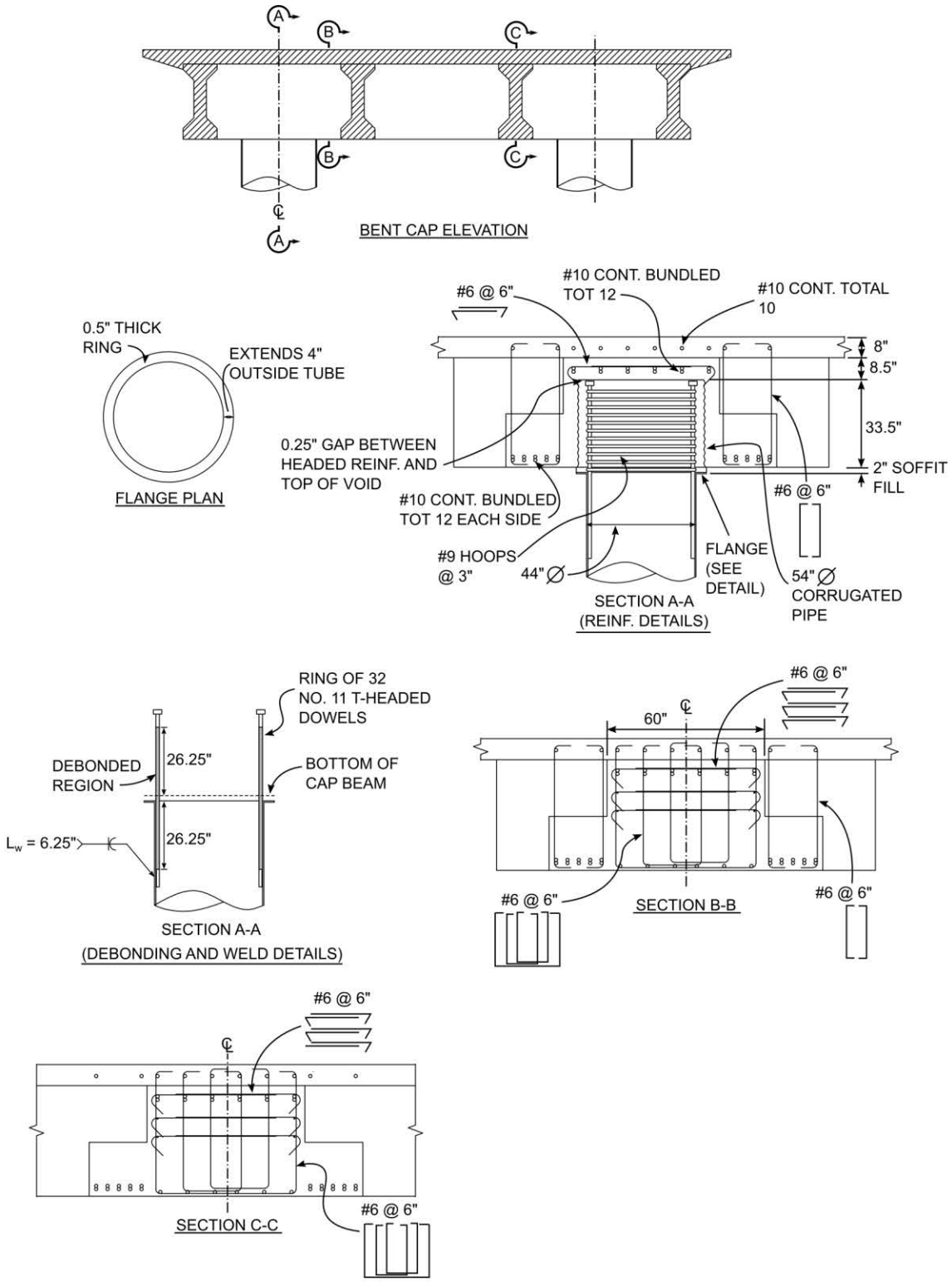

NOTE: DECK REINFORCING, DIAPHRAGM REINFORCING, CORBEL REINFORCING AND SIDE REINFORCING NOT SHOWN

Fig A9. Final Cap Beam Design

APPENDIX B: SPECIMEN REINFORCING DETAILS

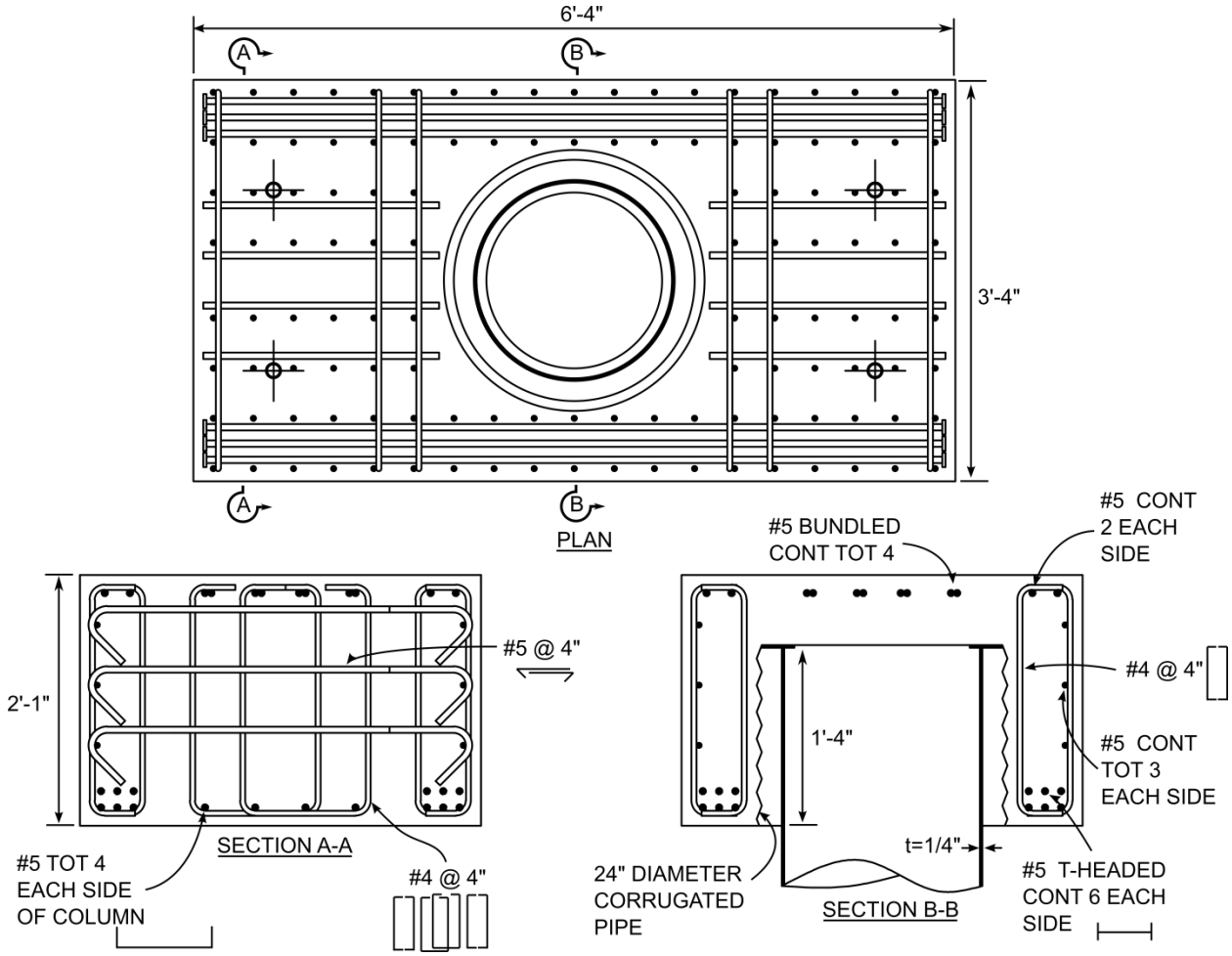

Fig. B1. ER80T Reinforcing Details

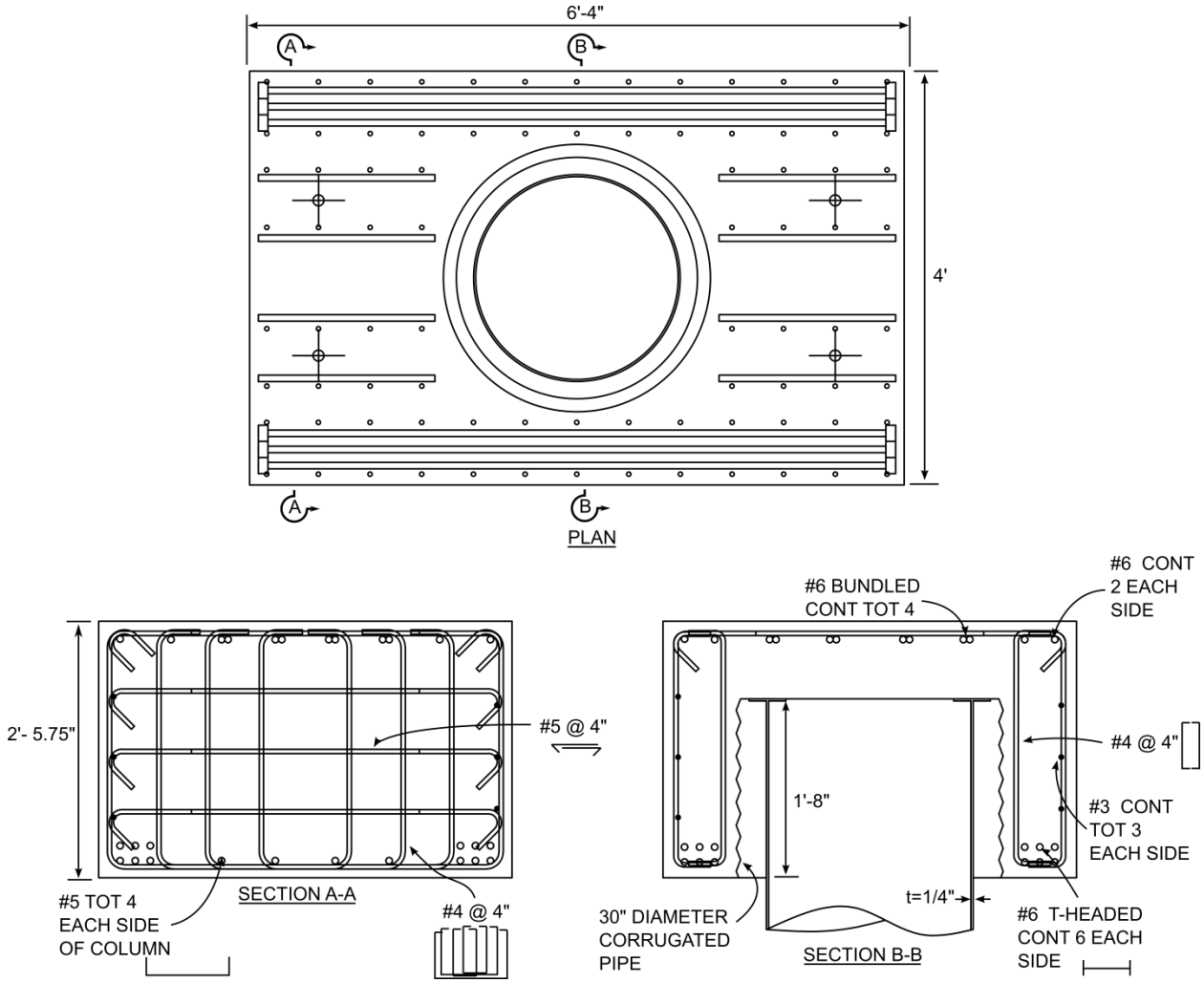

Fig. B2. ER96T Reinforcing Details

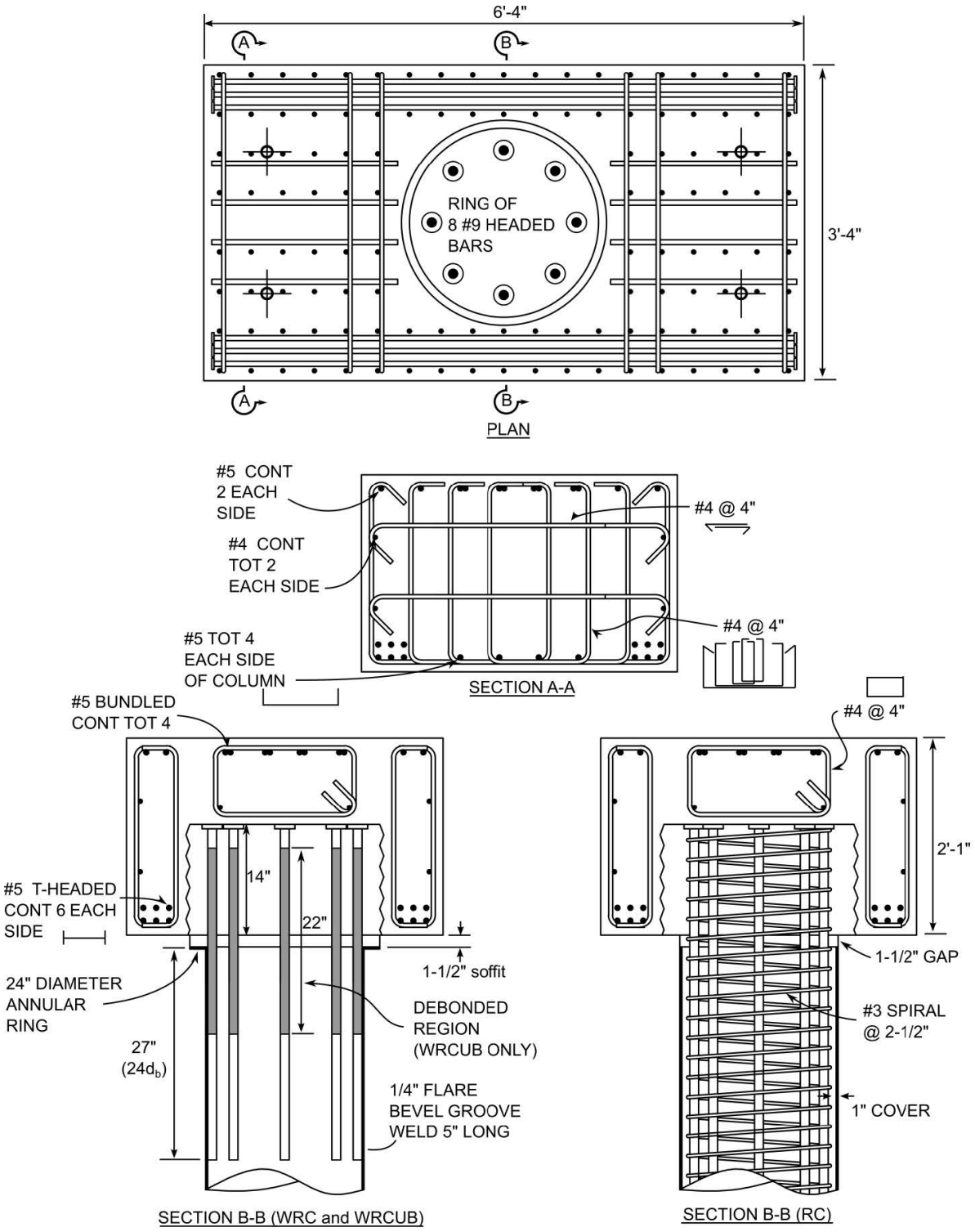

Fig. B2. WD80T1, WD80T2, and RC80T Reinforcing Details

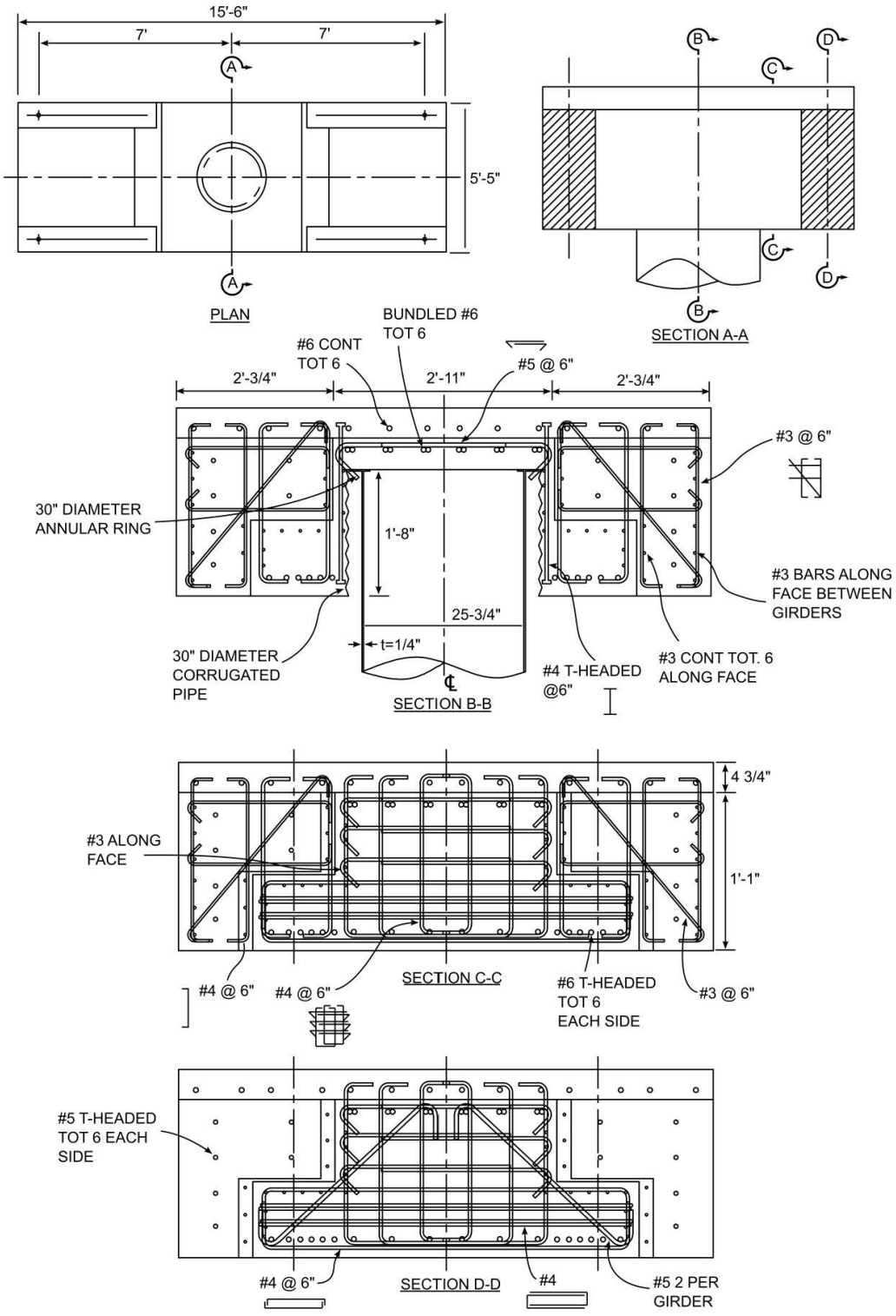

Fig. B3. ER103L Reinforcing Details

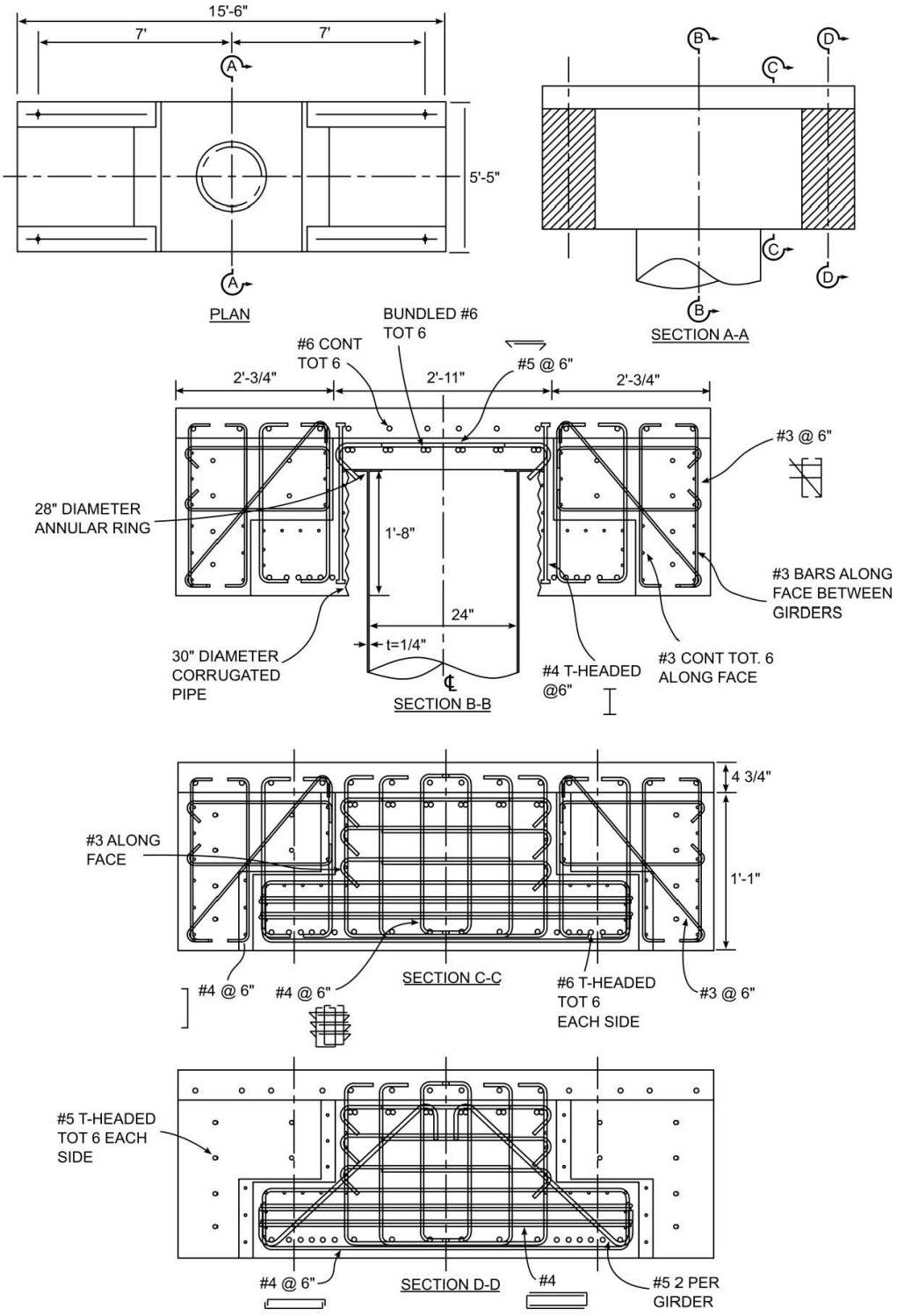

Fig. B4. ER96L Reinforcing Details

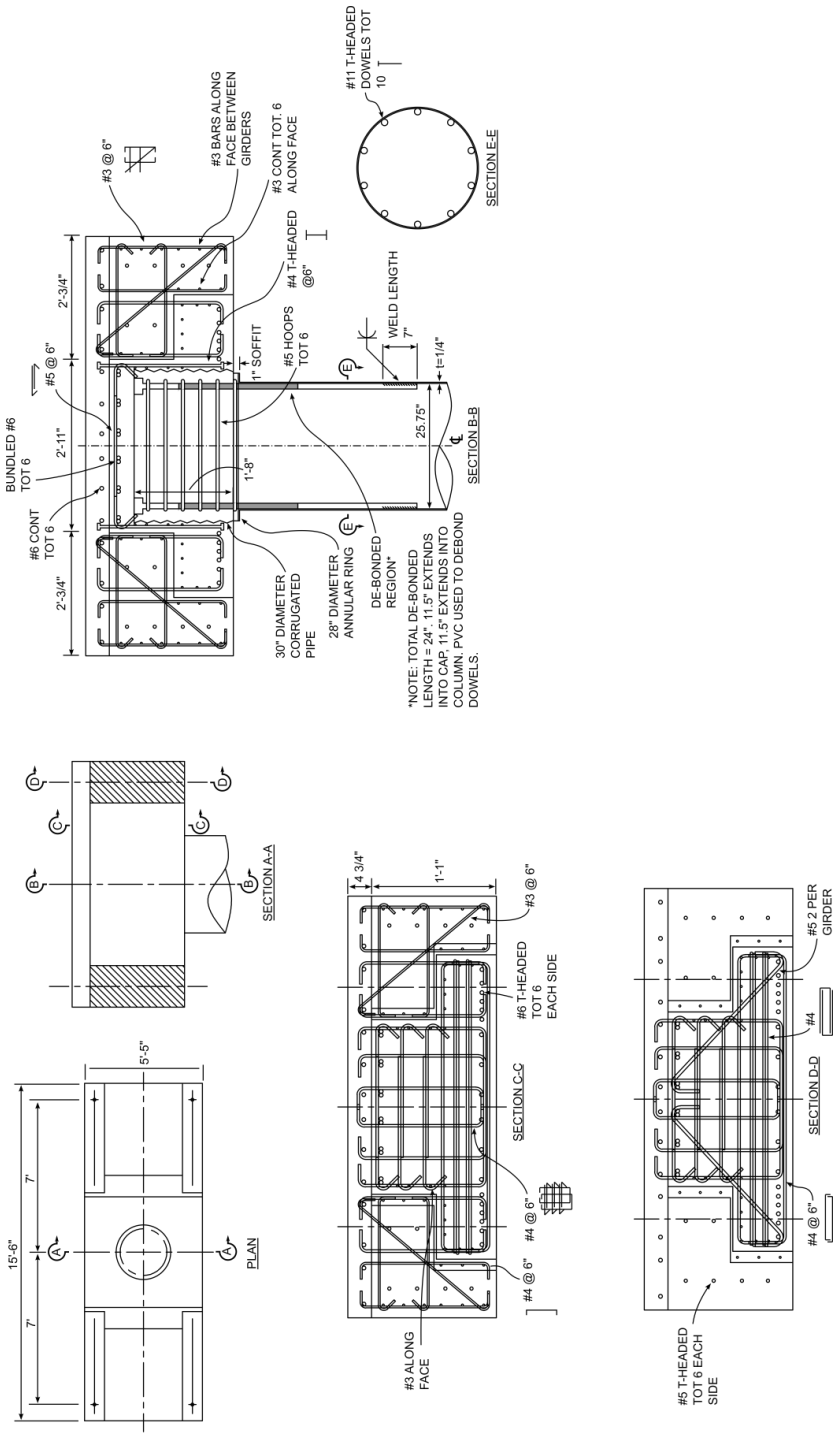

Fig. B5. WD103L Reinforcing Details

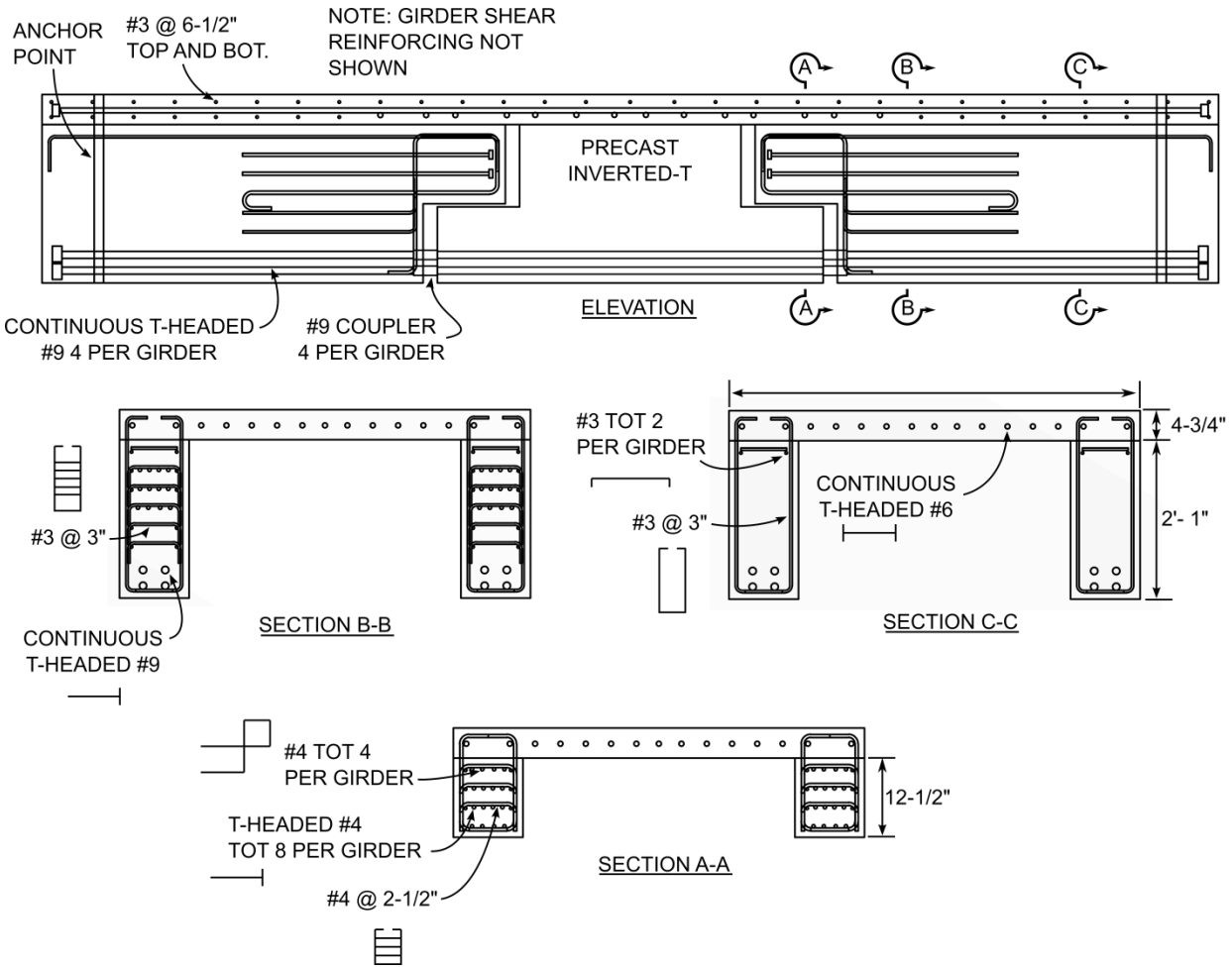

Fig. B6. Deck and Longitudinal Girder Reinforcing Details for Specimens ER96L, ER103L, and WD103

APPENDIX C: PROPOSED CODE LANGUAGE

1. Cap Beam Connections for CFT

1.1 General

CFT column to cap beam connections shall be designed using one of the following options:

1. An embedded ring (ER) connection in which the CFT column is embedded into the cap beam as illustrated in Figure 1.3.1.
2. A welded dowel (WD) connection in which a ring of reinforcing bars are welded inside the CFT column and extend into the cap beam as illustrated in Figure 1.4.1.
3. A reinforced concrete (RC) connection in which a ring of headed reinforcing bars is developed into the steel tube and extend into the cap beam as illustrated in Figure 1.5.1.

Each of these options can be employed using cast-in-place or precast super-structure components. Embedded ring connections shall be embedded into the reinforced concrete cap beam with an embedment depth and cap beam depth specified in Article 1.4. Welded dowel connections shall include reinforcing welded into the steel tube and extending into the cap beam and CFT column according to Article 1.5. Reinforced concrete connections shall include transverse and longitudinal reinforcing extending from the CFT column into the cap beam according to Article 1.6. Cap beam design for the embedded CFT connection shall conform to requirements in Article 1.3.3, while cap beam design for the welded dowel and embedded dowel connections shall conform to joint shear requirements in Section 7.4 of the Caltrans SDC V. 1.8 unless otherwise specified in the following sections.

1.1.1 Limitations of Application

None of these connections shall be used in bridges with skew greater than 20 degrees.

C1. Cap Beam Connections for CFT

C1.1 General

The CFT column to cap beam connections presented in Articles 1.4, 1.5, and 1.6 have been researched extensively (Lehman and Roeder 2012), and range in performance in terms of stiffness and strength. All of the connections can be implemented using cast-in-place or precast super-structure elements.

For precast construction, a void must be included in the precast elements through use of a corrugated pipe which meets the specifications in Article 1.2.3. The connections are to be grouted into place using fiber-reinforced grout which is designed according to Articles 1.2.1 and 1.2.2.

The three different connection types provide differing strengths and stiffness. The embedded ring connection is a full strength connection in which the strength is controlled by the capacity of the CFT column. The welded dowel connection can be designed as a full or partial strength connection depending on the longitudinal reinforcing ratio in the connection region. The reinforced concrete connection is a partial strength connection which cannot achieve the plastic moment capacity of the CFT without exceeding a longitudinal reinforcing ratio in the connection region of 4%.

C1.1.1 Limitations of Application

To date, no experimental testing has been conducted to evaluate the performance of these connections on bridges with a skew greater than 20 degrees.

1.2 Materials

Materials for the specified connections shall conform to the Caltrans standards, with several specific provisions included in Section 1.2 of this document.

1.2.1 Grout

The fiber-reinforced grout shall consist of prepackaged, cementitious grout which meets ASTM C-1107 for grades A, B, and C non-shrink grout. The grout shall conform to several additional performance requirements including compressive strength, compatibility, constructability, and durability. These requirements are summarized in Table 1.1.1. The 28-day grout strength f'_g must exceed f'_c of the surrounding concrete components. Grout using metallic formulations shall not be permitted, and grout shall be free of chlorides. No additives shall be added to pre-packaged grout.

Table 1.2.1.1 Grout Specifications

Property	Permitted Values
Mechanical Compressive Strength	Must exceed f'_c of surrounding concrete at 28-days. Minimum grout strength f'_g shall exceed 6-ksi.
Compatibility Non-Shrink	Grade A, B, or C Per ASTM C-1107.
Constructability Flow	Mix to flowable consistency according to manufacturer specification.
Durability Freeze thaw Sulfate resistance	300 cycles, relative durability factor 90% per ASTM C666. Expansion at 26 weeks < 0.3% per ASTM C1012

1.2.2 Fiber Reinforcing

Macro polypropylene fiber shall be included with a minimum volume of 0.2%, and shall be mixed according to manufacturer specification.

1.2.3 Corrugated Metal Duct

Corrugated metal ducts are used to provide voids in precast components. The ducts shall be galvanized

C1.2.1 Grout

Provisions in 1.2.1 have been included to ensure the grout has properties that provide adequate strength, are conducive to longevity, and provide constructability such that the grout can be placed efficiently for ABC. These requirements are based loosely on recommendations provided in NCHRP Report 651. Grouts with chloride are not permitted as these materials can accelerate corrosion in the connection reinforcing and steel tube. Additives are not permitted because pre-packaged grouts are proprietary mixes which should not be modified.

C1.2.2 Fiber Reinforcing

Macro polypropylene fiber (not micro) reinforcing is included to provide crack resistance and bounding characteristics between the tube and corrugated metal duct. Test results to date have not evaluated the use of alternative fibers including steel fibers.

C1.2.3 Corrugated Metal Duct

The use of corrugated metal ducts for grouted connections has been researched extensively. These ducts provide mechanical interlock between the cap

steel according to ASTM A653. Duct diameter shall be selected based on construction tolerances. Plastic ducts are not permitted.

1.2.4 Reinforcing

Reinforcing in the connection region shall conform to ASTM A706 Gr. 60 (or Gr. 80 if allowed) requirements for weldable reinforcing.

1.2.5 Tube Steel

Steel tubes may either be straight seam or spiral welded and must conform to either ASTM or API requirements. Spiral welded tubes must be welded using a double submerged arc welding process, and weld metal properties must match properties of the base metal and meet minimum toughness requirements of AISC demand critical welds (AISC 2010).

beam concrete and grout, and provide confinement in the joint region. Research on the behavior of the connections using plastic ducts is limited, and therefore their use is currently not permitted.

C1.2.4 Reinforcing

ASTM A706 places restrictions on the chemical composition of reinforcing bars to enhance welding properties. Welding requirements are discussed in Article 1.4.3.

C1.2.5 Tube Steel

Selection of tube material designation (ASTM or API) plays a role in the ductility of the full strength embedded CFT connection. API grade steels tend to be of higher quality than ASTM grade steels, and can therefore provide additional ductility for both spiral welded and straight seam tubes. Experiments were conducted on API and ASTM tubes which slightly exceeded the upper bound slenderness requirements for CFTS specified in the AISC Steel Construction Manual (2010). Results from these tests showed that embedded CFT connections which utilize API steel can exceed 8% drift prior to tube fracture, while connections which use ASTM grade steels tend to fracture at 6% drift. Additional ductility can be expected for tubes with lower slenderness values (Lehman and Roeder, 2012).

1.3 Embedded Ring Connection

Embedded CFT connections shall be designed

C1.3 Embedded Ring Connection

The embedded ring connection utilizes a CFT fully

according to the requirements specified in Article 1.3.

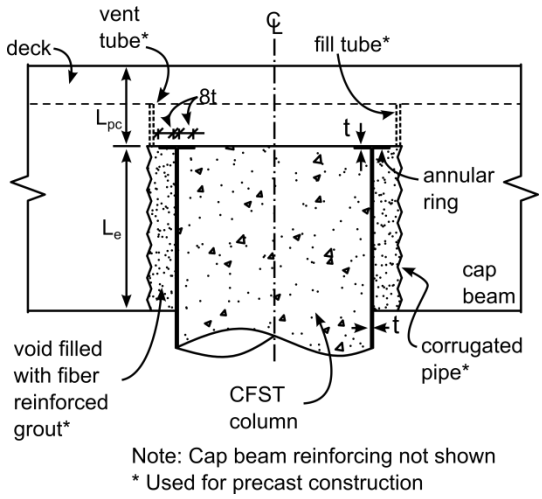

Figure 1.3.1 Embedded Ring Connection

1.3.1 Annular Ring

An annular ring shall be welded to the steel tube as illustrated in Figure 1.3.1. The annular ring shall have the same thickness of the steel tube with a yield stress equal to or greater than that of the steel tube. The ring shall extend outside the tube 8 times the thickness of the tube, and project inside the steel tube 8 times the thickness of the tube as illustrated in Figure 1.3.1.

The annular ring shall be welded to the steel tube using complete joint penetration (CJP) welds of matching filler metal, or fillet welds on both the inside and outside of the tube. The minimum size, w, of the fillets shall be determined using Equation 1.3.1.1 where F_{EXX} and $F_{u,tube}$ are the minimum tensile strength of the weld metal and steel tube in ksi or psi respectively.

$$w \geq \frac{1.31 F_{u,st} t}{F_{EXX}} \qquad \text{Equation 1.3.1.1}$$

Welds shall provide a minimum CVN toughness of 40-ft-lbs at 70˚F.

1.3.2 Embedment Depth

The tube shall be embedded into the cap beam a embedded into the cap beam. The strength and ductility of this connection type is to be controlled by the CFT component, not by the cap beam or other superstructure components. For practical construction, the precast cap would be placed onto the column after the column was set, and the recess between the tube and corrugated pipe would be filled with high strength fiber reinforced grout.

C1.3.1 Annular Ring

The annular ring is welded to the steel tube to provide anchorage and transfer stress to the concrete and reinforcing in the cap beam. This ring is welded according to Article 1.3.1 to ensure the weld can develop the full tensile capacity of the steel tube. The failure cone is assumed to have a 45-degree angle with a maximum concrete principle stress of 6sqrt($f'_{c,cap}$).

C1.3.2 Embedment Depth

The embedment requirement in Article 1.3.2 is required to develop the full tensile capacity of the CFT

distance L_e as defined by Equation 1.3.1.1 where f'_{ccap} is the compressive strength of the cap beam in psi, D is the outside diameter of the steel tube, D_o is the inside diameter of the corrugated pipe, and F_u is the minimum specified tensile strength of the steel tube in psi.

$$L_e = \sqrt{\frac{D_o^2}{4} + \frac{DtF_{u,st}}{6\sqrt{f'_{c,cap}}}} - \frac{D_o}{2} \qquad \text{Equation 1.3.1.2}$$

1.3.3 Requirements for Bridge Layout and Cap Beam Design

1.3.3.1 Bridge Layout

When using the embedded connection, the column shall be laid out between the longitudinal girders as illustrated in Figure 1.3.3.1 and Figure 1.3.3.2.

1.3.3.2 Required Cap Depth Above CFT Embedment

A minimum cap beam depth above the embedded CFT, L_{pc}, shall be included according to Equation 1.3.3.2.1 where C_c and C_s are the compressive forces (in lbs) in the concrete and steel due to the combined axial load and bending moment as computed using a plastic stress distribution method and $f'_{c,cap}$ is the compressive strength of the cap beam in psi.

member in flexure prior to developing a conical pullout failure of the connection as illustrated in Figure C1.3.2.1. The cone depth and maximum concrete principal stress limits were derived using results from an extensive experimental program (Lehman and Roeder 2012).

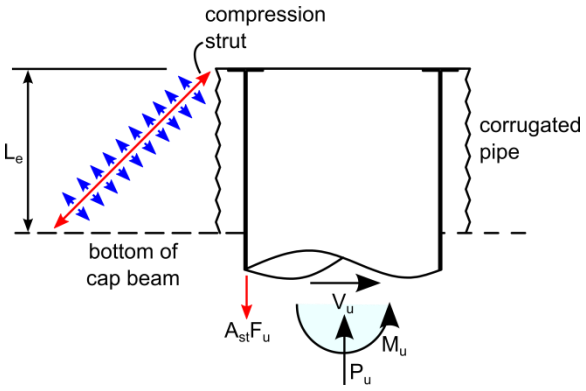

Figure C1.3.2.1 Transfer Mechanism

C1.3.3 Requirements for Bridge Layout and Cap Beam Design

C1.3.3.1 Bridge Layout

The column must be placed between the longitudinal girders to facilitate the development of corbel reinforcing in the cap beam as well as positive moment continuity in the girders.

C1.3.3.2 Required Cap Depth Above CFT Embedment

Adequate concrete depth must be provided above the tube to eliminate the potential for punching shear failure in the cap beam. The ACI 318 (2010) provisions for flat slabs in single shear were used as a basis to develop an expression for the minimum cap beam depth above the embedded CFT, L_{pc}, to avoid this failure mode.

$$L_{pc} \geq \sqrt{\frac{D_o^2}{4} + \frac{C_c + C_s}{4\sqrt{f'_{c,cap}}}} - \frac{D}{2} - L_e \qquad \text{Equation 1.3.3.2.1}$$

1.3.3.3 Cap Beam Reinforcing

(A) Flexural Reinforcing

Longitudinal flexural reinforcing in the column region shall be designed to resist $1.2M_p$ of the CFT column per requirements in the Caltrans SDC. Longitudinal flexural reinforcing shall be spaced uniformly across the width of the cap beam. A minimum of one layer of reinforcing shall pass above the embedded CFT in the cap beam as shown in Figure 1.3.3.3.3. Some longitudinal reinforcing in the bottom layer will be interrupted by the embedded corrugated pipe. The bottom layer of flexural reinforcing not interrupted by the corrugate pipe shall be designed to resist $1.2M_p$ of the CFT column. Interrupted bars shall still be included and arranged as illustrated in Figure 1.3.3.3.

(B) Vertical Stirrups

Vertical reinforcing, A_s^{jv}, shall be included according to Equation 1.3.3.3.1 where A_{st} is the total area of the steel tube embedded into the cap beam.

$$A_S^{jv} = 0.65 \times A_{st} \qquad \text{Equation 1.3.3.3.1}$$

Vertical stirrups or ties shall be distributed uniformly within a distance $D_c/2+L_E$ extending from the column centerline as shown in Figure 1.3.3.3.1 and Figure 1.3.3.3.3. These stirrups can be used to meet other requirements documented elsewhere including shear in the bent cap.

(C) Horizontal Stirrups

Horizontal stirrups or ties shall be placed transversely around the vertical stirrups or ties in two or more intermediate layers spaced vertically at not more than 18-in apart. The horizontal reinforcing area, A_s^{jh}, shall be included according to Equation 1.3.3.3.2 where A_{st} is the area of the steel tube embedded into the cap beam. The horizontal reinforcing shall be placed within a distance $D/2+L_E$ extending from the column

(B) Vertical Stirrups

Vertical reinforcing is included a distance extending $D/2+L_E$ from the column centerline to resist development of a conical pullout failure as discussed in Article C1.3.2. The vertical reinforcing is included to resist $4\sqrt{f'_c}$ of the maximum principal stress illustrated in Figure C1.3.3. The remaining $2\sqrt{f'_c}$ is carried by the concrete.

(C) Horizontal Stirrups

Horizontal reinforcing requirements are consistent with requirements in Article 7.4.4.3 of the Caltrans SDC V. 1.8 with the exception that the horizontal stirrups must be placed within a distance $D_c/2+L_E$ extending from the column centerline.

centerline as illustrated in Figure 1.3.3.3.2 and Figure 1.3.3.3.3.

$$A_S^{jh} = 0.1 \times A_{st}$$ Equation 1.3.3.3.2

In addition, the top layer of transverse reinforcing shall continue across top of the void in the cap beam as illustrated in Figure 1.3.3.3.3.

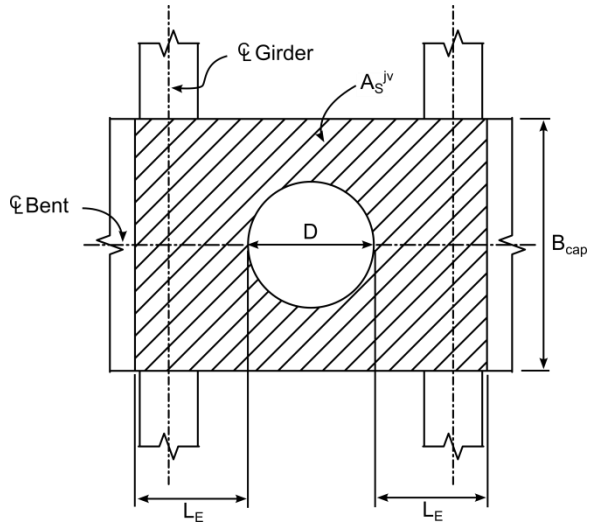

Figure 1.3.3.3.1 Location of Vertical Reinforcing

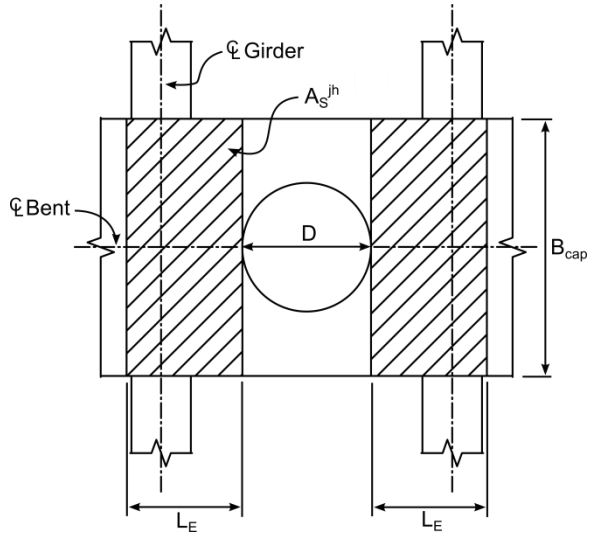

Figure 1.3.3.3.2 Location of Horizontal Reinforcing

(D) Horizontal Side Reinforcement

Horizontal side reinforcing shall be included

according to Article 7.4.4.3 of the Caltrans SDC.

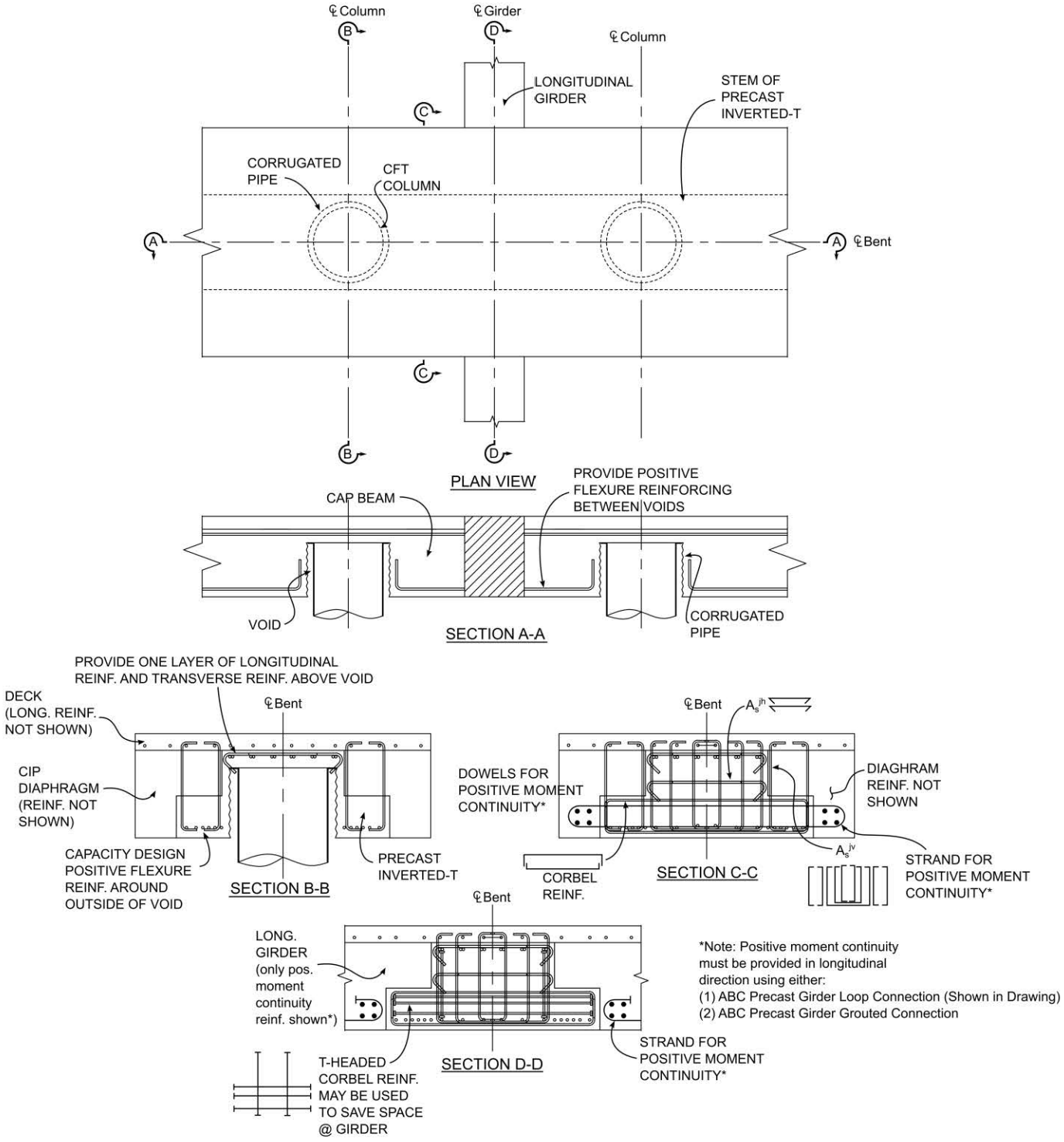

Figure 1.3.3.3 Cap Beam Details for Embedded Connection

1.3.4 Construction Sequence

The embedded ring connection shall be constructed according to the sequence defined in Article 1.3.4 and illustrated in Figure 1.3.4.1C.

(1) Cast foundation leaving a void for the steel tube using a corrugated pipe.
(2) Place the steel pipe with annular rings welded to the top and bottom.
(3) Grout the steel tube into the foundation using fiber-reinforced grout.
(4) Cast concrete fill.
(5) For precast construction, place precast element on top of the CFT. For CIP construction, build false work and cast cap beam around the CFT.
(6) For precast construction, grout the steel tube into the cap beam using fiber-reinforced grout.

C1.3.4 Construction Sequence

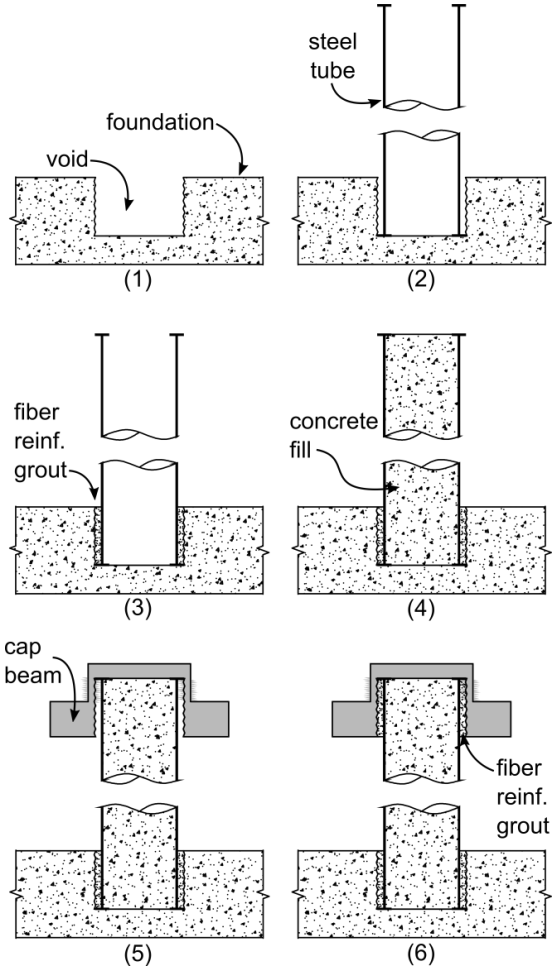

Figure 1.3.4.1C Construction Sequence for Embedded Ring Connection

1.4 Debonded Welded Dowel Connection

De-bonded welded dowel connections shall be designed according to requirements in Section 1.4.

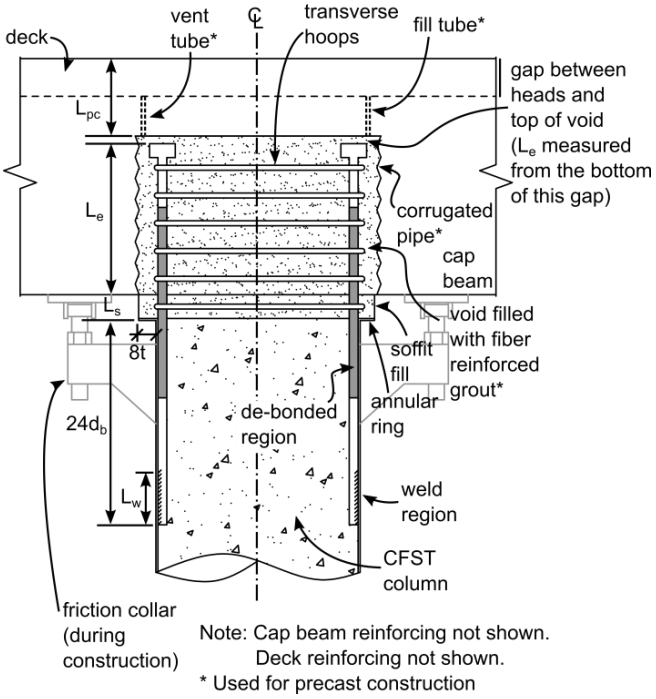

Figure 1.4.1 Welded Dowel Connection with De-bonded Reinforcing

1.4.1 Annular Ring

An annular ring shall be welded to the steel tube as illustrated in Figure 1.4.1. The annular ring shall have the same thickness of the steel tube with a yield stress equal to or greater than that of the steel tube. The ring shall extend outside the tube 8 times the thickness of the tube as illustrated in Figure 1.4.1.

The annular ring shall be welded to the steel tube using a fillet weld on the outside of the tube. The fillet weld shall be the largest allowable based on the tube thickness as specified in the AISC Construction Manual. Welds shall provide a minimum CVN toughness of 40-ft-lbs at 70˚F.

1.4.2 Reinforcing Embedment Depth

C1.4 Debonded Welded Dowel Connection

The debonded welded bar connection utilizes a ring of headed reinforcing bars which are welded into the tube and developed into the cap beam. The strength and ductility of this connection type is controlled by the reinforcing ratio of the longitudinal reinforcing which extends from the column into the cap beam. The welded detail is primarily intended to decrease the development length and utilize the maximum moment arm within the CFT column.

C1.4.1 Annular Ring

The annular ring is welded to the steel tube to provide a larger area to transfer compressive stress from the steel tube to the cap beam. This helps limit localized grout crushing. The fillet weld is designed to transfer to compressive stress from the tube into the annular ring.

1.4.2.1 Embedment into Cap Beam

Longitudinal reinforcing shall be embedded into a void in the cap beam. The embedment length shall be the maximum length calculated using Equation 1.4.2.1.1 where ψ_e is the reinforcing bar coating factor defined in ACI 318 (1.0 for uncoated bars, and 1.2 for epoxy coated bars), L_{db} is the debonded length of the reinforcing bar as defined in Article 1.4.4.2, $f'_{c,cap}$ is the compressive strength of the cap beam in psi, and $f_{y,bar}$ is the yield capacity of the longitudinal dowel in psi.

$$L_e = \frac{0.016\psi_e f_{y,b}}{\sqrt{f'_{c,cap}}} d_b \qquad \text{Equation 1.4.2.1a}$$

$$L_e = \frac{D}{2} + \sqrt{\frac{D^2}{4} + \frac{1.2 * f_{y,b} * A_{st}}{6\pi\sqrt{f'_{c,cap}}}} \qquad \text{Equation 1.4.2.1b}$$

$$L_e = 3d_b + 0.5L_{db} \qquad \text{Equation 1.4.2.1c}$$

1.4.2.2 Embedment into CFT Column

Longitudinal reinforcing shall extend a distance $24d_b$ into the CFT column.

C1.4.2.1 Embedment into Cap Beam

The headed reinforcing must extend into the cap beam for a length sufficient to fully develop the reinforcing bar while eliminating the potential for a conical pullout failure as illustrated in Figure C1.4.2.1.1. Equation 1.4.2.1.1a defines the required development length as specified in Article 12.6 of ACI 318, while Equation 1.4.2.1.1b defines the required embedment depth to eliminate conical pullout failure as determined using the transfer mechanism shown in Figure C1.4.2.1.1. The embedment depth requirement in Equation 1.4.2.1c has been included to ensure a minimum bonded length of $3d_b$ is included adjacent to the head on the end of the headed dowel as illustrated in Figure 1.4.1. This region of bonded reinforcing must be included to ensure adequate anchorage of the longitudinal reinforcing into the cap beam.

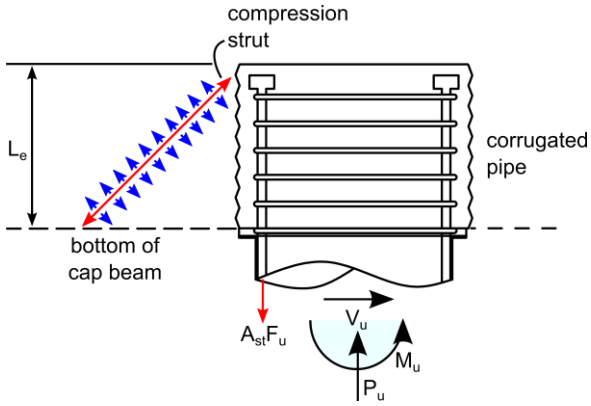

Figure C1.4.2.1.1 Transfer Mechanism

C1.4.2.2 Embedment into CFT Column.

The required reinforcing embedment into the CFT column specified in Article 1.4.2.2 is based on research conducted on the pullout strength of reinforcing welded into CFTs. Results suggest that the embedment can be decreased to as low as $16d_b$, however $24d_b$ is required to provide a reasonable factor of safety.

1.4.3 Reinforcing-to-Steel Tube Welds

Reinforcing bars shall be welded to the inside of the steel tube using flare bevel groove welds on both sides of the reinforcing bars as shown in Figure C1.4.3.1. The minimum length of the welds, L_w, shall be the maximum length calculated using Equation 1.4.3.1. All material strengths ($F_{y,bar}$ and F_{EXX}) are in ksi.

$$L_w = \frac{5.6 A_b F_{y,bar}}{F_{EXX} d_b} \qquad \text{Equation 1.4.3.1a}$$

$$L_w = \frac{0.83 A_b F_{y,bar}}{F_{y,tube} t} \qquad \text{Equation 1.4.3.1b}$$

$$L_w = \frac{1.11 A_b F_{y,bar}}{F_{u,tube} t} \qquad \text{Equation 1.4.3.1c}$$

1.4.4 De-bonded Reinforcing

Longitudinal reinforcing shall be de-bonded from the surrounding concrete in the connection region according to the requirements in Section 1.4.4. The de-bonded region is denoted as L_{db} in Figure 1.4.4.1.

C1.4.3 Reinforcing-to-Steel Tube Welds

The weld lengths specified in Article 1.4.3 are calculated to develop the yield capacity of the reinforcing bars based on typical weld limit states for flare bevel groove welds. These equations are based on welding requirements for reinforcing bars specified in AWS 1.4, which defines the effective throat width to be $0.2d_b$ as illustrated in Figure C1.4.3.1. Equation 1.4.3.1a is based on failure of the weld metal, Equation 1.4.3.1b is based on yielding of the tube steel, and Equation 1.4.3.1c is based on rupture of the tube steel. Strength reduction factors specified according to the AISC Construction Manual have been included in Equation 1.4.3.1.

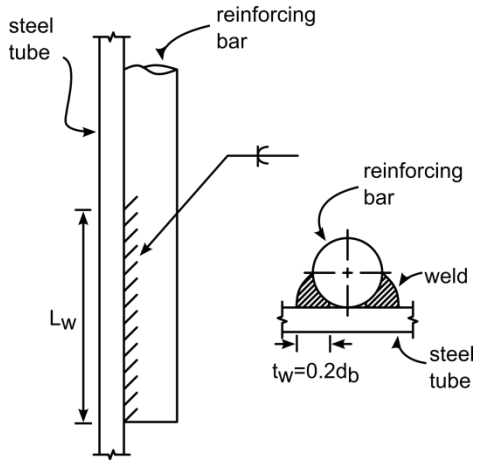

Figure C1.4.3.1 Flare Bevel Groove Weld

C1.4.4 De-bonded Reinforcing

Longitudinal reinforcing is de-bonded in the connection region with the intention of evenly distributing strain across the de-bonded length, thereby increasing the ductility of the connection.

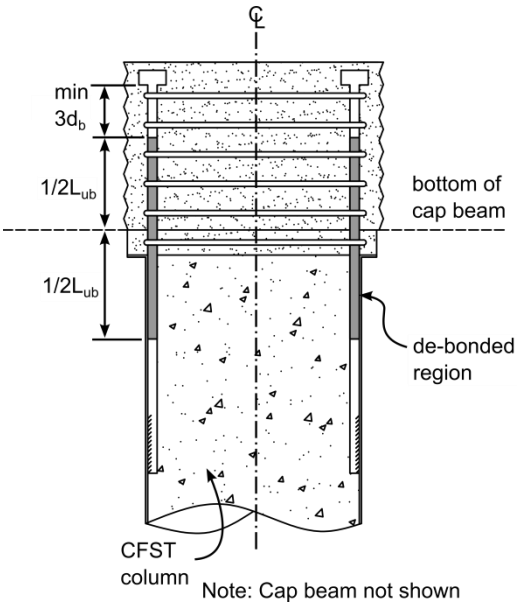

Figure 1.4.4.1 Welded Dowel Connection Debonding Details

1.4.4.1 De-bonding Methods

The Engineer shall specify the de-bonding method on project plans on a project by project basis.

1.4.4.2 De-bonded Length

Longitudinal reinforcing shall be de-bonded from the surrounding concrete in the connection region as illustrated in Figure 1.4.4.1. The de-bonded length, L_{db}, shall be calculated according to Equation 1.4.4.2.1 or Equation 1.4.4.2.2 where θ is the target rotation for reinforcing bar fracture, and φ_s is the curvature of the connection at a steel strain limit of $0.7\varepsilon_u$ as obtained from a moment curvature analysis. Half of the de-bonded length shall extend into the cap beam, and half of the de-bonded length shall extend through the soffit

C1.4.4.1 De-bonding Methods

Several de-bonding methods have been evaluated in previous research including encasing the bars in tight-fitting PVC pipe, or wrapping the bars with duct tape. Other methods may be considered so long as it has been shown that they adequately de-bond the reinforcing from the surrounding concrete.

C1.4.4.2 De-bonded Length

Equation 1.4.4.2.1 is a simplified method for estimating the required de-bonded length of the longitudinal reinforcing to achieve a pre-determined drift ratio prior to bar fracture. Although this method does not require a moment curvature analysis, it is highly approximate and results in larger de-bonded lengths than those calculated using a moment curvature analysis as is prescribed in Equation 1.4.4.2.2.

fill and into the CFT column as illustrated in Figure 1.4.1.

$$L_{db} = \frac{\tan\theta(D-t-d_b/2)}{0.7\varepsilon_u} \qquad \text{Equation 1.4.4.2.1}$$

$$L_{db} = \frac{\theta}{\phi_s} \qquad \text{Equation 1.4.4.2.2}$$

1.4.5 Transverse Reinforcing

Transverse reinforcing shall be included in the joint region in the form of spiral or discrete hoops as shown in Figure 1.4.1. The area and spacing of this reinforcing must conform to Equation 1.4.5.1. When discreet hoops are used, at least one hoop must be placed in the depth of the soffit fill.

1.4.6 Requirements for Bridge Layout and Cap Beam Design

1.4.6.1 Bridge Layout

The column shall be laid out between the longitudinal girders.

1.4.6.2 Cap Beam Reinforcing

(A) Flexural Reinforcing

Longitudinal flexural reinforcing shall be designed to resist $1.2M_p$ of the CFT column per requirements in the Caltrans SDC V. 1.8. Longitudinal flexural reinforcing shall be spaced uniformly across the width of the cap beam. Some longitudinal reinforcing in the bottom layer will be interrupted by the embedded corrugated pipe. The bottom layer of flexural reinforcing not interrupted by the corrugate pipe shall be designed to resist $1.2M_p$ of the CFT column. Interrupted bars shall still be included as shown in Figure 1.3.3.

(B) Vertical Stirrups

Vertical stirrups shall be included according to requirements in Article 7.4.4.2 in the Caltrans SDC V.

C1.4.5 Transverse Reinforcing

Transverse reinforcing is placed around the reinforcing bars to increase confinement in the joint region especially through the depth of the soffit fill.

1.8.

(C) Horizontal Stirrups

Horizontal stirrups shall be included according to requirements in Article 7.4.4.2 in the Caltrans SDC V. 1.8.

(D) Horizontal Side Reinforcing

Horizontal side reinforcing shall be included according to requirements in Article 7.4.4.2 in the Caltrans SDC V. 1.8.

1.4.6.1 Soffit Fill Depth

The soffit fill depth, L_{soffit}, shall be calculated according to Equation 1.4.6.1.1.

$$L_s = \sin(\theta_u)\left(\frac{D}{2} + 8t\right) \qquad \text{Equation 1.4.6.1.1}$$

1.4.6.2 Requirements for Headed Reinforcing

Minimum cover shall be provided when headed reinforcing is anchored in the cap beam according to requirements in Article 1.4.6.2. These requirements are summarized in Figure 1.4.6.2.

1. The thickness of side cover around the head must be equal to or greater than the diameter of the head
2. A minimum depth of $3d_h$ shall be included above the heads in the headed reinforcing where d_h is the diameter of the head.
3. Nominal amounts of longitudinal reinforcing (e.g. reinforcing steel in the plane orthogonal to the headed reinforcement) shall be placed above the head.

C1.4.6.1 Soffit Fill Depth

The soffit fill depth requirement in Equation 1.4.6.1.1 ensures that the annular ring does not come into contact with the cap beam at the maximum expected drift, θ.

C1.4.6.2 Requirements for Headed Reinforcing

Unlike straight bar anchorage conditions, for which the deformations along the length of the bar provide progressive anchorage, in a headed bar the head itself provides most of the anchorage. Under tensile loading the head reacts and transfers the force through strutting action, as shown in Figure 1. Under compression, the headed bar transfers the force to the concrete through strutting action towards the base. In both conditions, four aspects of dimensioning are important: (1) sufficient concrete depth to limit the shear stresses along the compression strut, (2) sufficient cover, (3) horizontal (longitudinal) reinforcement to resist the horizontal component of the strut and (4) vertical (transverse) reinforcement to resist the vertical component of the strut.

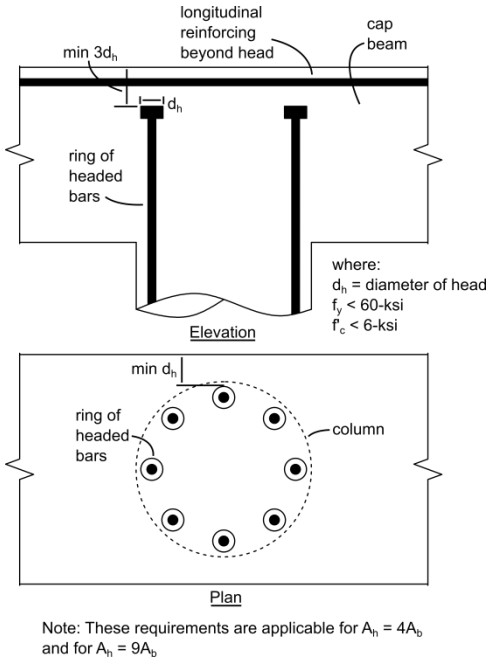

Figure 1.4.6.2.1 Cover Requirements for Headed Reinforcing

1.4.7 Construction Sequence

The welded dowel connection shall be constructed according to the sequence defined in Article 1.4.7 and illustrated in Figure 1.4.7.1C.

(1) Cast foundation leaving a void for the steel tube using a corrugated pipe.
(2) Place the steel pipe with annular ring welded to the bottom and longitudinal reinforcing and annular ring welded to the top.
(3) Grout the steel tube into the foundation using fiber-reinforced grout.
(4) Cast concrete fill.
(5) For precast construction, place precast element on top of the CFT with a friction collar. The headed reinforcing should not come into contact with the top of the void in the cap beam. For CIP construction, build false work and cast cap beam around the CFT.
(6) For precast construction, grout the welded reinforcing into the void in the cap beam.

C1.4.7 Construction Sequence

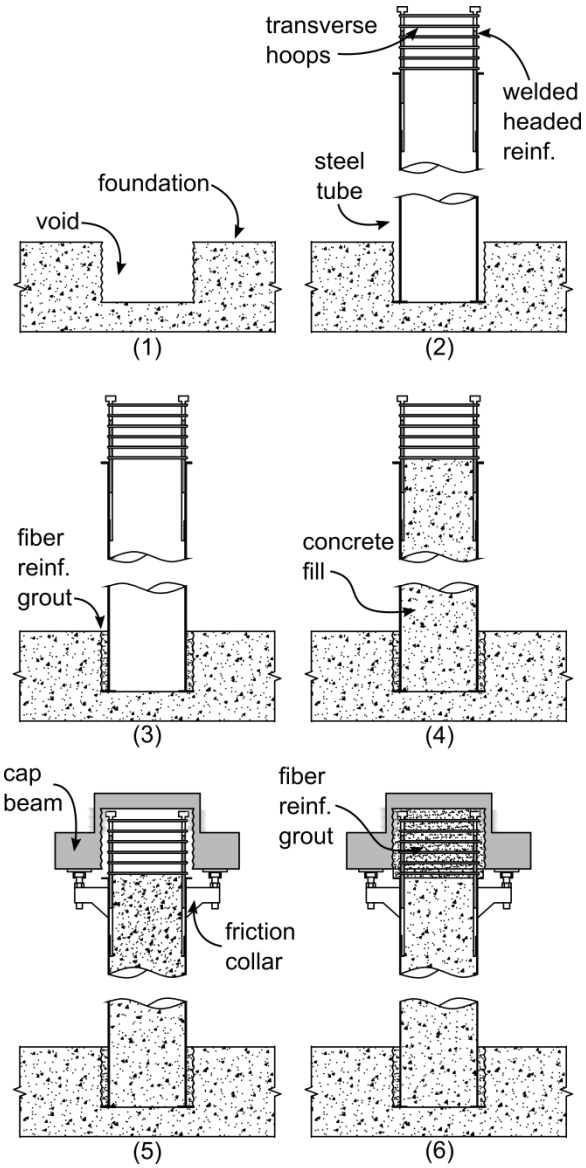

Figure 1.4.7.1C Welded Dowel Connection Construction Sequence

1.5 Reinforced Concrete Connection

Reinforced concrete connections shall be designed according to requirements in Section 1.5.

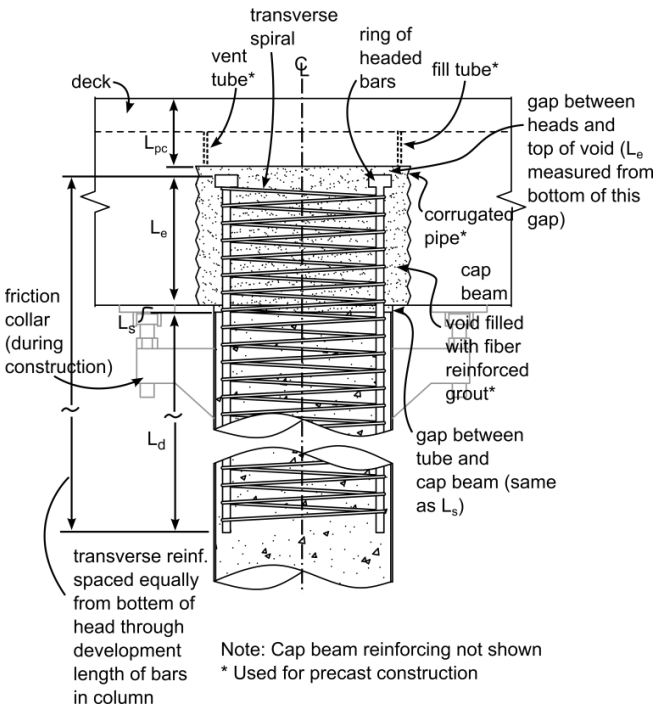

Figure 1.5.1 Reinforced Concrete Connection

1.5.2 Reinforcing Embedment Depth

1.5.2.1 Embedment into Cap Beam

Longitudinal reinforcing shall extend into the cap beam as specified in Article 1.4.2.1.

1.5.2.2 Embedment into CFT Column

Longitudinal reinforcing shall extend a distance L_d into the CFT column according to Equation 1.5.2.2.1 where ψ_e is the reinforcing bar coating factor as defined in ACI 318 (1.0 for uncoated bars, and 1.2 for epoxy coated bars), $f'_{c,fill}$ is the compressive strength of the concrete fill in psi, and $f_{y,bar}$ is the yield strength of the longitudinal dowels in psi.

C1.5 Reinforced Concrete Connection

The reinforced concrete connection consists of a more traditional reinforced concrete dowel connection, as both transverse and longitudinal reinforcing extend from the CFT column into the cap beam. The strength and ductility of this connection type is controlled by the reinforcing ratio and moment arm of the longitudinal reinforcing. Note that construction of this connection using precast super-structure components requires use of a friction collar to temporarily support the cap beam.

C1.5.2.2 Embedment into CFT Column

The headed reinforcing must extend into the CFT column for a length sufficient to fully develop the reinforcing bar. Equation 1.5.2.21 defines the required development length as specified in Article 12.2 of ACI 318. Equation 1.5.2.2.1 is a simplified development length equation which pertains to geometries commonly found in reinforced concrete bridge columns. For

$$L_d = \left(\frac{f_{y,b}\psi_e}{25\sqrt{f'_{c,fill}}}\right) d_b \qquad \text{Equation 1.5.2.2.1}$$

1.5.3 Transverse Reinforcing

Transverse reinforcing in the form of discrete hoops or spiral shall extend from the cap beam and into the column for a distance L_d as illustrated in Figure 1.5.1.

1.5.4 Requirements for Bridge Layout and Cap Beam Design

1.5.4.1 Bridge Layout

The column shall be laid out between the longitudinal girders.

1.5.4.2 Cap Beam Reinforcing

(A) Flexural Reinforcing

Longitudinal flexural reinforcing shall be designed to resist $1.2M_p$ of the CFT column per requirements in the Caltrans SDC V. 1.8. Longitudinal flexural reinforcing shall be spaced uniformly across the width of the cap beam. Some longitudinal reinforcing in the bottom layer will be interrupted by the embedded corrugated pipe. The bottom layer of flexural reinforcing not interrupted by the corrugate pipe shall be designed to resist $1.2M_p$ of the CFT column. Interrupted bars shall still be included as shown in Figure 1.3.3.

(B) Vertical Stirrups

Vertical stirrups shall be included according to requirements in Article 7.4.4.2 in the Caltrans SDC V. 1.8.

(C) Horizontal Stirrups

Horizontal stirrups shall be included according to requirements in Article 7.4.4.2 in the Caltrans SDC V. 1.8.

(D) Horizontal Side Reinforcing

Horizontal side reinforcing shall be included according uncommon geometries or reinforcing layouts, The Engineer shall reference Article 12.2 of ACI 318.

to requirements in Article 7.4.4.2 in the Caltrans SDC V. 1.8.

1.5.4.1 Requirements for Headed Reinforcing

Cover for headed reinforcing shall be included according to requirements in Article 1.4.6.2.

1.5.5 Construction Sequence

The reinforced concrete connection shall be constructed according to the sequence defined in Article 1.5.5 and illustrated in Figure 1.5.5.1C.

(1) Cast foundation leaving a void for the steel tube using a corrugated pipe.
(2) Place the steel pipe with an annular ring welded to the bottom.
(3) Grout the steel tube into the foundation using fiber-reinforced grout.
(4) Temporarily support longitudinal reinforcing cage at the top of the column, and cast concrete fill.
(5) For precast construction, place precast element on top of the CFT using a friction collar. The headed reinforcing should not come into contact with the top of the void in the cap beam. For CIP construction, build false work and cast cap beam around the CFT.
(6) For precast construction, grout the longitudinal reinforcing cage into the cap beam using fiber-reinforced grout.

C1.5.5 Construction Sequence

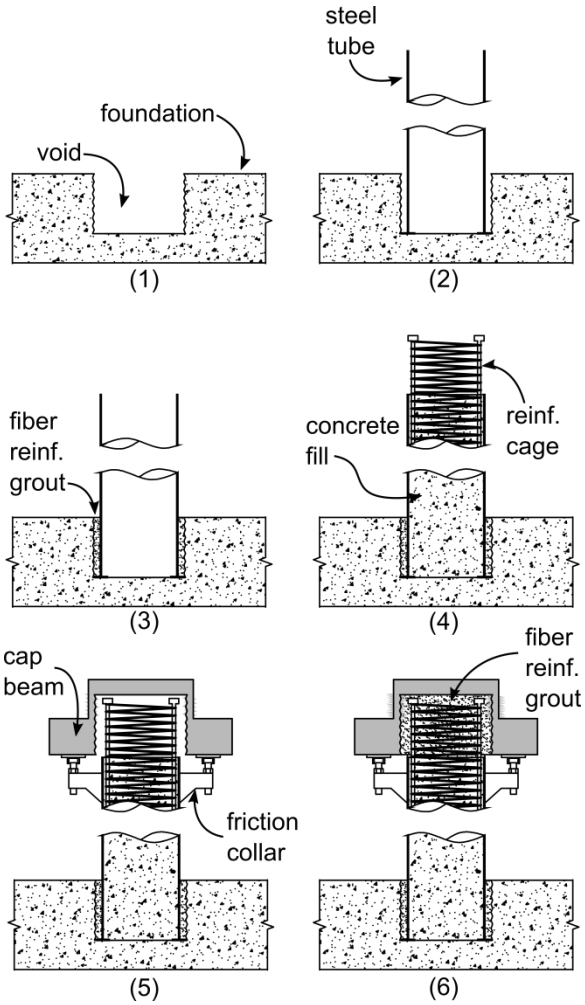

Figure 1.5.5.1C Reinforced Concrete Construction Sequence

1.6 Annotation List

A_b = Area of longitudinal reinforcing bar, Article 1.4.6.2.

A_h = Area of headed anchor on headed reinforcing bar, Article 1.4.6.2.

A_s^{jh} = Area of horizontal joint shear reinforcing, Articles 1.3.3.3, 1.4.6.2, 1.5.4.2.

A_s^{jv} = Area of vertical joint shear reinforcing, Articles 1.3.3.3, 1.4.6.2, 1.5.4.2.

A_{st} = Total area of longitudinal reinforcing extending into the cap beam, Article 1.3.3.3.

B_{cap} = Width of cap beam, Article 1.3.3.3.

C_c = Resultant compressive force in concrete as calculated using the plastic stress distribution method, Article 1.3.3.2.

C_s = Resultant compressive force in steel tube as calculated using the plastic stress distribution method, Article 1.3.3.2.

d_b = Diameter of reinforcing bar.

D = Diameter of steel tube.

D_o = Diameter of steel tube plus 4t (D+4t) when corrugated pipe is not used in cases of cast-in- place construction. Diameter of corrugated pipe when applicable.

F_{EXX} = Minimum tensile strength of weld metal, Articles 1.3.1, 1.4.2.

$F_{u,tube}$ = Ultimate strength of steel tube, Article 1.3.1.

$F_{y,bar}$ = Yield strength of longitudinal reinforcing bar. Article 1.4.2.1.

$F_{y,tube}$ = Yield strength of steel tube.

f'_c = Concrete strength.

$f'_{c,fill}$ = Compressive strength of concrete fill.

$f'_{c,cap}$ = Compressive strength of cap beam concrete, Articles 1.3.2, 1.3.3.2.

f'_g = Compressive strength of grout, Article 1.2.1.

L_{db} = Reinforcing bar debonded length, Article 1.4.4.2.

L_e = Steel tube or longitudinal reinforcing embedment depth into cap beam, Articles 1.3.2, 1.4.2.1, .

L_{pc} = Depth of the cap beam above the embedded CFT for the embedded CFT connection, or depth of the cap beam above the embedment of longitudinal reinforcing into cap beam for the dowel connections, Articles 1.3.3.2, 1.4.6.2.

L_w = Weld length, Article 1.4.3.

t = Thickness of steel tube.

w = Minimum fillet weld size between steel tube and annular ring, Articles 1.3.1, 1.4.1.

ε_u = Ultimate strain of longitudinal reinforcing, Article 1.4.4.2.

θ = Target deformation capacity (rad), Articles

φ_s = Curvature of the connection at a steel strain limit of $0.7\varepsilon_u$, Article 1.4.4.2.

ψ_e = Reinforcing bar coating factor as defined in ACI 318 (1.0 for uncoated bars, and 1.2 for epoxy coated bars), Articles 1.4.2.1, 1.5.2.2..

APPENDIX E: STANDARD CONNECTION DRAWINGS